Research on Regulation of Cytokinesis in *Trypanosoma brucei*

Sophie Frances May

BA (Hons)

A thesis submitted in the fulfilment of the requirement for the degree of Doctor of Philosophy in the Faculty of Biomedical and Life Sciences, University of Glasgow

Wellcome Trust Centre for Molecular Parasitology

Glasgow Biomedical Research Centre

University of Glasgow

United Kingdom

September 2010

Table of contents

List of Tables

List of Figures

Acknowledgements

I would like to thank my supervisor Dr Tansy Hammarton for giving me the opportunity to complete my PhD in the Hammarton lab, and for all the support and help, especially in the past year. I am grateful to Corinne Benz, Fiona McMonagle, Glynn Forsythe, Cristina Costa, Jiang Ma and Chris Stockdale for the advice, technical help and encouragement at the bench, and for all the good conversations.

Thanks also to Calvin Tiengwe and Will Proto, who have been so supportive through the failed experiments and late nights, and who always knew how to fix things.

I would also like to thank Elaine Brown and Margaret Mullin for being so helpful in the lab and for putting up with all the questions, and Kerry Woods and Daniella Tonn for showing me how to use the Delta Vision. Also thanks to everyone in the Mottram, Barry, Muller, Doerig and McCulloch groups for their friendship and for creating such a nice atmosphere to work in.

This project would have been so much harder without the support from my parents, especially my mum who has always made time to listen to the same old same old news from the lab, and never stopped encouraging me. Thanks for listening!

Finally, thanks to Mark, I don't know how you put up with the stress / having no living room for these past few months – but I couldn't have done it without you. Thanks for all the love and encouragement.

Author's Declaration

The research reported in this thesis is the result of my own original work, except where stated otherwise, and has not been submitted for any other degree.

Sophie Frances May

September 2010

List of Abbreviations

AIR9	auxin induced in roots cultures 9
APC	anaphase-promoting complex
Apo-L1	apolipoprotein L-1
AUK1	aurora kinase 1
BRDU	5'bromodeoxyuridine
BSF	bloodstream form
CDK	cyclin dependent kinase
CPC	chromosomal passenger complex
CRK	cdc2-related kinase
CYC	cyclin
DAPI	4', 6'-diamidino-2-phenylindole
DFMO	difluoromethylornithine
DIC	differential interference contrast
DMSO	dimethyl sulphoxide
FAZ	flagellum attachment zone
FC	flagellar connector
FP	flagellar pocket
FPC	flagellar pocket collar
GFP	green fluorescent protein
GST	glutathione-S-transferase

HA	haemagglutinin
HAT	Human African Trypanosomiasis
HDL	high density lipoprotein particle
HRP	horseradish peroxidase
IFT	intraflagellar transport
Ig	immunoglobulin
IPTG	isopropyl β-D-1 thiogalactopyranoside
K	kinetoplast
KAB	kinase assay buffer
KD	kinase domain
LA	Luria-Bertani agar
LB	Luria-Bertani broth
LSGI	lysis solution with glycerol and inhibitors
MAP	microtubule associated protein
MEN	mitotic exit network
MOB1	mps one binder 1
N	nucleus
ORF	open reading frame
PBD	polo-box domain
PBS	phosphate buffered saline
PC	polo-box cap
PCF	procyclic form

PCR	polymerase chain reaction
PFR	paraflagellar rod
PLK	polo-like kinase
RNAi	RNA interference
SAC	spindle attachment checkpoint
SDS PAGE	sodium dodecyl sulphate polyacrylamide gel electrophoresis
SEM	scanning electron microscopy
SIN	septation initiation network
SRA	serum resistance associated protein
TAC	tripartite attachment complex
TDB	trypanosome dilution buffer
TEM	transmission electron microscopy
Tet	tetracycline
TLF1	trypanolytic factor-1
UTR	untranslated region
VSG	variant surface glycoprotein
WT	wild type
λPPase	lambda protein phosphatase

Abstract

Trypanosoma brucei is a protozoan parasite, and the causative agent of Human African Trypanosomiasis and Nagana in cattle. The life cycle and cell cycle of the parasite is complex and unusual. In particular, cytokinesis regulation in *T. brucei* is divergent, and significantly does not involve the formation of an actomyosin contractile ring; instead, a furrow ingresses longitudinally along the cell following the axis of the subpellicular microtubules which form a cytoskeletal cage around the cell body. As the organelles are positioned longitudinally in the posterior half of the cell, and in different positions according to life cycle stage, the cleavage axis is therefore subject to a number of constraints which must be overcome for symmetrical allocation of organelles to the daughter cells. It is highly likely that the subpellicular microtubule cytoskeleton plays important roles in cytokinesis furrow ingression. Presumably this process must involve microtubule and membrane remodelling at the site of the furrow apex to form the two discrete daughter cell bodies, and this is likely to require changes in microtubule dynamics, at least locally. Additionally, the cytoskeleton could influence the position of the cleavage plane by denoting polarity, or the timing of furrow initiation through mechanosensing.

The divergent nature of *T. brucei* cytokinesis implies that regulators of this process could be exploited as a source of potential novel drug targets. The Polo-like kinase, PLK, has previously been shown to be required for furrow ingression during cytokinesis in bloodstream form *T. brucei*. This study aimed to further our understanding of the regulation of cytokinesis by PLK by investigating how its activity is regulated *in vitro* and *in vivo*. In other organisms, PLK is known to influence microtubule dynamics, and given the likelihood that microtubule dynamics are important for furrow ingression in *T. brucei*, this study also aimed to investigate the role of the cytoskeleton in cytokinesis. An orthologue of a microtubule-associated protein required for cytokinesis in plants, AIR9, was functionally characterised in *T. brucei*, and the role of subpellicular microtubules in cytokinesis was investigated via the use of microtubule inhibitors.

Soluble and active recombinant PLK was purified from *E. coli* as a 6X Histidine fusion protein (6XHis:PLK). 6XHis:PLK autophosphorylated prolifically, and removal of these phosphorylations with lambda protein phosphatase significantly reduced the ability of 6XHis:PLK to transphosphorylate generic kinase substrates. Further, the importance of a conserved threonine residue (T198) in the T-loop of *T. brucei* PLK, which is a major site for regulation by upstream kinases in other organisms, was investigated. Substitution of T198 with a non-polar (alanine or valine) or a phosphomimetic (aspartic acid) residue revealed that this residue was important for PLK activity *in vitro*. However, expression of T198 variants *in vivo* showed T198V and T198D to be functional, suggesting that PLK activity is not regulated *in vivo* by phosphorylation at this site. The role of the polo box domain (PBD) of PLK in regulating PLK activity was also investigated. In PLKs from other organisms, the PBD autoinhibits PLK activity. Here, while recombinant 6XHis:PBD could pull down full length ty:PLK from *T. brucei* lysates, kinase assays indicated that the PBD did not inhibit the activity of full length PLK. Thus, regulation of the activity of PLK in *T. brucei* appears to be divergent.

Functional characterisation of *T. brucei* AIR9 by RNAi mediated depletion revealed roles for this protein in the relative positions of organelles and the position of the cleavage plane in both life cycle stages. However, the phenotypes observed during RNAi experiments differed between procyclic and bloodstream form parasites. For procyclic form parasites, the defective cytokinesis resulting in non-equivalent progeny seemed to occur in cells with organelle positioning defects suggesting that problems with cytokinesis were secondary to the major organelle positioning defect. Abnormal organelle positioning was far less frequent in bloodstream form parasites, which none the less seemed impaired in the accurate positioning of the cleavage axis.

AIR9 was shown to localise to the cytoskeleton of bloodstream and procyclic trypanosomes using two different epitope tagging approaches, and following induction of *AIR9* RNAi, AIR9 was preferentially depleted from the posterior end of the cell, supporting a designation of AIR9 as a microtubule-associated protein. However, data do not support a role for AIR9 in cytoskeletal stability, since transmission electron microscopy showed the structure of cytoskeletal microtubules was not affected following depletion of AIR9. Hence, I suggest

that AIR9 is more likely to be a scaffold protein potentially involved in the integration of signalling pathways to control cell polarity and cytokinesis.

This study also demonstrated through the application of inhibitors of microtubule dynamics that microtubule dynamics are important for cytokinesis in *T. brucei*. Vinca alkaloid treatment of bloodstream form parasites arrested furrow ingression, while taxol inhibited initiation of cytokinesis in bloodstream form parasites and affected cleavage plane positioning in procyclic cells. In addition, organelle positioning was inhibited through the application of the vinca alkaloid, vinblastine, to procyclic form cells. Thus, although these studies indicate that there are differences in the cytoskeleton makeup of bloodstream and procyclic trypanosomes, the data obtained are consistent with microtubule dynamics playing crucial roles in cell polarity and cytokinesis in both life cycle stages.

1 Introduction

1.1 Cause and geographical distribution of the African Trypanosomiases

The African Trypanosomiases are a group of infectious vector-borne diseases caused by protozoan parasites of the genus *Trypanosoma* and transmitted by the bite of infected tsetse flies (*Glossina* species). *Trypanosoma brucei* species can infect humans, livestock and wild animals, and disease foci correspond to areas within tsetse fly habitats (10 million km^2) incorporating 37 sub-Saharan African countries and putting 50 million people and 48 million cattle at risk(Ilemobade, 2009). Human African Trypanosomiasis (HAT) is caused by the subspecies *T. b. gambiense* and *T. b. rhodesiense*, which are found in west and central Africa, and east and southern Africa, respectively. *T. b. brucei* is non-human infective, and causes the disease Nagana in livestock throughout sub-Saharan Africa.

In 2009, 9877 cases of HAT were reported (World Health Organisation, 2010), although due to incomplete surveillance and diagnosis, the real number of cases is likely to be far higher. In addition to the impact on public health, financial losses due to the effects of Nagana on the agricultural economy are believed to amount to $4.5 billion annually (Torr, 2005). The disease progression and epidemiology of HAT depends on the parasite species. Gambian sleeping sickness (caused by *T. b. gambiense*) accounts for 90 % of HAT cases; the clinical stages of this disease include a long asymptomatic period (which can last for several years after disease onset), followed by sub-acute febrile illness and finally late-stage chronic meningoencephalitis, which if untreated, can be fatal. This contrasts with the acute form of the disease, Rhodesian sleeping sickness which is characterised by a rapid onset of the late stage occurring within just a few months after infection. Disease progression for both types of HAT does not always occur with such predictable outcomes, and there is a spectrum of rates of progression and severity of pathology, thought to be influenced by both host and parasite genetics, and the presence of multiple infections in a single host (Sternberg, 2010). Environmental factors, such as exposure to tsetse flies may also play a role (Caljon et al., 2006).

The transmission cycles of *T. b .gambiense* and *T. b. rhodesiense* are different. *T. b. gambiense* has been isolated from wild and domestic animals; however, the epidemiological consequences of animal reservoirs have yet to be determined (Njiokou et al., 2006). It has been suggested that whilst these reservoirs may not be important during human epidemics, they may serve to maintain and circulate parasites to low levels, facilitating reemergence and reinfection of the human population. By contrast, both wild and domestic animal reservoirs have been shown to be important for the transmission cycle of the zoonotic species, *T. b. rhodesiense*, and trading of infected domestic cattle has been linked to disease foci of human epidemics (Fevre et al., 2001). *T. b. brucei* also has sylvatic hosts, which are of increasing relevance as climate change, population increases and altered land use lead to encroachment of cattle onto tsetse fly-infested regions populated by wild species (Van den Bossche et al., 2010). Understanding the transmission cycles of *Trypanosoma* species is important for the design and implementation of control programmes, and may become increasingly vital towards tackling the possible resurgence of zoonotic diseases in a changing environment.

1.2 Disease history and pathology

Trypanosomiasis is an ancient disease, and the *Glossina*-Trypanosome complex is believed to have existed before the divergence of hominid species, and to have played a role in hominid evolution (Lambrecht, 1985), which is a notion that has more recently been supported by phylogenetic evidence (Stevens and Gibson, 1999), and which may explain how arboreal primates (which live high above the tsetse fly swarming range) are trypanosensitive, whilst humans are largely trypanotolerant (with the exception of their sensitivity to *T. b. gambiense* and *T. b. rhodesiense*). The symptoms of trypanosome infection have been described since Antiquity, and it is believed that some early cattle rearing practices and tribal migrations were a reflection of the impact of Nagana on the lives of early peoples (Steverding, 2008). Despite this long shared evolutionary history, trypanosomes were only discovered to be the causative agent of Nagana and sleeping sickness in 1895 (by David Bruce) and 1902 (by Aldo Castellani), respectively, and it was only in 1903 that the transmission cycle was determined (by David Bruce). Astonishingly, treatments and intervention methods, which

proved hugely successful in controlling large epidemics at the turn of the century, are still in use today.

The earliest symptoms of infection include local inflammation at the site of the tsetse fly bite caused by proliferation of parasites at this lesion (Sternberg, 1998). Parasites rapidly multiply in the blood and lymphatic system, which can lead to the swelling of the lymph nodes referred to historically as 'Winterbottom's sign'. This may be accompanied by febrile episodes as successive waves of parasitaemia occur. The cyclical nature of parasite proliferation is the result of alternating immune evasion and destruction of circulating parasites facilitated by changes to the parasite surface antigen. Recognition and destruction of one particular antigenic type followed by emergence of a different, novel antigenic type allows the parasite to establish a chronic infection, and the high levels of circulating immunoglobulins resulting from the constant pressures on the immune system can cause anaemia. Eventually, parasites migrate into a variety of tissues including the spleen, liver and heart and ultimately the central nervous system. Transmigration across the blood brain barrier is associated with the release of inflammatory mediators, and alterations in the natural balance of pro- and anti-inflammatory molecules is thought to contribute to the clinical manifestations of late stage disease. Symptoms of neuroinflammation include mental disturbances, motor and sensory system involvement, sleep disturbances and finally if untreated, coma and death. Disturbance of natural sleep pattern led to description of the disease as a 'sleeping sickness', which despite the implications of the name, can refer to night time insomnia as well as day time somnolence.

1.3 Treatment of Human African Trypanosomiasis

There are no vaccines available for prophylactic immunisation against HAT, and the prospects of vaccine development are poor due to the ability of the parasites to frequently change their surface antigen. Current treatments are restricted to just four drugs: pentamidine, suramin, melarsoprol and eflornithine (also known as difluoromethylornithine (DFMO)), which, with the exception of eflornithine, were developed over 60 years ago (Burchmore et al., 2002). All four available drugs may be used to treat the early stage of the disease,

although pentamidine and eflornithine are ineffective against *T. b. rhodesiense*, and only melarsoprol and eflornithine are effective against the late stage of the disease. Application of all four drugs requires hospitalisation of the patient due to the mode of drug application and level of monitoring required. Suramin, melarsoprol and eflornithine are administered intra-venously and pentamidine, via intra-muscular injection; treatment regimes involve administration of these drugs over several days, sometimes with intervening recovery periods. Not only is current chemotherapy impractical and expensive, the toxicity of these drugs can also cause painful and serious side effects, particularly in the case of melarsoprol, which has a 5 % fatality rate due to the reactive encephalopathy which can ensue following treatment. Repeated application of the same drugs has led to drug resistance. Treatment failures of up to 30 % and 16 % have been recently reported for melarsoprol and eflornithine, respectively, suggesting that second stage drugs could soon be ineffective in the field (Balasegaram et al., 2009). Mechanisms of drug resistance have been shown to involve the loss of drug transporters: for example, the P2 amino-purine and HAPT1 transporters have been observed in pentamidine-resistant parasites, and loss of the P2 amino-purine transporter has also been implicated in melarsoprol resistance (Barrett et al., 2007). Pentamidine, suramin and melarsoprol are trypanolytic and the modes of action of these drugs are not understood, although inhibition of glycolysis (melarsoprol and suramin), interaction with kinetoplast DNA (pentamidine) and interaction with trypanothione (melarsoprol) have been proposed as possible explanations for trypanolytic activity. Eflornithine, by contrast, is a known inhibitor of ornithine decarboxylase, and was developed as an analogue of this enzyme for the treatment of neoplasmas. Inhibition of ornithine decarboxylase deprives cells of polyamines, resulting in growth arrest. As this drug has a trypanostatic effect, patients must have a functioning immune system to clear the growth-arrested parasites and therefore, this is an unsuitable treatment for patients suffering from immunosuppressive disorders. More recently, nifurtimox, a drug licensed for the treatment of Chagas disease, has been tested in drug trials, and although it is not sufficient to cure trypanosomiasis as a monotherapy, it has been used successfully in combination with other drugs. Trials using a combination of eflornithine and nifurtimox (Nifurtimox Eflornithine Combination Therapy, NECT) were successful at clearing *T. b. gambiense* infections using a reduced number of infusions for shorter

durations (Priotto et al., 2006), and as a result, in 2009, NECT was added to the WHO Essential List of Medicines for the treatment of human African trypanosomiasis (World Health Organisation, 2009).

The current situation is clearly not acceptable; without good prospects of a vaccine, rises in drug resistance and few compounds capable of treating late stage disease, it is critical that new, safer and cheaper drugs are developed.

1.4 Drug development approaches and new treatment prospects

Attempts to develop a vaccine are still ongoing, despite the problems associated with surface antigen variation. Vaccination with tubulin or the microtubule-associated proteins, p52 and p15, resulted in humoral protection against trypanosomes in mouse models (Balaban et al., 1995;Lubega et al., 2002;Rasooly and Balaban, 2004). Interestingly, immunisation with adenovirus expressing recombinant p15 caused a strong CD8+ T-cell response and an effective but non-specific clearance of trypanosomes (Rasooly and Balaban, 2004). However, the development of an effective vaccine that can be used clinically is still a long way off.

The drugs currently in use were developed from existing veterinary or antineoplastic compounds. This type of 'piggy back' approach is still useful, and a more recent example of this approach is Acivicin, an antineoplastic agent which targets CTP synthetase and has been shown to successfully treat trypanosomiasis in the mouse model (Fijolek et al., 2007). The sequencing of the *T. brucei* genome (Berriman et al., 2005), and the subsequent publications of the *T. brucei* kinome (Parsons et al., 2005) and phosphoproteome (Nett et al., 2009) have facilitated investigation into *T. brucei* protein kinases as potential drug targets and given that many of these kinases are conserved regulators of the mammalian cell cycle and already targeted by existing antineoplastic agents, there is great potential for fast tracking these candidates through such piggy back approaches to clinical trials. These advances in genomics and proteomics have not only increased the potential for utilisation of existing

antineoplastic drugs, but also provided opportunities for a target based approach in drug design.

Target assessment is first carried out by genetic validation using techniques such as RNAi or gene knockouts. Essential genes identified in this manner can then be analysed *in vitro* through the production of recombinant proteins, development of protein assays and ultimately screening of inhibitor libraries. If, in addition, the crystal structure of the target can be determined, designed improvements and modifications to individual inhibitors are possible. Finally, animal models and clinical trials are required to test inhibitors *in vivo*. With a targeted approach, it is possible to infer toxic effects in the mammalian host, track resistance occurring from mutations in the target protein, and assess whether the drug may be a good candidate for the treatment of other diseases (broad spectrum drugs may, for example, target conserved but kinetoplastid-specific proteins with potential for treating Chagas disease or Leishmaniasis). This approach has recently been used to good effect in the identification of N-myristoyltransferase inhibitors (Frearson et al., 2010) and inhibitors of trypanothione synthetase (Torrie et al., 2009). Other compounds under investigation include the Oxaborole 6-carboxamides (Nare et al., 2010) and DB289 and its derivatives (Wenzler et al., 2009); the latter are currently in Phase III trials, and as these drugs can be orally administered and some of these compounds are effective against early and late stage disease, these are currently the most promising alternatives to traditional treatments.

1.4.1 Alternative strategies for drug discovery – exploiting natural resistance mechanisms

Human serum is trypanolytic to *T. b. brucei*, and contains high density lipoprotein particles (HDLs), containing a protein called 'Apolipoprotein L-I' (Apo-LI). This protein has been shown to enter trypanosomes via the endocytic pathway, where it is trafficked to the lysosomes (Vanhamme et al., 2003b). Apo-LI forms pores in the lysosomal membrane, causing an influx of chloride ions into the lysosome, which results in osmotic swelling (Perez-Morga et al., 2005;Vanhamme et al., 2003a;Vanhamme et al., 2003a). The swollen lysosome eventually occupies most of the cell body, and it is thought that this could

compromise the outer plasma membrane, and ultimately kill the parasites (Perez-Morga et al., 2005). *T. b. rhodesiense* can be resistant (depending on antigenic variation) to the effects of Apo-LI due to the production of a protein called 'Serum resistance associated protein' (SRA), and it has been shown that SRA interacts with Apo-LI though a coiled-coil protein-protein interaction, the consequence of which is to abolish the liposome fusogenic activity of Apo-LI, thus allowing the parasite to evade Apo-LI induced lysosomal swelling (Vanhamme et al., 2003a). Variant forms of Apo-LI which possess mutations at the binding site of SRA can still kill *T. b. rhodesiense* parasites, and it has been shown that these Apo-LI variant genes are common in African Americans, but absent from European Americans; suggesting that the acquisition of this variant form of Apo-LI is a relatively recent event (Genovese et al., 2010). It appears that humans have evolved a way to counter the *T. b. rhodesiense* resistance mechanism, albeit at cost, as inheritance of the resistant form of Apo-LI was found to be associated with two genes involved in kidney disease (focal segmental glomerulosclerosis (FSGS) and hypertension-attributed end-stage kidney disease (H-ESKD).

T. b. gambiense, which does not express SRA, is still able to infect humans. It has recently been found that resistance to the trypano-toxic HDL particles in human serum (trypanolytic factor-1 (TLF-1)) is associated with downregulation of a receptor for TLF-1: TbgHpHbR (Kieft et al., 2010). The equivalent receptor in *T. b. brucei* (TbbHpHbR) binds to another component of TLF-1, the haptoglobin (Hp)-related protein (Hpr) (and co-factor Hb), a high affinity interaction which occurs at the flagellar pocket and leads to uptake of TLF-1 into the parasites, ultimately leading to killing of *T. b. brucei*. Reduced expression of this receptor was found to be associated with resistance of *T. b. brucei* to TLF-1. Ectopic expression of TbbHpHbR but not TbgHpHbR (which has some amino acid changes compared to TbbHpHbR) in TLF-1 resistant *T. b. brucei* restored TLF-1 sensitivity. Thus, resistance mechanisms to TLF-1 in *T. b. gambiense* could involve decreased expression of TbgHpHbR, or coding sequence mutations in the receptor, which may alter the affinity of this receptor towards Hpr (Kieft et al., 2010).

In addition to TLF, small hydrophobic peptides produced by the mammalian immune system including defensins, cathelicidins and neuropeptides have been

shown be effective against trypanosomes *in vitro* (Delgado et al., 2008;Haines et al., 2009;McGwire et al., 2003). These molecules, like Apo-LI have the ability to disrupt membranes, and possess a highly positively-charged amphipathic alpha helical structure. Neuropetides, for example, were found to lyse bloodstream form parasites via a mechanism involving uptake into the endocytic pathways, disruption of lysosome integrity, cytosolic distribution of metabolic enzymes and ultimately metabolic failure (Delgado et al., 2008). The association with parasite membranes probably results in more than osmotic disruption, and it has been proposed that signalling pathways could also contribute the their trypanocidal effect (McGwire and Kulkarni, 2010). Recently it has also been shown that hydrophobic peptides (derived from the signal sequences of haptoglobin related protein (SHP-1) and paraoxonase-1 (SHP-2)) can affect both motility and membrane rigidity, and that these effects occur before any evidence of osmotic swelling, providing evidence that there are more complex processes involved in the trypanocidal effects of these peptides (Harrington et al., 2010).

Knowledge of these and possibly other natural resistance mechanisms will hopefully prove useful towards developing drugs which mimic components of the natural killing mechanisms so effective against *T. b. brucei* species. Indeed, molecules which mimic or modify the host response could provide useful alternatives to chemical inhibitors, and some have been shown to effectively treat trypanosome infections in mice. For example, a truncated form of Apo-LI which lacks the SRA interaction domain caused trypanosome lysis when the truncated molecule was targeted to the cell surface through conjugation with a nanobody (a single-domain antigen-binding fragment) targeted against variable surface glycoproteins (Baral et al., 2006). The antibiotic minocycline inhibits the immune response to neuroinflammation by decreasing leukocyte invasion into the central nervous system, and has also been shown to inhibit the expression or activity of adhesion molecules involved in leukocyte transmigration. Interestingly, trypanosome invasion of the central nervous system has similarities to leukocyte invasion, and treatment of trypanosome-infected mice with minocycline alleviated late stage disease symptoms and reduced parasite invasion (Masocha et al., 2006).The reduction in leukocyte and trypanosome invasion and consequential reduction in cytokine production in the brain were described as probable explanations for alleviation of late stage symptoms.

Although minocycline cannot be used as a monotherapy, it is a potential candidate for use in combination with other treatments (Masocha et al., 2006). Methods of disease prevention that are based on naturally produced immune defence molecules, or which modulate the immune system, could have advantages over chemical inhibitors as potential toxic effects in the host organism may be less likely, which would increase patient adherence to treatment programmes.

1.5 Transmission intervention strategies

Methods which target the trypanosome transmission cycle rather than the disease itself can also be useful intervention strategies e.g. selective breeding of trypanotolerance in cattle (based on red blood cell percentage), the use of pour-on cattle insecticides, and large scale insecticide application (Bauer et al., 1995;Kgori et al., 2006;Murray et al., 1990). Sterilisation of tsetse flies through gamma irradiation has also successfully reduced tsetse fly populations on the island of Unguja in Zanzibar, although this is not a practical approach for mainland Africa (Vreysen et al., 2000).

Improvements in disease surveillance and diagnosis are also important considerations for control of HAT. Current diagnosis of HAT uses serological and parasitological techniques. The card agglutination test is a useful aid in detecting individuals producing *T. b. gambiense* antibodies. However, this alone is not sufficient to confirm trypanosome infection, and in addition, blood and lymph samples must be analysed by microscopy for the detection of trypanosomes. Stage determination involves lumbar puncture and extraction of cerebrospinal fluid for detection of trypanosomes and monitoring of white blood cell count. The necessity for invasive procedures and analysis of samples by microscopy stipulates that health workers have training and equipment, which can be problematic in field situations.

Investigation into new diagnostic approaches is ongoing, and focussed on producing a test that is non-invasive and easy to use. Advances in molecular techniques have enabled the development of polymerase chain reaction (PCR) tests which are capable of differentiating between *T. b. gambiense* and *T. b.*

rhodesiense (Radwanska et al., 2002), which is impossible by morphological analysis, and the development of loop-mediated isothermal amplification (Njiru et al., 2008) should eliminate the need for field PCR (thermocycling reactions). Simpler methods for interpretation of PCR results are also in progress. The 'molecular dipstick' test uses oligochromatography to detect a positive PCR product, which is an extremely quick procedure resulting in the presence or absence of a single line, very much like a pregnancy test (Deborggraeve et al., 2006). Whilst these methods still rely on blood sampling, tests which use salivary samples are also being developed (Lejon et al., 2006). Replacing lumbar puncture for stage determination is more problematic and sleep-rapid eye movement tests using polysomnography are unreliable. Hopefully identification of stage makers in serum, urine or saliva will replace the need for this highly invasive procedure (Simarro et al., 2008). The development of new drugs, diagnostic tests and implication of intervention strategies requires collaboration between Governments, aid agencies, academic institutions and pharmaceutical companies. The World Health Organisation has a central role in these efforts and in 2000, African Governments launched the Pan African Tsetse and Trypanosomiasis Erradication Campaign, and with Governmental backing, it is more likely that these efforts could lead to eradication of this terrible disease.

1.6 The life cycle of *T. brucei*

The cyclical life cycle of *T. brucei* parasites (Figure 1-1) involves alternation of replicative and differentiated forms in the vector and host organisms. The parasites are exposed to different environmental conditions in the tsetse fly vector and mammalian hosts, and exhibit an array of adaptations in order to survive, varying from metabolic and morphological changes to expression of different surface antigens.

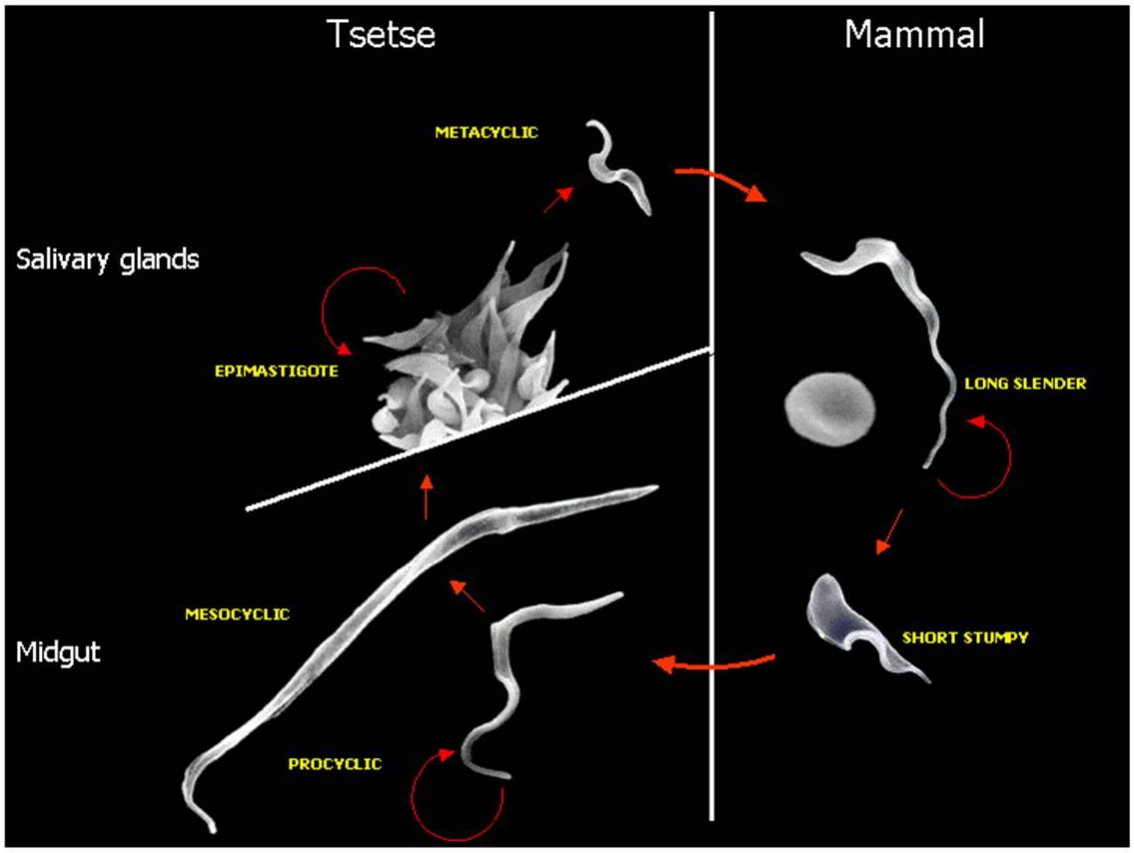

Figure 1-1 -The life cycle of *T. brucei*.
Scanning electron microscope images showing the life cycle stages of *T. brucei* in the mammalian and tsetse fly hosts. Circular arrows indicate replicative life cycle stages. Reproduced with permission from Dave Barry.

1.6.1 Life cycle stages in the mammalian host and immune evasion mechanisms

The biting tsetse fly deposits metacyclic trypanosomes within the dermal connective tissue of the mammalian host where localised inflammation facilitates the entry of trypanosomes into the draining lymphatics and bloodstream. These cell cycle arrested metacyclic parasites quickly undergo morphological changes and cell cycle re-entry, proliferating rapidly in the bloodstream and lymphatic system as a long slender bloodstream trypomastigote. Proliferation is accompanied by antigenic variation. The cell surface is coated in a monolayer of variant surface glycoprotein homodimers (VSG), which comprise 10-15 % of the total cell protein, and act to shield other cell surface membrane epitopes from the immune system of the mammalian host. The diploid trypanosome genome encodes around 1700 distinct *VSG*s at subtelomeric loci; around 1500 of these are located in silent gene arrays, around 200 are found on minichromosomes, and 20 are located at *VSG* expression sites

(McCulloch, 2004). *VSG* expression sites are transcribed as polycistronic mRNAs by RNA polymerase I and consist of tandem gene arrays containing *VSG* and expression site associated genes (ESAGs, which in *T. b. rhodesiense*, include the serum resistance associated (*SRA*) gene). For transcription of a particular *VSG* gene, it must be located at the single active expression site, found in a sub-compartment of the nucleus known as the expression site body (Navarro and Gull, 2001). *VSG* switching occurs at a rate of approximately 10^{-2} per cell per cell cycle (Turner and Barry, 1989), and occurs in a stochastic and spontaneous manner, independently of host antibody presence (Lythgoe et al., 2007). Expression of different *VSG*s in the early stages of infection is ordered to an extent, and this is thought to result from hierarchical differences in the probabilities of expression site activation (Morrison et al., 2005). Coincident silencing and activation of different expression sites is referred to as epigenetic or '*in situ*' switching. For the parasite to increase its *VSG* repertoire beyond those encoded in the 20 expression sites, it must move *VSG* genes from the minichromosomes or silent gene arrays into an expression site. This occurs through gene conversion, whereby homologous recombination at the 70 bp repeats located upstream of the *VSG* gene, and the conserved 3' end of the *VSG* gene results in *VSG* replacement at the expression site. At chronic stages in the infection, complex gene conversion can result in the expression of chimeric or mosaic *VSG*s. Complex gene conversion makes use of the many *VSG* pseudogenes, which are otherwise non-functional.

In addition to antigenic variation, clearance of bound antibody from the cell surface is important for immune evasion. Bloodstream form parasites appear to remove bound antibody though a combination of directional cell motility and high rates of membrane recycling. Directional cell motility is important for generating forces involved in selectively trafficking VSG/antibody complexes to the cell posterior and flagellar pocket where endocytosis occurs, a process referred to as hydrodynamic sorting (Engstler et al., 2007). Further, as discussed above (Section 1.4.1), *T. b. rhodesiense* is largely resistant to the effects of host Apo-LI as a result of expression of the SRA protein. This protein is a truncated form of VSG and can bind to apolipoprotein L-I in early endocytic vesicles, and this prevents apolipoprotein L-I activation, thus protecting the parasite (reviewed in (Wheeler, 2010)).These immune evasion strategies allow the

parasites to survive in the mammalian host for long periods, during which time parasites can enter a multitude of different organs including the central nervous system, producing the typical symptoms associated with Trypanosomiasis.

Bloodstream form parasites (slender form) can proliferate rapidly in the mammalian host due to the abundant supply of nutrients, and glucose can passively enter the cytoplasm and subsequently the spherical glycosomes where the majority of glycolysis takes place (Vickerman, 1965). The mitochondrion of bloodstream form cells is tubular, lacks cristae and most Krebs cycle enzymes, and is incapable of oxidative phosphorylation. One of the functions of the mitochondrion in bloodstream form parasites is to oxidise glycerol-3-phosphate and therefore quell the excess of reducing power generated by glycolysis. This occurs at the inner mitochondrial membrane where glycerol-3-phosphate oxidase is located (Hannaert et al., 2003b). Bloodstream form slender parasites can differentiate to stumpy form parasites during periods of high parasitaemia. Differentiation is density dependent and is thought to initiate in response to an unidentified 'stumpy induction factor'. The mechanism of differentiation involves asymmetric cell division of slender parasites, resulting in shorter daughter flagellum extension in the daughter cell; after cell division, both daughter cells becomes committed to differentiation (Tyler et al., 2001b). Cells that are undergoing differentiation are called intermediate forms, which undergo dramatic changes to the mitochondrial morphology. The tubular mitochondria become swollen and develop cristae, and also contain enzymes associated with amino acid-based metabolism. These changes represent preadaptations to the tsetse fly environment (Vickerman, 1985). Stumpy form parasites do not undergo VSG switching, which leaves them vulnerable to attack by host antibodies. However, increased pinocyctosis (and the ability to clear antibodies by hydrodynamic sorting), lysosomal activity and cholesterol content of the surface membrane (and therefore greater rigidity) can help compensate for this weakness.

Molecular regulation of slender form differentiation is known to involve the PX-FVYVE family zinc finger kinase (ZFK), and the mitogen-activated protein kinase family member TbMAPK5 (Pfister et al., 2006;Vassella et al., 2001). Stumpy form parasites are prevented from differentiating further, into procyclic form cells by the activity of the tyrosine phosphatase TbPTP1 (Szoor et al., 2006), and one

target of TbPTP1 has recently been identified as the DxDxT phosphatase, TbPIP39 (Szoor et al., 2010). In the absence of TbPTP1, TbPIP39 exhibits increased phosphorylation (transferred by an unknown kinase), enabling it to accumulate in the glycosomes from where it can promote a differentiation response. A preadaptation to stumpy differentiation in the tsetse fly is the expression of the surface transporter proteins, Protein Associated with Differentiation proteins PAD1 and PAD2 (Dean et al., 2009). PAD1 is found on the cell surface at the stumpy form cells, and thus acts as a molecular marker for this life cycle stage. When stumpy form parasites are taken up by the tsetse fly, and enter the tsetse fly midgut, they experience both a drop in temperature, and change in chemical environment. Citrate and cis-aconitate (CCA) have long been known to trigger the differentiation of stumpy parasites, although the levels required *in vitro* were much higher than those present in a tsetse fly environment (reviewed in (MacGregor and Matthews, 2010)). A decrease in temperature however can increase sensitivity to CCA to physiological levels (Engstler and Boshart, 2004), and this hypersensitivity is mediated by both PAD1 and PAD2, the surface translocation of the latter being induced by the decrease in temperature (Dean et al., 2009). These studies imply that the PAD proteins are the environmental sensors in the differentiation response responsible for the transition from stumpy to procyclic form parasites, whose downstream effect is the inactivation of TbPTPI, and the activation and glycosomal localisation of TbPIP39, where possible targets could include regulators of metabolism.

1.6.2 Life cycle stages in the tsetse fly vector

Tsetse flies become infected when they take a blood meal from an infected mammalian host. Ingested stumpy form parasites accumulate in the crop and midgut lumen of the tsetse fly, where they differentiate into procyclic form parasites (Vickerman et al., 1988). The differentiation process is characterised by morphological and metabolic changes, which include increased cell length accompanied by kinetoplast migration, extensive mitochondrial branching and increased mitochondrial volume, increased expression of mitochondrial enzymes and proteins (including Krebs cycle enzymes and respiratory chain proteins), alterated glycosome morphology (from spherical to bacilloform), reduced endocytosis and replacement of the VSG surface coat with procyclins

(EP/GPEET). The changes to mitochondrial morphology and protein/enzyme expression allow metabolism of the amino acid substrate proline which is abundant in the tsetse fly midgut. As the infection of the tsetse fly midgut progresses, parasites move across the peritrophic membrane into the ectoperitrophic space and migrate to the salivary glands via the oesophagus, mouthparts and salivary glands, a route which is necessary to avoid trypanolysis in the haemocoel. During migration, the parasites are cell cycle arrested and experience an increase in length to become mesocyclics. These proventricular mesocyclics no longer express GPEET procyclin on the cell surface. After differentiation, mesocyclics undergo cell division, which involves extension of a short new daughter flagellum, and nuclear migration towards the cell posterior during mitosis, such that the kinetoplasts and nuclei appear to switch position. Asymmetric cell division of these proventricular mesocyclics produces long and short daughters, and the latter are able to differentiate into an epimastigote upon arrival at the salivary gland (Sharma et al., 2007). These short, unattached epimastigotes are believed to represent the sexual stage of the trypanosome life cycle. This evidence was obtained by infecting tsetse flies with parasites expressing either red or green fluorescent protein, and screening infected tsetse flies for yellow hybrids. These hybrids were observed in the tsetse fly salivary glands as unattached short epimastigotes. In addition, genetic markers confirmed genetic exchange had occurred, implying meiosis like mechanisms occur (Gibson et al., 2008).

Epimastigote differentiation involves huge structural changes. Dendritic outgrowths appear at the flagellum (‘flagellipodia’) which wrap around the microvilli of the salivary gland epithelium, and together with newly formed hemidesmosome like junctional complexes facilitate epimastigote adherence (Vickerman et al., 1988). Epimastigotes proliferate whilst remaining attached to the salivary gland epithelium, which is probably facilitated by the more anterior positioning of the basal body and kinetoplast (Vickerman et al., 1988). Epimastigotes express alanine rich surface proteins (BARP) in place of procyclins (Urwyler et al., 2007). Differentiation of epimastigotes to metacyclics occurs at later stages of infection, which involves two intermediate stages before full maturation to metacyclic parastites. These intermediate stages are cell cycle arrested and described as pre- and nascent metacyclics (Vickerman et al., 1988).

These cells display increasingly reduced flagellar outgrowths (but maintain attachment to salivary epithelial cells via junctional complexes), changes to the mitochondrial and glycosomal morphology (mitochondria lose the extensive branching and cristae, and glycosomes become more spherical), and increasing expression of VSG surface protein. There are over 20 metacyclic-specific *VSG* expression sites (Turner et al., 1988), and the expression of metacyclic-specific VSG prior to detachment from the epithelium of the salivary gland prepares the metacyclics for invasion of the mammalian host (Tetley et al., 1987).

1.7 The basic structure of the *T. brucei* cell

The structure of the cytoskeleton and associated cytoskeletal organelles (Figure 1-2) are described in detail in Chapter 2. Briefly, the shape of the *T. brucei* cell is defined by the subpellicular microtubule corset. Covering the cytoskeleton is a membrane coated with antigenic surface proteins, and at the posterior end of the cell this features a region of endo and exocytosis (Overath and Engstler, 2004), which is referred to as the flagellar pocket, as a result of also being the site for the emergence of the single flagellum. The flagellum extends from the mature basal body, which is associated with an immature or probasal body, and adheres to the cell body via junctional complexes collectively referred to as the flagellum attachment zone (Vaughan et al., 2008). A single mitochondrion runs along the length of the cell body, and the mitochondrial DNA is contained in a single organelle called the kinetoplast, found at the posterior end of the mitochondrion. The kinetoplast DNA is composed of catenated maxi and minicircles (Klingbeil and Englund, 2004), the latter encoding guide RNAs which are essential for the unique form of kinetoplast RNA editing. The kinetoplast and basal bodies are connected by a set of filaments at a differentiated region of the mitochondrial membrane referred to as the tripartite attachment complex (Ogbadoyi et al., 2003). The region between the flagellar pocket and single nucleus is a major site for vesicle trafficking, and also contains the single lysosome, where protein degradation occurs (reviewed in (Field and Carrington, 2004)). The single Golgi stack can also be found within this posterior region. The many glycosomes are distributed throughout the cytoplasm and represent the locations for compartmentalised metabolic processes.

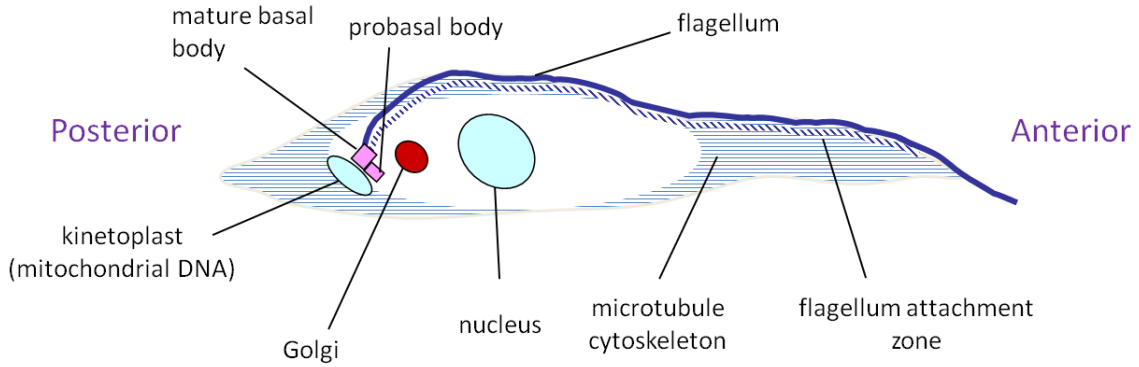

Figure 1-2 -The basic structure of the *T. brucei* cell.
A simplified cartoon of the *T. brucei* cell adapted with permission from Tansy Hammarton.

Cell division in *T. brucei* features requires faithful replication and segregation of its single copy organelles (Figure 1-2 and Figure 1-3) in order to generate viable progeny. The timing of cell cycle events varies according to life cycle stage, and in general, the cell cycle duration in bloodstream and procyclic form parasites lasts around 6 or 8.5 hours, respectively (Tyler et al., 2001a;Sherwin and Gull, 1989a). Early cell cycle events include maturation of the probasal body and assembly of the new flagellum at the newly matured basal body, which is accompanied by basal body duplication to form two new probasal bodies(Lacomble et al., 2010;Sherwin and Gull, 1989a). Golgi duplication also occurs at the beginning of the cell cycle, commencing just after basal body duplication, and involving the *de novo* appearance of a new Golgi close to the endoplasmic reticulum exit site and partially derived from the old Golgi (He et al., 2004). Replication of the subpellicular corset occurs in a semi-conservative manner throughout the cell cycle (Sherwin and Gull, 1989b). Nuclear and kinetoplast replication cycles are independent, and kinetoplast replication occurs earlier, and lasts for a shorter duration (Woodward and Gull, 1990). Kinetoplast segregation is followed by branching of the mitochondrion, although the final detachment of the duplicated mitochondria occurs after mitosis is completed (Tyler et al., 2001b). Mitosis in procyclic form cells is accompanied by migration of the nucleus towards the anterior end of the cell, between the recently segregated basal body and associated kinetoplast (Robinson et al., 1995), producing a linear arrangement of organelles described as ‘KNKN’ (where K and N refer to kinetoplasts and nuclei, and the order is taken from posterior to

anterior). Basal body segregation in bloodstream form cells is not so extensive, and the result is a 'KKNN' organelle configuration (Tyler et al., 2001b).

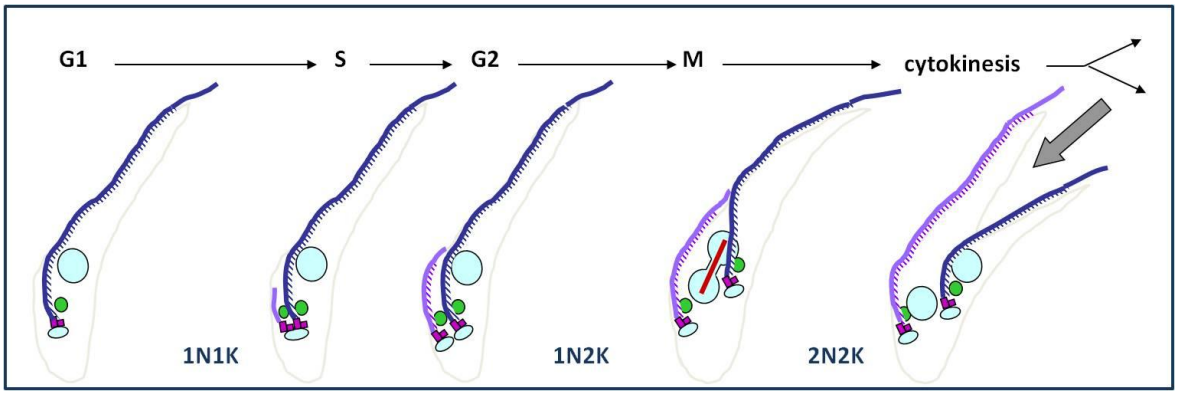

Figure 1-3 –The order of major events in the *T. brucei* cell cycle.
Organelle replication and positioning during the cell cycle is shown for a procyclic form cell. The cell cycle stage (top; G1/G2: gap phases; S: DNA synthesis; M: mitosis), and the number of nuclei (N) and kinetoplasts (K) at different cell cycle stages (bottom) are indicated. The nuclei and kinetoplasts are shown in light blue, basal bodies in pink, Golgi in green, flagella and flagellum attachment zones in purple (the new flagellum and flagellum attachment zone are in the lighter purple), and spindle in red. The grey arrow indicates the direction of furrow ingression. Adapted with permission from Tansy Hammarton.

The equal distribution of organelles between daughter cells at cytokinesis involves the lateral ingression of a furrow, which proceeds until daughter cells remain attached at their posterior ends (Figure 1-4). The final event in cytokinesis is referred to as abscission, and describes the detachment of these nascent daughters into separate cells (reviewed in(Hammarton, 2007)).

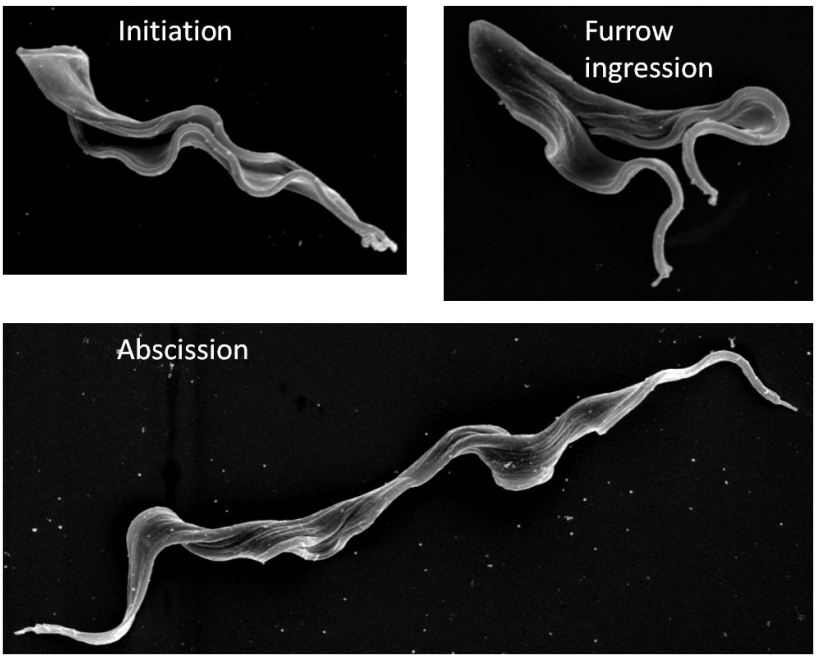

Figure 1-4 -The three stages of cytokinesis in *T. brucei*.
Scanning electron microscope images showing bloodstream form *T. brucei* parasites at the three stages of cytokinesis.

1.8 Tools for studying the cell cycle in *T. brucei*

1.8.1 Assessing cell cycle stage

Cell cycle stage in *T. brucei* can be broadly assessed through classification of cells according to DNA content. This can be achieved through the application of 4',6-diamidino-2-phenylindole (DAPI) stain, which can penetrate both the nucleus (N) and kinetoplast (K), and bind to DNA. Excitation of DAPI stain with ultraviolet light leads to the emission of blue fluorescence. Due to the staggered timing of kinetoplast and nuclear replication cycles, 1N1K, 1N2K and 2N2K categories are taken to represent cells at G1 or S, G2 or M, or post-mitotic stages of the cell cycle, respectively (illustrated in Figure 1-3). To distinguish cells undergoing S phase, cells can be treated with 5'-bromodeoxyuridine (BrdU), a synthetic nucleoside and thymidine analogue which can substitute for thymidine during DNA replication. Detection of BrdU by immunofluorescence can be used to distinguish whether 1N1K cells are at the G1 or S stage of the cell cycle. Flow cytometry is a useful tool for assessing the ploidy of whole populations of cells. Propidium iodide staining of the DNA in individual cells followed by determination of whole cell fluorescence using a laser based detection system ensures a high frequency of measurements is obtained (e.g. 10000 cells per sample), allowing comparison of the proportions of cells at G1, S and G2/M stages of the cell cycle across different samples. This is a useful tool for detecting cell cycle problems, as cells with abnormal ploidy due to abnormal cell division or inhibition of cytokinesis will exhibit abnormal levels of fluorescence.

1.8.2 Determining subcellular localisation

In order to study the function of a protein, it is very useful to be able to localise the protein by immunofluorescence. Where an antibody is unavailable, genetic manipulation can be carried out in order to add an epitope tag or fluorescent protein to the N or C terminus and the latter method has become increasingly popular (Shaner et al., 2007). Green fluorescent protein was originally isolated from the jellyfish *Aequorea Victoria*, and subsequent modifications have given rise to blue, cyan and yellow derivatives; additionally, proteins are available

that emit fluorescence from the other end of the spectrum including red fluorescent protein from non-bioluminescent reef coral.

For some proteins it is necessary to use an inducible expression system, as near endogenous levels of the protein may be difficult to detect. Inducible expression enables selection of genetically modified parasites without the need to express a potentially toxic gene product, and a tetracycline-inducible expression system has been developed for trypanosomes(Biebinger et al., 1997;Wirtz and Clayton, 1995). Tetracycline inducible gene expression utilises the tet operator and the tetracycline repressor (*TetR*) gene from the prokaryotic transposon Tn10 (Hillen and Berens, 1994). TetR is a DNA binding protein which inhibits expression of genes situated downstream from the tet operator. TetR is extremely sensitive to small amounts of tetracycline-Mg^{2+}, which cause conformational changes preventing further interaction with the tet operator, allowing transcription of downstream genes. Trypanosome cell lines expressing constitutive levels of TetR can be used in conjunction with expression vectors featuring the desired epitope tagged protein under the control of a modified promoter (for example, the procyclin acidic repetitive protein (PARP) promoter) containing tetracycline operator sites. Expression vectors also contain a selectable marker (antibiotic resistance gene) under the control of an alternative, constitutively regulated promoter (commonly the *VSG* promoter) to allow selection of genetically modified parasites. The expression vector is designed to integrate at a transcriptionally silent region, for example the ribosomal DNA locus to minimise the possibility for unregulated gene expression.

However, to study the localisation of cell cycle regulators, it may be preferable to express them at near to endogenous levels, as these proteins are often toxic in large amounts. In addition, it is also desirable to minimise the possibility of binding site saturation to avoid misinterpreting the localisation of the protein. A series of plasmid constructs for N- or C-terminal tagging of the protein of interest with a variety of epitope and fluorescent protein tags have been developed and allow expression from the endogenous locus (Kelly et al., 2007;Alsford et al., 2005;Alsford and Horn, 2008). The level of expression achieved is likely to be near to but not equivalent to endogenous levels, since either the 5` or 3` UTR is disrupted by integration of the expression construct.

However, N-terminal tagging is believed to be less disruptive to gene expression in comparison to C-terminal tagging (Clayton, 2002).

1.8.3 Cell cycle synchronisation

In asynchronous trypanosome cultures, a large proportion of cells are at the G1 and S phases of the cell cycle, making it difficult to characterise large numbers of cells that are undergoing mitosis or cytokinesis. Recently, methods of cell synchronisation using hydroxyurea have been adapted for use with *T. brucei* cultures (Chowdhury et al., 2007;Forsythe et al., 2009). Treatment of cells with hydroxyurea stalls DNA synthesis through inhibition of ribonucleotide reductase, and subsequently depletion of dNTPs. This can be lethal to the parasites at high concentrations; however, through optimisations of the concentration and duration of treatment it is now possible to stall cells of both life cycle stages reversibly at S phase. Synchronisation is extremely useful for investigating proteins which have a dynamic localisation and/or expression pattern in the cell cycle, which is a common feature of cell cycle regulators, although it must always be borne in mind that any chemical treatment of cells may cause off-target effects. Alternative Fluorescence Associated Cell Sorting (FACS) approaches, which may help to alleviate this issue, have been described using Vybrant DyeCycle Orange and Vybrant DyeCycle Violet for procyclic and bloodstream form cells, respectively (Siegel et al., 2008;Kabani et al., 2010).

1.8.4 Gene knock out and RNA interference

Studying the function of a protein traditionally involves the generation of knock out cell lines. Knock out cell lines can be generated through targeted gene replacement of both alleles for single copy genes. However, this is not a useful method for investigating the function of cell cycle regulators, which are likely to be essential. As an alternative, the tetracycline inducible system can be used to generate conditional null mutants, whereby exogenous expression of the target gene can compensate for the loss of endogeous expression during selection. Additionally, dominant negative cell lines (generated, for example, by the inducible ectopic expression of an inactive (dead) mutant enzyme) may be useful for characterising protein function. However, following the discovery of a

functional RNA interference (RNAi) pathway in *T. brucei*, faster and simpler methods for generating a knock down phenotype are possible. RNAi is an evolutionarily conserved mechanism believed to have originated as a defence mechanism against transposable elements or viruses, and has also been shown to be a means of post-transcriptional gene regulation (reviewed in (Cerutti and Casas-Mollano, 2006). RNAi mediated gene silencing involves recognition and cleavage of double stranded RNA (dsRNA) by a dicer endoRNase into small 21-26 nucleotide fragments known as silencing RNAs (siRNAs). These small fragments are subsequently recognised and loaded onto a protein complex called RISC, which is activated by removal of one of the siRNA strands allowing the remaining siRNA strand to act as a guide for another endo-RNAse known as Slicer. Slicer subsequently identifies and selectively degrades corresponding mRNAs. Two Dicer nucleases and one Slicer nuclease have been shown to be involved in the *T. brucei* RNAi pathway (Durand-Dubief and Bastin, 2003;Patrick et al., 2009). While dsRNA can be transfected into *T. brucei* to transiently knock down the gene of interest, stable RNAi lines require the integration of an RNAi plasmid into the genome, allowing the inducible expression of dsRNA. The RNAi plasmid can either be a stem-loop plasmid where two identical inverted fragments of the desired gene are separated by an irrelevant 'stuffer' sequence and expressed via a tetracycline-inducible promoter (Shi et al., 2000a), or can feature two opposing tetracycline-inducible T7 promoters either side of a fragment of the gene of interest (LaCount et al., 2000), which are expressed by integrating this RNAi plasmid into a *T. brucei* cell line constitutively expressing T7 polymerase and TetR (Wirtz et al., 1999).

1.9 The cell cycle

Cell replication involves growth, organelle replication and segregation, and distribution of organelles and cytoplasm between daughter cells. These processes are typically carried out in a precise order, which is determined by the activity of key regulatory proteins including cyclins, and cyclin-dependent kinases or CDKs (reviewed in (Hochegger et al., 2008)). CDKs are generally expressed throughout the cell cycle, but only become active once bound by a cyclin partner. Cyclin interaction also acts to target the CDK to appropriate substrates. Control of CDK activity is further exerted through activatory or

inhibitory phosphorylations, and through interaction with inhibitory proteins (which cause conformational change at the CDK active site). Cyclin abundance is regulated through transcriptional control, and through ubiquitylation and proteolysis.

The cell cycle stages in order are referred to as G1, S, G2, M, and cytokinesis, where G1 and G2 describe 'gap' phases, where cell growth may occur, S describes the DNA synthesis phase and M refers to mitosis (nuclear division). Cytokinesis is typically defined as the division of cytoplasm. To ensure that cell cycle processes only occur under favourable conditions, environmental and internal signals influence the relative abundance, localisation and activity of cyclin/CDK complexes, and only when a threshold level of activity is breached can the cell cycle proceed. These checkpoints control the timing of major cell cycle transitions, and are vital for ensuring the viability of daughter cells. If conditions are not favourable for growth, or upon differentiation, cells can enter a quiescent stage known as G0. This quiescent state is irreversible for some cell types, but for others sufficient mitogenic signals can cause re-entry to the cell cycle at G1.

In addition to the general cell cycle stage descriptors, mitosis can itself be divided into different stages. These stages refer to the major mitotic events including: chromosome condensation and spindle assembly (prophase), chromosome attachment to the spindle (prometaphase), chromosome alignment (metaphase), chromosome segregation (anaphase), and finally chromosome decondensation (telophase). Spindle generation requires the duplication and maturation of the centrosome, a complex containing γ-tubulin which can nucleate microtubule polymerisation and regulate microtubule dynamics. The spindle is unstable and highly dynamic. Located at the growing ends of microtubules are microtubule-associated proteins which interact with centromeric chromatin to 'capture' chromosomes, mediating their attachment at regions called kinetochores. Sister chromatids are held attached to each other until anaphase by protein complexes called cohesins. At anaphase, the activity of the conserved cell cycle regulatory complex called the 'anaphase-promoting complex' (APC), which ubiquitylates cell cycle regulators, targeting them for degradation by the proteosome, results in the activation of separase. Separase

cleaves a component of the cohesins allowing sister chromatids to separate, a process that is facilitated by forces generated by mitotic spindle dynamics.

In mammalian cells, cytokinesis is included as a sixth stage of mitosis, since mitosis in these cells involves the breakdown of the nuclear envelope, and the spindle therefore bisects the whole cell during cytokinesis where it is well placed to direct cleavage plane positioning, assembly of the cleavage apparatus (an actomyosin contractile ring) and vesicle targeting during abscission. Specialised regions of the spindle known as the spindle midzone and the mid-body are important for early and late cytokinesis mechanisms, respectively. The 'chromosomal passenger complex' (CPC) describes proteins which localise to centromeres and then relocate to the spindle midzone. The CPC is vital for maintenance of the spindle midzone and for regulation of important cytokinesis events.

1.9.1 Cell cycle regulation in T. brucei

T. brucei possesses several conserved homologues of cyclins (CYCs) and CDKs termed cdc2-related kinases (CRKs); these include CRK1-4, CRK6-12 and CYC2-11. The CYC/CRK complexes which have been identified involve CRK3 which can bind to CYC2 and CYC6 (Hammarton et al., 2003;Van Hellemond et al., 2000), and there is also some evidence to suggest that CRK1 and CRK2 can interact with CYC2 (Gourguechon et al., 2007). However the latter evidence is debatable, since it came from *in vitro* data only and a previous *in vivo* study was not able to demonstrate these interactions (Van Hellemond et al., 2000).

RNAi has been used extensively to investigate the roles of these putative cell cycle regulators in trypanosomes, and these studies revealed that regulation of the G1/S transition involves CRK1, CYC2 and possibly also CYC4 (Hammarton et al., 2004;Li and Wang, 2003). RNAi of *CRK2*, *CRK4* and *CRK6* independently had no effect on the cell cycle; however, when these kinases were depleted simultaneously with *CRK1*, they seemed to accentuate the effect of CRK1 on the G1/S transition, suggesting that they may have accessory roles at this cell cycle stage(Tu and Wang, 2005). RNAi studies have also revealed regulators of the G2 and M phases, which were shown to include CRK3 and CYC6 (Hammarton et al., 2003; Li and Wang, 2003; Tu and Wang, 2004) and CRK9 (Gourguechon and

Wang, 2009). These experiments revealed differences in cell cycle checkpoints between bloodstream form and procyclic form parasites. Pairwise knockdown of *CRK1* and *CRK2* blocked DNA synthesis in procyclic but not bloodstream form cells, implying differences in regulation of the G1/S transition (Tu and Wang, 2005a). Additionally, while *CYC6* downregulation inhibited mitosis in both bloodstream and procyclic trypanosomes, this only prevented cytokinesis in bloodstream form parasites, suggesting that procyclic form cells lack a mitotic exit checkpoint (Hammarton et al., 2003).

1.9.1.1 Mitosis

The *T. brucei* genome consists of 11 diploid pairs of megabase chromosomes, 1-5 intermediate chromosomes, and around 100 minichromosomes of uncertain ploidy (Gottesdiener et al., 1990; Melville et al., 1998). The megabase chromosomes encode the housekeeping genes, and the smaller chromosomes are thought to function largely as a reservoir for *VSG* genes. Organisation of genetic material requires association with histone proteins. *T. brucei* possesses four canonical histones (H2A, H2B, H3 and H4), four variant histones (H2Az, H2Bz, H3v and H4v) and one divergent H1 linker histone (reviewed in (Figueiredo et al., 2009)). Post-translational modification of histone proteins is important for transcriptional activation, chromatin organisation, and signalling for DNA repair. Histone modifications observed in *T. brucei* include acetylation and methylation and these modifications are important for mitotic progression (Ingram and Horn, 2002; Janzen et al., 2006; Kawahara et al., 2008). Unusually, chromosome condensation has not been observed in *T. brucei* (Galanti et al., 1998), and nuclear membrane disintegration does not occur (Ogbadoyi et al., 2000) during mitosis. The formation of the mitotic spindle therefore occurs inside the nuclear membrane. Spindle generation does not appear to involve typical microtubule organising centres (centrioles), and spindle nucleation sites can be observed by transmission electron microscopy as small fibrous ring shaped structures found close to the nuclear envelope with emergent microtubules (Ogbadoyi et al., 2000). Nucleation of spindle microtubules requires γ-tubulin, which localises in late mitotic cells to either end of the spindle poles as two punctate dots (Scott et al., 1997), and depletion of γ-tubulin prevents spindle formation and mitosis (McKean et al., 2003). Molecular regulation of spindle formation involves proteins of the *T. brucei* chromosomal passenger complex (CPC), which include

Aurora kinase 1 (AUK1), CPC1, and CPC2, and also proteins which interact with this complex, including Tousled-like kinase 1 (TLK1), Kinesin A (KINA) and Kinesin B (KINB). These proteins were shown to localise to the nucleus and spindle (including the spindle midzone (AUK1, KINA and B, and CPC1 and 2) and spindle poles (TLK1)), and downregulation of any of these proteins in procyclic or bloodstream form parasites inhibited mitosis (Li et al., 2007; Li et al., 2008a; Li and Wang, 2006; Li et al., 2008b; Tu et al., 2006). Analysis of the nuclei in procyclic form cells in which either CPC components or CPC interacting proteins had been depleted, revealed a lack of spindle formation (Li et al., 2007; Li et al., 2008a; Tu et al., 2006) which was also observed following the depletion of AUK1 in bloodstream form cells (Li et al., 2009). Therefore, despite the lack of a canonical microtubule organising centre, the roles of γ-tubulin and an Aurora kinase (AUK1) in spindle generation at least are conserved in *T. brucei*. The attachment of spindle microtubules to chromosomes, and their segregation at anaphase, however, occurs in an unusual and divergent manner.

The components of the *T. brucei* kinetochore have not yet been identified, although kinetochore-like structures have been observed as electron dense laminated plaques penetrated by up to four microtubules (Ogbadoyi et al., 2000), and interestingly, these seem to undergo changes during mitosis, whereby a new, opaque layer forms prior to chromatid separation. However, only 100 spindle microtubules, and eight kinetochore-like structures have been observed, which does not correspond to the total number required to segregate all *T. brucei* chromosomes with one kinetochore and two spindle microtubules attached to each. Additionally, segregation of megabase chromosomes and minchromosomes were shown by fluorescent *in situ* hybridisation to have different dynamics (Ersfeld et al., 1998), suggesting that anaphase mechanisms for different chromosomes vary. Megabase chromosomes but not smaller chromosomes possess sites of enriched Topoisomerase II activity (Obado et al., 2007), which localise to strand switch regions where the DNA sequence is repetitive (these regions represent points at which transcription of polycistronic mRNA changes to the opposite strand). Topoisomerase II is required for decatenation of DNA which is important for separation of sister chromatids at the centromeric regions of chromosomes. Differences in the separation kinetics of megabase and smaller chromosomes and the small numbers of spindle

microtubules and kinetochores observed suggested that megabase chromosomes probably segregate via classical mechanisms, but smaller chromosomes use different means of segregation. It has been proposed that intermediate and minichromomes segregate through association with antiparallel microtubules and that interaction with motor proteins directed towards the negative ends of microtubules would propel the sister chromatids to opposite spindle poles (Gull et al., 1998).

The mechanisms by which chromosomes interact with the mitotic spindle are not understood, since a centromere specific histone protein has not yet been identified in *T. brucei*, and the only potential candidate (H3v) was found to be dispensable for cell viability and moreover was found to associate with minichromomes rather than megabase chromosomes (Lowell and Cross, 2004). Post-translational modifications of histones may play roles in signalling during mitosis, as inferred from the sudden appearance of dimethylated histone H3 at the onset of mitosis, and its disappearance at G1 (Janzen et al., 2006). Intriguingly, investigations into the role of histone modifications revealed that bloodstream form *T. brucei* parasites do not possess a checkpoint to ensure that only replicated chromosomes are segregated during anaphase. Reduced methylation of histone H3 or reduced acetylation of histone H4 resulted in the appearance of 1N1K cells with a 1C DNA content, or 2N2K cells with a 2C DNA content, respectively, providing evidence that anaphase occurred in the absence of DNA synthesis (Janzen et al., 2006; Kawahara et al., 2008).

Despite *T. brucei* possessing divergent mechanisms for chromosome segregation, the attachment of sister chromatids is believed to involve conserved SMC complexes, and components of cohesin and condensin complexes have been identified (Gluenz et al., 2008). Depletion of SCC1 (a homologue of α-kleisin in the cohesin complex) led to mitotic arrest during metaphase (inferred from the presence of kinetochores in abnormal nuclei) in both procyclic and bloodstream form parasites. Mutation of a conserved cleavage site (targeted by separase to trigger chromatid separation) caused a similar mitotic arrest; implying conserved upstream mechanisms for anaphase regulation are functional in *T. brucei*. Seven core components of the APC are conserved in *T. brucei* and two components, APC1 and CDC27 have essential roles in mitotic progression (Kumar and Wang, 2005). In procyclic form parasites, depletion of either of these proteins led to a

metaphase arrest (as judged from the spindle morphology), suggesting a conserved mechanism of anaphase initiation, although in bloodstream form parasites, mitosis was arrested at a later stage implying that other regulators or the combined action of multiple APC components control anaphase initiation at this life cycle stage.

Spindle dynamics are important for anaphase, and it is not known how spindle dynamics are regulated in *T. brucei*. One hypothesis is that microtubule severing enzymes could stimulate catastrophe events, contributing to the rapid collapse and extension associated with spindle behaviour. *T. brucei* possesses homologues of the microtubule severing enzymes fidgetin and spastin (Casanova et al., 2009). Spastin (with the addition of either an N- or C-terminal GFP tag) was found to localise at the nucleus and more specifically, to discrete foci at perinucleolar regions (in procyclic form cells), and these cells additionally displayed abnormal nuclear morphology. Despite the intriguing localisation exhibited by spastin, overexpression or depletion of spastin had no effect on mitosis in procyclic form parasites; similarly no mitotic defects were observed following the overexpression or depletion of fidgetin in procyclic form cells.

Mitosis requires the coordination of many diverse proteins, which can involve enzymes other than the kinases traditionally thought of as 'master regulators' (e.g. AUK1); for example, PRMT6 (a methyltransferase), and ubiquitin-like modifier SUMO (involved in SUMOylation, a type of reversible modification involving covalent attachment of SUMO to target proteins in coordination with activating and conjugating enzymes). Depletion of either protein led to mitotic arrest in procyclic form parasites (Fisk et al., 2010; Liao et al., 2010), and binding partners of PRTM6 included nuclear pore proteins and histones, indicating that methylation could influence trafficking into the nucleus during mitosis (Fisk et al., 2010). Coordination of signalling pathways in mitosis may require scaffold proteins, which are molecular chaperones capable of interacting with multiple and diverse binding partners. 14-3-3 proteins are important for a wide range of processes in mammalian cells, plants and yeast, including cell cycle regulation. *T. brucei* possess two 14-3-3 homologues, 14-3-3 I and 14-3-3 II, both of which were localised to the cytoplasm, and downregulation of either protein affected cell cycle progression (Inoue et al., 2005). Further, downregulation of 14-3-3 I (but not 14-3-3- II) caused inhibition of mitosis. The

binding partners of these proteins are not known, and although it was suggested that protein phosphatase 1 could be a potential candidate, no interaction with this protein could be determined.

1.9.1.2 Cytokinesis

Mitosis is succeeded by cytokinesis, and the transition from mitosis to cytokinesis has been shown to involve the *T. brucei* CPC (comprising AUK1, CPC1 and CPC2). TLK1, KINA and KINB are necessary for the translocation of the CPC components to the anterior tip of the nascent daughter cell, which is the site of furrow initiation. During furrow ingression, this novel complex migrates along the furrow apex (Li et al., 2008b). Depletion of either the components of the CPC, TLK1, KINA or KINB inhibited cytokinesis in both procyclic and bloodstream parasites (Li et al., 2007; Li et al., 2008a; Li et al., 2008b). The effect of CPC depletion on cytokinesis was found not to be a downstream effect of mitotic block. This was demonstrated through the application of an AUK1 inhibitor to hydroxyurea-synchronised procyclic form parasites. Treatment of parasites with the AUK1 inhibitor 3 hours after release from S-phase allowed these parasites to complete mitosis, but inhibited migration of the CPC to the site of furrow initiation, preventing cytokinesis (Li et al., 2009). This implied that the CPC can independently regulate mitosis and cytokinesis, although phenotypes obtained with synchronised and drug-treated parasites must be interpreted with caution.

Mitotic constraints on the regulatory mechanisms associated with cytokinesis vary according to life cycle stage. Completion of mitosis is not required for cytokinesis in procyclic form parasites, even though this results in the generation of anucleate daughter cells (Hammarton et al., 2003; Ploubidou et al., 1999). By contrast, inhibition of mitosis was shown to prevent cytokinesis in bloodstream form cells (Hammarton et al., 2003). This apparent dissociation of mitotic exit from cytokinesis in procyclic form parasites is highly unusual. In yeasts, the mitotic exit network (*S. cerevisiae*) and septation initiation network (*S. pombe*) are important for both mitotic exit, and for mitotic exit-independent regulation of cytokinesis, and therefore, these pathways link these important cell cycle events. A description of how this occurs is given below.

1.9.1.2.1 Regulation of mitotic exit and cytokinesis in yeast

SIN and MEN involve the yeast orthologues of polo-like kinase (PLK), Mps One Binder 1 (MOB1) and nuclear DBF1-related (NDR) kinases. Both of these pathways are initiated by GTPase activity at spindle poles, resulting in activation of a kinase cascade and culminating in the activation of MOB1/NDR kinase complexes (reviewed in (Balasubramanian et al., 2004; Bardin and Amon, 2001; Wolfe and Gould, 2005)). NDR/MOB1 activation leads to phosphorylation of Cdc14 (Clp1 in *S. pombe*) causing this phosphatase to be retained in the cytoplasm, ultimately leading to mitotic exit. The NDR/MOB1-mediated cytoplasmic retention of Cdc14 occurs through different mechanisms in *S. pombe* and *S. cerevisiae*. Phosphorylation occurs at residues adjacent to the nuclear localisation signal of Cdc14 and phosphorylated Cdc14 which exits the nucleus is not able to re-enter (Mohl et al., 2009), while Clp1 is phosphorylated at a binding site for the 14-3-3 scaffold protein Rad24, and the Clp1 which exits the nucleus is sequestrated in the cytoplasm through interaction with Rad24 (Chen et al., 2008; Mohl et al., 2009). In *S. cerevisiae*, the cytoplasmic localisation of Cdc14 is important for the dephosphorylation of Cdh1 and Swi5, proteins which upon dephosphorylation, are able to enter the nucleus, and activate the APC or stimulate the transcription of Sic1 (an inhibitor of the mitotic CDK), respectively. In *S. pombe*, Clp1 has a role in mitotic exit through dephosphorylation of the CDK activating phosphatase Cdc25 (for a review of yeast Cdc14 phosphatases, see (Queralt and Uhlmann, 2008)).

Cytokinesis regulation by both the SIN and MEN pathways involves several components. Cytokinesis regulation by the yeast polo kinase homologues Cdc5 (*S. cerevisiae*) and Plo1 (*S. pombe*), is discussed in Section 7.2. Briefly, Cdc5 is involved in the contraction of the actomyosin contractile ring, through activation of the GTPase Rho1 (Yoshida et al., 2006) and Plo1 is involved in the positioning of the actomyosin contractile ring as a result of its role in the translocation of Mid1 from the nucleus, and in the formation of Mid1 'nodes' at the cell equator prior to mitosis and cytokinesis onset (Bahler et al., 1998). SIN/MEN components other than PLK proteins also have direct roles in cytokinesis. For example, recruitment of Clp1 by Mid1 to the contractile ring is required for dephosphorylation of Cdc15, a protein which contributes to the stability of this ring (Clifford et al., 2008). Further, in *S. cerevisiae*, the MEN pathway was found to be required for translocation of the Inn1, Cyk3 and Chs2

proteins to the bud neck (Meitinger et al., 2010). Chs2 is a chitin synthase involved in chitin deposition at the primary septum (the chitin cell wall), while Inn1 and Cyk3 are part of a complex involved in formation of the primary septum, which initially separates the nascent daughter cells prior to secondary septum deposition.

1.9.1.2.2 The function and localisation of T. brucei orthologues of yeast SIN and MEN proteins

T. brucei PLK, MOB1A and MOB1B, and the NDR kinases, PK50 and PK53, were shown to have direct roles in cytokinesis in bloodstream form parasites (Hammarton et al., 2005; Hammarton et al., 2007; Kumar and Wang, 2006; Ma et al., 2010). Depletion of PK50 led to a rapid increase in post-mitotic cells that had not initiated cytokinesis (Ma et al., 2010), whilst depletion of PK53, PLK or MOB1 proteins caused an increase in post-mitotic cells undergoing furrow ingression (Hammarton et al., 2005; Hammarton et al., 2007; Ma et al., 2010). The roles of PLK and MOB1 proteins have additionally been investigated in procyclic form parasites. Depletion of these proteins at this life cycle stage also affected cytokinesis, but there were differences in the resultant phenotypes compared to the bloodstream form life cycle stage. Depletion of MOB1 proteins did not inhibit furrow ingression, but compromised the accuracy of furrow ingression (Hammarton et al., 2005). PLK depletion inhibited the initiation of cytokinesis, resulting in the generation of multinucleate cells, although basal body replication and kinetoplast segregation were also inhibited following *PLK* depletion, and it was not possible to determine whether inhibition of cytokinesis was a direct result of *PLK* depletion or solely a downstream effect of delayed basal body/kinetoplast segregation (Hammarton et al., 2007). In a separate study, Golgi bilobe (described in Section 2.1.2) and Golgi biogenesis were also found to be affected in procyclic form parasites depleted of PLK (Graffenried et al., 2008). Cells depleted of PLK produced malformed Golgi bilobes associated with an abnormally high number of Golgi. This further suggests that cytokinesis inhibition in these parasites may be a downstream effect of other cell cycle problems.

The localisation of regulatory proteins of the SIN and MEN pathways in yeasts is highly dynamic, involving movement between the spindle poles, spindle midzone and finally the cleavage site (septum or bud neck in *S. pombe* and *S. cerevisiae*,

respectively). The nuclear localisation of these proteins is of fundamental importance to their function in mitotic exit, and intriguingly the *T. brucei* homologues of these proteins do not exhibit nuclear localisation. MOB1 and the NDR kinases exhibit a cytoplasmic pattern of localisation (Hammarton et al., 2005; Ma et al., 2010), while PLK localises to the basal bodies, Golgi bilobe and the flagellum attachment zone (Graffenried et al., 2008; Kumar and Wang, 2006; Umeyama and Wang, 2008). Localisation of PLK to the flagellum attachment zone (FAZ) is cell cycle-related. Appearance of PLK at the posterior end of the FAZ occurs at S phase, and later some PLK co-migrates with the extending FAZ to the mid-dorsal region of the cell. Both signals at the posterior and mid-points of the FAZ disappear at anaphase, when PLK disperses into the cytoplasm and then disappears. Therefore, 1N2K cells display distinctive PLK localisation while 2N2K cells do not appear to express PLK (Li et al., 2010c; Umeyama and Wang, 2008). Interestingly, the CPC is found at a similar location to PLK, but at later stages in the cell cycle, and treatment of synchronised cells with an inhibitor of PLK, or depleting PLK in these cells by RNAi, prevented CPC components from localising to the anterior tip of the cell (Li et al., 2010b). The role of PLK in cytokinesis, and the apparent requirement for PLK in the localisation of the CPC after its disappearance from post-mitotic cells, suggests that PLK can activate the relevant proteins early on in the cell cycle, when it is localised at the FAZ, implying that signals deposited before anaphase can persist until cytokinesis when CPC migration and cytokinesis initiation occur.

1.9.1.2.3 The role of scaffold proteins and checkpoints in T. brucei *cytokinesis*

Localisation is an important factor in regulating the activity of cell cycle regulators, and also for bringing these proteins into contact with other regulators and substrates. Scaffold proteins, which can bind to multiple different binding partners, can integrate different molecular pathways, and one scaffold protein, 14-3-3 II has been shown to have a role in cytokinesis in *T. brucei* procyclic form parasites (Inoue et al., 2005). Cells depleted of 14-3-3 II were inhibited at the stage of cytokinesis initiation, resulting in the accumulation of multinucleated cells. Receptor for activated C- kinase 1 (RACK) is another scaffold protein with multiple signalling roles, and a homologue has been identified *T. brucei* (Rothberg et al., 2006), which was shown to localise to the cytoplasm and perinuclear regions of cells, and was found to be a component of

the translational apparatus through association with eukaryotic translation elongation factor 1a (Regmi et al., 2008). Depletion of TbRACK1 inhibited cytokinesis in both bloodstream and procyclic form cells; procyclic form parasites were unable to complete furrow ingression, whilst bloodstream form cells could not initiate furrow ingression (Rothberg et al., 2006). The furrow arrested procyclic form parasites were capable of reentering the cell cycle, again arresting at furrow ingression, resulting in the accumulation of multinucleate cells with many furrows. Application of an inhibitor of translation (anisomycin) did not have the same effect, although it did act synergistically to increase the number of furrow arrested cells following TbRACK1 depletion in procyclic form parasites (Regmi et al., 2008). These results suggested that the cytokinesis defect was caused by decreased translation of another protein (which was exacerbated further by the translational inhibition by anisomycin), and not due to global inhibition of translation.

The furrow ingression arrest described for procyclic form cells depleted of TbRACK1 (described above) reflects a common theme for the depletion of cytokinesis regulators, whereby furrow ingression appears to be inhibited at a specific point along the cell body (Hammarton et al., 2005; Hammarton et al., 2007; Ma et al., 2010). This may imply the presence of a novel furrow ingression checkpoint in *T. brucei*. Whilst depletion of individual molecular regulators revealed the possibility of checkpoints in furrow ingression, ablation of VSG synthesis or inhibition of mitochondrial fission also produced phenotypes which alluded to the presence of cytokinesis-specific checkpoints. VSG depletion in bloodstream form parasites caused a very specific and unique cell cycle arrest whereby cells accumulated at the pre-cytokinesis stage of the cell cycle; unusually, this post-mitotic arrest was not succeeded by additional rounds of organelle replication implying that this was a very stringent cell cycle arrest (Sheader et al., 2005). Depletion of dynamin and inhibition of mitochondrial fission had a similar effect on the cell cycle, although post-mitotic cells accumulated partway through cytokinesis, but again without subsequent rounds of organelle replication (Chanez et al., 2006). The tight control over the cell cycle exerted by VSG synthesis and mitochondrial fission suggested that there are unique checkpoints associated with very specific processes, and that these are activated at cytokinesis.

In addition to the involvement of molecular regulators in cytokinesis, the cytoskeleton, flagella, and flagellar-associated organelles are important for furrow initiation, ingression and abscission, and the role of these cytoskeletal elements in cytokinesis is discussed in Chapter 2.

2 Review of the trypanosome cytoskeleton, and its role in cell division

2.1 The composition of the trypanosome cytoskeleton

The complexity of the *T. brucei* cytoskeleton creates unique challenges during cell division, and unusual physical mechanisms are employed to ensure accurate daughter cell generation. Although the main component of the cytoskeleton comprises the subpellicular microtubule corset, which encompasses the cell and denotes cell shape, it is generally accepted that the flagellum and associated organelles are also important features (Figure 2-1).

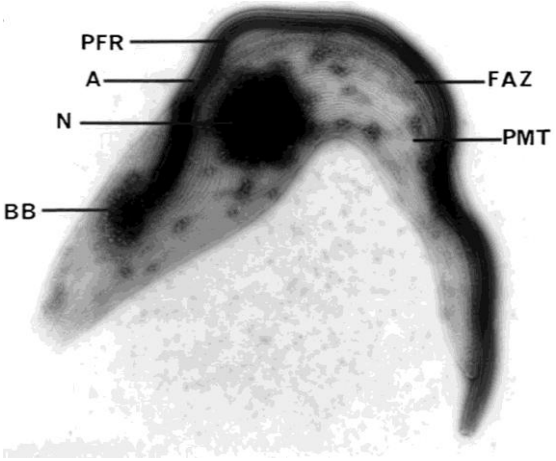

Figure 2-1 -Negatively stained electron microscopic image of a *T. brucei* cytoskeleton obtained by detergent extraction.
The basal bodies (BB), flagellar axoneme (A), paraflagellar rod (PFR), flagellum attachment zone (FAZ), subpellicular microtubules (PMT), and nucleus (N) are indicated. Adapted with permission from (Gull, 1999).

2.1.1 The subpellicular microtubule corset

The subpellicular corset is a tubulin-based structure (Kleinschmidt and Kinder, 1950), and the microtubules are arranged in parallel and form a left handed helix ((Angelopo, 1970); see also Figure 2-6). The corset is extremely stable, and displays resistance to cold and to classical inhibitors of microtubule stability (Macrae and Gull, 1990); in part this stability is conferred by the presence of microtubule-associated proteins (MAPs), which link adjacent microtubules

(Sherwin and Gull, 1989a). Stability is not compromised during growth of the subpellicular corset, as replication occurs in a semi-conservative manner: new microtubules are inserted into the microtubule array between older microtubules (Sherwin and Gull, 1989b). Initiation of a new microtubule occurs at randomly distributed nucleation sites (Scott et al., 1997), where microtubules can grow to varying lengths (Angelopo, 1970). All microtubules of the subpellicular corset have common polarity, and with their plus end extending towards the posterior end of the cell (Robinson et al., 1995). At the extreme posterior end is a small ring-like opening, which may represent a cap, stabilizing positive microtubule ends (Rindisbacher et al., 1993). The corset accommodates two specialised regions: the flagellum attachment zone (FAZ, Figure 2-2) and the flagellar pocket (Figure 2-3). In order for the flagellum to attach along the cell body, a gap exists between two microtubules, wherein lies a filament of relatively unknown composition (Sherwin and Gull, 1989a) and also four microtubules that are associated with membrane of the endoplasmic reticulum (Taylor and Godfrey, 1969). These four specialized microtubules are nucleated near to the basal bodies and exhibit opposite polarity relative to those within the corset. The flagellar pocket is the sole site of endo- and exocytosis, and is an invagination of the pellicular membrane, separated from the corset by an electron dense structure (Sherwin and Gull, 1989a) which is described as the flagellar pocket collar (Bonhivers et al., 2008). These structures are discussed in more detail below.

2.1.1.1 Post-translational modifications of cytoskeletal tubulin

Tubulin within the cytoskeleton is subject to post-translational modifications, which include acetylation, detyrosination and polyglutamylation. Acetylation of α-tubulin at a conserved lysine residue (Woods et al., 1989) is a feature of tubulin in the flagellum and, to a lesser extent, in the subpellicular corset (Schneider et al., 1987). Both α- and ß-tubulin contain a C-terminal tyrosine residue which can be removed and replaced. Detyrosination of α-tubulin (but not ß-tubulin) appears to be a feature of tubulin incorporation into growing microtubules (Sherwin and Gull, 1989b), and as such, is a useful marker for cell cycle events and cell polarity (Sherwin et al., 1987a). Glutamylation of both α- and ß-tubulin (at glutamic acid residues 445 and 435, respectively) is unusually extensive and is observed in both flagellar and subpellicular microtubules

(Schneider et al., 1997). The function of this extensive post-translational modification in *T. brucei* is not known, but it may serve to facilitate binding of MAPs as this has been demonstrated for some major neuronal MAPs (Bonnet et al., 2001).

2.1.2 The flagellar axoneme and associated organelles

The flagellar axoneme of *T. brucei* exhibits the classical '9 + 2' structure of nine outer doublet microtubules and two central single microtubules (Figure 2-2); other conserved features of the axoneme include inner and outer dynein arms, radial spokes, nexin links, and components of a dynein regulatory complex and intraflagellar transport system (Ralston et al., 2009). The flagellum extends from a mature basal body, which comprises nine triplet microtubules that become doublets to form the transition zone. Nucleation of the central pair is initiated at this transition zone at a region termed the basal plate to form the full flagellar axoneme. Incorporation of tubulin into the axoneme seems to involve a process of flagellum-specific quality control at transitional fibres associated with the basal body (Stephan et al., 2007).

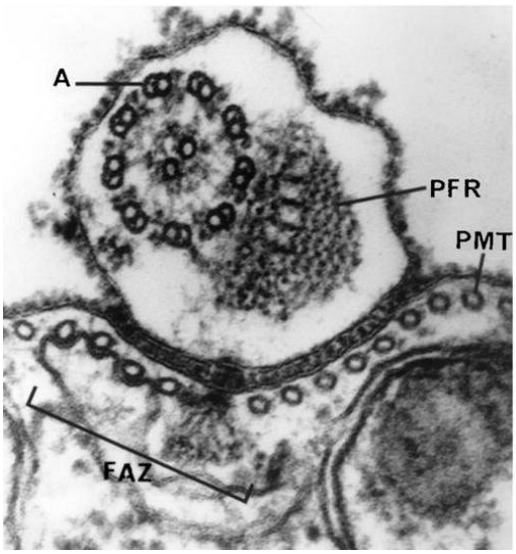

Figure 2-2 -Transverse section through the flagellum of a *T. brucei* cell.
The transmission electron microscopy section shows the flagellar axoneme (A), paraflagellar rod (PFR), subpellicular microtubules (PMT) and flagellum attachment zone (FAZ). The electron dense structure to the right of the microtubule quartet is the FAZ filament, and the membrane in the region of these microtubules is derived from the endoplasmic reticulum but forms part of the FAZ. Reproduced with permission from (Gull, 1999).

T. brucei parasites are highly motile and swim in a corkscrew-like fashion at speeds of up to 20 μm per second (Hutchings et al., 2002). Directionality is achieved by the production of a low amplitude and high frequency tip to base flagellar beat (Absalon et al., 2007a), which is occasionally interspersed with base to tip beating of high amplitude and low frequency, causing 'tumbling' and reorientation of the parasite (Baron et al., 2007a; Hutchings et al., 2002). Recently, bioinformatic (Baron et al., 2007b) and proteomic studies (Broadhead et al., 2006; Portman et al., 2009; Zhou et al., 2010) have identified conserved and novel components of the *T. brucei* flagellum, and there are ongoing studies to investigate the roles of these proteins in this highly complex and unusual mechanism of motility. Adjacent to the flagellar axoneme lies an accessory structure called the paraflagellar rod (PFR) (Vickerman, 1962). This structure has a lattice-like composition and is attached to both the flagellar axoneme (at doublets 4-7) and flagellum attachment zone (Figure 2-2 and Figure 2-3). The lattice has three distinct layers (proximal, intermediate and distal domains) constructed from core components, PFR A and C. Ablation of PFR A causes paralysis (although some abnormal 'twitching' of the flagellum occurs), suggesting a role for the PFR in motility (Bastin et al., 1999; Bastin et al., 2000). Interestingly, recent studies have localized cyclic nucleotide and calcium signalling pathways to the PFR, suggesting an additional role in environmental sensing (Portman and Gull, 2010), and also supporting a more regulatory role in motility (for example, as a phosphotransfer relay, supplying ATP to the distal portions of the flagellum).

The flagellum is attached to the cell body at the FAZ via regularly spaced fibres connecting the FAZ filament to the axoneme and paraflagellar rod (Vickerman, 1969). Adjacent to the FAZ filament lie four specialized microtubules and associated endoplasmic reticular membrane (Figure 2-2). FAZ1 and FLA1 are two proteins that have been shown to be components of the FAZ (LaCount et al., 2002; Vaughan et al., 2008). Trypanin also appears to localize to the FAZ and is required for flagellum attachment as well as acting as a regulator of flagellum motility (Hutchings et al., 2002). In addition to being attached to the cell body, the flagellum is attached via the basal body to the mitochondrial DNA (kDNA), by the tripartite attachment complex (TAC), composed of interstitial and exclusion zone filaments, at the mitochondrial and cytoplasmic faces of a region of

differentiated mitochondrial membrane (Ogbadoyi et al., 2003). Only two components of the TAC have so far been identified: p166, a nuclear encoded protein, and AEP-1, a kinetoplast encoded protein which is expressed from alternatively edited mRNA for cytochrome *c* oxidase III (Ochsenreiter et al., 2008; Zhao et al., 2008). Both p166 and AEP-1 are required for kDNA segregation, and AEP-1, which binds kDNA, has been shown to play a role in the maintainance of kDNA. Therefore the TAC has dual roles, anchoring the kDNA to the basal bodies, and maintaining the integrity and structure of kDNA (Ochsenreiter et al., 2008). Additional structural cohesion within the cytoskeleton is demonstrated by the existence of the 'bilobe' which links the basal body to the Golgi, and marks the site of Golgi assembly (He et al., 2005). Although both Centrin2 and Centrin4 are located at the bilobe, only depletion of Centrin2 was shown to inhibit Golgi assembly (Shi et al., 2008).

In addition to attachment to internal structures, a mobile junction called the flagellar connector (Moreira-Leite et al., 2001) (Figure 2-3) couples the external old and new flagella during procyclic form replication (Briggs et al., 2004), and differentiation to epimastigotes (Sharma et al., 2008). The flagellar connector has a distinctive trilaminar structure with a thicker central core between the two layers abutting the flagella. The overall structure is asymmetric and triangular in appearance. This structure has been implicated as a possible facilitator of the cytotaxis concept (Sonneborn, 1964), as it appears to have roles in both basal body segregation and positioning the elongating daughter flagellum (Absalon et al., 2007a;Absalon et al., 2007a). Growth of the flagella and associated paraflagellar rod utilises a system of intraflagellar transport (Bastin et al., 1999). The transport machinery operates along specific tracks in antero and retrograde directions along axonemal tubules 3-4 and 7-8 (Absalon et al., 2008b). Surprisingly, assembly and motility of the flagellar connector occurs independently of this system (Davidge et al., 2006a).

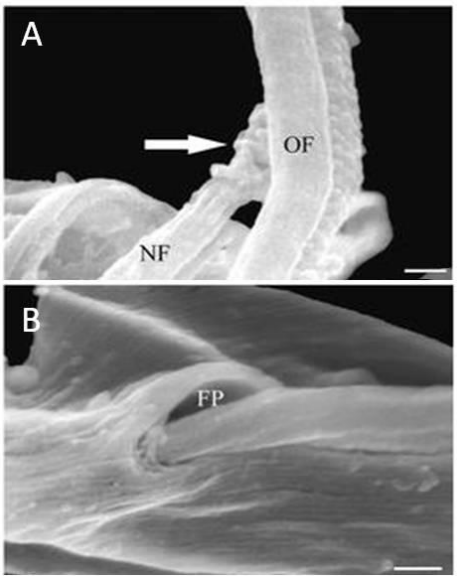

Figure 2-3 -Field emission scanning electron microscope images of *T. brucei* flagellar structures.
A: The new (NF) and old (OF) flagella in a dividing cell. It is possible to distinguish the paraflagellar rod (the lattice-like structure to the right of the old flagellum), and the flagellar connector (arrow) connecting the new and old flagella. B: The helical arrangement of subpellicular microtubules and the flagellar pocket (FP). Scale bars: 1.6 µm (panel A) and 1.8 µm (panel B). Adapted with permission from (Sant'Anna et al., 2005).

The flagellar pocket (Figure 2-3B) itself is not a cytoskeletal structure, but there is evidence that cytoskeletal elements are involved in its replication, positioning and function (Absalon et al., 2008a; Bonhivers et al., 2008), and in defining subdomains within the pocket (Gadelha et al., 2009). The regions within the pocket include the flagellar pocket neck, a constricted site defined by the flagellar pocket collar (FPC), and the lumen, which contains a collarette at the base where the flagellum enters the pocket (Field and Carrington, 2009). Recently, a flagellar pocket channel has also been identified (Lacomble et al., 2009). This is a region adjacent to an individual short subpellicular microtubule and the specialised microtubule quartet, and is thought to function as the main site of endocytosis into the lumen (Gadelha et al., 2009). The horseshoe-shaped FPC is an important structure as it is required for maintaining a barrier between the flagellar pocket lumen and the cell surface membrane (Absalon et al., 2008a). BILBO1 is the first protein found to localise to the FPC (Bonhivers et al., 2008).

2.1.3 Perspectives

The main cytoskeletal components, the subpellicular corset and flagellum (and associated organelles) are tightly associated, forming a cohesive unit, which in

turn, associates with the kinetoplast via the TAC. This structural cohesion dictates that tight orchestration of organelle replication is required during cell division, and implies that novel checkpoints are likely to operate in the regulation of these events. The role of minor cytoskeletal elements in the replication of organelles like the Golgi and flagellar pocket, demonstrates how structural elements can act to define and facilitate the replication of internal structures.

2.2 Timing of cell cycle events

2.2.1 Spatial and temporal analysis of the major cell cycle events

The tight order of cell cycle events in *T. brucei* was evident from detailed morphological analysis of procyclic cells growing as asynchronous cultures (Sherwin and Gull, 1989a). Temporal linkage of major events was carried out by relating generation time to cumulative percentage of cells at different predetermined stages (according to the particular organelle or event in question). To facilitate classification, organelles or structures were labelled with antibodies, DAPI stain and/or BrdU as appropriate. The outcome of these experiments was a timeline of the duration of major events, including nuclear and kinetoplast replication and segregation, basal body replication, and paraflagellar rod elongation. These were described in terms of 'cell cycle units' (Sherwin and Gull, 1989a;Woodward and Gull, 1990). Intriguingly, the kinetoplast and nuclear replication events were temporally independent, with the kinetoplast cycle being of a shorter duration and occurring earlier.

Spatial changes to the *T. brucei* cytoskeleton during the cell cycle have been extensively investigated. It is now known that the cell length increases throughout the cell cycle (from 18.9 ±0.3 to 24.9 ±0.3 μm in procyclic form Lister 427 cells (Robinson et al., 1995)), although the temporal and spatial pattern of microtubule extension varies (Sherwin et al., 1987b). Measurements of relative organelle positions revealed that basal body segregation is associated with cell extension and flagellum elongation. The increase in cell length was similar to maximum inter-basal body distance (Robinson et al., 1995). Intriguingly, flagellum extension rate relative to basal body separation altered at

a particular point, which coincided with an inter-basal body distance of ~2 µm; and a flagellar extension of 0.5 of a cell length (Robinson et al., 1995). This is also the distance at which flagellar connector migration ceases (Absalon et al., 2007a; Davidge et al., 2006b).

With the sequence of the main cell cycle events in place, both temporally and spatially, it is possible to position the replication and segregation of other cytoskeletal features within this framework.

2.2.2 Replication of the basal bodies, Golgi bilobe, tripartite attachment complex and flagellar pocket

At the G1/S transition, basal body maturation occurs. This involves the extension of the probasal body to form the transition zone and basal plate, from where flagellum extension is initiated. The probasal body is positioned anterior to the existing flagellum/basal body, which is counterintuitive, given that the new flagellum is positioned at the posterior end of the cell. This contradiction has recently been resolved through an elegant tomography study, which revealed that during flagellum extension, after invasion of the flagellar pocket and association with the flagellar connector, the basal body and extending flagellum rotates around the old flagellum, a movement involving anticlockwise rotation of the flagellar connector (Lacomble et al., 2010). This rotation positions the new flagellum at the posterior end of the cell. It was suggested that the new microtubule quartet, which is initiated before probasal body maturation, could provide the forces required for this rotational movement as it is closely associated with the basal body, and extends in a helical fashion around the basal body and flagellum before inserting into the subpellicular corset after the rotation has occurred (which would generate forces opposing those produced by extension of the microtubule quartet). Probasal body duplication was shown to precede the rotational event and the duplicated basal bodies were located at anterior positions relative to their respective basal body/flagellum complexes. It was suggested that one reason for the basal body/flagellum complex rotation could be to facilitate segregation of the flagellar pocket membrane, which was shown to involve partitioning of the existing membrane as opposed to *de novo* generation of a separate flagellar pocket. In accordance with this suggestion,

the FPC was formed during the rotation, which would coincide with the proposed membrane segregation.

Basal body replication and kinetoplast S-phase occur at similar times. Kinetoplast S-phase coincides with the replication of the TAC and remodelling of the kDNA/TAC association (Ogbadoyi et al., 2003), and also coincides with the duplication of the Golgi bilobe (He et al., 2005) and growth and duplication of the FPC (Bonhivers et al., 2008). Flagellar pocket segregation is completed by the end of kinetoplast S-phase; however, segregation of the duplicated bilobes occurs later, during basal body segregation.

2.2.3 The replication of the flagellar axoneme, flagellar connector, flagellum attachment zone, and paraflagellar rod

Flagellum extension at the matured basal body coincides with the assembly of the FAZ. Once the flagellum has entered the flagellar pocket, PFR assembly is initiated. The rates of PFR and FAZ assembly differ, and although extension of the FAZ is initiated earlier, PFR assembly occurs more rapidly (Kohl et al., 1999). There is evidence that the flagellar connector is associated with the new flagellum within the flagellar pocket, coincident with initiation of the central pair singlet microtubules (Briggs et al., 2004). The rate and extent of flagellar connector migration appears to be consistent, although dissociation of the flagellar connector is variable (cells can occasionally remain attached by the flagellar connector following cytokinesis). It has frequently been shown that the daughter flagellum is shorter than the old flagellum, a discrepancy that appears to be due to continued flagellum extension beyond cytokinesis (Farr and Gull, 2009). The events described are shown within the context of nuclear and kinetoplast phases in Figure 2-4.

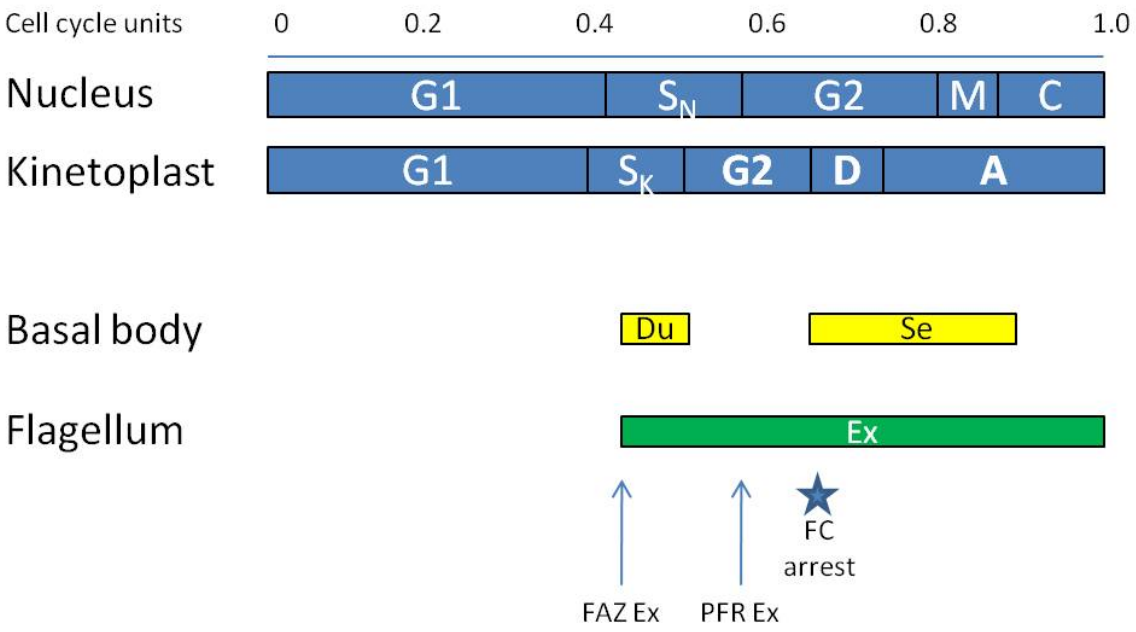

Figure 2-4 -Schematic representation of the major events in the *T. brucei* cell cycle. Cell cycle units and the relative timing of nuclear and kinetoplast cell cycles are shown at the top (Woodward and Gull, 1990) (M: mitosis; C: cytokinesis; S_N and S_K: nuclear and kinetoplast S phase, respectively; D: kinetoplast division; A: kinetoplast segregation). Estimates for the duplication (Du) and segregation (Se) of the basal bodies and extension (Ex) of the flagellum are indicated. Arrows indicate the extension of the FAZ and PFR, and the star indicates the arrest of the flagellar connector (FC). Adapted with permission from (Ploubidou et al., 1999).

2.3 Coordination of cell cycle events

2.3.1 The interplay between kinetoplast and basal body segregation

Kinetoplast replication can be inhibited by the application of Topoisomerase II inhibitors, for example ethidium bromide, teniposide and acriflavine, which affect decatenation and catenation of the minicircles of the kinetoplast DNA. Application of these inhibitors to procyclic *T. brucei* cultures affected kinetoplast segregation, but not basal body segregation, and the basal bodies remained attached to the kinetoplasts (Robinson and Gull, 1991). However, it has also been demonstrated that in the absence of attachment of the TAC to kDNA, basal body segregation still occurs (Ogbadoyi et al., 2003). Inhibition of microtubule dynamics though the application of ansamitocin did not inhibit kDNA replication, but inhibited both basal body and kinetoplast segregation (Robinson and Gull, 1991). A similar phenotype was observed through the application of okadaic acid, which inhibits protein phosphatases (Das et al., 1994;Li et al., 2006).

Genetic studies have also demonstrated that kinetoplast segregation is absolutely dependent on the basal bodies. TbLRTP is a negative regulator of basal body biogenesis, and overexpression of this protein dramatically reduced basal body duplication, resulting in an increase of cells with unsegregated kinetoplasts (Morgan et al., 2005). Centrins 1 and 2 are positive regulators of basal body duplication, and downregulation of these proteins had a similar effect on kinetoplast segregation (He et al., 2005). NKRC and KMP11 are regulators of basal body segregation; cells deficient in NKRC display delayed basal body segregation and accumulate at the four basal body stage. The effect on kinetoplast morphology was not described for these cells (it was only recorded that kinetoplast enlargement occurred in cells with abnormal numbers of basal bodies) and no cell cycle arrest was observed (Pradel et al., 2006). More dramatically, downregulation of KMP11 abolished basal body replication and cells with enlarged kinetoplasts appeared (Li and Wang, 2008).

The combined evidence from chemical and genetic studies suggests therefore that kinetoplast replication can occur in the absence of basal body duplication, but that kinetoplast segregation requires both duplication and segregation of the basal bodies. Conversely, basal body duplication and segregation appear to be independent of kinetoplast replication.

2.3.2 The role of the flagellum, flagellum attachment zone and flagellar connector in kinetoplast and basal body replication and segregation

When the structure of the flagellar axoneme is disrupted, motility defects can arise; frequently, cells displaying defective motility also have problems with basal body segregation. Downregulation of different axonemal components caused different motility phenotypes. Axonemal defects and cell paralysis were reported following simultaneous downregulation of two PACRG homologues (Dawe et al., 2005) and the paralysed PACRG mutants also displayed basal body segregation defects, although flagellar motility was not investigated. In other cases, however, the motility defect was analysed in detail, and particular flagellar wave forms were associated with different mutants. When assembly of the central pair was ablated (through knockdown of PF16 or PF20 (Absalon et

al., 2007b), both types of flagellar wave formation were abolished (tip to base and base to tip). When components of the dynein arms were downregulated (dynein intermediate chain (DNAI1) and dynein light chain (LC1)), tip to base motility was abolished, although the parasites still exhibited base to tip motility. In the case of DNAI1 downregulation, cells were totally paralysed (Absalon et al., 2007b), while LC1 depleted parasites displayed backwards swimming (Baron et al., 2007a). Inhibition of base to tip (central pair mutants) but not tip to base (DNAI1 mutant) wave forms affected basal body migration. Motility defects are not limited to axonemal mutants, however. A mutant lacking a PFR was paralysed due to an almost total deficiency of tip to base and base to tip flagellar movement (Branche et al., 2006); this mutant did not exhibit basal body segregation defects, which implied that occasional base to tip flagellar motility could be sufficient for basal body segregation.

The flagellar connector is also likely to be important for basal body segregation, since the halting of flagellar connector migration coincides with basal body segregation, and when the flagellar connector is absent (as is the case when TBBC (Trypanosome Basal Body Protein), a cytoskeletal protein, is downregulated), basal body segregation is inhibited (Absalon et al., 2007b). The flagellar connector may be required to transduce the forces generated by base to tip flagellar movement, which could be important for basal body segregation, or alternatively it could be involved in signal transduction, and halting of flagellar connector migration may trigger a signalling cascade, stimulating basal body segregation. Bloodstream form parasites, which appear not to possess a structure analogous to the flagellar connector, may not require such a structure to segregate basal bodies, as the distance involved is much smaller.

Interference with the intraflagellar transport (IFT) system affects construction of the flagellum, PFR and FAZ, and therefore can also influence basal body segregation. The severity of flagellar defects observed when IFT system components are downregulated is dependent upon the particular component and the duration of downregulation. Che2 downregulation had no effect on the flagellum-associated organelles (FAZ or flagellar connector) but completely abolished assembly of the axoneme (Davidge et al., 2006). Downregulation of IFT20, IFT88 and DHC1b inhibited both flagellum and FAZ assembly, causing the appearance of cells only capable of producing short flagella and FAZs, which

were frequently abnormal. Basal body segregation was inhibited when the FAZ was abnormal (IFT20 and DHC1b mutants (Absalon et al., 2007b)), or absent (IFT88 mutant (Kohl et al., 2003), but surprisingly, was unaffected in the total absence of a flagellar axoneme with intact FAZ and flagellar connector (Che2 depletion). This would imply that an intact FAZ/flagellar connector (rather than force or motility) is essential for basal body segregation, but this does not hold true in all cases. For example, the flagellum attachment defects present in FAZ1 or FLA1 mutants do not cause inhibition of basal body segregation (LaCount et al., 2002; Vaughan et al., 2008). Therefore, it is most likely that basal body segregation requires the combined presence of three functional structures: the flagellar axoneme, (providing base to tip motility forces), the flagellar connector (for force transduction or signalling/checkpoint regulation), and the FAZ (for flagella attachment and positioning cues).

It should also be noted that flagellum extension is independent of flagellar pocket formation, and *vice versa*; however, the positioning of either in the absence of the other is abnormal, demonstrating another example of structural cohesion within the cytoskeleton (Absalon et al., 2008a; Bonhivers et al., 2008).

2.4 The cytoskeleton and cytokinesis

2.4.1 Stages of cytokinesis

Cytokinesis can be considered as a three stage process, comprising initiation, furrow ingression and abscission. If a cell becomes committed to cytokinesis in the absence of successful organelle replication or segregation, abnormal daughter cells will arise which may not be viable. Cytokinesis initiation pathways are usually associated with mitotic exit to avoid the generation of anucleate cells; however, in *T. brucei*, initiation is also associated with replication and segregation of cytoskeletal elements. Furrow ingression in *T. brucei* is longitudinal and appears to follow the axis of the subpellicular microtubules. The pathways governing furrow placement, and the mechanism of furrow ingression are unknown at present. Abscission is the process responsible for remodelling the region of daughter cell attachment following furrow ingression. The region of cytoplasmic continuity between daughter cells is spanned by small

numbers of microtubules and has a small surface area, and evidence suggests that abscission in *T. brucei* may be accomplished by mechanical breakage. The roles of individual components of the cytoskeleton in cytokinesis are discussed in detail below.

2.4.2 Basal bodies

The kinetoplast organelle is unique to Kinetoplastids. As described above, it has been demonstrated that the nuclear and kinetoplast cycles are temporally independent, and in *T. brucei*, successful kinetoplast replication seems to have a more prominent role in cytokinesis regulation, since inhibition of nuclear S phase or mitosis does not prohibit cytokinesis (Ploubidou et al., 1999), but inhibition of kinetoplast and/or basal body segregation does (Das et al., 1994; He et al., 2005; Li and Wang, 2008a; Morgan et al., 2005; Pradel et al., 2006; Robinson and Gull, 1991). To ensure faithful segregation of the kinetoplast organelle, basal body duplication and segregation must proceed correctly, as the two organelles are linked by the TAC. Evidence implies that basal body segregation is in fact the main regulator of cytokinesis in *T. brucei*, as cells treated with acriflavine do not undergo kinetoplast replication, but still segregate basal bodies and undergo cytokinesis (Ogbadoyi et al., 2003).

2.4.3 Flagellum attachment zone

The FAZ is well placed to have roles in determination of cell polarity as it is associated with the flagellar pocket and the flagellum, and in close proximity to the kinetoplast and basal bodies. Polarity is important for the correct positioning of the cleavage plane in cells which have a linear arrangement of organelles. Furthermore, it has been identified as a putative site for furrow ingression because the gap in the subpellicular microtubules at this site could facilitate membrane ingression (Dolan et al., 1986). There has also been speculation with regards to the section of endoplasmic reticular membrane associated with the microtubule corset, which could potentially be involved in localised release of calcium, thus affecting signalling or microtubule dynamics (Dolan et al., 1986). Analysis of cells undergoing cytokinesis by electron microscopy clearly identifies the anterior end of the cell as the site of furrow initiation. Furthermore,

flagellum length directly correlates with cell length (Sherwin and Gull, 1989a). The FAZ has been shown to be essential for cytokinesis and correct positioning of the cleavage plane through the downregulation of FLA1 (LaCount et al., 2002) and FAZ1 (Vaughan et al., 2008), respectively.

It has been demonstrated on multiple occasions that inhibition of the IFT system can inhibit the assembly of FAZ and flagellum (Absalon et al., 2008b), resulting in inhibition of cytokinesis. Detailed analysis of IFT88 and DHC1b mutants, where dividing cells assembled a short daughter flagellum and FAZ, revealed that division of these cells was asymmetric. The length of the FAZ and flagellum in the daughter cells correlated with cell length, suggesting that the cell inheriting the shorter flagellum received a proportional quota of the cytoplasm and cytoskeleton, implying that the cleavage plane is determined by flagellum or FAZ extension. Furthermore, cells producing a short daughter FAZ, but lacking a flagellum, were still capable of dividing, thus emphasising that the FAZ and not the flagellum determines the cleavage site (Kohl et al., 2003).

2.4.4 Flagellum

Through the recent advances in identification of putative flagellar proteins, there is an accumulation of evidence that the flagellum is important for cytokinesis, and interestingly, the role of the flagellum in this process differs dramatically according to life cycle stage. When components of the flagellar axoneme or PFR are downregulated in procyclic form cells, the parasites frequently display abscission defects, and clusters of parasites attached by their posterior ends accumulate (Baron et al., 2007b; Broadhead et al., 2006; Ralston et al., 2006). The cytokinesis defect observed upon depletion of PFR2 (Ralston et al., 2006) was not described previously (Bastin et al., 2000); however, these original mutants were later found to exhibit cytokinesis defects and the differences in the severity of these defects were attributed to differences in the generation of mutants or culture technique (discussed in (Ralston et al., 2006)). The abscission defect could be reversed by shaking the culture medium (Ralston et al., 2006), perhaps suggesting that *in lieu* of membrane insertion or microtubule severing, membrane and microtubule attachments at cell posterior ends could be broken by the rotational forces generated from the two flagella

beating in opposite directions. In bloodstream form parasites, downregulation of axonemal or PFR components caused inhibition of cytokinesis initiation, resulting in the production of multinucleated cells with a distinctive morphology comprising loss of cell polarity, enlargement of the flagellar pocket, and multiple flagella which occasionally possessed two axonemes (Broadhead et al., 2006). This phenotype could not be reversed by growth of these mutants *in vivo*, suggesting that, unlike in procyclic form parasites, a lack of flagellar motility could not be compensated for by shear forces (Griffiths et al., 2007).

2.4.5 Subpellicular corset

The subpellicular corset is present throughout the cell cycle, which is a predicament for furrow ingression, as presumably the cell membrane must invaginate and coalesce during cell division. The cytoskeleton is highly stable, a consequence of microtubule crosslinking by microtubule-associated proteins. Additionally, MAPs attach the cell membrane to the subpellicular corset (shown in Figure 2-6). Although the cytoskeleton does not disassemble globally at any point during the cell cycle, it has been proposed that local disassembly must occur for the ingression of the furrow and to allow remodelling of the membrane bilayers, although this has not yet been observed. Downregulation of α-tubulin causes a dramatic phenotype, characterised by cell rounding and inhibition of cytokinesis (Ngo et al., 1998). These cells have been dubbed ‘fat cells’; so dramatic and reproducible is the phenotype, it has been used to test the efficacy of new RNAi systems (Shi et al., 2000b). Inhibition of cytokinesis following induction of α-tubulin RNAi was rapidly induced, and whilst this was attributed in part to axonemal and FAZ defects, the cytokinesis phenotype was not reversible, suggesting that α-tubulin turnover and cytoskeletal assembly could represent an important cytokinesis checkpoint. The unsubtle and global effect on the *T. brucei* cytoskeleton makes depletion of tubulin an unsuitable method for investigating furrow ingression. Other methods of studying the role of the cytoskeleton in furrow ingression include the application of inhibitors of microtubule dynamics (discussed in Chapter 6) and the manipulation of expression levels of MAPs that regulate stability of the microtubule corset (Section 2.6.2.1).

2.5 Microtubule structure and dynamics

Microtubules are hollow tubes constructed from polymerised tubulin protofilaments, with typically thirteen protofilaments making up one microtubule (Amos and Schlieper, 2005). For polymerisation of tubulin to occur, α and ß isoforms of tubulin first dimerise producing heterodimers. The incorporation of these heterodimeric subunits into protofilaments requires hydrolysis of GTP. Protofilaments interact with other protofilaments in a lattice sheet, which folds to form a hollow tube. In typical microtubules, the protofilament lattice is an 'A' lattice, meaning that α and ß subunits in adjacent protofilaments alternate. The subunits within the lattice are slightly offset, forming a shallow helix. This pattern of alternating isoforms is not continuous in a typical microtubule (due to the odd numbers of protofilaments), and there is a region along one side of the tubule where identical isoforms are adjacent, referred to as the microtubule seam.

The α- and ß–tubulin isoforms each possess two globular domains, which are spatially separated by a core helix (Figure 2-5), and have different functions. The larger globular domain, located at the N-terminus, contains a GTP binding site. The second globular domain contains three important regions: the activation domain (which comprises loop T7 and helix 8), the taxol binding pocket, and the M-loop. The activation loop stimulates GTP hydrolysis, the taxol binding pocket is important for interactions with MAPs (and small molecules, for example, taxol), and the M-loop is involved in maintaining inter-protofilament bonds. There are two crucial differences between α- and ß-tubulin isoforms. Firstly, the GTP bound to the α-tubulin is not hydrolysed due to a substitution of glutamic acid for lysine within helix 8 of the ß-tubulin activation domain, preventing the association of ß-tubulin helix 8 with the GTP binding site of α-tubulin from resulting in hydrolysis. GTP is therefore permanently bound at the α-tubulin subunit. The second difference concerns the taxol binding pocket, which is closed in α-tubulin due to an extension of the L-loop obstructing the pocket opening. In addition to the globular domains and core helix, there is a C-terminal domain consisting of two helices, a U-turn and crucially, a disordered domain of 13 (α-tubulin) or 9 (ß-tubulin) residues that are acidic. These are believed to project from the microtubule polymer where they can form binding

sites for basic and positively-charged MAPs. The C-termini are frequently modified by post-translational modifications, which are believed to mediate interactions with MAPs.

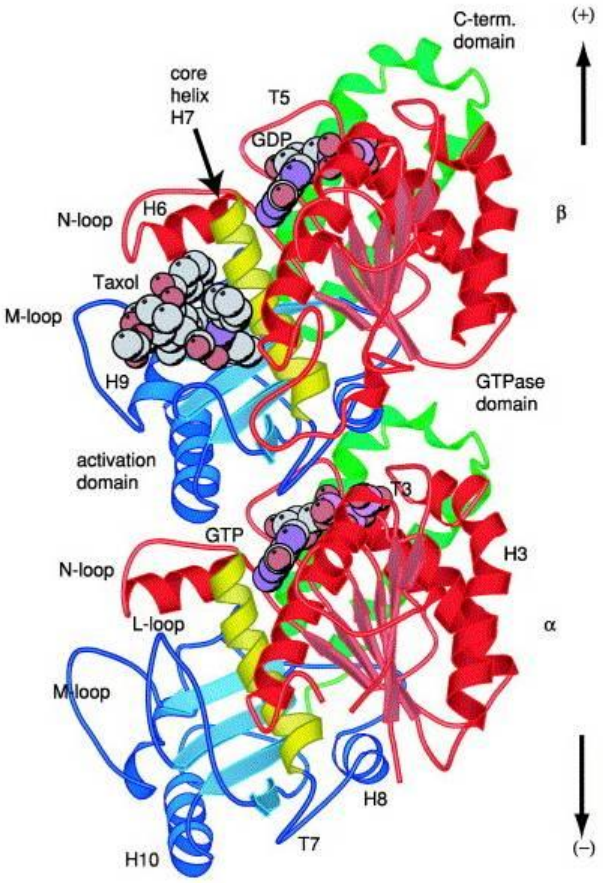

Figure 2-5 -Ribbon diagram of an α/β tubulin heterodimer.
Electron crystallography structure of bovine brain tubulin in complex with taxol orientated to correspond to the inside view of a microtubule. Red: GTPase domains; blue: activation domains; yellow: the core helix connecting the two globular domains; green: C-terminal domain on the external surface. GTP, bound to α-tubulin by loops T7-T6 and making contact with loop T7 of β-tubulin, is shown between the α and β subunits of each heterodimer. The nucleotide bound to β-tubulin has been hydrolysed to GDP through contact with helix H8 and loop T7 of the activation domain of another α-tubulin subunit. Taxol sits at the taxol binding pocket of β-tubulin. Reproduced with permission from (Amos and Schlieper, 2005).

GTP hydrolysis is important for the polarity and dynamics of microtubule assembly. GTP-bound heterodimers associate more readily with positive microtubule ends, resulting in polarized microtubule growth. When net loss at the negative pole and net gain at the positive pole reach equilibrium, the length of the microtubule remains constant, a process known as ‘treadmilling’. GTP hydrolysis is also responsible for conformational changes within the tubulin heterodimer, and GTP-bound heterodimers form straight protofilaments which become curved upon GTP hydrolysis. This phenomenon can be observed when a

microtubule is growing; growing microtubule ends form straight sheet-like structures, whilst shrinking microtubules appear to curve outwards, shedding ring-like pieces of protofilaments (Howard and Hyman, 2003).

The pattern of microtubule assembly features four phases: nucleation, elongation, stationary phase and disassembly (Valiron et al., 2001). Nucleation and assembly can occur spontaneously *in vitro*, providing the conditions are right, which is evidence that self assembly is an intrinsic property of tubulin. *In vitro* assembly has also shown that the initial concentration of GTP-bound heterodimers is important for nucleation. *In vivo*, the dynamics of tubulin assembly are similar; however, nucleation only occurs at designated microtubule organising centres, such as centrioles. Protein complexes called γ-tubulin rings are found at these regions and are thought to act as templates, mimicking microtubule ends to recruit tubulin heterodimers (Job et al., 2003). Once protofilaments begin to elongate, the energy released by GTP hydrolysis keeps GDP-bound heterodimers in a straight but strained conformational state, and continued incorporation of GTP-bound heterodimers with naturally straight ends act as a cap, stabilising the structure beneath. If incorporation of tubulin ceases, then the cap is lost, and the microtubule disassembles. The cap can be as small as one layer thick. Loss of the cap may occur stochastically, even when conditions for assembly are favourable, and this is described as a catastrophe event. Catastrophe events do not necessarily cause the whole microtubule to disintegrate, and rescue events can restore microtubule extension.

The simplest way to alter microtubule dynamics *in vitro* is to increase the supply of GTP-bound tubulin heterodimers. Temperature is also important for mammalian microtubules, which are unstable at 4°C. Regulation of microtubule dynamics *in vivo* is far more complex, as there are different layers of regulation involving post-translational modifications and association of MAPs. The field of MAP research is biased towards those MAPs linked to degenerative neurological diseases, and comparatively little is known about other MAPs. However, current knowledge suggests that microtubule binding domains, and binding sites within microtubules are diverse. Perhaps this diversity reflects the plethora of functions which range from general roles in cell morphology and polarity, and cell cycle roles at mitosis and cytokinesis, to cell type-specific roles in vesicle transport, and motility.

2.5.1 General features of common microtubule-associated proteins

MAPs can inhibit microtubule disassembly by counteracting the tendency of GDP-bound microtubules to bend outwards by forming intra-protofilament bonds, and by forming links between adjacent heterodimers to strengthen lateral associations (non-specifically or at the lattice seam). MAPs frequently possess repetitive regions, enabling them to contact more than one heterodimer, and frequently these regions contain basic and positively-charged residues, which mediate the interaction with the acidic C-terminus of tubulin. These proteins often have a random coiled structure, and some may only form an ordered structure upon binding to the microtubule, which makes it very difficult to predict how and where a MAP binds.

'Typical' MAPs are exemplified by MAP2 and Tau. Both proteins bind microtubules via their C-termini which contain PGGG repeats and proline-rich repeats, which each bind independently to microtubules. The PGGG repeats bind to the taxol binding pocket of ß-tubulin (Kar et al., 2003), laterally joining up to as many as four heterodimers along the inside face of the microtubule, whilst the proline-rich repeats have less specificity, and bind to the acidic microtubule surface linking heterodimers longitudinally along microtubule ridges (Al Bassam et al., 2002).

'Unusual' MAPs include MAP1A, doublecortin and members of the Ds1 / TOG family. MAP1A controversially possesses an acidic microtubule binding domain: the 'SS2' domain. This domain is thought to assemble an α helix, and the regular intervals between acidic and basic residues suggests that these cluster on opposite sides of the helical loop, an arrangement that could allow protein interactions at one side, and microtubule binding to the acidic microtubule surface at the other (Cravchik et al., 1994). Microtubule binding does not always involve repetitive regions or α-helices. Doublecortin, for example, has two DCX motifs, which share a common ubiquitin-like fold; moreover, the C-terminal motif has globule-like properties suggesting that it is in fact a disordered structure. Both domains can bind to microtubules, and it has been suggested that the C-terminal DCX motif binds free tubulin, supplying heterodimers to the

growing microtubule (Moores et al., 2003). The site of doublecortin binding has been mapped to 'valleys' between heterodimers, whereby one doublecortin molecule can interact with four heterodimers, thus stabilising both longitudinal and lateral bonds (Moores et al., 2004). The Dis1/TOG family encompasses a large group of highly conserved proteins which possess distinctive motifs called TOG domains. The TOG domain is a paddle-like structure, and has two wide faces composed of HEAT repeat helices flanking a hydrophobic core (Al Bassam et al., 2007). Members of this family can possess multiple TOG domains, and it has been shown that different TOG domains within a protein can have preferential affinity for different tubulin isoforms, which could allow the proteins to interact with more than one heterodimer. The exact binding mechanism has not yet been elucidated. This family of proteins have diverse cellular functions, and the TOG domain is believed to facilitate interactions with many different proteins in addition to tubulin (Ohkura et al., 2001).

These examples represent just a small number of microtubule-associated proteins. There are other classes of MAPs, which bind preferentially to growing microtubule ends (for example EB1), or possess ATPase activity for microtubule severing (katanins) or trafficking (dynein and kinesins). The diversity observed in well studied eukaryotic systems seems to be increasing; however, very little is currently known about MAPs in *T. brucei*.

2.6 Microtubule-associated proteins in *T. brucei*

2.6.1 Identification of T. brucei microtubule-associated proteins

MAPs can be visualised by electron microscopy of *T. brucei* subpellicular microtubule arrays (Figure 2-6). Cytoskeletons of *Trypanosoma* species are highly immunogenic, and immunisation of mice and rabbits with either whole cytoskeletons, or the salt extracts thereof, has proven to be a successful method for the identification of novel MAPs. Verification of sera specificity can be achieved by immunofluorescence microscopy analysis, and the epitope recognised by the sera can be assigned to a particular protein by screening expression libraries. Proteins identified though immunological methods include

WCB (Woods et al., 1992), CAP5.5 (Hertz-Fowler et al., 2001) and Autoantigen I/6 (Detmer et al., 1997).

MAPs have also been isolated directly from cytoskeletons, either by purifying proteins found in salt-extracted cytoskeletal fractions using gel filtration, or by passing the salt-extracted fractions through a tubulin affinity column, and analysing the eluted proteins. Proteins isolated by these methods were characterised either by peptide sequencing, or through the production of antibody and screening of expression libraries. Proteins identified from cytoskeletal fractions included p15 (Balaban and Goldman, 1992), p52 (Balaban et al., 1989), MARP1 and MARP2 (Schneider et al., 1988b).

Other MAPs were identified indirectly; for example, GB4 was identified in a screen for cell surface proteins (Rindisbacher et al., 1993), CAP15 and CAP17 (Vedrenne et al., 2002) were identified primarily as stage-specific proteins (CAP15 is expressed in bloodstream form parasites, whereas CAP17 is expressed in procyclic form parasites), and a metabolic labelling study to identify fatty acid-associated proteins led to the discovery of the MAP, p41 (Schneider et al., 1988a).

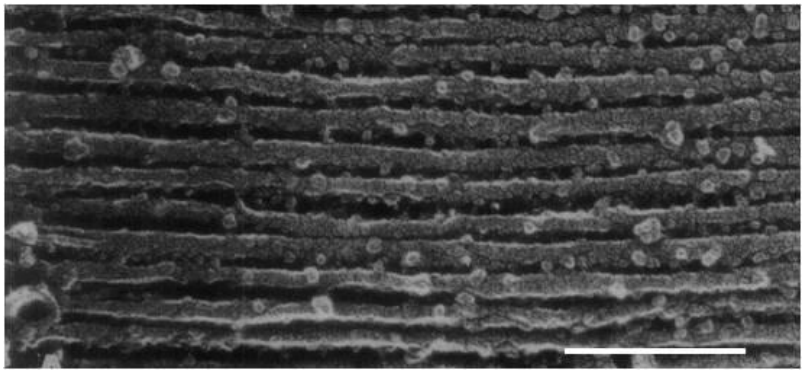

Figure 2-6 -Quick-freeze deep-etch electron microscope image showing the localisation of MAPs in a *T. brucei* subpellicular microtubule array.
The high density of MAPs localised at the membrane-oriented face of the subpellicular microtubule array can be seen (protein knobs above). The cytoplasmic face is relatively smooth (not shown). Occasionally, MAPs can be seen bridging adjacent microtubules. Scale bar: 197 nm. Adapted with permission from (Hemphill et al., 1991).

2.6.2 Characterisation of microtubule-associated proteins

2.6.2.1 Roles in microtubule stability

Techniques for purification of calf brain, porcine and *Trypanosoma* tubulin have enabled the binding, and polymerisation capabilities of MAPs to be assessed *in vitro*. Tubulin polymerisation in the presence or absence of the MAP in question can be assessed biochemically (by monitoring the dynamics of polymerisation), or visually using electron microscopy. Additionally, S-tubulin, a form of tubulin, which lacks the C-terminal region usually associated with the binding of MAPs, can be used in affinity assays to probe the nature of the binding interaction.

To assess the effect of MAPs on microtubule stability *in vivo*, different genetic approaches have been used. Expression of MAPs in mammalian cell lines is a useful method for testing whether a protein has a stabilising effect on microtubules. Mammalian microtubules are not stable at low temperatures or in the presence of destabilising agents like nocodazole. Therefore, the morphology of the mammalian cell cytoskeleton can be compared in the presence or absence of a trypanosome MAP. This method effectively showed that MARP1 and MARP2 and CAP15 can stabilise microtubules (Affolter et al., 1994; Hemphill et al., 1992; Vedrenne et al., 2002). Genetic techniques, for example RNAi and protein overexpression, have been used to alter the levels of some MAPs in *T. brucei* cells. Parasites with an altered level of a particular MAP were analysed by electron microscopy in order to determine the impact on cytoskeletal organisation and integrity. RNAi was used to investigate the roles of CAP5.5, CAP5.5v and WCB (Baines and Gull, 2008; Olego-Fernandez et al., 2009). Parasites subjected to the downregulation of these MAPs displayed abnormal cytoskeletal morphologies. Cells depleted of WCB exhibited uneven spacing of the microtubules and poor membrane/microtubule attachment, indicating that WCB is involved in linking the subpellicular corset to the cell membrane. (Baines and Gull, 2008). Additionally, cytoskeletons showed a loss of integrity following detergent extraction, and downregulation of WCB caused an accumulation of 2N2K cells and the production of equal numbers of 0N1K and 2N1K cells, suggesting cytokinesis was delayed, and that the cleavage plane was then abnormally positioned (Baines and Gull, 2008) generating these abnormal daughter cells. Cells depleted of CAP5.5 or CAP5.5v exhibited abnormal

microtubule spacing, and possessed bundles of microtubules beneath the cell membrane, defects, which were more severe at the posterior ends of cells, and abnormal placement of the cleavage furrow was observed (Olego-Fernandez et al., 2009). Overexpression of CAP15 or CAP17 (Vedrenne et al., 2002) also caused abnormal cleavage furrow placement, although this may have been a consequence of inhibited kinetoplast segregation also observed in these cell lines. Hence, although few *T. brucei* MAPs have been identified to date, four have been shown to have roles in cytokinesis.

In addition to microtubule binding, some MAPs were identified as potentially interacting with membranes. Liposome binding assays identified p15 as a protein involved in crosslinking microtubules to phospholipid membranes (Rasooly and Balaban, 2002).

2.6.2.2 The structural characterisation of *T. brucei* microtubule-associated proteins

No crystal structures for the *T. brucei* MAPs have been determined; however, protein structure has been investigated through bioinformatic approaches. Some proteins displayed features characteristic of MAPs, namely the presence of repetitive motifs and regions rich in basic amino acids. MAPs containing repeat sequences include MARP1 and MARP2, which contain repeats of 38 amino acids which have a low pI (Affolter et al., 1994); p15, which contains sixteen repeats rich in positive and hydrophobic amino acids that are predicted to be distributed equally around an α-helix (Rasooly and Balaban, 2002); Autoantigen I/6, which contains six tandem repeats each eight amino acids in length (Detmer et al., 1997); and WCB, which possesses five repeats all 32 amino acids in length (interestingly incorporating alternating acidic and basic residues) (Baines and Gull, 2008). MARP1 and MARP2 possess basic N-termini (Affolter et al., 1994), and CAP5 and CAP5.5v possess proline-rich N-termini (Hertz-Fowler et al., 2001). The non-repetitive N-terminus of MARP2 has been shown to bind microtubules (Affolter et al., 1994; Hemphill et al., 1992). In some cases, common sites of post-translational modification were present, including sites for fatty acid addition by palmitoylation or myristoylation (p41 (Schneider et al., 1988a), CAP5 and CAP5.5v (Hertz-Fowler et al., 2001)), glycosylation (GB4 (Rindisbacher et al., 1993)), and phosphorylation (WCB (Woods et al., 1992)). These observations

have functional implications; fatty acid addition suggests a role in membrane interaction, and phosphorylation could suggest a signalling role.

The cellular localisation for most of these proteins has now been determined (excluding p52 and p41). Proteins that are evenly distributed throughout the microtubule array include MARP1, MARP2, WCB, Autoantigen I/6, CAP15, CAP17 and p15 (Detmer et al., 1997; Hemphill et al., 1991; Vedrenne et al., 2002; Woods et al., 1992). CAP5, CAP5.5v and GB4 show different localisation patterns within the corset; CAP5 and CAP5.5v are found only in the anterior region (Olego-Fernandez et al., 2009), whilst GB4 forms a ring-like distribution at the posterior end (Rindisbacher et al., 1993).

MAPs in the subpellicular corset of *T. brucei* are a diverse collection of molecules. From a structural angle there are no strong patterns that would implicate a common binding site within the microtubule structure. The unusual properties of *T. brucei* MAPs are highlighted by the MARP proteins, which perversely exhibit the classical MAP structural features, yet do not bind the acidic tubulin C-terminus. These unique proteins clearly have a role in maintaining the integrity of the microtubule structure in the subpellicular corset, but there are several indications that some proteins could have other roles, for example, in signalling, cell polarity, cytokinesis, and differentiation.

2.6.3 Microtubule-associated proteins, cytokinesis and parallels with other organisms

The subpellicular corset has obvious roles in maintaining cell shape and polarity, and via the FAZ, it is also associated with the flagellum. These factors place the subpellicular corset in a uniquely advantageous position for determining the cleavage plane and regulating furrow ingression, which is all the more poignant given the absence of an actomyosin contractile ring, and unusually reduced importance of mitosis in regulating these processes.

Novel MAPs may provide a link to bridge cytoskeletal replication and cytokinesis regulation. MAPs can regulate microtubule dynamics, establish membrane/microtubule association, interact with signalling pathways (involving kinase-mediated phosphorylation), and recruit other proteins (i.e. by acting as

scaffolds). These properties strongly implicate this group of proteins as key putative regulators of cytokinesis. Potential roles for MAPS in *T. brucei* cytokinesis include: marking the initiation site, perhaps through association with the CPC (Section 1.9.1.2); recruiting other proteins to the site of furrow initiation or ingression (either directly or by participating in signalling pathways); in the mechanical process of furrow ingression (by remodelling the microtubules and microtubule/membrane association along the furrow); or finally in positioning the cleavage axis (localisation of MAPs is likely to be necessary for maintaining cell polarity).

Microtubules and their associated proteins are important for cytokinesis in mammalian cells. However, the microtubules in this case are those comprising the spindle, not the cortical cytoskeleton. Since *T. brucei* can undergo cytokinesis in the absence of mitosis, there may be more mechanistic parallels to be drawn between plant cytokinesis processes, than mammalian ones, as positioning of the cleavage axis in plants involves novel cytoskeletal structures and MAPs.

2.7 Cytokinesis in plants

2.7.1 General principles

In plants cells, the cleavage plane is positioned prior to mitosis, via the formation of a structure called the ‘preprophase band’, which is composed of cortical microtubules and actin filaments. The preprophase band disassembles at the transition between prophase and prometaphase, but markers deposited at the site of the preprophase band remain, comprising the ‘cortical division site’. During late telophase, the phragmoplast forms. This microtubule-based structure is the target for vesicle trafficking from the Golgi, and at the phragmoplast midzone, these vesicles fuse to form the cell plate, a membranous structure containing cell wall precursors and enzymes. Cell plate expansion continues until the plate encounters the cortical division site; contact with this region coincides with cross wall maturation, which finally separates the two daughter cells (reviewed in (Jurgens, 2005;Muller et al., 2009)).

2.7.2 Cleavage plane determination, the preprophase band and the cortical division site

The strong correlation between preprophase band position and cell wall insertion implied a role for the preprophase band in cleavage plane determination. However, the mechanism behind this process has only recently been revealed through the discovery of preprophase band components, and there is still much to be elucidated. Summarised below is an account of preprophase band formation (see also Figure 2-7) and a description of the roles of preprophase band components in cytokinesis (reviewed by (Jurgens, 2005; Muller et al., 2009; Van Damme et al., 2007; Van Damme and Geelen, 2008)).

During interphase, microtubule nucleation occurs at discrete sites throughout the cortical array, and is thought to involve acentrosomal γ-tubulin complexes (although the exact role of γ-tubulin is not understood). The accumulation of microtubules to form the preprophase band appears to occur at the expense of cortical microtubules, and this process requires the MAPs MOR1 and MAP65, which can both bind to, and cause bundling of, microtubules. The transition from cortical to preprophase band microtubule assembly is probably a consequence of changes in microtubule dynamics mediated by these MAPs. The preprophase band stretches across the cell bilaterally, and contact with the cell wall is thought to be assisted by CLASP, a positive microtubule end-associated protein. Initiation of preprophase band formation requires a putative homologue of the regulatory subunit of protein phosphatase 2a called FASS (or Discordia and Alternative Discordia in maize) which is thought to regulate TON1, a protein with homology to centrosomal proteins; absence of either of these proteins completely inhibits preprophase band formation. Both preprophase band formation and the expression of kinesins POK1 and POK2 are vital for the recruitment of TAN and RanGAP1 to the cortical division site. The preprophase band is implicated in the establishment of spindle bipolarity and nuclear orientation, and RanGAP1 is suspected of coordinating nucleus/preprophase band interactions. At the onset of mitosis, the CDKA/cyclinB kinase complex signals degradation of the preprophase band (this process may also involve AURORA 1 kinase), but the cortical attachment site persists and plays a role in guiding the cell plate to the cell wall during telophase. The cell plate is located

at the centre of the phragmoplast, which is a microtubule-based structure composed of overlapping microtubules of opposite polarity, and Golgi-derived vesicles. The phragmoplast also incorporates some of the proteins previously located at the preprophase band, including the MAPs, MOR1, AIR9, MAP65 and CLASP (Figure 2-7). The cell plate contains cytokinesis regulators TPLATE (a protein with homology to adaptin and ßCOP coat proteins), the kinesin, KCA1, and RanGAP1, in addition to cell wall precursors and enzymes (Figure 2-7). TPLATE and AIR9, also localise to the cortical division site immediately before it comes into contact with the cell plate, implicating these proteins in cell plate positioning. Contact between the cell plate and the cortical division site is believed to be required for cell wall maturation, as demonstrated by AIR9, which migrates from the cortical division site into the maturing cross wall where it influences maturation processes (probably through microtubule-mediated mechanisms). Ectopically inserted cell plates do not exhibit AIR9 labelling and do not mature into cell walls. It has been proposed that the cortical division site could have dual roles in cell plate guidance and localisation of cross wall maturation factors. In contradiction to this theory, POK1/2 double mutants display ectopic cell plate insertion and normal cell wall maturation.

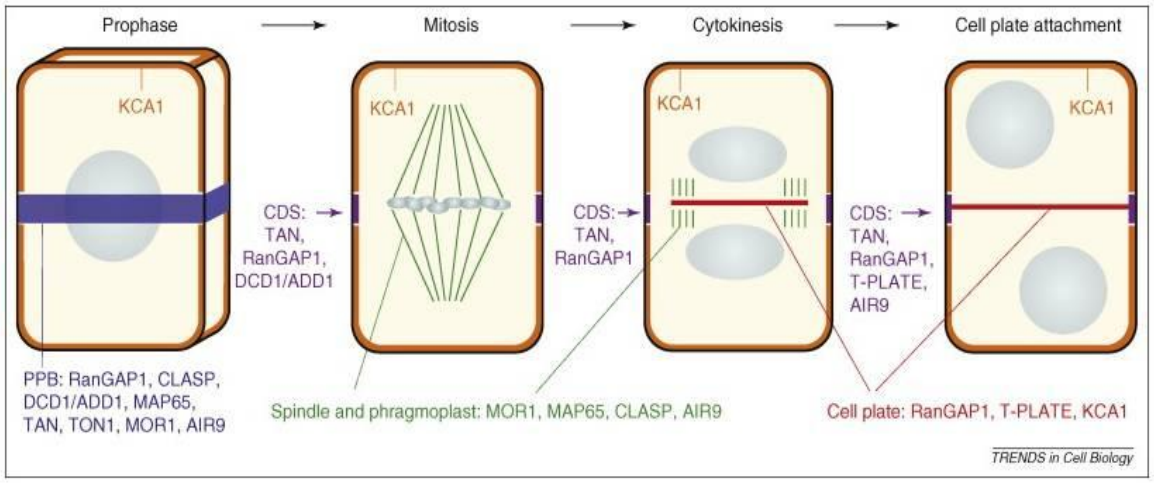

Figure 2-7 -Schematic of plant cytokinesis with preprophase band and cortical division site regulators.
The prophase cell is illustrated as a 3D projection, and other cell cycle stages are shown as mid-plane cross sectional views. The preprophase band (PPB) is coloured blue, the cortical division site (CDS), purple; the spindle and phragmoplast microtubules, green; and the cell plate, red. Proteins which associate with the structures described are indicated in the corresponding colours, and not all of the cytokinesis regulators are shown for simplicity. Reproduced with permission from (Muller et al., 2009).

This condensed description of plant cell cytokinesis processes emphasises the prominent role of microtubule-based structures in cytokinesis, and although

knowledge of this process is patchy, MAPs comprise a large proportion of known cytokinesis regulators. Plant cell cleavage plane determination at preprophase rather than after mitosis does not preclude the nucleus from influencing cleavage site selection, however, as demonstrated by the physical displacement of nuclei in onion cotyledon cells (Mineyuki et al., 1991). Nuclear displacement resulted in the formation of two phragmoplasts, one at the site of the displaced nucleus, and one positioned midway along the cell. This suggests that whilst the preprophase band can form in a position where there is no nucleus, there is an element of redundancy, which ensures that in adverse circumstances, production of anucleate cells can be prevented by formation of a phragmoplast in the absence of preprophase band assembly. Small changes of nuclear positioning can also be corrected for by the preprophase band, suggesting that cells are able to compensate for slight positioning problems, and under normal circumstances, given the robust structure of the plant cell, physical deformation and subsequent nuclear displacement are unlikely to occur (reviewed in (Van Damme and Geelen, 2008)). For plant cells, early determination of the cleavage plane is likely to be an advantage as it gives the cell longer to prepare for the complex cell wall assembly and there are minimal risks that organelle segregation could be compromised.

Plant and *T. brucei* cytoskeletons are quite similar in the way that microtubules are nucleated, cross-linked, and positioned beneath the plasma membrane. It is tempting to speculate that less stringent association between mitosis and cytokinesis may suggest that *T. brucei* cells determine the cleavage axis in ways which parallel the formation of a pre-prophase band in plant cells; that is, through deposition of molecular markers at the site of furrow initiation or maybe even along the site of ingression, before mitosis occurs. It is possible that the *T. brucei* chromosomal passenger complex (Section 1.9.1.2) localises to the site of furrow initiation as a result of such signals, perhaps via MAPs. Intriguingly, AIR9, a component of the pre-prophase band in plants (Section 2.7.2) is conserved in *T. brucei*. The results of investigations into the function of this *T. brucei AIR9* orthologue are discussed in Chapter 5.

3 Project aims

To date, little is known about the molecular pathways regulating cytokinesis in *T. brucei,* and while a number of proteins are known to play important roles in this process, how individual regulators are connected remains unclear in many cases, and little is known about how the activity of key players such as protein kinases are regulated. Additionally, the physical mechanism of furrow ingression remains to be elucidated. It is not, for example, understood how the cytoskeleton is divided during furrow ingression, or clear what role microtubule dynamics might play during this process or to what extent microtubule-associated proteins contribute to furrow ingression.

Initially, this project aimed to follow on from RNAi studies of PLK (Section 1.9.1.2.2 and Hammarton et al., 2007) to address how PLK activity is regulated *in vitro* and *in vivo*. Additionally, since PLK plays an important role in furrow ingression in bloodstream form parasites, and microtubule dynamics are likely to be important in this aspect of cytokinesis, a second aim was to investigate whether microtubule inhibitors affected cytokinesis in *T. brucei* parasites and to compare any effects on furrow ingression with the *PLK* RNAi phenotype, where depletion of PLK blocked furrow ingression part way through. PLK has been shown to influence microtubule dynamics in other organisms (McNally et al., 2002; Yarm, 2002; Archambault et al., 2008; see also Chapter **Error! Reference source not found.**) and it was therefore hypothesised that cell cycle regulators such as PLK might control the mechanical aspects of furrow ingression, potentially through regulation of microtubule dynamics, and that there could be novel furrow ingression checkpoints which control this process.

During the course of this project, literature searching coupled with bioinformatic analyses also indicated that a plant MAP, AIR9, with roles in plant cytokinesis (Section 2.7.2), was likely to be conserved in *T. brucei* (Section 5.1.2) and had not previously been studied in the parasite. Given the important roles of MAPs in microtubule stability (Sections 2.1.1 and 2.5), the likely importance of microtubule dynamics in trypanosome cytokinesis (Section 2.4.5), and studies

indicating that depletion of other *T. brucei* MAPs compromises cytokinesis (Section 2.6.2.1), it was therefore of interest to functionally characterise the *T. brucei* AIR9 protein.

Hence, this project covered three different aspects of cytokinesis: the roles of microtubule dynamics and putative microtubule-associated protein AIR9; and investigations into the activity of PLK.

Specifically the project aims were:

- To determine whether a putative *T. brucei* orthologue of the plant cytoskeleton-associated protein, AIR9, is microtubule-associated and to characterise its role in cytokinesis and the cell cycle more generally
- To investigate the importance of microtubule dynamics in cytokinesis by characterising cell cycle progression in *T. brucei* cells treated with microtubule inhibitors
- To determine how PLK activity is regulated in *T. brucei*

AIR9 characterisation and microtubule inhibitor studies are described in Chapters 5 and 6, respectively, while the investigation of the regulation of PLK activity is discussed in Chapter 7.

4 Materials and Methods

4.1 Chemicals

All chemicals and reagents were obtained from Sigma-Aldrich Company Ltd unless otherwise stated. Before use, media and solutions were autoclaved at 121^{o}C, 15 psi for 20 minutes, or filter sterilised using a 0.1 µm syringe filter (Sartorius) for small volumes or 0.1 µm bottle top filters (Millipore) for larger volumes, as appropriate.

4.2 Cell culture: Routine techniques

4.2.1 Culture of bacterial cells

4.2.1.1 Bacterial strains

Details of bacterial strains and plasmids used and generated during this study are given in Table 4-1, Table 4-2, Table 4-3 and Table 4-4.

Table 4-1 -*E. coli* strains used in this study

Strain	Genotype	Company	Application and notes
XL-1Blue	*recA*1 *endA*1 *gyrA*96 *thi*-1 *hsdR*17 *supE*44 *relA*1 *lac*[F' *proAB*$^+$ *lacI*^{q}ZΔ*M*15] Tn10(Tc^r)	Stratagene	Host strain for plasmid transformations, plasmid purifications and maintenance of plasmids via glycerol stocks.
BL21(DE3)	F- *ompT* *hsdS*$_B$(r$_B$-m$_B$-) *gal dcm* (DE3[*lacI* *lacUV5*-T7 gene 1 *ind*1 *sam7* *nin5*])	Stratagene	IPTG-inducible protein expression driven by T7 polymerase promoter. DE3 encodes T7 polymerase regulated by *LacUV* promoter.
BL21(DE3)pLysS	F- *ompT* *hsdS*$_B$(r$_B$-m$_B$-) *gal dcm* (DE3 [*lacI* *lacUV5*-T7 gene 1 *ind*1 *sam7* *nin5*]) pLysS (Cam^R)	Invitrogen	Tightly regulated IPTG-inducible protein expression driven by T7 polymerase promoter. Particularly useful for expression of toxic proteins. pLysS encodes T7 lysozyme which inhibits T7 polymerase and reduces basal expression from T7 promoter.
Rosetta (DE3)pLysS	F- *ompT* *hsdS*$_B$(r$_B$-m$_B$-) *gal dcm* (DE3 [*lacI* *lacUV5*-T7 gene 1 *ind*1 *sam7* *nin5*]) pLysSRARE (Cam^R)	Novagen	Tightly regulated IPTG-inducible expression and enhanced expression of eukaryotic proteins containing codons rarely used in *E. coli* due to supply of tRNAs for rare codons.
SCS110	*rpsL* (Str^r) *thr* leu *endA* *thi-1* *lacY* *galK* *galT* *ara* *tonA* *tsx* *dam* *dcm* *supE44* Δ(*lac-proAB*) [F´ *traD36* *proAB* *lacI*qZΔ*M15*]	Stratagene	Generation of unmethylated DNA due to lack of DNA adenine cytosine methylation genes.
Solopack Gold	Tet^r Δ (*mcr*A) 183 Δ (*mcr*CB-*hsd*SMR-*mrr*) 173*end*A1 *sup*E44 *thi*-1 *rec*A1 *gyr*A96 *rel*A1 *lac*Hte [F'*pro*AB *lacI*^{q}ZΔM15 Tn10 (Tc^r) Amy Cam^r]	Stratagene	Transformation host for pSC-A and pSC-B ligations Contains *LacI*^{q}*ΔM15* on F' episome for blue/white screening.
TOP 10	F$^-$ *mcr*A Δ(*mrr-hsd*RMS-*mcr*BC) Φ80*lac*ZΔM15 Δ*lac*X74 *rec*A1 *ara*D139 Δ(*ara-leu*)7697 *gal*U *gal*K *rps*L (Str^r) *end*A1 *nup*G	Invitrogen	Transformation host for pCR4-TOPO ligations. Contains *LacI*^{q}*ΔM15* on F' episome for blue/white screening.

Table 4-2 –Plasmid vectors for cloning and recombinant protein expression in *E. coli*.

Vector	Details	Source
pSC-A	Amp^r. Cloning vector for inserts with A overhangs	Stratagene
pSC-B	Amp^r. Cloning vector for blunt inserts	Stratagene
pCR4-TOPO	Amp^r, Kan^r. Cloning vector for inserts with A overhangs	Invitrogen
pGEX-5X1	Amp^r. Glutathione-S-transferase fusion protein vector (for N-terminal tagging)	GE Healthcare
pET28a(+)	Kan^r. 6XHistidine fusion protein vector (for N or C terminal tagging)	Novagen

Table 4-3 –Plasmid vectors for RNAi and recombinant protein expression in *T. brucei.*

Plasmid	Description	Reference / source
pT27^{Ti}A	Amp^{r}.Ble^{r}. RNAi vector. Gene fragment of choice is cloned in between opposing T7 promoters, in place of the *GFP* coding sequence. Vector is linearised for transfection by digestion with NotI and integrates into the *rRNA* locus.	(LaCount et al., 2000;LaCount et al., 2002)
pENT-6-Blast eGFP-TY	Amp^{r}. Bsd^{r}. Expression vector for N-terminal tagging at the endogenous locus. Contains TYGFPTY epitope tag. Incorporation of 5'UTR and 3'ORF DNA fragments for gene of choice at XbaI and BamHI sites displaces second TY epitope. Vector is linearised for transfection by digestion with a unique restriction site engineered into the 5'UTR and ORF oligonucleotides (sense and antisense, respectively).	(Kelly et al., 2007)
Orc-_6XHA_Ble	Amp^{r}. Ble^{r}. Expression vector for C-terminal tagging at the endogenous locus. Contains 6XHA epitope tag. Modification of pNAT$^{6myc}{}_{x}$ (Alsford and Horn, 2008). Vector is linearised for transfection by digestion with a unique restriction site engineered into the inserted gene of choice.	(Alsford and Horn, 2008)/ C. Tiengwe
pGL1278	Amp^{r}. Hyg^{r}. Inducible ty:PLK WT expression vector	(Hammarton et al., 2007)
pGL1279	Amp^{r}. Hyg^{r}. Inducible ty:PLK N169A expression vector	(Hammarton et al., 2007)

Table 4-4 -Plasmids generated in this study.

Plasmid	Description
pGL1785	Amp^r. *AIR9* (bases 1803-2215) in pSC-A amplified using oligonucleotides OL2696 and OL2697
pHG27	Amp^r. Ble^r. *AIR9* (bases 1803-2215) subcloned as HindIII / BamHI fragment from pGL1785 into same sites in pT27^{Ti}A
pHG108	Amp^r. *AIR9* 5' UTR (269 bases upstream from start codon) in pSC-A amplified using PR94 and PR95
pHG109	Amp^r. *AIR9* (bases 4-358) in pSC-A amplified using PR96 and PR97
pHG129	Amp^r. *AIR9* (bases 4-2979) in pSC-A amplified using PR226 and PR227
pHG172	Amp^r. Bsd^r. *AIR9* 5'UTR (269 bases upstream from start codon) and *AIR9* ORF (bases 4-358) subloned from pHG108 and pHG109 as XbaI / NheI or NheI / BclI fragments, respectively into BamHI / XbaI sites in pENT-6-Blast eGFP-TY in a threeway ligation
pHG182	Amp^r. Ble^r. *AIR9* (bases 2253-2979) subcloned as HindIII / XbaI fragment from pHG184 into same sites in Orc-_6XHA_Ble
pHG184	Amp^r. *AIR9* (bases 2253-2979) in pSC-A amplified using PR228 and PR229
pGL1525	Amp^r. Kan^r. *PLK WT* (bases 4-879) amplified from pGL1278 using OL2142 and OL2141 to produce a truncated protein comprising amino acids 2-294.
pGL1526	Amp^r. Kan^r. *PLK N169A* (bases 4-879) amplified from pGL1279 using OL2142 and OL2141 to produce a truncated protein comprising amino acids 2-294.
pGL1530	Amp^r. *PLK WT* (bases 4-879) subcloned from pGL1525 as a BamHI / XhoI fragment into same sites in pGEX-5X1
pGL1531	Amp^r. *PLK N169A* (bases 4-879) subcloned from pGL1526 as a BamHI / XhoI fragment into same sites in pGEX-5X1
pGL1780	Amp^r. Kan^r. *PLK WT* (bases 4-2289) in pCR4-TOPO amplified from pGL1278 with OL2138 and OL2139
pGL1781	Amp^r. Kan^r. *PLK N169A* (bases 4-2289) in pCR4-TOPO amplified from pGL1279 with OL2138 and OL2139
pHG3	Kan^r. *PLK WT* subcloned from pGL1780 as a NheI / XhoI fragment into same sites in pET-28a(+)
pHG4	Kan^r. *PLK N169A* subcloned from pGL1781 as a NheI / XhoI fragment into same sites in pET-28a(+)
pHG123	Kan^r. Site directed mutagenesis of pHG3 with PR126 and PR127 to generate *PLK T198V*
pHG148	Amp^r. *PLK* (bases 1291-2289) amplified from pGL1278 with OL2139 and PR172 to produce a truncated protein comprising amino acids 430-763
pHG152	Amp^r. pSC-B containing *PLK H705K K707A* (bases 4-2289) amplified as two PCR products from pGL1278 using OL2138 and PR171, and OL2139 and PR172 joined together by Gene SOEing PCR with OL2138 and OL2139
pHG153	Kan^r. *PLK* (bases 1291-2289) subcloned from pHG148 as a NheI / XhoI fragment into same sites in pET-28a(+)
pHG157	Kan^r. Site directed mutagenesis of pHG3 with PR124 and PR125 to generate *PLK T198A*
pHG158	Amp^r. Hyg^r. Site directed mutagenesis of pGL1278 with PR126 and PR127 to generate ty:*PLK T198V*
pHG163	Kan^r. Site directed mutagenesis of pHG3 with PR168 and PR169 to generate *PLK T198D*
pHG164	Amp^r. Hyg^r. Site directed mutagenesis of pGL1278 with PR168 and PR169 to generate ty:*PLK T198D*
pHG169	Kan^r. *PLK H705A K707A* subcloned from pHG152 as a NheI / XhoI fragment into same sites in pET28a(+)

4.2.1.2 Media and growth conditions

Strains were cultured at 37 ˚C in Luria-Bertani broth (L-broth) medium (Miller.J.H., 1972) or 2X-YT broth medium, with shaking at 200 rpm to ensure adequate aeration, or on L-agar (LA). Overnight cultures were obtained after 12-

16 hours of aerated growth; single bacterial colonies were visible on L-agar plates after the same period of growth.

L-broth comprised 86 mM NaCl, 10 gL^{-1} tryptone, and 5 gL^{-1} yeast extract. The pH of the medium was adjusted to pH 7.0 with NaOH. To generate L-agar, L-broth was supplemented with 15 gL^{-1} agar. L-agar plates were made by heating L-agar until homogenous in a microwave, allowing to cool to ~60 ˚C and pouring the warm medium into petri dishes. L-agar plates were stored at 4 ˚C for up to 1 month. 2X-YT broth comprised 171 mM NaCl, 16 gL^{-1} tryptone, and 10 gL^{-1} yeast extract, adjusted to pH 7.64 with NaOH.

Media were supplemented with antibiotics (from 1000X stock solutions) as appropriate to give the final concentrations: 100 μgml^{-1} ampicillin, 20 μgml^{-1} tetracycline, 25 μgml^{-1} chloramphenicol, and 25 μgml^{-1} kanamycin. Ampicillin and kanamycin were dissolved in dH20, while chloramphenicol and tetracycline were dissolved in 50 % ethanol. Antibiotic stock solutions were stored at -20 ˚C.

4.2.1.3 Determination of cell density

Cell density was determined by sampling 1 ml of the bacterial culture, placing in a cuvette (Fisher Scientific) and measuring the OD_{600nm} using a spectrophotometer (Shimadzu Biospec-mini DNA/RNA/protein analyser).

4.2.1.4 Storage of strains

Bacterial strains grown on L-agar plates were stored for up to 2 weeks at 4˚C. For long term storage, strains were maintained as glycerol stocks at -80 ◦C. To make a glycerol stock, 5-10 ml cells were harvested from an overnight culture by centrifugation at 5285 x *g* for 5 minutes at 4 ◦C to pellet the bacteria. The pellet was resuspended in a 1/10 volume of sterile L-broth and added to an equal volume of a 2 % peptone / 40 % glycerol mix. The glycerol stock was stored at -80 ◦C. When needed, a small amount of glycerol stock was defrosted and streaked onto an LA plate to give single bacterial colonies after overnight incubation at 37 ◦C.

4.2.2 Culture of T. brucei *parasites*

4.2.2.1 *T. brucei* strains

Details of *T. brucei* strains used and generated during this study are given in Table 4-5 and Table 4-6.

Table 4-5 -*T. brucei* strains used in this study.

Life cycle stage	Genotype	Description / application
Bloodstream form	Lister 427	Wild type
Procyclic form	Lister 427	
Bloodstream form	Lister 427 pLew13 pLew90	Tetracycline-inducible RNAi (Wirtz et al., 1999)
Procyclic form	Lister 427 pLew13 pLew29	
Procyclic form	Lister 427 pHD449	Tetracycline-inducible expression (Wirtz and Clayton, 1995;Biebinger et al., 1997)
Procyclic form	Lister 427 pHD449 pGL1278 Pool 2	Expression of ty:PLK WT (Hammarton et al., 2007)
Procyclic form	Lister 427 pHD449 pGL1279 Pool 2	Expression of ty:PLK N169A (Hammarton et al., 2007)

Table 4-6 -*T. brucei* strains generated in this study.

Life cycle stage	Genotype	Description / application
Procyclic form	Lister 427 pLew13 pLew29 pHG27 clone 4	*AIR9* RNAi
Procyclic form	Lister 427 pLew13 pLew29 pHG27 clone 5	
Procyclic form	Lister 427 pLew13 pLew29 pHG27 clone 4 pHG172 clone 2	*AIR9* RNAi and expression of tyGFP:AIR9 from endogenous locus
Procyclic form	Lister 427 pLew13 pLew29 pHG27 clone 5 pHG172 clone 2	
Procyclic form	Lister 427 pHG172 clone 2	Expression of tyGFP:AIR9 from endogenous locus
Procyclic form	Lister 427 pHG172 clone 3	
Procyclic form	Lister 427 pHG182 clone 1	Expression of AIR9:6XHA from endogenous locus
Procylic form	Lister 427 pHG182 clone 3	
Bloodstream form	Lister 427 pLew13 pLew90 pHG27 clone 1	*AIR9* RNAi
Bloodstream form	Lister 427 pLew13 pLew90 pHG27 clone 2	
Bloodstream form	Lister 427 pLew13 pLew90 pHG27 clone 1 pHG172 clone 2	*AIR9* RNAi and expression of tyGFP:AIR9 from endogenous locus
Bloodstream form	Lister 427 pLew13 pLew90 pHG27 clone 2 pHG172 clone 1	
Bloodstream form	Lister 427 pHG172 clone 8	Expression of tyGFP:AIR9 from endogenous locus
Bloodstream form	Lister 427 pHG172 clone 15	
Bloodstream form	Lister 427 pHG182 clone 1	Expression of AIR9:6XHA from endogenous locus
Bloodstream form	Lister 427 pHG182 clone 3	
Procyclic form	Lister 427 pHD449 pHG158 clone 6	Expression of ty:PLK T198V
Procyclic form	Lister 427 pHD449 pHG158 clone 7	
Procyclic form	Lister 427 pHD449 pHG164 clone 1	Expression of tyPLK T198D
Procyclic form	Lister 427 pHD449 pHG164 clone 2	

4.2.2.2 Media and growth conditions

Bloodstream form *T. brucei* parasites were cultured at 37 ˚C in HMI-9 medium (Section 4.2.2.2.1) in the presence of 5 % CO_2 and passaged to maintain mid-log phase growth (1 x 10^5 - 1 x 10^6 cellsml^{-1}). Procyclic form *T. brucei* parasites were grown at 27 ˚C in SDM-79 medium (Section 4.2.2.2.2) in the presence of 5 % CO_2 and passaged to maintain mid-log phase growth (1 x 10^6 - 1 x 10^7 cellsml^{-1}). Antibiotics were added to media as appropriate (Table 4-7) to select for integrated plasmid constructs or in the case of tetracycline, to induce the RNAi response in appropriate cell lines.

Table 4-7 –Antibiotic concentrations for the culture of *T. brucei*.
Final concentrations of antibiotics are given for both life cycle stages.

Drug	Procyclic form	Bloodstream form	Company
Neomycin	10 μgml^{-1}	2.5 μgml^{-1}	Calbiochem
Hygromycin	50 μgml^{-1}	5 μgml^{-1}	Calbiochem
Phleomycin	-	2.5 μgml^{-1}	Invivo Gen
Zeocin	10 μgml^{-1}	-	Calbiochem
Blasticidin	20 μgml^{-1}	10 μgml^{-1}	Calbiochem
Tetracycline	1 μgml^{-1}	1 μgml^{-1}	Sigma

For downstream analyses, trypanosomes were harvested by centrifuging at 600 x *g* (procyclic form) or 1500 x *g* (bloodstream form), and where required, cells were washed in phosphate buffered saline (PBS: 137 mM NaCl, 2.7 mM KCl, 8 mM Na_2HPO4 and 1.8 mM KH_2PO_4, adjusted to pH 7.4, procyclic form) or trypanosome dilution buffer (TDB: 20 nM Na_2HPO_4, 2 mM $NaH_2PO_4.2H_20$, 80 nM NaCl, 5 mM KCl, 1 mM $MgSO_4.7H_2O$, and 20 mM glucose, adjusted to pH 7.4, bloodstream form).

4.2.2.2.1 HMI9 medium

HMI-9 medium (Hirumi and Hirumi, 1989) was made by dissolving one pot of HMI9 powder (sufficient for 5 L HMI9, custom made by Invitrogen), 15 g $Na(CO_3)_2$ and 71.5 µl ß-mercaptoethanol in 4 L dH_2O and stored at 4 ˚C.

Prior to use, HMI-9 was supplemented with 10 % (v/v) heat-inactivated tetracycline-free foetal bovine serum (BioSera), 10 % (v/v) serum plus (JRH Biosciences), 500 Uml^{-1} penicillin and 50 μgml^{-1} streptomycin, and preheated to 37 ˚C.

4.2.2.2.2 SDM79 medium

SDM-79 medium (Brun and Schonenberger, 1979) was made by dissolving one pot of SDM79 powder (sufficient for 5 L SDM79, custom made by Invitrogen) and 10 g $Na(CO_3)_2$, in 4.5 L dH_2O, adjusting the pH to pH 7.3 with NaOH before adding 10 ml hemin stock (25 $mgml^{-1}$ in 50 mM NaOH) and storing at 4˚C. Prior to use, SDM-79 was supplemented with 10 % (v/v) heat-inactivated tetracycline-free fetal calf serum (BioSera), 500 Uml^{-1} penicillin and 50 μgml^{-1} streptomycin, and preheated to 27˚C.

4.2.2.3 Determination of cell density

A 10 µl sample of cell suspension (or an appropriate dilution) was loaded into the chamber of a Neubauer Improved haemocytometer, and at least 200 cells were counted by phase contrast microscopy. The concentration was determined using the following calculation: cells ml^{-1} = average number of cells counted per 1 mm^2 x 10^4 x dilution factor.

4.2.2.4 Storage of *T. brucei* strains

T. brucei parasites were typically passaged to maintain a density corresponding to the mid-log phase of growth for 3 -7 days prior to making stabilates. Cells (typically 10 ml of a mid-log phase culture) were harvested (Section 4.2.2.2 and resuspended in a 4 ml culture medium supplemented with 5 % (v/v) glycerol and 1 ml aliquots placed into cryotubes. Stabilates were frozen in an insulated container at -80 ˚C overnight before being transferred to liquid nitrogen. Stabilates removed from liquid nitrogen were slowly defrosted at room temperature before transferring to 10 ml pre-warmed HMI-9 or SDM-79 (without antibiotics). Parasites were grown in medium lacking antibiotics for 1 day following removal from stabilate before appropriate selective drugs were added.

4.3 Genetic manipulation

4.3.1 Transformation of bacterial cells

4.3.1.1 Production of chemically competent cells

From an appropriate overnight bacterial culture, cells were diluted 1/100 into 50 ml L-broth supplemented with the appropriate antibiotics and cultured at 37 ˚C with shaking at 200 rpm until the culture density reached an OD_{600nm} of 0.6. The culture was incubated on ice for 10 minutes, and then centrifuged at 957 x *g* for 15 minutes at 4 ˚C to pellet the bacteria. The pellet was resuspended in 16 ml cold RF1 buffer (100 nM RbCl, 50 mM $MnCl_2{\cdot}4H_20$, 30 mM CH_3COOK, 10 mM $CaCl_2$, and 15 % (v/v) glycerol, adjusted to pH 5.8 with acetic acid) by slow vortexing. The suspension was incubated on ice for 15 minutes, and then centrifuged at 775 x *g* for 15 minutes at 4 ˚C to pellet the bacteria. The pellet

was resuspended in 4 ml cold RF2 buffer (10 mM MOPS, 10 mM RbCl, 75 mM $CaCl_2 \cdot 4H_20$, and 15 % glycerol, adjusted to pH 6.8 by addition of NaOH) and incubated on ice for 1 hour. Cells were aliquoted (100 µl), frozen rapidly in a dry ice/ethanol slurry, and stored at -80 ˚C.

4.3.1.2 Transformation of chemically competent *E. coli* with plasmid DNA or ligation product

Competent cells (Section 4.3.1.1) were thawed on ice, before the addition of ß-mercaptoethanol (0.85 µl per 100 µl cells) and DNA (10 ng plasmid DNA or 5 µl of a ligation product). The cells were shaken gently to mix the DNA and incubated on ice for 15 minutes prior to a 45 second heat-shock at 42 ˚C. Following the heat-shock treatment, 500 µl L-broth were added, and the cells were incubated with shaking at 37 ˚C, 200 rpm for 30-60 minutes. To obtain single colonies, cells were harvested by centrifugation at 17 968 x *g* for 1 minute, resuspended in 100 µl L-broth and spread on an L-agar plate containing the appropriate selective antibiotic. To control for cell viability and efficacy of antibiotic selection, separate aliquots of competent cells received equivalent volumes of dH_20 instead of DNA and were grown on LA plates in the absence or presence of appropriate antibiotic, respectively.

To transform ligation products involving pSC-A/pSC-B or pCR4-TOPO vectors (Table 4-2), SoloPack Gold competent cells (Stratagene), or TOP10 cells (Invitrogen), respectively (Table 4-1), were used in accordance with the manufacturers' instructions.

4.3.2 Transfection of T. brucei

4.3.2.1 Purification of linearised plasmid DNA for transfection of *T. brucei* parasites

To prepare plasmid DNA for transfection, 100 µg was digested with the appropriate restriction enzyme (Section 4.5.2) and the digestion efficiency verified by analysis of 1 µl of the digestion product by agarose gel electrophoresis (Section 4.5.1) prior to purification. To purify the DNA, 1/2 volume of phenol and 1/2 volume of chloroform:isoamyl alcohol (24:1) were

added and the mixture was vortexed for 30 seconds prior to being centrifuged at 17 968 x *g* at room temperature for 2 minutes to separate the lower organic phase (containing precipitated proteins) from the upper aqueous layer (containing the DNA). The aqueous layer was decanted and further purified by the addition of 1 volume chloroform:isoamyl alcohol, and centrifuging as described above. The aqueous layer was decanted, and the chloroform extraction step repeated. To precipitate the extracted DNA, 1/10 volume 3 M CH_3COONa (pH 5.2), and 1 volume of isopropanol were added to the aqueous phase, and the mixture was vortexed before the precipitated DNA was pelleted by centrifugation at 17 968 x *g* for 15 minutes at 4 ˚C. The DNA pellet was washed in 1 ml ice cold 70 % ethanol, following which the ethanol solution was decanted under a sterile hood, and the DNA pellet was air dried and resuspended in dH_2O to a final concentration of 1 $\mu g \mu l^{-1}$. Linearised plasmid DNA was stored at -20 ˚C prior to transfection.

4.3.2.2 Transfection of *T. brucei* cells using an Amaxa Nucleofector

Cells were grown to mid-log phase and 3-5 x 10^7 cells were harvested by centrifugation (Section 4.2.2.2) of an appropriate volume of cell culture. The medium was decanted, and any residual medium removed using a pipette before the cells were resuspended in 100 µl Amaxa human T-cell nucleofactor solution (Amaxa Biosystems) and transferred to a cuvette (Amaxa Biosystems) containing 10 µg purified linearised DNA (Section 4.3.2.1). The DNA/cell suspension was mixed by slow pipetting before transferring to an Amaxa Nucleofector II machine and transfecting the parasites using programme X-001. The transfected parasites were transferred immediately to 30 ml (bloodstream form) or 10 ml (procyclic form) of warmed medium, (which for procyclic form cells was supplemented with 30 % conditioned medium (prepared by growing procyclic form Lister 427 wild type parasites in SDM-79 to a density of 1 x 10^7 cells ml-1, pelleting the cells by centrifugation (Section 4.2.2.2), decanting and filter sterilising the spent medium). Selection of genetically modified parasites was carried out by limiting dilution and growth in the presence of the appropriate selective antibiotic (Table 4-4 and Table 4-7). The exact method used varied according to life cycle stage. For bloodstream form parasites, immediately after transfection, 10 fold serial dilutions (10-1 – 10-3) were prepared before plating 1 ml aliquots in 24 well plates and allowing cells to recover for 6 hours at 37 ˚C prior to the

addition of an equivalent volume of medium containing a 2X concentration of selective antibiotic (Table 4-7). Clonal parasites were typically obtained after 1 week of selection and growth at 37 ˚C. Clonal cell lines were deemed to be those populations that derived from a well on a plate where less than 10 % of the wells contained living parasites after the selection period. For procyclic form parasites, immediately following transfection, three 10^{-1} dilutions were prepared from the neat cell suspension of transfected parasites and the cells were allowed to recover for 16 hours at 27 ˚C before addition of the appropriate selective antibiotic. Appropriate dilutions (10^{-1} – 10^{-3}) in SDM79/30 % conditioned medium were prepared from the neat culture flask and the three independent 10^{-1} dilution flasks, and 100 µl aliquots plated in 96 well plates Clonal parasites were typically obtained 3 weeks following transfection.

Once clonal cell lines had been obtained, culture volumes were gradually increased, with cell lines being transferred to larger well plates and flasks as appropriate, until stabilates could be generated (Section 4.2.2.4).

4.4 DNA preparation

4.4.1 *Preparation of plasmid DNA from* E. coli

The QIAprep spin Miniprep or Midi prep kits (Qiagen) were used for small or large scale purification of plasmid DNA, from 3 ml or 50 ml overnight culture, respectively. Purification of plasmid DNA was carried out in accordance with the manufacturer's instructions.

4.4.2 Preparation of genomic DNA from T. brucei

Genomic DNA was extracted from *T. brucei* cells using the DNeasy blood and tissue kit (Qiagen). 5 x 10^6 parasites were harvested (Section 4.2.2.2) and washed once in TDB (Section 4.2.2.2, bloodstream form cells) or PBS (Section 4.2.2.2, procyclic form cells). DNA was extracted from the cell pellets according to the manufacturer's instructions.

4.4.3 Determination of DNA concentration

DNA concentration was determined using a spectrophotometer (Eppendorf biophotometer) or Nanodrop (Nanodrop 1000, Thermoscientific) by measuring the absorption at OD_{260nm}. Ratios of OD_{260nm}/OD_{280nm} were also obtained to assess the purity of the DNA, with a ratio of 1.8 – 2 indicated low levels of protein contamination. Alternatively, when an estimate of DNA concentration was sufficient, 1 µl of DNA was analysed by agarose gel electrophoresis (Section 4.5.1). The mass of DNA was estimated from its intensity relative to the 1650 bp band of the 1 kb plus ladder (Section 4.5.1), which had a known mass of 41 ng when 10 µl ladder were loaded.

4.5 DNA manipulation

4.5.1 Agarose gel electrophoresis

DNA was prepared for agarose gel electrophoresis by the addition of 6X DNA loading buffer (15 % Ficoll, 0.25 % xylene cyanol and 0.25 % bromophenol blue) to give a final concentration of 1X. Agarose gels were prepared by adding agarose (0.5-1 % (w/v)) to 0.5X TBE buffer (44.6 mM Tris base, 44.5 mM boric acid and 1 mM EDTA) and heating in a microwave oven until all agarose dissolved. The agarose/TBE solution was cooled before adding SYBR Safe stain (Invitrogen; diluted 1/30,000 from the 10,000X stock) and pouring into a suitable gel tray. Once set, the gel was placed in a gel tank and immersed in 0.5X TBE buffer prior to the loading of suitably prepared DNA samples and 10 µl of 1 kb plus DNA ladder (0.052 $\mu g \mu l^{-1}$ in 1X DNA loading buffer, Invitrogen). DNA was electrophoresed at 100 V for typically 45 minutes and visualised under blue or UV light.

4.5.2 Restriction endonuclease digestion of DNA

Restriction endonucleases and buffers were purchased from New England Biolabs (NEB), with the exception of AspI, which was obtained from Roche.

To confirm or check the identity of plasmid DNA, 0.2 µg plasmid DNA was incubated with 10 U of the chosen restriction endonuclease, 1X appropriate buffer and, if recommended by the manufacturer, 1X bovine serum albumin (BSA, NEB) in a total volume of 10 µl at the appropriate temperature for 1 hour.

Variations in this protocol were employed for digestion of plasmid DNA for subcloning (which typically involved digestion of 2 µg DNA with 20 U enzyme in a total volume of 50 µl for 2 hours) and for linearising DNA for transfection of *T. brucei* parasites (which typically involved digestion of 100 µg DNA with 40 U enzyme in a total volume of 500 µl for 16 hours). In all cases, digested DNA was analysed by agarose gel electrophoresis (Section 4.5.1) prior to using it for downstream applications.

4.5.3 Extraction of restriction endonuclease digested DNA fragments from agarose gels

To purify DNA fragments (eg from a restriction endonuclease digestion (Section 4.5.2) from an agarose gel, the desired fragment(s) was/were visualised under blue light and excised from the gel using a clean scalpel blade. The gel slices were weighed and DNA was extracted from them using the QIAEX spin gel extraction kit (Qiagen) according to the manufacturer's instructions.

4.5.4 Polymerase chain reaction (PCR)

PCR was used for multiple applications, including amplification of specific regions of plasmid (Section 4.4.1) or genomic (Section 4.4.2) DNA, mutation of genes by Gene SOEing (splicing by overlap extension (Horton et al., 1990)) or site directed mutagenesis (Section 4.5.5), and in colony screening of *E. coli*. PCR reactions were carried out in a 'pX2 Therma Cycler' PCR machine (Thermo Electron Coorporation) using the active tube system, or for a gradient PCR, the heat block system. PCR reactions used Taq DNA polymerase (NEB), or if the target sequence was to be used subsequently for cloning, the high fidelity proof reading polymerases Pfu Turbo (Stratagene) or Phusion DNA polymerase (Finnzymes) which have 3'→5' exonuclease activity were used.

Typical reaction mix compositions are given for each enzyme in Table 4-8.

Table 4-8 -Typical compositions of PCR reaction mixes.

	PCR enzyme		
Reagent	**Taq**	**Pfu Turbo**	**Phusion**
Buffer	1X Taq PCR mix*	1X Pfu Turbo buffer	1X Phusion HF buffer
dNTPs (dATP, dCTP, dGTP & dTTP)	Included in PCR mix	250 µM	200 µM
Each oligonucleotide	20 ng	20 ng	20 ng
DNA**	1-200 ng	1-200 ng	1-200 ng
Enzyme	1U	0.5U	0.4U
Final volume	20 µl	20 µl	20 µl

*10 X Taq PCR mix: 1.13 $mgml^{-1}$ BSA, 450 mM Tris (pH 8.8), 110 mM $(NH_4)_2SO_4$, 45 mM $MgCl_2$, 0.47 % (v/v) ß-mercaptoethanol, 44 µM EDTA (pH 8) and 10 mM dNTPs (Invitrogen).

** genomic or plasmid DNA, or PCR product(s), or alternatively a small portion of an *E. coli* colony

PCR reaction cycles were typically as follows:

1 cycle of 95 °C for 30 s;

25-35 cycles of 95 °C for 50 s, T_m for 50 s, T_e for 1-2 minutes;

1 cycle of T_e for 5-10 minutes.

The annealing temperature (T_m) was adjusted according to the melting points of the primers. Extension temperatures (T_e) were 68 °C (Phusion DNA polymerase) or 72 °C (Taq and Pfu Turbo polymerases) and the extension time was adjusted according to the length of the product being amplified. For colony PCR, the length of the initial denaturation step was increased to 5 minutes to ensure cell lysis. The oligonucleotides used for PCR are listed in Table 4-9 and Table 4-10.

Table 4-9 -*AIR9* oligonucleotides.

Oligonucleotide	5'→3' sequence and restriction site	Properties
OL2696	GATGAAGCTTGGATGTGGGCAAGTGTTTG HindIII	Sense oligonucleotide to amplify *AIR9* (bases 1803-2215)
OL2697	GAGGGGATCCGAAGTTCGTCTGGGGAATG BamHI	Antisense oligonucleotide to amplify *AIR9* (bases 1803-2215)
PR94	CCTGCTAGCCGTCATCTTCGGTGGCAACA NheI	Sense oligonucleotide to amplify a region of the 5' AIR9 UTR (269 bases upstream from the start codon of *AIR9*)
PR95	CGCTGATCACGTGTATACCAGAAATAACC BclI	Antisense oligonucleotide to amplify a region of the 5' AIR9 UTR (269 bases upstream from the start codon of *AIR9)*
PR96	GCGTCTAGAAGTGCGTCTGCGATAAGGCG XbaI	Sense oligonucleotide to amplify *AIR9* (bases 4- 358)
PR97	CCGCTAGCCAATCCCTCAAAACTGT NheI	Antisense oligonucleotide to amplify *AIR9* (bases 4-358)
PR226	GGACGCGT**ATG***GAGGTCCATACTAACCAGGA CCCACTTGAC*AGTGCGTCTGCGATAAGGCG MluI	Sense oligonucleotide to amplify *AIR9* (bases 4-2979) and introduce a start codon (bold) and TY epitope tag (doubly underlined)
PR227	CATGATCACTATGCGCCGTCAGTCCGGG BclI	Antisense oligonucleotide to amplify *AIR9* (bases 4-2979)
PR228	GGAAGCTTGAGTTGGAAGTGGAGTAC HindIII	Sense oligonucleotide to amplify *AIR9* (bases 2253-2976)
PR229	CGCTCTAGATGCGCCGTCAGTCCG XbaI	Antisense oligonucleotide to amplify *AIR9* (bases 2253-2976)

Table 4-10 -*PLK* oligonucleotides.

Oligonucleotide	5'→3' sequence and restriction site or mutation	Properties
OL2138	CCAAGCTAGCATGCACGCAACCGCTGAGAC NheI	Sense oligonucleotide to amplify *PLK*
OL2139	GGTTCTCGAGCTAAATATCACGGTTTTGTATG XhoI	Antisense oligonucleotide to amplify *PLK*
OL2141	CCCCTCGAGCTAATGTGAACGAATTTCCAGC XhoI	Antisense oligonucleotide to amplify the kinase domain of *PLK* (bases 4-879)
OL2142	CCAAGGATCCACGCAACCGCTGAGACGTG BamHI	Sense oligonucleotide to amplify *PLK*
PR124	CGGGGAGCGGAAACGC**GC**C**C**ATTTGTGGCACGCCCA T198A	Sense oligonucleotide for site directed mutagenesis of *PLK* bases 592 and 594 (A→G and T→C respectively)
PR125	TGGGCGTGCCACAAAT**GGC**GCGTTTCCGCTCCCCG T198A	Antisense oligonucleotide for site directed mutagenesis of *PLK* bases 592 and 594 (A→G and T→C respectively)
PR126	CGGGGAGCGGAAACGC**GTC**ATTTGTGGCACGCCCA T198V	Sense oligonucleotide for site directed mutagenesis of *PLK* bases 592-594 (ACT→GTC)
PR127	TGGGCGTGCCACAAAT**GAC**GCGTTTCCGCTCCCCG T198V	Antisense oligonucleotide for site directed mutagenesis of *PLK* bases 592-594 (ACT→GTC)
PR168	CGGGGAGCGGAAACGC**GAC**ATTTGTGGCACGCCC T198D	Sense oligonucleotide for site directed mutagenesis of *PLK* bases 592-594 (ATC→GAC)
PR169	TGGGCGTGCCACAAAT**GTC**GCGTTTCCGCTCCCCG T198D	Antisense oligonucleotide for site directed mutagenesis of *PLK* bases 592-594 (ATC→GAC)
PR170	CTATTCAGGTTTGTTTT**GCC**GAT**GCA**GCGGAGGTT H705A K707A	Sense oligonucleotide to amplify PLK (bases 4-2130) for Gene SOEing PCR to mutate bases 2113-2115 (CAT→GCC) and bases 2119-2121 (AAG→GCA)
PR171	CGAACTTAGAATAACCTCCGC**TGC**ATC**GGC**AAAACAA H705A K707A	Antisense oligonucleotide to amplify *PLK* (bases 2095-2289) for Gene SOEing PCR to mutate bases 2113-2115 (CAT→GCC) and bases 2119-2121 (AAG→GCA)
PR172	CGGCTAGCGCGGTGAGCATCCCGTCACC NheI	Sense oligonucleotide to amplify a C-terminal region of *PLK* comprising the putative polo-box cap and downstream sequence (bases 1291-2289)

PCR reactions were analysed by agarose gel electrophoresis (Section 4.5.1). Optimisation of PCR reactions was frequently required, which involved alterations to the annealing temperature (increasing the annealing temperature increased the specificity of the reactions giving a cleaner PCR product, whilst decreasing the annealing temperature increased yield but sometimes produced multiple PCR products), the extension time (to allow the completion of more PCR reactions), the number of cycles (to increase yield), or the efficiency (which involved the addition of 5 % dimethyl sulphoxide (DMSO) to decrease the secondary structure of the DNA, allowing greater access for the primers).

4.5.4.1 Addition of 3' adenine residues

PCR products generated using Pfu Turbo or Phusion DNA polymerase were generally used for downstream cloning procedures. These enzymes produce PCR products with blunt ends. Thus, these products were either cloned into the blunt

ended cloning vector pSC-B (Strataclone), or were modified by the addition of a 3` A tail to allow cloning into vectors pSC-A (Strataclone) and pCR4-TOPO (Invitrogen), which possess 5' U overhangs (Table 4-2). To A-tail PCR products, 1 U Taq DNA polymerase was added to the PCR reaction mix and the mix was incubated at 72 °C for 8-10 minutes before placing the PCR product on ice and proceeding with the ligation reaction.

4.5.4.2 Purification of PCR products

PCR product purification was carried out before performing Gene SOEing PCR reactions (Section 4.5.4). PCR products were purified using the QIAquick PCR purification kit (Qiagen) according to the manufacturer's instructions.

4.5.5 Site-directed mutagenesis

Site-directed mutagenesis was performed using the QuikChange II Site-Directed Mutagenesis kit (Stratagene) according to the manufacturer's instructions. Oligonucleotides (Table 4-10) containing the desired mutation were designed according to the parameters recommended by the manufacturer. Following transformation of the mutagenised plasmid into XL1-Blue supercompetent cells (Stratagene), plasmid DNA was prepared (Section 4.4.1) from selected colonies and analysed by DNA sequencing (Section 4.5.8) to confirm the introduction of the desired mutation and the absence of any other changes to the sequence of the mutagenised gene.

4.5.6 Cloning of PCR products into generic cloning vectors

PCR products were routinely ligated into a generic cloning vector (pSC-A, pSC-B or pCR4-TOPO; Table 4-2) according to the manufacturers' instructions to facilitate sequencing of the PCR product and to provide a source of sequenced PCR product for use in downstream subcloning applications. Ligations were transformed into SoloPack Gold (pSC-A/pSC-B ligations) or TOP10 (pCR4-TOPO ligations) cells according to the manufacturers' guidelines, and to facilitate the identification of colonies harbouring inserts, transformed cells were plated onto LA plates spread with 40 µl 5-bromo-4-chloro-3 indolyl-ß-D galactopyranoside (X-Gal; 2% (w/v) in dimethylformamide). The multiple cloning site within each

cloning vector is located within the *LacZ* gene. Colonies harbouring empty vectors should retain a functional *LacZ* gene and therefore be able to metabolise X-Gal to a blue product, while colonies harbouring vectors containing an insert will have a disrupted LacZ gene and remain white. Further screening of white colonies was performed by colony PCR (Section 4.5.4) and by appropriate restriction endonuclease digests of DNA preparations (Section 4.4.1) from the colonies (Section 4.5.2). The sequence of the PCR products was also checked by DNA sequencing (Section 4.5.8) to confirm that no mutations had been introduced during the PCR.

4.5.7 Subcloning of PCR products from generic cloning vectors into destination plasmids

PCR-amplified DNA fragments were excised from the generic cloning vectors pSC-A, pSC-B or pCR4-TOPO (Table 4-2) by appropriate restriction endonuclease digestion (Section 4.5.2), analysed by agarose gel electrophoresis (Section 4.5.1) and purified from agarose gels (Section 4.5.3) before being ligated into the appropriate destination vector (also appropriately digested, analysed and purified). Where required, the destination vector was treated with calf intestinal alkaline phosphatase (CIP) to prevent the vector self-ligating during the ligation reaction. Following restriction endonuclease digestion of the destination vector, 1 U CIP was added to the reaction, before incubating it at 37 ˚C for 1 hour to remove 5` phosphate groups and then heating the reaction to 65 ˚C for 15 minutes to inactivate CIP.

To determine the appropriate relative amounts of insert and vector to use for the ligation reaction, the concentration of the purified DNA fragments was first determined (Section 4.4.3) before using the formula below (Equation 1) to calculate the desired quantities. Generally a ratio of 1:3 (insert:vector) was used for ligations, and to control for self-ligation of the vector, a separate reaction comprising only vector was carried out.

Equation 1 -Formula to calculate quantities of insert for ligation of DNA fragments into plasmids.

$$\frac{(100\ ng\ vector \times\ kb\ insert)}{(kb\ vector)} \times \frac{Ratio\ of\ insert}{Ratio\ of\ vector} = ng\ insert$$

$$\frac{(100\ ng\ vector \times\ kb\ insert)}{(kb\ vector)} \times \frac{Ratio\ of\ insert}{Ratio\ of\ vector} = ng\ insert$$ To ligate the DNA fragments, 1X T4 DNA ligase buffer and 0.4 U of T4 DNA ligase were added to the DNA fragments and sterile dH_2O was added to a final volume of 10 µl. The ligation reaction was incubated for 16 hours at 17 ˚C prior to transformation into XL-1Blue *E. coli* (Section 4.3.1). Colony PCR (Section 4.5.4) was used to identify colonies harbouring plasmids with the desired insert, before overnight cultures were set up for selected colonies to facilitate DNA preparation (Section 4.4.1) and restriction digests (Section 4.5.2) to check that the ligation had been successful. Where appropriate, plasmids were also analysed by DNA sequencing (Section 4.5.8).

4.5.8 DNA sequencing

DNA sequencing was performed by the University of Dundee sequencing service (http://www.dnaseq.co.uk/home.html), using an ABI automatic sequencer. The oligonucleotides used for DNA sequencing are listed in Table 4-11.

Table 4-11 -Oligonucleotides for DNA sequencing

Oligonucleotide	5'→3' sequence	Properties
M13 Fwd (-20)	GTAAAACGACGGCCAGT	Universal sequencing oligonucleotide
M13 Rev	GGAAACAGCTATGACCATG	Universal sequencing oligonucleotide
T7	TAATACGACTCACTATAGGG	Universal sequencing oligonucleotide
T7 terminator	TATGCTAGTTATTGCTCAG	3' pET-X sequencing oligonucleotide (binds at the 3' end of the multiple cloning site)
OL42	GGGCTGGCAAGCCACGTTTGGTG	5' pGEX-5X1 sequencing oligonucleotide (binds within the GST coding sequence)
OL43	CCGGGAGCTGCATGTGTCAGAGG	3' pGEX-5X1 sequencing oligonucleotide (binds at the 3' end of the multiple cloning site)
OL2015	GGTTGACGGCGTTGCGGTG	*PLK* antisense oligonucleotide
OL2223	CAGTTCACGCCGCCGTCAGC	*PLK* sense oligonucleotide
OL2224	GCCACCCGCACACAAACC	*PLK* sense oligonucleotide
PR163	CCCAGTTACCTTCAAGGTTTCTGG	*AIR9* sense oligonucleotide
PR164	GCGGTACAGAGGGTGAGAGC	*AIR9* sense oligonucleotide
PR165	CGGTACTCGTAGTCACCGGC	*AIR9* antisense oligonucleotide
PR166	GCCAAACACTTGCCCACATCC	*AIR9* antisense oligonucleotide
PR167	CCCGCAGCGCCAAGTTCTGC	*AIR9* antisense oligonucleotide

4.6 Protein techniques

4.6.1 Polyacrylamide gel electrophoresis

Polyacrylamide gel electrophoresis (PAGE) was used to separate denatured proteins according to their electrophoretic mobility. Both NuPAGE (Invitrogen) and sodium dodecyl sulphate PAGE (SDS PAGE) systems were used and are described below. To determine the molecular weight of proteins analysed using either buffer system, the unstained protein standard Benchmark protein ladder (Invitrogen) prepared according to the manufacturer's instructions, or prestained protein standard See Blue Plus 2 ladder (Invitrogen) were used for Coomassie staining and Western blotting, respectively.

4.6.1.1 SDS PAGE

A 12 % SDS PAGE separating gel was prepared by adding all the reagents described with the exception of TEMED and ammonium persulphate (Table 4-12), mixing and then adding the final components and mixing again before pouring the gel into a gel case (Invitrogen) and covering with a thin layer of isopropanol. Once the separating gel had set, the 4 % stacking gel was prepared. The stacking gel components with the exception of TEMED and ammonium persulphate were mixed (Table 4-13), before adding the final reagents and mixing again. The isopropanol layer was decanted, the stacking gel poured into the gel case, and a comb inserted. The set gels were used immediately or stored at 4 ˚C in moist conditions for up to 1 week.

Table 4-12 -12 % Separating gel.

Reagent	Volume
1.5 M Tris HCl pH 8.8	2.5 ml
20 % (w/v) SDS	50 µl
30 % / 0.8 % (w/v) Acrylamide / Bis acrylamide	4 ml
10 % (w/v) Ammonium persulphate	50 µl
TEMED	5 µl
dH_2O	3.4 ml

Table 4-13 -4 % Stacking gel.

Reagent	Volume
1.5 M Tris HCl pH 8.8	2.5 ml
20 % (w/v) SDS	50 µl
30 % / 0.8 % (w/v) Acrylamide / Bis acrylamide	4 ml
10 % (w/v) Ammonium persulphate	50 µl
TEMED	5 µl
dH_2O	3.4 ml

Samples were prepared for SDS PAGE by adding Laemmli loading dye (4 X Laemmli buffer: 20 mM Tris, 10 % (w/v) SDS, 40 % (v/v) glycerol, 28 % (v/v) β-mercaptoethanol, 0.2 % Bromophenol blue), to a final concentration of 1X, and boiling for 3 minutes. Laemmli buffer was stored at 4 ˚C. For electrophoresis, gels were immersed in SDS running buffer (25 mM Tris, 250 mM glycine and 0.1 % SDS). After loading the samples, gels were electrophoresed at 200 V for approximately 1 hour at room temperature.

4.6.1.2 NuPAGE

4-12 % Bis-Tris gradient gels or 12 % Bis-Tris gels (Invitrogen) were used with a 1X MES running buffer (Invitrogen). Prior to running the gels, an antioxidant solution was added to the inner chamber (according to the manufacturer's instructions). Samples were prepared for NuPAGE by adding NuPAGE sample buffer (Invitrogen) to a final concentration of 1X and heating to 70 ˚C for 10 minutes. NuPAGE gels were electrophoresed at 200 V for approximately 45 minutes.

4.6.2 Coomassie staining

Following PAGE, proteins were stained by incubating the SDS PAGE/NuPAGE gels in a solution containing 0.25 % Coomassie Blue R-250, 10 % acetic acid, and 45 % methanol for at least 2 hours at room temperature before destaining with 10 % acetic acid, and 45 % methanol for approximately 2 hours at room temperature. Stained gels were dried using a BioRad gel dryer (model 583) between filter paper and cellophane, or air dried between pre-wetted cellophane sheets.

4.6.3 Western blotting

To analyse proteins by Western blotting, proteins were first transferred from PAGE gels (Section 4.6.1) onto PVDF or nitrocellose membrane by electrotransfer.

PVDF transfer membrane (Perkin Eimer) or Hybond ECL nitrocellulose membrane (GE Healthcare), were prepared by incubating for 10 minutes in 100 % methanol or transfer buffer, respectively. For SDS-PAGE gels, transfer buffer comprised 1X SDS-PAGE running buffer and 20% methanol, while for NuPAGE gels, 1X NuPAGE transfer buffer (Invitrogen) supplemented with 20 % methanol was used. The transfer module (Invitrogen) was assembled by placing a layer of transfer buffer-soaked sponges, soaked filter paper (2 layers) and the protein gel into the module and covering with prepared membrane, soaked filter paper (2 layers) and soaked sponges. The assembled module was inserted into the gel tank and transfer buffer was added to cover the membrane, gel and sponges, before filling the outer compartment with dH_2O. Transfer was carried out at 30 V (constant voltage) for 2 hours at room temperature. Following transfer, proteins

were visualised by staining with Ponceau reagent at room temperature for 5 minutes before washing in dH_2O to reveal the stained proteins.

Following transfer and Ponceau staining, membranes were blocked in the appropriate blocking solution (PBS-T/milk or TBS-T/BSA, see Section 4.6.3.1) for 2 hours at room temperature or for 16 hours at 4 ˚C. The blocking solution was decanted, the blot washed briefly in PBS-T or TBS-T before primary antibody diluted appropriately in blocking solution (Table 4-14) was added and the blot incubated for 2 hours at room temperature on a shaking platform or for 16 hours at 4 ˚C. Blots were washed three times for 10 minutes at room temperature in PBS-T or TBS-T on a shaking platform to remove unbound antibody. Membranes were then incubated, shaking, in an appropriate dilution of secondary antibody (Table 4-15) in PBS-T/milk or TBS-T/BSA for 45 minutes at room temperature. The membranes were then washed once for 30 minutes and twice for 10 minutes in PBS-T or TBS-T before adding a chemiluminescent detection agent (Pierce). West Dura reagent was generally used to detect *T. brucei* proteins from cell lysates, while West Pico reagent was used for analysing recombinant proteins. However, occasionally, where a higher level of sensitivity was required, Supersignal West Femto reagent was used. Blots were incubated with the chemiluminescent detection reagents (prepared according to the manufacturer's instructions) for 5 minutes, before being drained and exposed to X-ray film (Kodak). Films were processed using an X-Omat automatic developer machine.

4.6.3.1 Buffer solutions

PBS-T: PBS (Section 4.2.2.2) plus 0.5% (v/v) Tween 20

PBS-T/milk: PBS-T plus 5% (w/v) Marvel skimmed milk powder

Tris buffered saline (TBS): 500 mM NaCl and 20 mM Tris-Cl. TBS-T: TBS plus 0.5% (v/v) Tween 20

TBS-T/BSA: TBS-T plus 3% bovine serum albumin

4.6.3.2 Antibodies for Western blotting

Table 4-14 -Primary antibodies for Western blotting.

Antibody	Source	Stock	Dilution
Anti-GST (B-14) mouse monoclonal IgG1	Santa Cruz Bio technology	0.1 $\mu g ml^{-1}$	1/1000
Anti-tetra-his mouse monoclonal IgG1	Qiagen	0.2 $\mu g ml^{-1}$	1/2000
Anti-phosphoserine rabbit polyclonal	Zymed laboratories	0.25 $mg ml^{-1}$	1/250
Anti-phosphothreonine rabbit polyclonal	Zymed laboratories	0.25 $mg ml^{-1}$	1/250
Anti-GFP mouse monoclonal IgG2a	Santa cruz Bio technology	200 $\mu g ml^{-1}$	1/1000-1/2000
Anti-HA rat monoclonal (clone 3F10)	Roche	100 $\mu g ml^{-1}$	1/1000
Anti-EF1-α mouse monoclonal (clone CBP-KK1)	Millipore	1 $mg ml^{-1}$	1/25 000
Anti-β-tubulin mouse monoclonal IgG2b (clone KMX)	Millipore	1 $mg ml^{-1}$	1/4000
Anti-PFR A /PFR C mouse monoclonal (clone L13D6)	Gull laboratory (Bastin et al., 1996b)	Purified antibody	1/1000
Anti-oligopeptidase B (OPB) sheep polyclonal	Mottram laboratory	Purified serum	1/1000
Anti-TY mouse monoclonal IgG1 (clone BB2)	Matthews laboratory (Bastin et al., 1996a)	Neat antibody	1/50

Table 4-15 -Secondary antibodies for Western blotting.

Antibody	Company	Stock	Dilution
Anti-mouse IgG horseradish peroxidise (HRP) conjugate	Promega	1 $mg ml^{-1}$	1/10 000
Anti-sheep IgG HRP conjugate	Santa cruz Bio technology	400 $\mu g ml^{-1}$	1/10 000
Anti-rabbit IgG HRP conjugate	Promega	1 $mg ml^{-1}$	1/10 000
Anti-rat IgG HRP conjugate	Sigma	-	1/10 000

4.6.4 Recombinant protein purification from bacteria

4.6.4.1 Expression of recombinant proteins in *E. coli*

The expression of recombinant proteins was carried out using BL21-derived *E.coli* strains (Table 4-1). Overnight cultures of appropriate bacterial strains were diluted 1/100 in L-broth and grown at 37 ˚C, shaking at 200 rpm to a density of 0.6 -1 OD_{600nm} (Section 4.2.1.3). Cultures were cooled, if necessary, to the expression temperature (optimised individually for each protein, but between 15 ˚C-37 ˚C) before protein expression was induced by the addition of isopropyl-beta-D-thiogalactopyranoside (IPTG) to a final concentration (0.5 mM – 1 mM, as optimised for each individual protein, see Section 7.8.2). After an appropriate period of growth under the optimal conditions for expression, cells were harvested by centrifugation at 5285 x *g* for 10 minutes at 4 ˚C. The cells were resuspended in a 1/50 or 1/20 volume of ice cold lysis buffer. For 6XHis tagged proteins, this comprised 50 mM NaH_2PO_4, 300 mM NaCl, 10 mM imidazole, adjusted to pH 8 using NaOH, while for GST-tagged proteins, PBS was used. The cell suspension was incubated with lysozyme (1 $mgml^{-1}$) and DNAseI (5 μgml^{-1}) in the presence of 1X complete EDTA free protease inhibitor cocktail (Roche) on ice for 1 hour. The resulting lysate was divided into 5 ml aliquots and immediately placed in an ice/water slurry before sonicating for 18 cycles of 10 seconds on/10 seconds off using a Soniprep 150 sonicator at 22 µ amplitude. The insoluble and soluble fractions were separated by centrifugation at 17 418 x *g* for 20 minutes at 4 ˚C.

4.6.4.2 Purification of recombinant proteins from *E. coli*

4.6.4.2.1 Purification of His-tagged proteins

6XHis tagged proteins were purified using 250 µl of a 50% slurry of nickel NTA beads (Qiagen) per ml of cleared cell lysate. Beads were prepared by washing them in 16 bed volumes of wash buffer (50 mM NaH_2PO_4, 300 mM NaCl, 20 mM imidazole, adjusted to pH 8 using NaOH) before transferring them to a 5 ml disposable polypropylene column (Pierce). The washed beads were incubated with the soluble fraction of cell lysate (Section 4.6.4.1) for 1 hour on a rotary mixer at 4 ˚C in order to allow 6XHis-tagged proteins to bind. The lysate was then drained, the flow through fraction containing unbound proteins collected,

and the beads washed in 16 bed volumes of chilled wash buffer to remove the remaining traces of unbound proteins. Elution was carried out by incubating the beads and interacting proteins with 1 bed volume of cold elution buffer (50 mM NaH_2PO_4, 300 mM NaCl, 250 mM imidazole, adjusted to pH 8 using NaOH) for 15 minutes, before collecting the proteins by draining the column. This was repeated four times. To determine the efficiency of the purification, samples were collected at each stage and prepared for PAGE (Section 4.6.1) and analysed by Coomassie staining (Section 4.6.2) and/or by Western blotting (Section 4.6.3) with anti-tetra-His antibody (Table 4-14).

4.6.4.2.2 Purification of GST-tagged proteins

GST-tagged proteins were purified using glutathione sepharose beads (GE Healthcare). A 75 % slurry of glutathione sepharose beads was centrifuged at 500 x *g* to and the beads were washed in cold PBS (Section 4.2.2.2) and centrifuged again (as above), before being resuspended in an appropriate volume of PBS to achieve a 50 % slurry. Cell lysate (Section 4.6.4.1) was incubated with a 1/50 volume of the 50 % slurry of glutathione sepharose beads for 1 hour at 4 °C on a rotary mixer. The lysate/bead mixture was then transferred to a 5 ml polypropylene column (Pierce), the unbound proteins were allowed to flow through, before washing the beads 3 times with 1/10 of the lysate volume of cold PBS. GST-tagged proteins were eluted from the beads by adding 1/100 lysate volume of elution buffer (10 mM glutathione, 50 mM Tris HCl, pH 8), incubating for 15 minutes on ice, and collecting the eluate from the column. This was repeated four times. To determine the efficiency of the purification, samples were collected at each stage and prepared for PAGE (Section 4.6.1) and analysed by Coomassie staining (4.6.2) and/or Western blotting (4.6.3) with anti-GST antibody (Table 4-14).

4.6.5 Determination of protein concentration by Bradford assay

The concentration of purified protein in eluates was determined using a Bradford assay. Protein standards for the assay were obtained by performing serial dilutions of bovine serum albumin (BSA; 31.25 - 500 $\mu g ml^{-1}$). Protein standards, appropriate dilutions of protein sample, and a sample buffer control, were transferred to a 96 well plate (10 µl per well) before 200 µl Bradford reagent was added and the samples mixed gently and incubated at room temperature for

5 minutes. The plate was analysed at a wavelength of 595 nm using a Versamax spectrophotometer and Softmax Pro 5 software. The A_{595nm} values for the BSA protein standards were used to plot a standard curve of A_{595nm} against standard concentration, and the formula of the regression line was used to calculate the sample protein concentration.

4.6.6 Dialysis of proteins

Dialysis tubing (Medicell International, cut off 12-14 kDa) was prepared by immersing in 1 L of 2 % (w/v) $NaHCO_3$, 1 mM EDTA, and boiling for 10 minutes; the tubing was then rinsed in dH_2O before being boiled again in dH_2O for 10 minutes. The tubing was removed from the dH_2O and stored in 50 % ethanol, 1 mM EDTA at 4 ˚C. Before use, the prepared dialysis tubing was rinsed in dH_20. Protein samples were added to sealed portions of dialysis tubing and incubated at 4 ˚C with stirring, in the appropriate buffer. After 3-4 hours, the buffer was removed and replaced with fresh buffer and the process was repeated. The process was repeated once more, for a longer duration of 16 hours.

4.6.7 Storage of proteins

For long term storage, proteins were dialysed into a buffer comprising 40 mM Tris HCl (pH 7.6), 50 mM NaCl, 2 mM DTT, 10 % (w/v) glycerol and 1X EDTA free protease inhibitor (Roche), frozen in a slurry of dry ice and ethanol and stored at -80 ˚C.

4.6.8 Mass spectrometry

Proteins were prepared for mass spectrometry by dialysis into a buffer comprising 40 mM Tris HCl pH 7.6, 50 mM NaCl, 2 mM DTT and 1X EDTA free protease inhibitor (Roche). Mass spectrometry analysis was performed by Richard Burchmore, Sir Henry Wellcome Functional Genomics Facility, University of Glasgow. Samples were digested with trypsin and analysed using a Q Star Pulsar I spectrometer (set to detect positive ions), in conjunction with Mascot Software.

4.6.9 Preparation of cell extracts from T. brucei *parasites*

To prepare *T. brucei* whole cell lysates, cells were harvested (Section 4.2.2.2) and washed twice in 5 volumes of PBS (procyclic form) or TDB (bloodstream form). For downstream analysis by SDS-PAGE or NuPAGE (Section 4.6.1), cell pellets were resuspended 1X Laemmli or NuPAGE loading buffer at a concentration of 10^5 cells μl^{-1} and boiled for 3 minutes or heated to 70 ˚C for 10 minutes, respectively, before being stored at -20 ˚C. For all other downstream analyses, cell pellets were frozen in a slurry of dry ice and ethanol and stored at -80 ˚C for at least one hour before proceeding. When needed, 1 ml of ice-cold lysis buffer (LSGI, 4.6.9.1) per 5 x 10^7 cells was added to the frozen cell pellet, which was left on ice until the cell pellet had thawed. Cells were resuspended in lysis buffer by vortexing and then incubated on ice for 15 minutes before being centrifuged at 100, 000 x *g* for 45 minutes in an ultracentrifuge at 4 ˚C to separate soluble and insoluble fractions for use in downstream analyses. Samples of these fractions were prepared for analysis by SDS PAGE/NuPAGE (Section 4.6.1) and Western blotting (Section 4.6.3) by the addition of Laemmli or NuPAGE sample buffer to a final concentration of 1X and heating the samples as described above.

4.6.9.1 LSGI buffer

Lysis solution with glycerol and inhibitors (LSGI; (Mottram and Grant, 1996)) comprises LSG buffer (50 mM MOPS (pH 7.4), 100 mM NaCl, 1 mM EDTA, 1 mM EGTA, 10 mM NaF, 1 mM NaOVa, 1 % Triton X-100 and 10 % glycerol), supplemented with protease inhibitors (100 μgml^{-1} leupeptin, 0.5 mM PMSF (in ethanol), 5 μgml^{-1} pepstatin A (in methanol), 0.5 mgml-1 pefabloc SC, and 1 mM 1,10 phenanthroline (in 50 % ethanol).

4.6.10 Preparation of cytoskeletal and flagellar fractions from T. brucei *parasites*

Preparation of cytoskeletons and flagella preparations was based on the protocol described in (Broadhead et al., 2006). *T. brucei* cells were harvested (Section

4.2.2.2), washed once in PBS or TDB, resuspended in ice cold PEME buffer (100 mM PIPES, 2 mM EGTA, 0.1 mM EDTA, 1 mM $MgSO_4$, adjusted to pH 6.9) containing 1 % (v/v) Nonidet P40 detergent and supplemented with 1X complete EDTA-free protease inhibitor cocktail (Roche), and incubated for 2 minutes on ice before being centrifuged at 800 x *g* for 10 minutes. Following centrifugation, cytosolic proteins were located in the supernatant (S1), while cytoskeletons were present in the pellet (P1). The cytoskeletons were resuspended in an ice cold high salt buffer (PEME with 1 M NaCl, supplemented with 1X complete EDTA free protease inhibitor cocktail (Roche), 200 $\mu g ml^{-1}$ DNAse I, and 50 $\mu g ml^{-1}$ RNAse A) and incubated on ice for 10 minutes to partially depolymerise the cytoskeletons. Depolymerised cytoskeletons (P2) were harvested by centrifugation at 16 000 x *g* for 15 minutes at 4 ˚C, leaving extracted microtubule-associated proteins and tubulin present in the supernatant (S2). The cytoskeletal pellet was incubated with the high salt buffer for a second time and centrifuged as above, in order to extract any remaining non-flagellar MAPS and tubulin (S3) and to obtain flagella in the pellet (P3). Samples from the various stages of fractionation were prepared for PAGE. Pellets containing cytoskeletons, depolymerised cytoskeletons, and flagella were resuspended in 1X NuPAGE sample buffer (Section 4.6.1.2) to a concentration equivalent to 0.5-1 x 10^5 cells μl^{-1}. Supernatants corresponding to the cytosolic and solubilised cytoskeletal fractions (including MAPs and tubulin) were diluted in NuPAGE sample buffer equivalent to a concentration of 5 x 10^4 cells μl^{-1}. The samples were heated at 70 ˚C for 10 minutes and stored at -20 ˚C until analysed by PAGE (Section 4.6.1) and Western blotting (Section 4.6.3).

4.6.11 Immunoprecipitation of TY epitope tagged proteins from T. brucei *cell lysates*

For immunoprecipitation, 5 x 10^7 *T. brucei* cells were harvested (Section 4.2.2.2) and resuspended in 1 ml high salt lysis buffer (50 mM MOPS (pH 7.4), 500 mM NaCl, 1 mM EDTA, 1 mM EGTA, 10 mM NaF, 1 mM NaOVa, 1 % Triton X 100 and 10 % glycerol) supplemented with protease inhibitors as described in Section 4.6.9.1, before being centrifuged at 100, 000 x *g* for 45 minutes at 4 ˚C. Following centrifugation, 1 ml of the S100 lysate was incubated with 50 µl anti-TY antibody (Table 4-14 and (Bastin et al., 1996)) and 100 µl of a 50 % slurry of

protein G agarose beads (prepared by washing 1 bed volume of protein G agarose slurry (Pierce) three times in 5 bed volumes of PBS and resuspending the beads in 1 bed volume of high salt lysis buffer with protease inhibitors). The lysate, anti-TY antibody and protein G beads were incubated for 2 hours on a rotary mixer at 4 ˚C, before the beads were pelleted by centrifugation at 366 X *g* for 3 minutes. The beads were washed 4 times in 1 ml high salt buffer containing protease inhibitors. After the final wash, the beads were resuspended in an appropriate buffer for downstream analyses (Section 4.7).

4.7 Kinase assays

4.7.1 Kinase reactions

Kinase assays were performed with recombinant proteins or proteins immunoprecipitated from trypanosome cell lysates. Purified recombinant proteins were dialysed (Section 4.6.6) into kinase assay buffer (KAB: 50 mM MOPS (pH 7.4), 20 mM $MgCl_2$, 2 mM DTT, 10 mM EGTA (pH 8), and equal amounts of each recombinant protein were added to kinase assay mix (4 µM ATP, 5 µg substrate and 0.37 MBq γ32P-ATP per reaction in KAB) prewarmed to 30 ˚C to give a final volume of 20 µl. Generic kinase substrates used in these assays included histone HI (Calbiochem), α- or ß-casein (Invitrogen) or myelin basic protein (Invitrogen). Kinase assays were incubated at 30 ˚C with shaking for up to 30 minutes, before the reaction was halted by the addition of protein sample buffer (NuPAGE or SDS PAGE (Section 4.6.1)) to 1X final concentration, and boiling for 5 minutes. The kinase assay reactions were stored at -20 ˚C or analysed immediately.

When a preincubation step was required, the relevant recombinant proteins were added to KAB (without ATP) to a final volume of 10 µl, and incubated at 30 ˚C for the desired amount of time before adding a further 10 µl of KAB containing a 2X (8 µM) concentration of ATP, 0.74MBq γ^{32P}ATP and 5 µg substrate (if required).

To analyse kinase activity of proteins immunoprecipitated from *T. brucei* cell lysates (Section 4.6.11), proteins immobilised on protein G sepharose beads

were equilibrated in an equal volume of kinase assay buffer and warmed for 5 minutes at 30 ˚C with shaking. The protein/bead complexes were pelleted by centrifugation at 366 X *g* for 3 minutes, before 50 µl of prewarmed kinase assay mix was added and kinase assays performed as described above.

4.7.1.1 Analysing kinase activity

Proteins in kinase assay samples were separated by PAGE (Section 4.6.1) and visualised by Coomassie staining (Section 4.6.2). Stained gels were dried using a BioRad gel dryer (model 583) between filter paper and cellophane before exposing to a phosphor-imaging screen overnight at room temperature. Radiolabelled proteins were detected by scanning the phosphor-imager screen using a Typhoon scanner.

4.8 Dephosphorylation of recombinant proteins

To dephosphorylate proteins, 10 µg of recombinant protein were treated with 200 U lambda protein phosphatase (New England Biolabs) in a reaction buffer comprising 1X supplied lambda phosphatase buffer and 2 mM $MnCl_2$ in a total volume of 50 µl at 30 ˚C for 1 hour with shaking, before halting the reaction by the addition of NuPAGE sample buffer (to 1X final concentration) and heating for 10 minutes at 70 ˚C. To perform time course experiments, 10 µl aliquots were removed at the desired intervals and the reaction was halted as described. The samples were analysed by PAGE (Section 4.6.1) and Coomassie staining (Section 4.6.2).

4.8.1 Preparation of dephosphorylated recombinant proteins for kinase assays

Where dephosphorylated recombinant proteins were required for kinase assays, their purification was carried out as described (Section 4.6.4), but halted after the washing stage (Section 4.6.4.2.1). An equal volume of 1X lambda protein phosphatase (λPPase) buffer (Section 4.8) was then added to the washed beads to create a 50 % slurry. The beads were pelleted by centrifugation of 200 µl of slurry at 91 x *g* for 30 seconds and resuspended in 500 µl 1X λPPase buffer

containing 2000 U λPPase (New England Biolabs) or the equivalent volume of dH_2O (untreated control). The reaction was incubated for 1 hour at 30 ˚C with shaking, before the bead suspension was transferred to a 5 ml polypropylene column (Pierce) and purification of the recombinant protein was continued, commencing from the washing stage (Section 4.6.4.2.1). Samples of the eluted proteins were prepared for PAGE (Section 4.6.1), Coomassie staining (Section 4.6.2) and Western blotting (Section 4.6.3) with anti-phosphothreonine antibody (Table 4-14) to determine the efficiency of the dephosphorylation reaction. Fractions with the highest protein concentration determined by Coomassie staining (Section 4.6.2) were transferred to an Amicon Ultra-15 centrifugal device with a 50 kDa cut off, to which kinase assay buffer (Section 4.7.1) was added, and the samples were centrifuged at 300 x *g* for 10 minutes. The flow through was removed and the process was repeated four times to remove any residual λPPase (25 kDa). The protein concentration of the retentate was determined (Section 4.6.5) before proceeding with kinase assays (Section 4.7).

4.9 Binding assays

To investigate the interaction of 6XHis:PBD with ty:PLK, purification of 6XHis:PBD was carried out as described (Section 4.6.4), but halted after the washing stage (Section 4.6.4.2.1). Twenty microlitres of 6XHis:PBD-bound beads or a beads only control washed and resuspended with high salt lysis buffer (Section 4.6.11) were incubated with 1 ml S100 lysates (Section 4.6.9) of cells expressing ty:PLK (or of a non-induced control) prepared in the same lysis buffer supplemented with protease inhibitors (Section 4.6.11) on a rotary mixer for 2 hours at 4 ˚C. After the incubation, the beads and interacting proteins were pelleted by centrifugation at 91 x *g* for 30 seconds and washed twice in 8 bed volumes of wash buffer (Section 4.6.4.2.1). 6XHis:PBD and any interacting proteins, were eluted from the beads by incubating in 1 bed volume of elution buffer (Section 4.6.4.2.1) for 15 minutes followed by centrifugation as above. Samples were prepared for PAGE (Section 4.6.1) and Western blotting with anti-TY antibody (Section 4.6.3 and Table 4-14).

4.10 Flow cytometry

To prepare cells for DNA content analysis by flow cytometry, 4 X 10^6 cells were harvested (Section 4.2.2.2) and washed in 1 culture volume of either TDB or PBS for bloodstream and procyclic form cells, respectively. Cell pellets were fixed in 1 ml of 70% methanol/30 % PBS, and stored at 4 ˚C for 16 hours-1 month prior to analysis. The fixed cells were harvested by centrifugation, washed once in 10 mls of PBS, resuspended in 1 ml of PBS containing 10 μgml^{-1} propidium iodide and 10 μgml^{-1} RNAse A, and incubated for 45 minutes at 37 ˚C in the dark. DNA content analysis was carried out with a Becton Dickinson FACSCalibur using detector FL2-A. Data were analyzed using the software CellQuest Pro.

4.11 Microscopy

4.11.1 DAPI staining and fluorescence microscopy

DAPI staining was employed to visualise nuclei and kinetoplasts in trypanosome cells. 5 x 10^5 cells were harvested (Section 4.2.2.2), resuspended in approximately 50 µl medium dispensed onto glass slides (prepared by incubating in a 1/10 dilution of poly-L-lysine solution for 5 minutes before air drying), and spread using a cover-slip. Cells were allowed to air dry before being fixed in methanol (-20˚C) for 30 minutes to 16 hours prior to analysis. To analyse the cells, the slides were allowed to air dry, and PBS was added to rehydrate the cells at room temperature for 10-15 minutes. After rehydration, the PBS was decanted, and one drop of Vectashield (Vector Laboratories), a mounting medium containing 4,6-diamidino-2-phenylindole (DAPI) to stain DNA, was added and spread by the application of a cover-slip, which was sealed with nail varnish. Microscopy was performed using a Zeiss Axioskop fluorescent microscope at 1000 X magnification with oil immersion. Cell morphology was analysed by differential interference contrast (DIC) microscopy, and UV light with a 480 nm filter set was used to visualise fluorescently stained kinetoplast and nuclear DNA. Images were processed and analysed with Openlab Version 5.5 software.

For visualisation of GFP tagged proteins, cells were fixed and prepared as described above and visualised with a Zeiss Axioskop fluorescent microscope

under UV light with a FITC (540 nm) filter set, or alternatively, were fixed and visualised as described in Section 4.11.2.

4.11.2 Immunofluorescence microscopy

For immunofluorescence microscopy, 1 x 10^6 *T. brucei* cells were harvested (Section 4.2.2.2) and washed in 1 culture volume of TDB or PBS for bloodstream and procyclic form cells, respectively. The cells were then resuspended in 500 µl PBS or TDB (as appropriate), placed onto an area of 1.0 cm^2 on poly-L lysine coated slides (Section 4.11.1) which had been outlined by nail varnish, and incubated for 15 minutes at room temperature to adhere the cells to the slides. The cells were fixed in freshly prepared 1 % formaldehyde in PBS for 30 minutes at room temperature, before being washed twice in PBS for 10 minutes. Alternatively, cytoskeleton preparations fixed in methanol (Section 4.11.3) were used. Slides were transferred to a dark box lined with moist tissues and the cell coated area of each slide was covered with 1 % Triton X-100 in PBS and incubated at room temperature for 5 minutes to permeablise the cells. The 1 % Triton X-100/PBS solution was replaced with 1 M glycine in PBS for 10 minutes to neutralize free aldehyde bonds and diminish any background fluorescence. This was then replaced with 0.1 % Triton X-100, 0.1 % BSA containing primary antibody at the appropriate concentration (Table 4-16). Cells were incubated with primary antibody for 1 hour and then washed with 10 X 1 ml aliquots of PBS. Secondary antibody (Table 4-17) was diluted 1/1000 in 0.1 % Triton X-100, 0.1 % BSA, and incubated with the cells for 1 hour before washing with 20 X 1 ml aliquots of PBS. The residual PBS and the nail varnish were removed, and Vectashield mounting medium with DAPI (Vector laboratories) was added to the stained cells before covering with a cover-slip, and sealing with nail varnish. Sample fluorescence was observed under UV light with DAPI (480 nm), FITC (540 nm) or RHO (580 nm) filter sets, as appropriate, while cell morphology was visualised by DIC microscopy. Cells were viewed using a DeltaVision RT Epifluorescence Imaging System (Applied Precision), or using a Zeiss Axioskop fluorescent microscope at 1000 X magnification with oil immersion and image processing was carried out using SoftWoRx (for deconvolution of images acquired with the DeltaVision) or Openlab Version 5.5 software (Axioskop).

Table 4-16 -Primary antibodies used for immunofluorescence microscopy.

Primary antibody	Source	Stock concentration	Dilution
Anti-HA rat polyclonal	Roche	100 $\mu g ml^{-1}$	1/100
Anti-β-tubulin mouse monoclonal sera (clone KMX)	Matthews lab (Birkett et al., 1985)	Purified antibody	1/50
Anti-β-tubulin mouse monoclonal IgG2b (clone KMX)	Millipore	1 $mg ml^{-1}$	1/1000

Table 4-17 -Secondary antibodies used for immunofluorescence microscopy.

Secondary antibody	Source	Stock concentration	Dilution
Alexa Fluor 594 conjugated anti-rat goat IgG (H+L)	Molecular probes/Invitrogen	2 $mg ml^{-1}$	1/1000
Alexa Fluor 488 conjugated anti-rat donkey IgG (H+L)	Molecular probes/Invitrogen	2 $mg ml^{-1}$	1/1000
Alexa Fluor 594 conjugated anti-mouse goat IgG2b	Molecular probes/Invitrogen	2 $mg ml^{-1}$	1/1000
Alexa Fluor 488 conjugated anti-mouse goat IgG2b	Molecular probes/Invitrogen	2 $mg ml^{-1}$	1/1000

4.11.3 Preparation of trypanosome cytoskeletons for analysis by microscopy

1 x 10^6 cells were harvested, washed and settled onto slides as described in Section 4.11.2. Cytoskeletons were prepared by adding 1 % NP40 in PEME (Section 4.6.10) buffer (procyclic form) or 0.75 % NP40 in PEME buffer (bloodstream form) and incubating for 1 minute or 30 seconds, respectively. The buffer was decanted and the cells were either immediately fixed in methanol at -20 ˚ C for 30 minutes prior to analysis by DAPI staining and fluorescence microscopy (Section 4.11.1), or by immunofluorescence microscopy (Section 4.11.2), or processed further (procyclic form only) to obtain depolymerised cytoskeletons. To depolymerise microtubules, 1 M NaCl/PEME supplemented

with protease inhibitor cocktail, DNAse I (200 $\mu g ml^{-1}$) and RNAse A (50 $\mu g ml^{-1}$) was added and the cells were incubated for 15 minutes at 4 ˚C. The depolymerised cytoskeletons were either fixed in methanol or incubated in 1M NaCl/PEME a second time to obtain flagella before being fixed and analysed by DAPI staining/immunofluorescence.

4.11.4 Transmission Electron Microscopy

To examine subcellular structures in detail, 5 x 10^7 - 1 x 10^8 procyclic cells were harvested (Section 4.2.2.2) and the culture medium decanted, leaving a residual layer to help stabilise the cells. Fixation was carried out by adding fixative (2.5 % glutaraldehyde in 0.1 M sodium cocodylate buffer) and incubating for 1 hour at room temperature. Downstream processing of the specimens was carried out by Mrs Margaret Mullin under the direction of Dr Laurence Tetley in the Integrated Microscopy Facility, University of Glasgow. In summary, fixed cells were washed three times (5 minutes each) in 4 ˚C 0.1 mM sodium cocodylate buffer, before being incubated in 1 % osmium tetroxide/0.1 mM sodium cocodylate for 1 hour at room temperature. Three 10 minute rinses in dH_2O were then carried out before treating with 0.5 % uranyl acetate for 1 hour in the dark, performing three 5 minute washes in dH_20 and dehydrating the samples in an alcohol series. Cells were incubated for 10 minutes at room temperature in 30 % ethanol, 50 % ethanol, 70 % ethanol, 90 % ethanol, followed by two 10 minute incubations in absolute alcohol and one 3 minute incubation in propylene oxide. The cells were incubated for approximately 16 hours in a 1:1 mix of propylene oxide and epon resin before performing three 30 minute incubations in pure epon resin. The samples were then placed in fresh embed, in gelatine capsules and heated in an oven at 60 ˚C until polymerised. Samples were sectioned to a thickness of 60 -70 nm, and contrast stained by treating the sections for 5 minutes each with 2 % methanol/aqueous uranyl acetate, and Reynold's lead citrate.

Specimens were viewed on a Leo 912 AB energy filtering transmission electron microscope using an Olympus camera, and images were analysed using iTEM imaging platform software (Olympus).

4.11.5 Analysis of vincristine-treated cells by Scanning Electron Microscopy

Bloodstream form cells were treated with 0.2 µM vincristine sulphate (Section 4.12) for 6 hours before being harvested and washed in TDB (Section 4.2.2.2). Cells were fixed in 2.5 % (v/v) glutaraldehyde/0.1 M sodium phosphate buffer (NaPi) for 1 hour at room temperature with mixing by slow inversion. After fixation, cells were harvested by centrifugation and washed 3 times and resuspended in 0.1 M NaPi buffer before transferring approximately 1 x 10^7 cells per sample to poly-L-lysine-coated cover-slips (Section 4.11.1) and leaving to settle for 30 minutes. Cell-coated cover-slips were incubated in 1 % osmium tetroxide (w/v) in 0.1 M NaPi buffer for 1 hour at room temperature. The cells were washed in 0.1 M NaPi buffer (three 10 minute rinses) before incubating them in a 0.5 % aqueous uranyl acetate solution for 1 hour at room temperature in the dark. This was followed by two five minute rinses in distilled water before the samples were dehydrated in an alcohol series. Cells were incubated for 10 minutes at room temperature in 30 % ethanol, 50 % ethanol, 70 % ethanol, 90 % ethanol, followed by two incubations each in absolute alcohol and dried absolute alcohol. The cells were then incubated in hexamethyldisilazane (HMDS) for 5 minutes, and this step was repeated before transferring specimens to a dessicator for 16 hours before mounting. Samples were mounted on aluminium stubs with copper double sided tape and silver paint, and an approximately 20 nm thick coating of gold-palladium was applied using a Polaron SC515 SEM coating machine. Samples were viewed on a Jeol 6400 Scanning Electron Microscope.

4.12 Microtubule inhibitor experiments

Microtubule inhibitors (Vincristine sulphate, Vinblastine sulphate and Paclitaxol (taxol)) were obtained from Calbiochem, and stored at 4 ˚C (vincristine and vinblastine) or -20 ˚C (taxol). 10 mM stock solutions were prepared using dH_2O (vincristine), methanol (vinblastine) or dimethyl sulphoxide (DMSO) (taxol) solvents; further 1000X stock solutions corresponding to the final concentrations listed in Table 4-18 were also produced. Lister 427 procyclic and bloodstream form cells were diluted to a density corresponding to low to mid log phase

growth (Section 4.2.2.2) in a volume of 10 ml; inhibitor (to a final concentration of 1X) or equivalent volume of solvent or dH_2O) was added and determination of cell density (Section 4.2.2.3) and sampling for DAPI staining (Section 4.11.1) were carried out at regular intervals.

Table 4-18 Concentrations of microtubule inhibitors (μM) used to treat *T. brucei* cells.

Inhibitor	Life cycle stage	
	Bloodstream form	Procyclic form
Vincristine	0, 0.05, 0.2, 1.0, 5.0, 10	0, 5.0, 10, 15, 20
Vinblastine	0, 0.05, 0.2, 1.0, 5.0	0, 5.0, 10, 15, 20
Taxol	0, 0.2, 1.0, 5.0, 10	0, 0.2, 1.0, 5.0, 10

4.13 Statistical Analyis

Values were expessed as means ± standard error of the mean (SEM). Levels of significance were calculated by unpaired t-tests using the Data Analysis add-on of Microsoft Excel. Differences were considered significant at a p value < 0.05.

5 The role of AIR9 in *T. brucei*

5.1 AIR9: structure and function

5.1.1 AIR9 in plants

AIR9 (Auxin induced in root cultures 9) was first identified in a screen to detect auxin-induced genes in lateral root cells of *Arabidopsis thaliana* using a cDNA expression library (Neuteboom et al., 1999); a separate screen to identify genes involved in male gametophytic development using transposon insertion mutants found that AIR9 was required for male and female gametophytic transmission (Lalanne et al., 2004), suggesting that it was an essential *Arabidopsis* gene. A further study isolated AIR9 protein from plant microtubules, and subsequently identified cell cycle functions of AIR9 (Buschmann et al., 2006), which were first investigated through localisation studies, and subsequently through the expression of truncated recombinant proteins *in vivo* to determine the molecular basis for localisation and function. These findings are described below.

Structural analysis revealed that there were three characteristic regions in the AIR9 protein (Figure 5-1): an N-terminal disordered basic serine-rich domain, a leucine-rich repeat domain (containing six repeats), and a C-terminal domain containing eleven tandemly-repeated A9 domains (Buschmann et al., 2006). The C-terminal A9 repeats were found to be immunoglobulin (Ig)-like domains which are generally involved in protein:protein interactions.

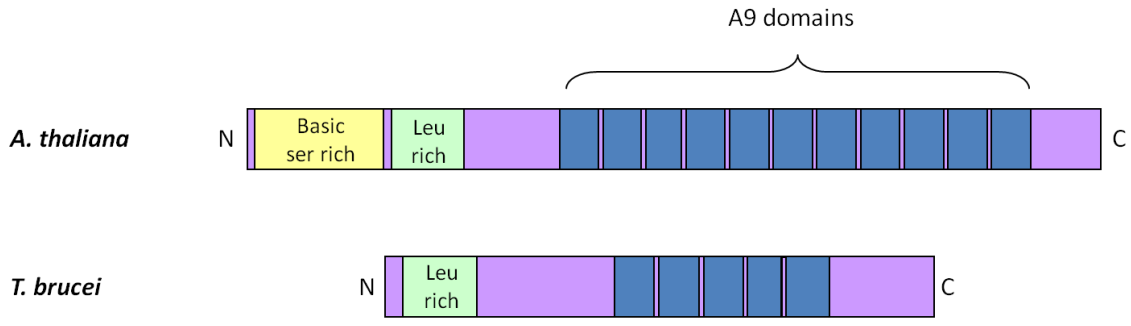

Figure 5-1 -Schematic to show the structural domains of AIR9 proteins from *Arabidopsis* and *T. brucei* (Tb11.01.8770).
The N-terminal basic domain (yellow), the leucine rich repeats (green) and the A9 domains (blue; 11 for *A. thaliana* AIR9 and 5 for the *T. brucei* homologue) are shown.

Full length AIR9 was expressed in BY-2 (Bright Yellow Tobacco) cells as a GFP fusion protein, and analysis of cells at different stages revealed a precise cell cycle-dependent localisation pattern (Buschmann et al., 2006). Briefly, the cortical microtubules were labelled at interphase, the preprophase band at G2, and weak labelling of the spindle was observed during metaphase. At the onset of cytokinesis, GFP:AIR9 labelled the phragmoplast and also the cortical division site. Localisation at the cortical division site appeared to occur immediately prior to contact between this region and the cell plate and, intriguingly, labelling seemed to spread from the cortical division site into the immature cross wall. The staining pattern was at first homogenous but became filamentous as the cross wall matured (suggesting GFP:AIR9 was associated with microtubules). Induction of ectopic phragmoplast insertion prevented GFP:AIR9 migration into the cross wall, and this also inhibited the conversion of callose to cellulose, which accompanies maturation. GFP fusion proteins corresponding to different truncations of AIR9 revealed that localisation to the cortical microtubules required the basic serine-rich N-terminus, whereas localisation to the cortical division zone and cross wall required the C-terminal A9 repeats.

Whilst this study highlights the dynamic nature of AIR9, there are some issues that were not addressed. For instance, while the filamentous microtubule-like distribution of AIR9 in the cross wall was noted for full length AIR9 and it was remarked that this could be a consequence of microtubule association, there was no comment regarding the distribution of N-terminally truncated AIR9 at the cross wall. If truncated AIR9 was capable of localising to microtubules specifically within the cross wall this would be very interesting, as it could indicate an indirect association via other MAPs, or perhaps an association of the C-terminal region specifically with the phragmoplast as opposed to cortical microtubules.

5.1.2 AIR9 in Trypanosomatids

AIR9 is of interest to parasitologists as there are homologues of AIR9 in several protozoan parasites including the Trypanosomatids (Buschmann et al., 2007). AIR9 is also found in other land plants (although not green and red algae), but is absent from fungi, metazoan and Amoebozoa genomes (Figure 5-2).

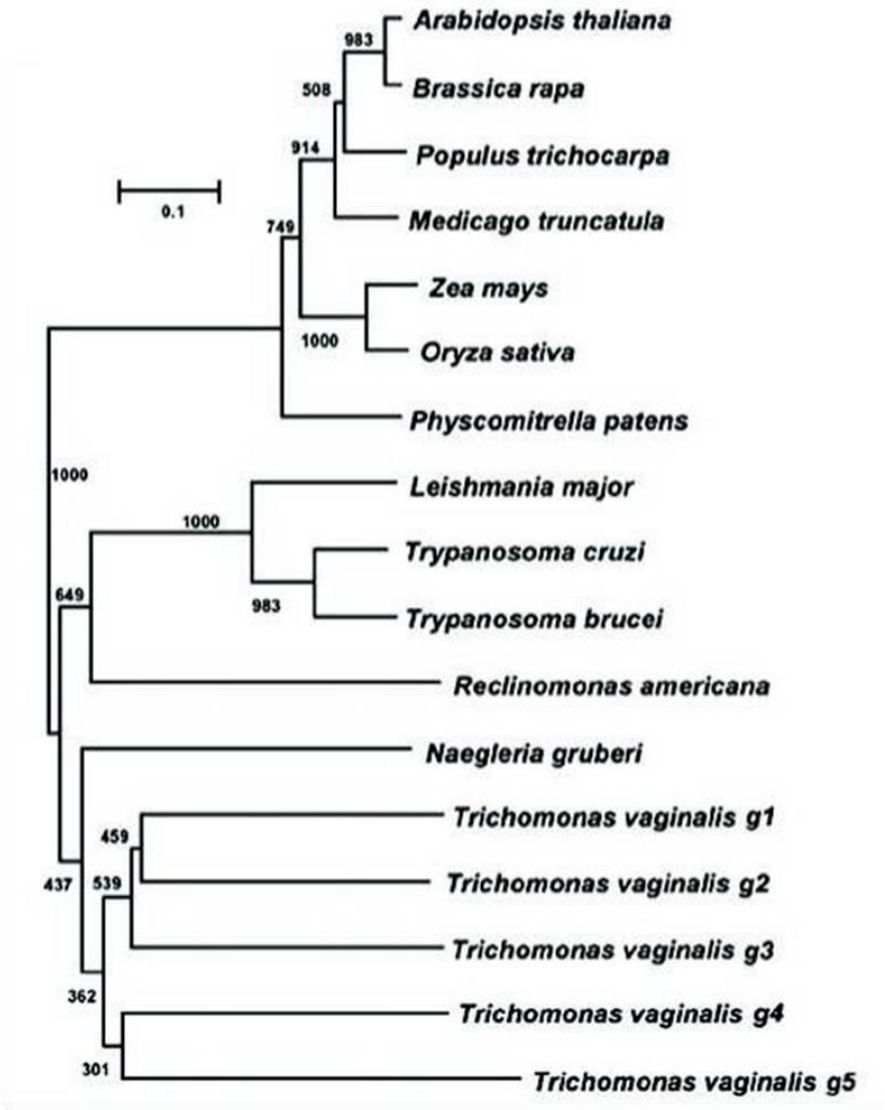

Figure 5-2- Phylogenetic relationship of AIR9-like proteins.
Phylogenetic comparison based on the leucine-rich repeat domain. Reproduced with permission from (Buschmann et al., 2007).

T. brucei AIR9 possesses five conserved A9 domains, and a leucine-rich repeat region (Figure 5-1, Figure 5-3 and Figure 5-4). However analysis of N-terminal amino acids by amino acid scanning did not detect significant enrichment of serine, arginine or lysine residues in the 104 most N-terminal residues for Trypanosomatid AIR9 homologues, indicating that the microtubule binding domain was not conserved.

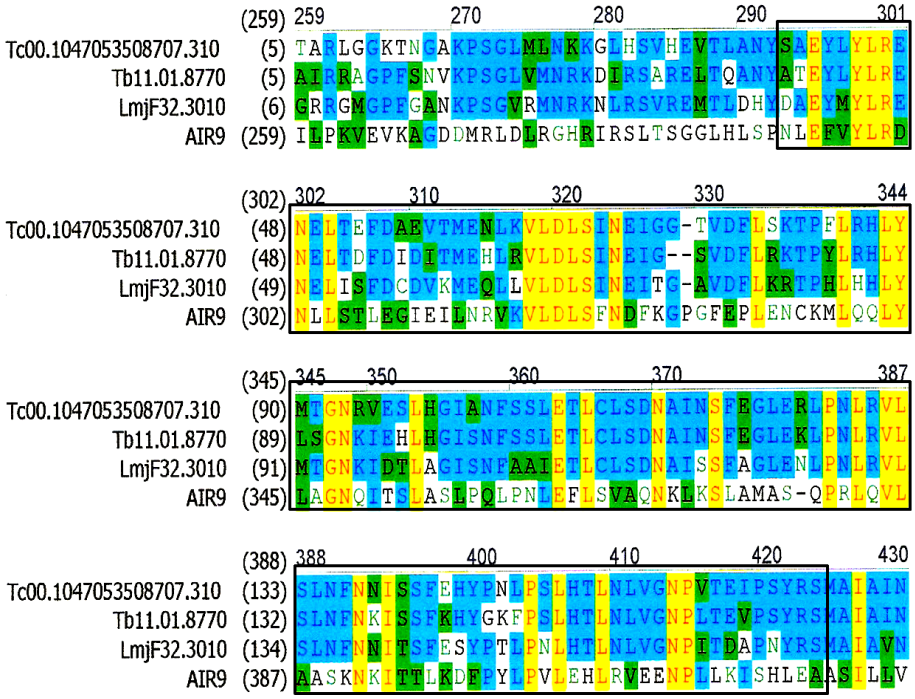

Figure 5-3 -Multiple alignment of the leucine-rich repeat region of AIR9.
The amino acid sequences for *A. thaliana* AIR9 (bottom) and its trypanosomatid homologues (accession numbers from top to bottom correspond to *T. cruzi*, *T. brucei* and *L. major* AIR9) were aligned to show conservation of the leucine-rich repeat region (black box). Sequences were sourced from GeneDB (www.genedb.org) and aligned using AlignX software.

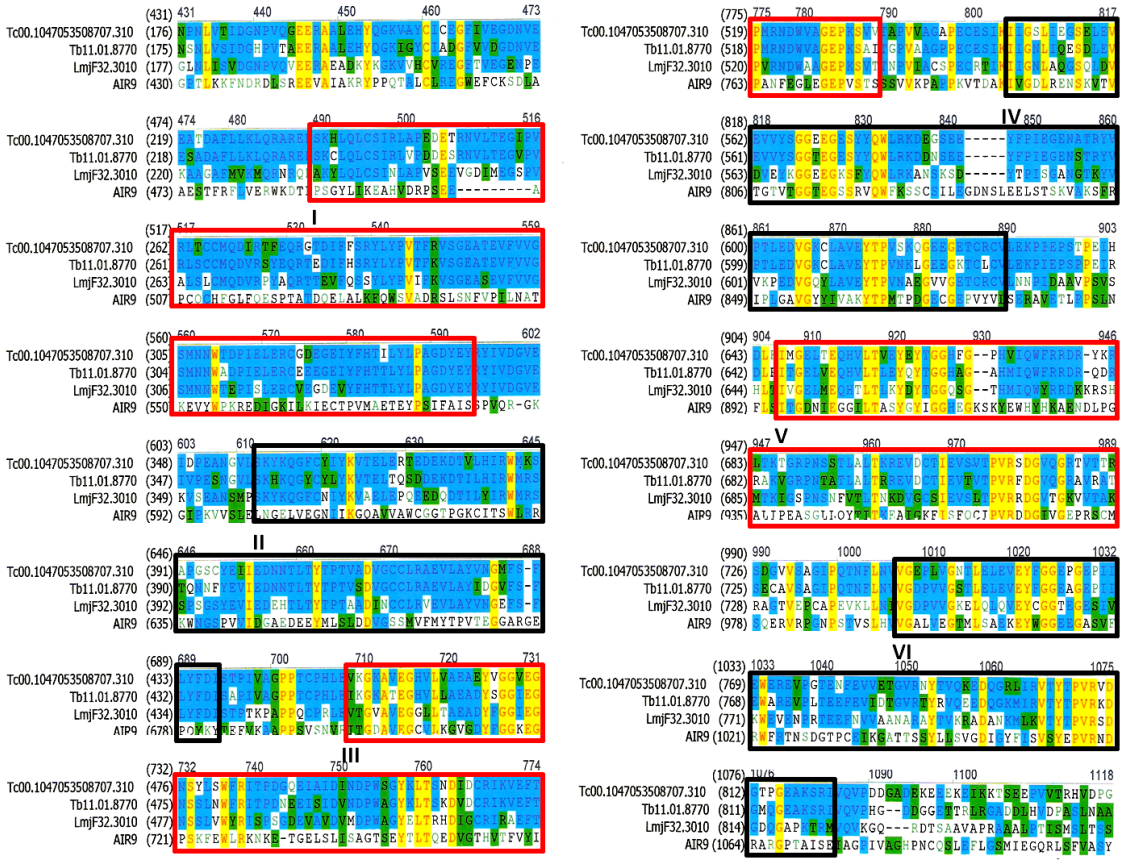

Figure 5-4-Multiple alignment of A9 domains of AIR9.
The amino acid sequences for *A. thaliana* AIR9 (bottom) and its Trypanosomatid homologues (accession numbers from top to bottom correspond to *T. cruzi*, *T. brucei* and *L. major* AIR9) were aligned to show conservation of the A9 domains. The first six A9 domains

of *A. thaliana* AIR9 are labelled I-VI, with alternating A9 domains shown in red and black boxes for clarity. Note that the first A9 domain is not conserved in Trypanosomatid parasites. Sequences were sourced from GeneDB and aligned using AlignX software.

5.1.3 Acquisition of T. brucei AIR9

AIR9 is one of several proteins in *T. brucei* to be described as a plant homologue, and the origins of plant-like genes in this parasite are the source of great debate.

The Trypanosomatids, Bodenida and Euglenida form the order Eugelozoans. Some Euglenida are phototrophic, which has led some to believe that Trypanosomatids, Bodenida and some Euglenida once possessed a plastid but have subsequently lost it (Hannaert et al., 2003a). Comparisons of cytoskeletal morphology and phylogenetic analysis imply, however, that this is not the case.

Euglenida are free living, and are a diverse collection of bacterivorous, eucaryovorous and phototrophic organisms. Their mode of nutritional acquisition is reflected in their cytoskeletal morphology. Bacterivorous and eukaryovorous Euglenida possess elaborate feeding apparata, which involves the highly developed flagellar pocket (for prey ingestion), and in some cases, a feeding rod and vane (eukaryovorous Euglenida). The mode of motility in bacterivoric and eukaryovoric Euglenida is a gliding mechanism known as Euglenoid movement. Phototrophic Euglenida have a reduced ingestion apparatus, and the ‘vane’ is used for swimming motility; these Euglenida show reduced or absent Euglenoid motility. Another feature of the phototrophic Euglenida is their large cell size and reduced number of pellicle strips, which may help to increase light harvesting (Kivic and Walne, 1984). Phylogeny has shown that eukaryovorous Euglenida are derived from bacterivorous ancestors, and that phototrophic Euglenida have eukaryovoric ancestors. The change in feeding apparatus accompanying the transition of prey choice (from small bacteria to larger eukaryotic cells) is believed to have led to a secondary endosymbiosis with a green alga, resulting in phototrophy (Leander, 2004). Together, the specialised specific cytoskeletal adaptations exhibited by phototrophic Euglenida, and the phylogeny analysis imply late acquisition of the plastid in evolutionary terms, which does not explain the presence of plant-like traits in other Euglenozoans.

T. brucei and *Leishmania* possess genes with apparently both prokaryotic and plant sources, which would suggest that another, earlier, secondary endosymbiosis event actually occurred in a Euglenozoan ancestor (Hannaert et al., 2003a). The situation looks more complicated when individual genes are studied. For example, genes representing components of the pyrimidine pathway are present (6-phosphogluconate dehydrogenase, adenylate kinase, fructose1,6-bisphosphate aldolase, and trypanothione reductase) suggesting a cyanobacterial origin from a primary endosymbiosis; the presence of YC4F-related proteins (which contain AAA-type ATPase domains and cytochrome P450-like domains) suggests a green algal origin implying a secondary endosymbiosis; and finally, phylogenetic analysis of components of the biosynthetic pathway for fatty acids, for example the enzyme Δ4 desaturase, groups the Trypanosomatid enzyme with haptophytes and stramenophiles, which evolved from an endosymbiosis with a red alga. This evidence supports a tertiary endosymbiosis of a haptophyte alga by a Trypanosomatid ancestor (Bodyl et al., 2010). This presents a rather confusing picture of multiple endosymbioses and subsequent losses of the plastids. A rather more elegant explanation for the origin of plant-like traits in Trypanosomatids is given in (Opperdoes and Michels, 2007). Briefly, this study suggested that a primary endocytosis of a cyanobacterium by an ancestral Euglenozoan led to gene transfer of plastid genes to the nucleus and the formation of glycosomes, and that following plastid loss, subsequent acquisition of genes occurred through lateral gene transfer, probably by viruses encountered in the arthropod vector.

Whatever the source of plant-like genes, the absence of these genes from mammalian cells indicates that the glycosome and plant-like proteins in trypanosomes could be good drug targets. What is interesting about the endosymbiosis theory is that it implies that only a small percentage of genes were retained. Selective gene retention could suggest that those genes retained aided in the adaptation to a parasitic lifestyle. A possible example would be dihydroorotate dehydrogenase (DHODase), which in trypanosomes is a soluble version of the ‘inner mitochondrial membrane-bound DHODase’, and as such, it donates electrons to fumarate as opposed to the mitochondrial respiratory chain, which could be an advantage in the absence of a functional mitochondrial respiratory chain. Incidentally *S. cerevisiae* also possesses soluble DHODase and

this is believed to be an important modification for allowing anaerobic growth (Opperdoes and Michels, 2007).

The presence of AIR9 in the *T. brucei* genome is not surprising viewed from the context of such a complex evolutionary history, and the selective retention of 'useful' genes suggests that *T. brucei* AIR9 could have a functional role. Moreover, both plants and trypanosomes possess a rigid cell structure, namely the plant cell wall and the subpellicular corset, respectively, features which might suggest convergent evolution of pre-mitotic cleavage site selection during cytokinesis. As a component of both the preprophase band and cortical division site, AIR9 has a proven function in this process in plants. One of the aims of this project is to address whether AIR9 has a comparative role in cytokinesis in *T. brucei*.

5.2 Strain differences between Lister 427 and TREU 927 GUTat.10.1

T. brucei Lister 427 was used as the host strain for all experiments in this study. To investigate the possibility of strain variation between *T. brucei* Lister 427 and the genome strain, TREU 927 GUTat.10.1, *AIR9* was PCR-amplified (Section 4.5.4) from Lister 427 genomic DNA (Section 4.4.2) using oligonucleotides PR226 and PR227 (Table 4-9); two independent PCR products were then cloned into pSC-A (Section 4.5.6) and sequenced (Section 4.5.8). The sequence of each PCR product was identical, and the plasmid generated was named pHG129 (Table 4-4). The Lister 427 and TREU 927 GUTat.10.1 *AIR9* sequences were compared to each other using Vector NTI software and the differences between them are listed in Table 5-1. *T. brucei AIR9* possesses a conserved leucine rich repeat region, and 5 A9 domains (Figure 5-1 and (Buschmann et al., 2007)). The base pair changes amounted to 4 amino acid mutations, only one of which (V773L) was located within a conserved region of AIR9 (the fifth A9 domain); K226N was located between the leucine rich repeat region and the first A9 domain, whilst D896G and G920D were located at the variable C-terminus of the protein. In addition, a number of deletions were present at the 3' end of the gene, causing a deletion of 12 amino acids in the C-terminal region of AIR9.

Table 5-1-A comparison of *AIR9* for the *T. brucei* genome strain, TREU 927 GUTat.10.1, and strain Lister 427.
Sequence differences for *AIR9* between the *T. brucei* genome strain (TREU 927 GUTat.10.1) and the laboratory strain used in this study (Lister 427) are detailed in the Table, and the effect of these DNA sequence changes on AIR9 protein sequence are also indicated.

Base	TREU 927 GUTat.10.1	Lister 427	Effect of mutation
171	T	C	Silent
237	G	A	Silent
495	G	C	Silent
678	G	C	K226N
942	C	G	Silent
1080	A	G	Silent
1698	C	T	Silent
2317	G	T	V773L
2687	AC	GT	D896G
2759	GT	AC	G920D
2795	GTGCTG	Deleted	Deletion of GAEKSTEAAADE (αα 932-943)
2802	GAAAT	Deleted	
2808	TACT	Deleted	
2812	AAG	Deleted	
2817	ACGCGC	Deleted	
2830	G	Deleted	
2832	CGCTG	Deleted	
2839	AAG	Deleted	

5.3 Downregulation of AIR9 in the bloodstream form and procyclic form life cycle stages of *T. brucei*

In order to study the function of AIR9 in *T. brucei*, inducible RNAi cell lines were constructed in procyclic and bloodstream form parasites and analysed for defects in proliferation or cell cycle progression following depletion of AIR9.

5.3.1 Construction of plasmid pHG27 for inducible expression of AIR9 *dsRNA in* T. brucei

Primer design for the amplification of a small, unique fragment of the *AIR9* gene (Tb11.01.8770) was carried out using 'TrypanoFAN RNAit' software (trypanofan.path.cam.ac.uk/software/RNAit.html; (Redmond et al., 2003)); additionally the exclusivity of the selected 413 bp sequence was verified using BLAST software. The primers OL2696 and OL2697 (Table 4-9) were used to PCR-amplify (Section 4.5.4) the *AIR9* fragment from 427 genomic DNA (Section 4.4.2), which was subsequently ligated into the cloning vector pSC-A (Strataclone,

Section 4.5.6), generating pGL1785 (Table 4-4), sequenced (Section 4.5.8) and subcloned (by restriction digest using enzymes BamHI and HindIII (Section 4.5.2)) into the RNAi vector pT27^{Ti}A (LaCount et al., 2000; LaCount et al., 2002), generating pHG27 (Figure 5-5 and Table 4-4), which was verified by performing suitable analytical restriction digests.

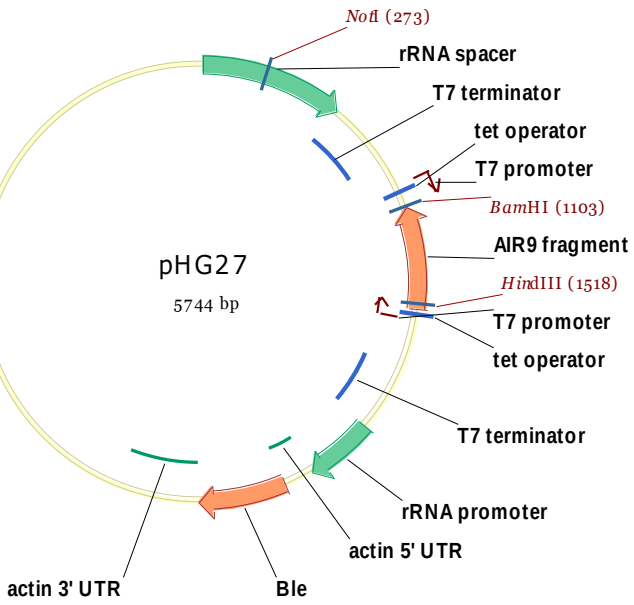

Figure 5-5 -Plasmid map for pHG27.
The features annotated on the plasmid map indicate the location of the opposing T7 promoters and T7 terminators which flank the *AIR9* fragment (bp 1803-2215), the opposing tetracycline operators ('Tet operators') which regulate expression from the T7 promoters, the NotI restriction site for linearization, the ribosomal DNA sequences for integration into genomic DNA, the HindIII and BamHI restriction sites used to clone the *AIR9* fragment into the RNAi vector (pT27^{Ti}A (LaCount et al., 2000; LaCount et al., 2002), and the bleomycin resistance gene (selectable marker), with flanking actin 5' and 3' UTR sequences.

5.3.2 Downregulation of AIR9 in the procyclic form life cycle stage of T. brucei

5.3.2.1 Generation of procyclic form RNAi cell lines

The *AIR9* RNAi plasmid (pHG27; Figure 5-5) was linearised by NotI restriction digest (Section 4.5.2 and Section 4.3.2.1) and transfected into procyclic form 427 pLew13 pLew29 cells (Wirtz et al., 1999) (Section 4.3.2.2). Clones were selected by limiting dilution in medium supplemented with hygromycin, G418 and zeocin (the latter to select for the RNAi plasmid). Six independent clones were generated and of these, four failed to thrive in culture. Subsequent experiments were performed with clones 4 and 5 only.

To verify targeted AIR9 downregulation following RNAi induction, additional cell lines were generated expressing tyGFP:AIR9 from the endogenous locus. Construction of the tyGFP:AIR9 expression construct is described in Section 5.4.1. The tyGFP:AIR9 expression plasmid (pHG172) was linearised (by restriction digest using NotI) and transfected into cell lines 427 pLew13 pLew29 pHG27 clone 4 and 5 (as above). Clones were selected by limiting dilution in medium supplemented with hygromycin, G418, zeocin and blasticidin (the latter to select for the expression construct). Six independent clones were obtained from each transfection. The clones were screened by Western blotting of cell lysates with anti-GFP antibody (Section 4.6.3), which revealed that two clones derived from RNAi cell line ‘clone 4’, and one clone derived from RNAi cell line ‘clone 5’ expressed tyGFP:AIR9 (Figure 5-6). Subsequent experiments were performed with cell lines 427 pLew13 pLew29 pHG27 clone 4 pHG172 clone 2, and 427 pLew13 pLew29 pHG27 clone 5 pHG172 clone 2.

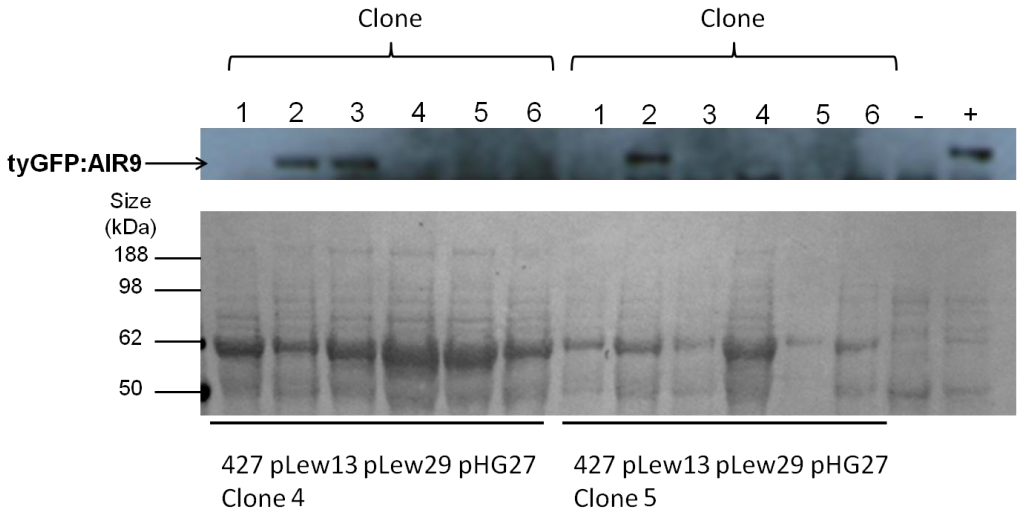

Figure 5-6-Western blot analysis of cell lysates from procyclic form RNAi cell lines transfected with pHG172 for endogenous expression of tyGFP:AIR9.
Procyclic RNAi cell lines transfected with pHG172 (Section 5.4.1) were screened for expression of tyGFP:AIR9 by preparing cell lysates for SDS PAGE and Western blotting (upper panel) with anti-GFP antibody. The parental RNAi cell lines are indicated at the bottom, and the clones derived from these cell lines are indicated at the top. The positive (+) and negative (-) controls corresponded to cell lysates from bloodstream form 427 pHG172 clone 3 (Section 5.4.2), and procyclic form 427 parasites, respectively. To control for loading, the blot was stained with Ponceau reagent (lower panel). The signal for tyGFP:AIR9 (upper panel) was observed at its predicted size of 137 kDa.

5.3.2.2 Kinetics of AIR9 downregulation in procyclic form *AIR9* RNAi cell lines expressing tyGFP:AIR9

Two independent *AIR9* RNAi cell lines expressing tyGFP:AIR9 from the endogenous locus were grown in the presence or absence of tetracycline for three days (Section 4.2.2.2). Western blotting (Section 4.6.3) of cell lysates revealed a dramatic decrease in the level of tyGFP:AIR9 by 24 hours, and by 48 hours little tyGFP:AIR9 remained (Figure 5-7). The amount of tyGFP:AIR9 detected was slightly variable for the uninduced cells over time, which may reflect a degree of inconsistent repression of the tetracycline-inducible T7 promoter. However, these results show that in this system, AIR9 can be efficiently downregulated at the protein level, to the extent that AIR9 expression is undetectable by 72 hours post-induction.

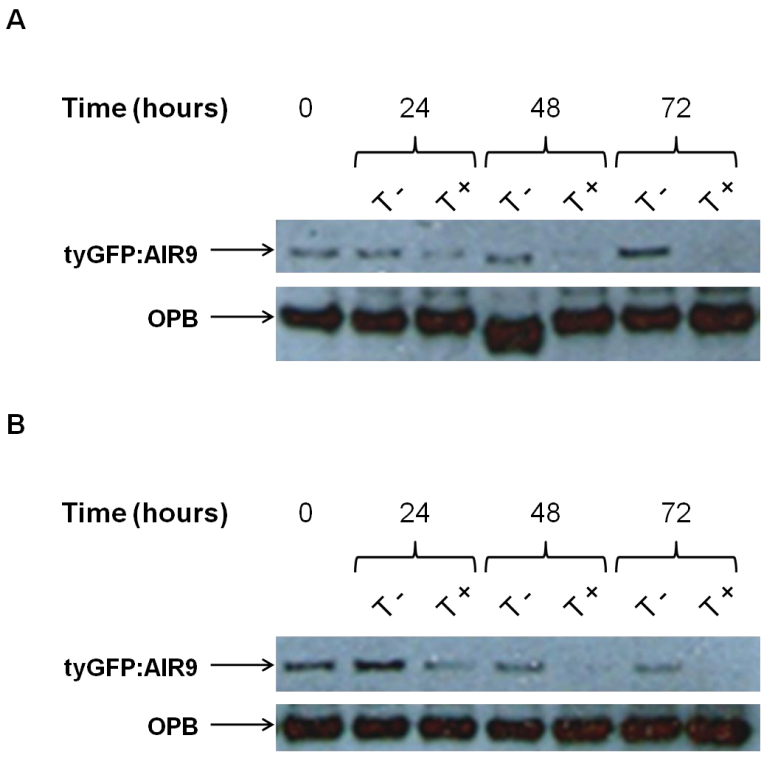

Figure 5-7 -Downregulation of tyGFP:AIR9 in procyclic form *AIR9* RNAi cell lines. Cells expressing tyGFP:AIR9 derived from procyclic form *AIR9* RNAi cell lines: 427 pLew13 pLew29 pHG27 clone 4 pHG172 clone 2 (panel A), and 427 pLew13 pLew29 pHG27 clone 5 pHG172 clone 2 (panel B); were grown in the presence (T +) or absence (T -) of 1 µgml^{-1} tetracycline for 3 days, and cell lysates were prepared at 24 hour intervals for analysis by SDS PAGE and Western blotting with anti-GFP antibody (to detect tyGFP:AIR9), and anti-OPB antibody (to control for loading).

5.3.2.3 The effect of AIR9 downregulation on growth and DNA content in procyclic form parasites

Growth of the two independent *AIR9* RNAi cell lines was affected by 72 hours of induction with tetracycline (Figure 5-8) with cells proliferating at a slower rate, although no growth arrest was observed throughout the period of induction (174 hours). The slow growth phenotype appeared to coincide with the point at which AIR9 protein had diminished to undetectable levels (Figure 5-7), implying that low levels of AIR9 may be sufficient for normal growth in culture.

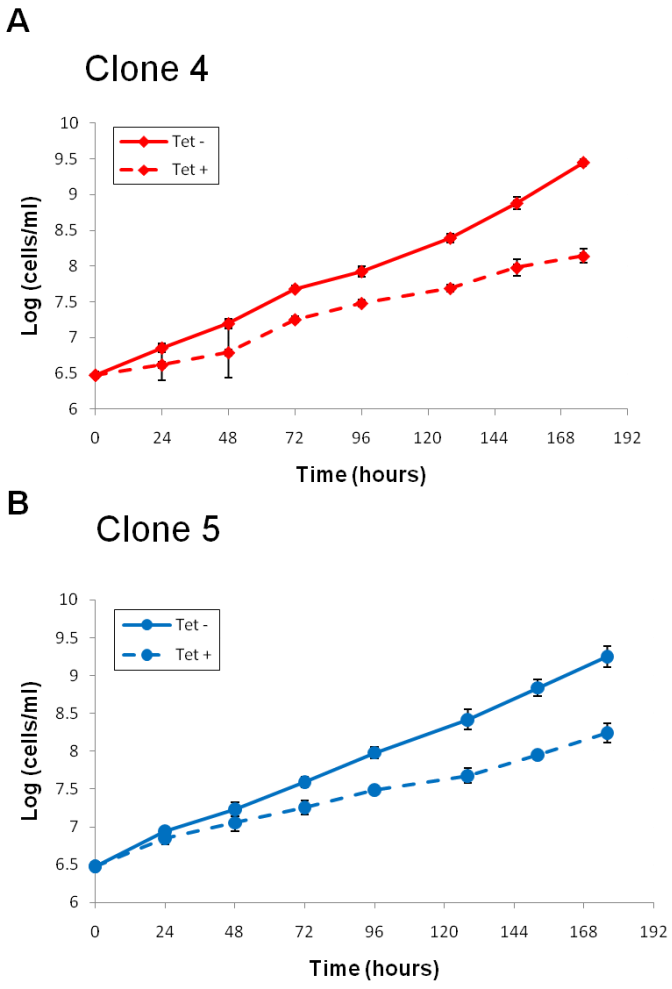

Figure 5-8 -Cumulative growth curves of procyclic *AIR9* RNAi cell lines.
Triplicate cultures of two independent *AIR9* RNAi cell lines (A: clone 4; B: clone 5) were grown in the absence (Tet-) or presence (Tet+) of 1 µgml^{-1} tetracycline; growth was analysed by determining the cell density at regular intervals (shown) over a period of 174 hours.

To investigate the possibility of cell cycle defects being responsible for the slow growth defect observed, the two independent RNAi cell lines were analysed by flow cytometry (Section 4.10). Uninduced and induced cells were sampled at approximately 24 hour intervals for the duration of the induction, fixed with

methanol and stained with propidium iodide prior to performing flow cytometry. Histograms of frequency versus whole cell fluorescence (FL2-A) were used to compare populations. 2C and 4C ploidy is easily discernable as two peaks, which represent cells in G0/G1, and G2/M, respectively (Figure 5-9, 'T=0'). Cells undergoing S-phase have intermediate fluorescence and are distributed between these peaks. Results for the induced clones are shown in Figure 5-9B and D; alterations in the cell cycle profile are apparent at 72 hours post-induction, when an abnormal peak arises, corresponding to a DNA content of less than 2C, which could represent cell debris or anucleate cells (e.g. 0N1K). At 96 hours post-induction, other abnormal peaks appear, representing cells emitting abnormally high levels of fluorescence which correspond to a more than 4C ploidy; and implies that individual cells are undergoing a second round of DNA replication. The abnormal peaks become more prominent over time, accompanied by a steady decrease in the height of the 2C peak. Together these changes suggest that cytokinesis might be impaired, and abnormalities in the DNA profile coincide with both growth inhibition and significant decreases in AIR9 expression. There was some variation between the sizes of 2C and 4C peaks in the uninduced controls (see Figure 5-9A and C), but cells with abnormal ploidy were not detected.

A. Clone 4 Tet-

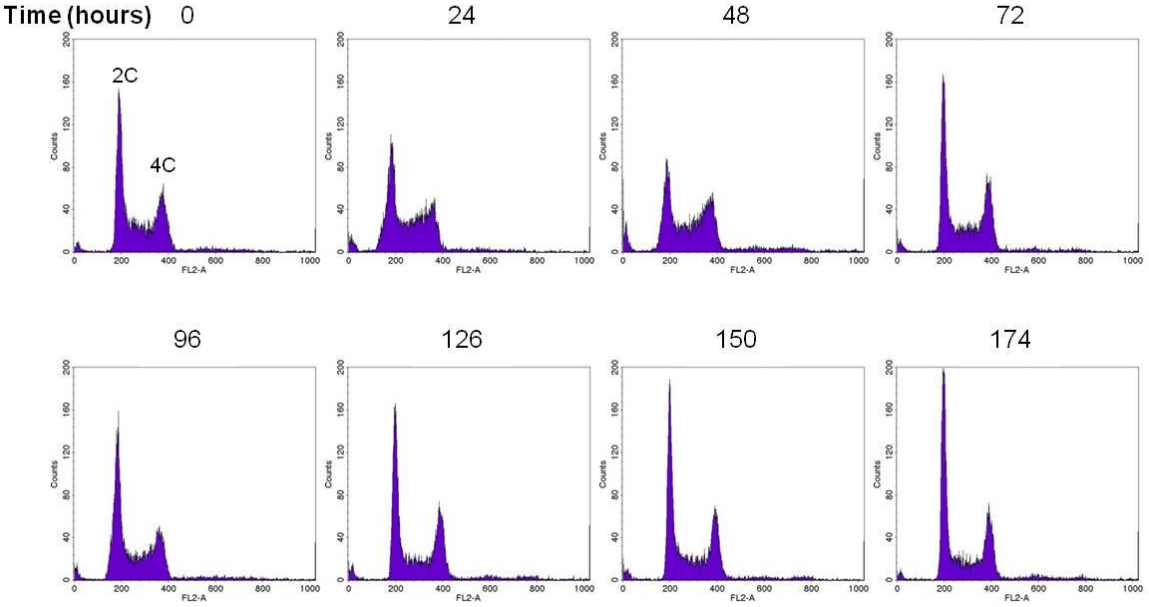

B. Clone 4 Tet +

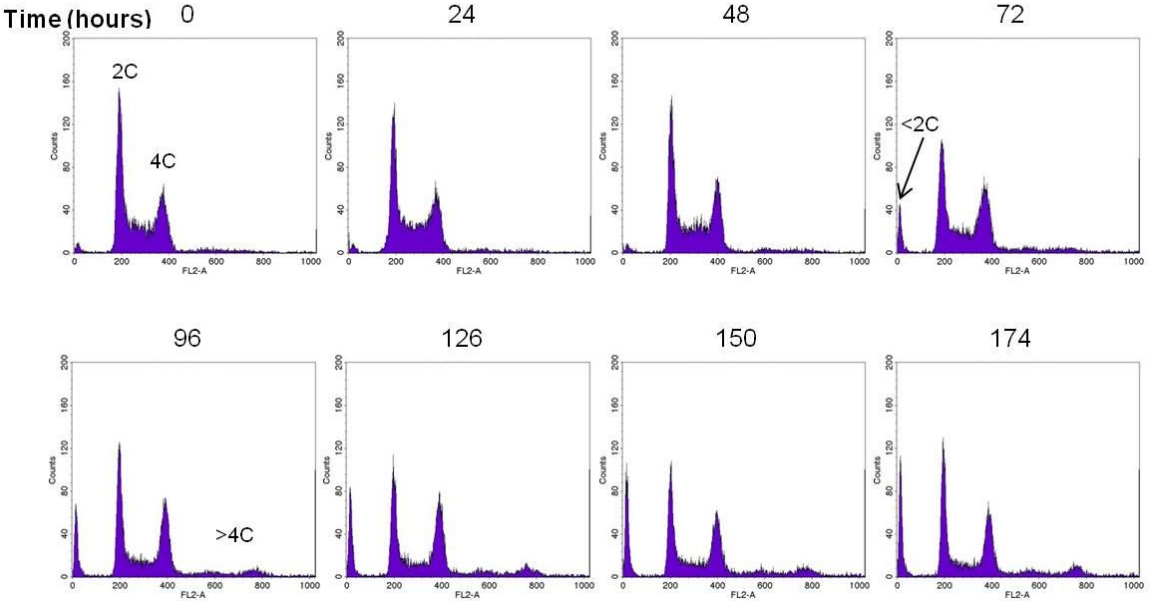

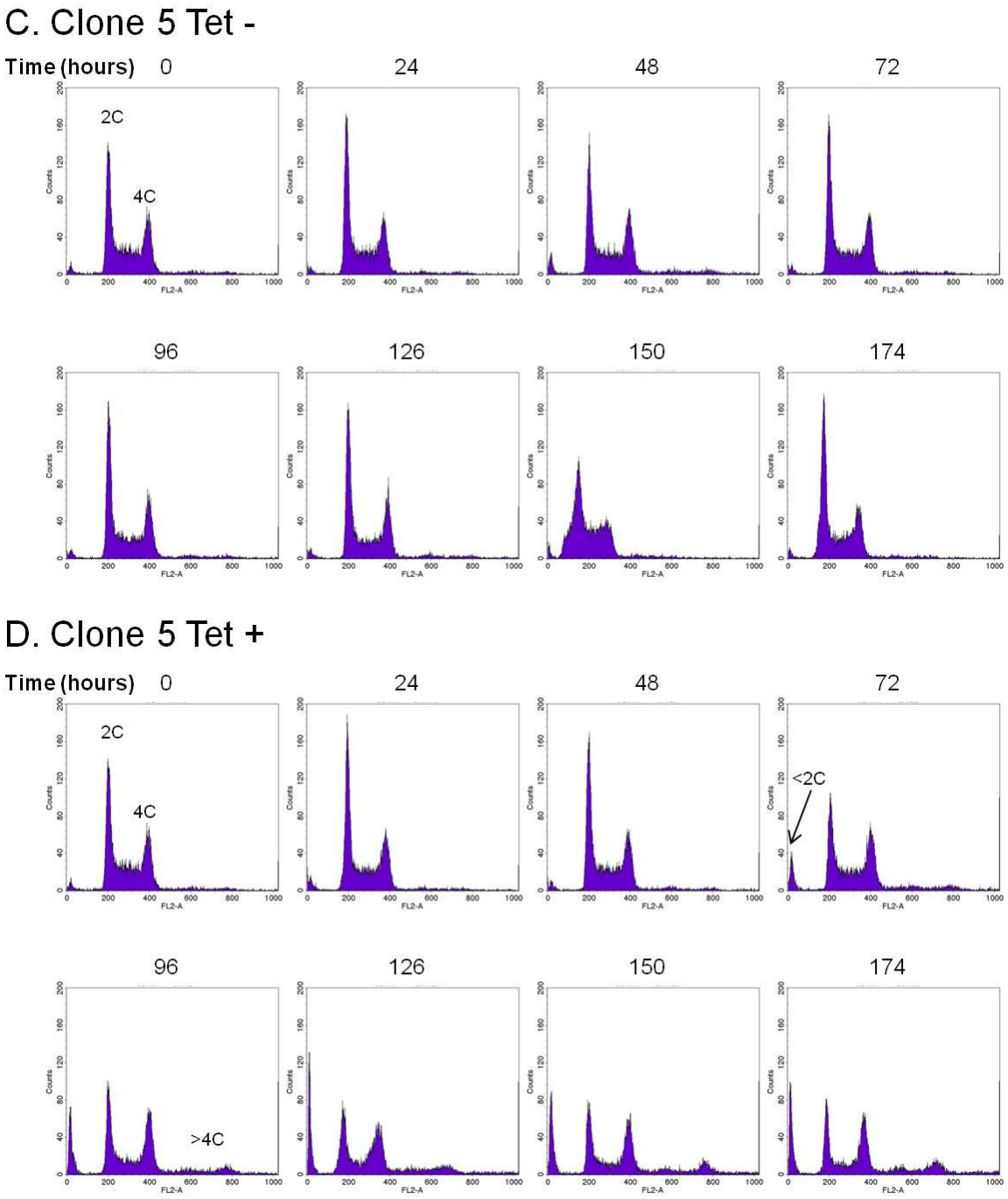

Figure 5-9 -Flow cytometry analysis of procyclic *AIR9* RNAi cell lines.
Two independent *AIR9* RNAi clones (A+B: clone 4; C+D: clone 5) grown in the absence (A+C: 'Tet –') or presence (B+D: 'Tet +') of tetracycline were analysed by flow cytometry (x-axis: FL2A; y-axis: cell count). Time points of sampling, and ploidy are shown.

5.3.2.4 Downregulation of AIR9 causes cytokinesis defects in procyclic form parasites

To further characterise any cell cycle defects appearing following the depletion of AIR9, cells grown in the presence or absence of tetracycline were sampled at approximately 24 hour intervals, fixed and stained with DAPI for analysis by

microscopy (Section 4.11.1). Over 200 individual cells were examined at each time point. Cells were classified according to the number of kinetoplasts and nuclei contained within them and the relative positions of these organelles; if relevant, the cytokinesis stage (no furrow, furrow, abscission) was recorded. Initially, the cell populations comprised 70-80% 1N1K cells, 10-20% 1N2K cells, 5-10% 2N2K cells with <3% cells exhibiting other (abnormal) N-K configurations (Figure 5-10). Images of cells with normal N-K configurations can be seen in Figure 5-12. In procyclic form parasites, the G2/M transition is marked by the dramatic basal body and coincident kinetoplast segregation and by the elongation of the replicated nucleus, and cells at early and late stages of this process (as implied from inter-kinetoplast distances and nuclear morphology) are shown in Figure 5-12Bi and Bii, respectively. Mitosis features segregation of the nuclei resulting in the typical KNKN organelle arrangement (from posterior to anterior), as shown in Figure 5-12C.

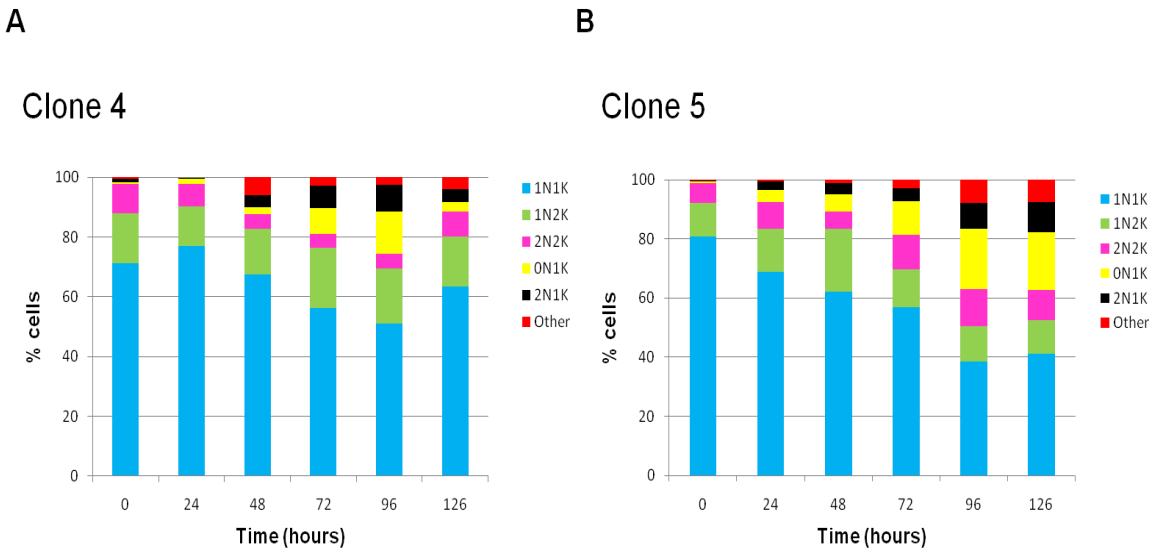

Figure 5-10 -DAPI staining of procyclic *AIR9* RNAi cell lines.
Procyclic *AIR9* RNAi cells (A: clone 4; B: clone 5) were grown in the presence of 1 µg ml^{-1} tetracycline and at the time points indicated, cells were stained with DAPI and >200 cells/time point were classified according to the number of nuclei and kinetoplasts per cell.

DAPI staining revealed a steady decrease over time in 1N1K cells (Figure 5-10). The decrease in 1N1K cells coincided with the appearance of 2N1K and 0N1K cells, images of which are shown in Figure 5-13A and B. These abnormal cell types were present in equal numbers at earlier stages of the induction, but at later time points, 2N1K cells were outnumbered by the 0N1K cells (Figure 5-10). Stastical analysis (Section 4.13) determined that although a small number of these abnormal cell types were sometimes observed in uninduced populations,

the numbers seen in induced populations were significantly higher at 72 or 24 hours post-induction for clones 4 and 5 respectively (Figure 5-11 and Table 5-2).The initial generation of equal numbers of these abnormal cell types suggests that they are sibling cells, which probably arose from a 2N2K parental cell.

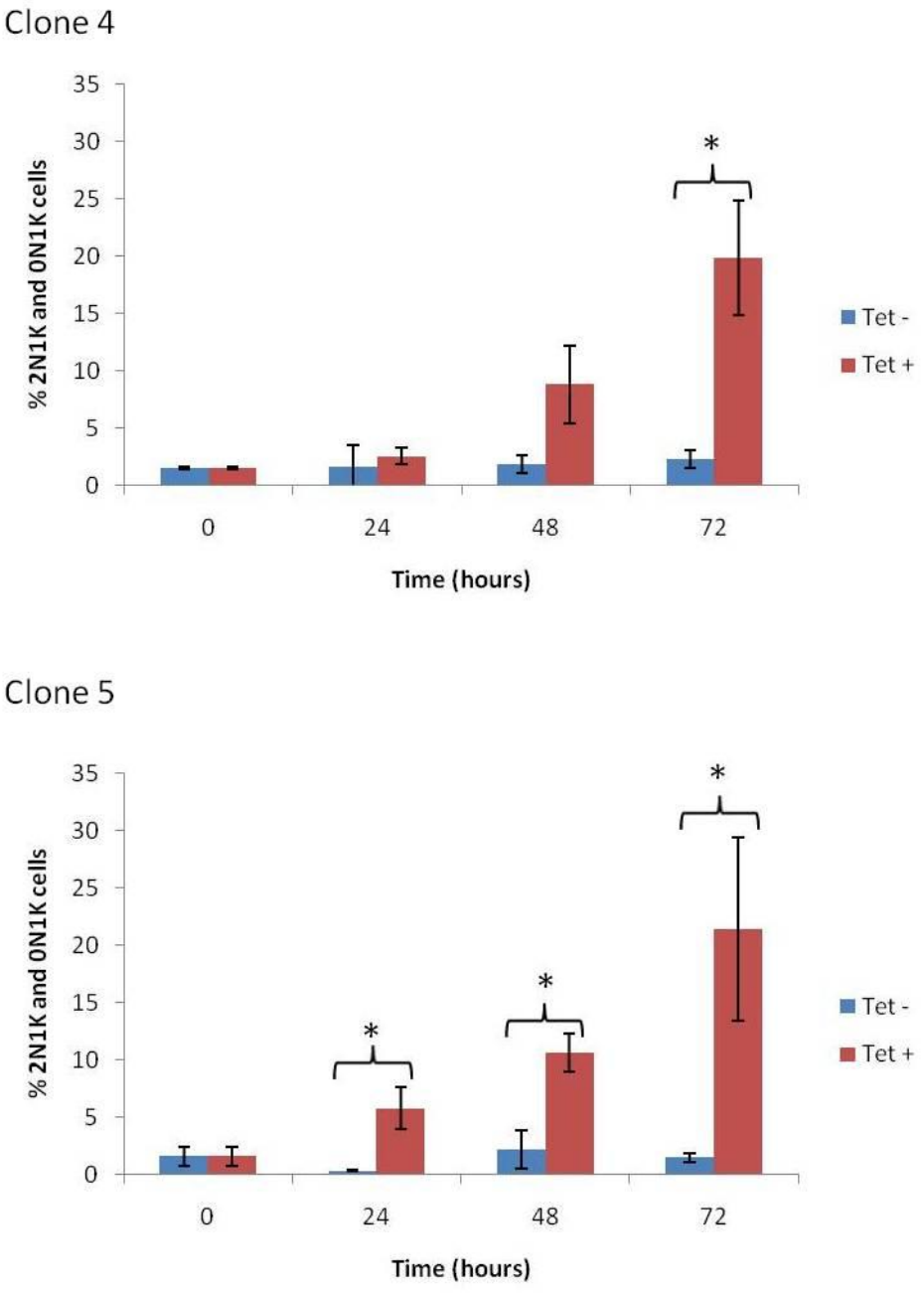

Figure 5-11 -Stastical analysis of 0N1K and 2N1K cells in AIR9 RNAi procyclic form cells. Procyclic form AIR9 RNAi cells grown in the absence or presence of 1 µgml^{-1} tetracycline ('Tet –' or 'Tet +', respectively) were analysed by DAPI staining and scored according to the whether cells contained two nuclei an one kinetoplast (2N1K) or were anucleate (0N1K). The results from two experiments were used to generate a mean, with values ±SEM. '*' indicates P=0.05 by an unpaired t-test (one-tail).

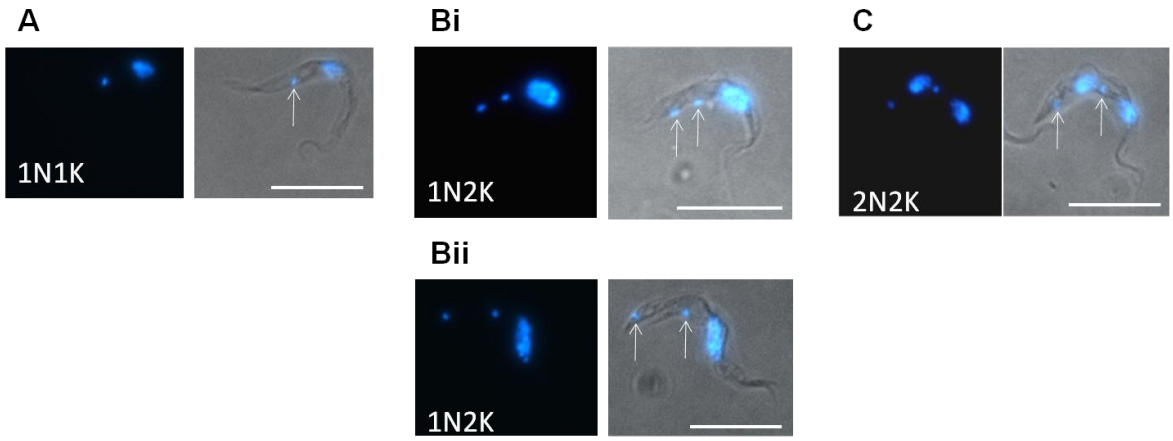

Figure 5-12 –Normal N-K configurations in procyclic form cells.
Representative DAPI-stained images of procyclic form cells containing normal quotas of nuclei (N) and kinetoplasts (K, arrows), as indicated. Left panels: DAPI; right panels: DAPI/DIC merge. Scale bars: 10 µm.

At later time points, multinucleate cells were observed (grouped within the 'Other' category in Figure 5-10), which in general resembled the cell shown in Figure 5-13C. Cells rarely possessed more than four nuclei and these cells maintained their characteristic spindle morphology. An example of a rare multinucleate cell with eight nuclei is shown in Figure 5-13D. Multinucleate cells were occasionally seen dividing to produce 0N1K daughters, which may have contributed to the asymmetric rise in 0N1K cells over 2N1K cells at these later time points.

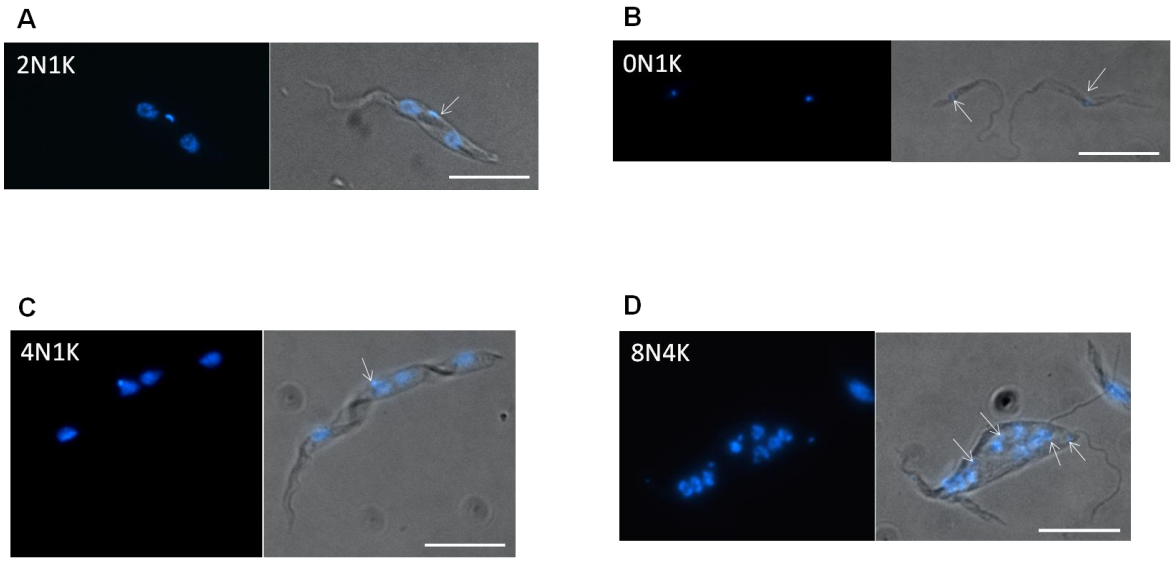

Figure 5-13 -Abnormal cell types observed following induction of *AIR9* RNAi in procyclic cells.
Representative DAPI-stained images of procyclic form *AIR9* RNAi cells (induced) containing abnormal quotas of nuclei (N) and kinetoplasts (K, arrows), as indicated. While some cells displayed normal morphology (cells A-C), others had an abnormal rounded morphology (see 8N4K cell, D). Left panels: DAPI; right panels: DAPI/DIC merge. Scale bars: 10 µm.

Both clones displayed some variability with regards to the proportions of 1N2K and 2N2K cells in their populations overtime, but since overall the proportion of these cell types did not change greatly (Figure 5-10), this implies that although the 2N2K cells appear to be dividing asymmetrically, cytokinesis still occurs at a similar rate.

These data are consistent with the flow cytometry analysis, which clearly showed a transition in the DNA profile of the population at 72 hours (Figure 5-9). The appearance of a small peak corresponding to an abnormally low DNA content coincided with a significant accumulation of 0N1K cells (comprising 8.6% or 11.3 % of the population for clones 4 and 5, respectively; Figure 5-10). Later, at 96 hours post-induction, the appearance of peaks corresponding to a DNA content greater than 4C coincided with an accumulation of multinucleate cells (comprising 2.5 % and 7.8 % of the population for clones 4 and 5, respectively).

5.3.2.5 Downregulation of AIR9 affected organelle positioning in procyclic form parasites

Examination of the DAPI-stained cells revealed that a striking proportion of cells with a normal quota of nuclei and kinetoplasts displayed atypical positioning of these organelles, as tabulated in **Error! Reference source not found.**. Despite the appearance of some cells with abnormal organelle positioning in non-induced populations, the proportion of cells with this phenotype were significantly greater in induced populations at 72 and 48 hours for clones 4 and 5 respectively (Figure 5-15 and Table 5-2).

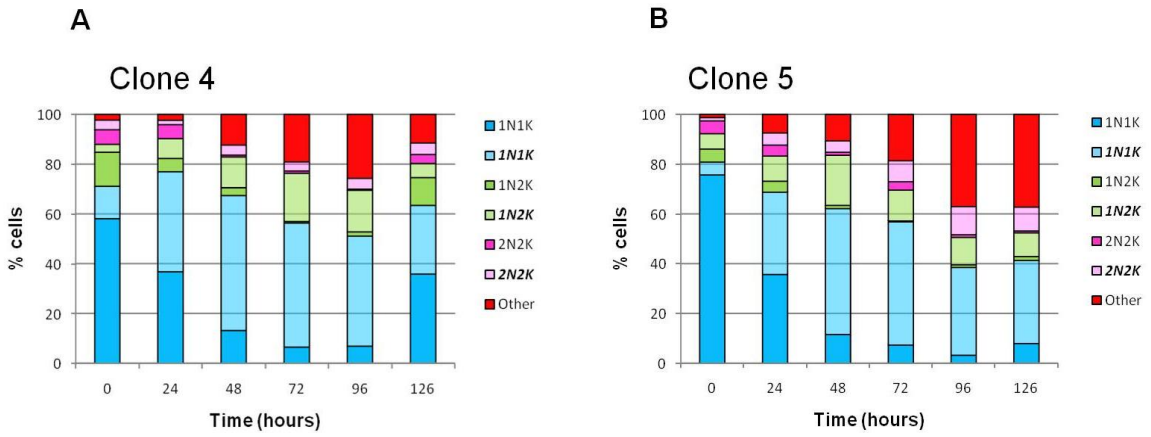

Figure 5-14-Organelle positioning defects observed following induction of AIR9 RNAi in procyclic cells.
Procyclic *AIR9* RNAi cells induced with 1 µgml^{-1} tetracycline and examined by DAPI staining (Figure 5-10), are presented here scored according to whether organelle positioning was normal (darker colours, standard font) or abnormal (lighter colours, italic font). 'Others' comprises those cells with an abnormal quota of nuclei (N) and/or kinetoplasts (K).

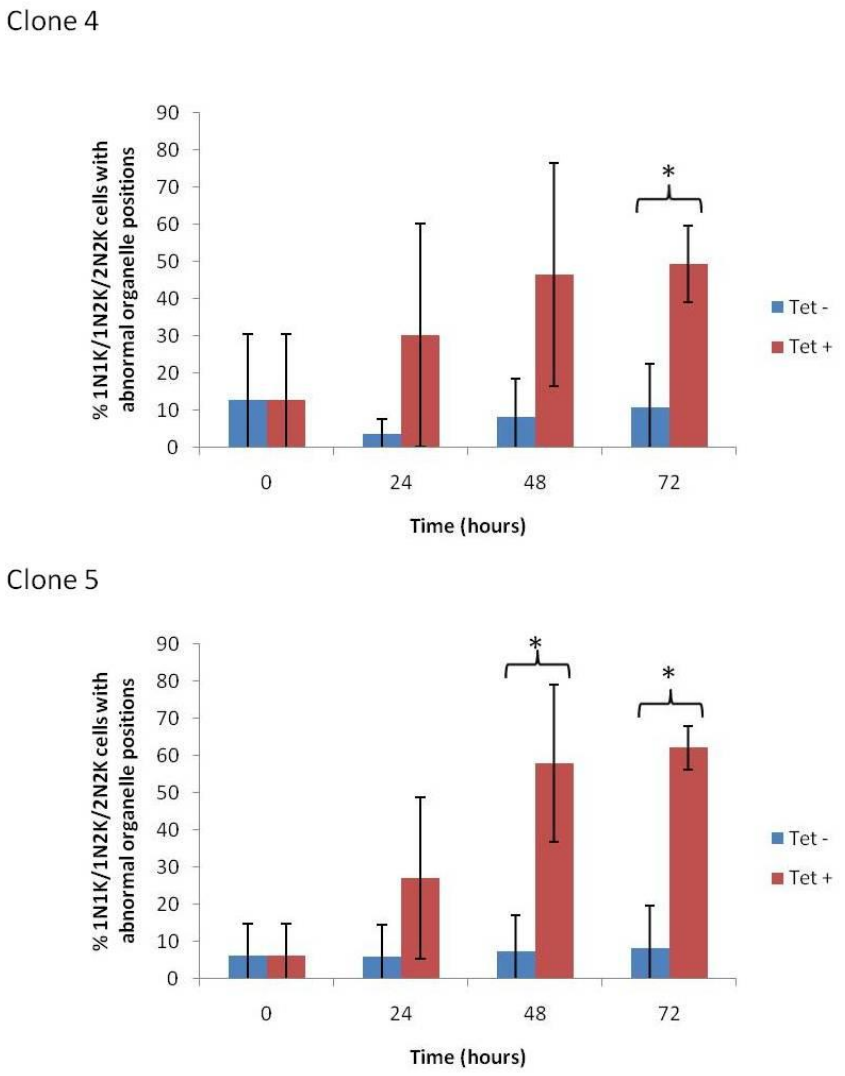

Figure 5-15-Stastical analysis of the organelle positioning defects in AIR9 RNAi procyclic form cells.
Procyclic form AIR9 RNAi cells grown in the presence or absence of 1 µgml^{-1} tetracycline ('Tet –' or 'Tet +', respectively) were analysed by DAPI staining and scored according to

whether organelle positioning was normal. The results from two experiments were used to generate a mean, with values ±SEM. '*' indicates P=0.05 by an unpaired t-test (one-tail).

Table 5-2-P values from unpaired t-tests assuming equal variance (one-tail) to determine the significance of the appearance of abnormal cell types in induced AIR9 RNAi procyclic cells. The significance of the appearance of abnormal cells in AIR9 RNAi procyclic form cell lines grown in the presence of 1μgml^{-1} tetracycline at different times during the experiments was determined by statistical analysis (Section 4.13) The results use data from two separate experiments. P=0.05.

Phenotype	Time (Hours)	P (T<=t)	
		Clone 4	Clone 5
% cells with abnormal organelle positioning	24	0.17062	0.16474
	48	0.115056	0.04555
	72	0.036247	0.013636
% 0N1K and 2N1K cells	24	0.284187	0.026232
	48	0.053816	0.018546
	72	0.019532	0.035996

The positioning defects in 1N1K cells included cells with the kinetoplast and nucleus positioned laterally to each other (sometimes the kinetoplast appeared to be directly above the nucleus when focussing through the cell), which are here referred to as 'K^N' cells, and cells where the kinetoplast was positioned anteriorly to the nucleus which are referred to as 'NK' cells. Example images of normal and both abnormal cell types are shown in Figure 5-16Ai-iii. The abnormal 1N1K cells comprised a large proportion of the whole population, and to compare the relative proportions of the different atypical cell types over the course of the induction, 1N1K cell types are displayed separately in Figure 5-16Bi-ii. Comparing the chronology of the appearance of K^N and NK cells reveals that K^N cells appear in larger numbers during the first three to four days, and afterwards, the proportion of 1N1K cells displaying the more severe NK phenotype increases to levels similar to the proportion of K^N cells within the whole population. This indicates a gradual increase in the severity of the positioning defect.

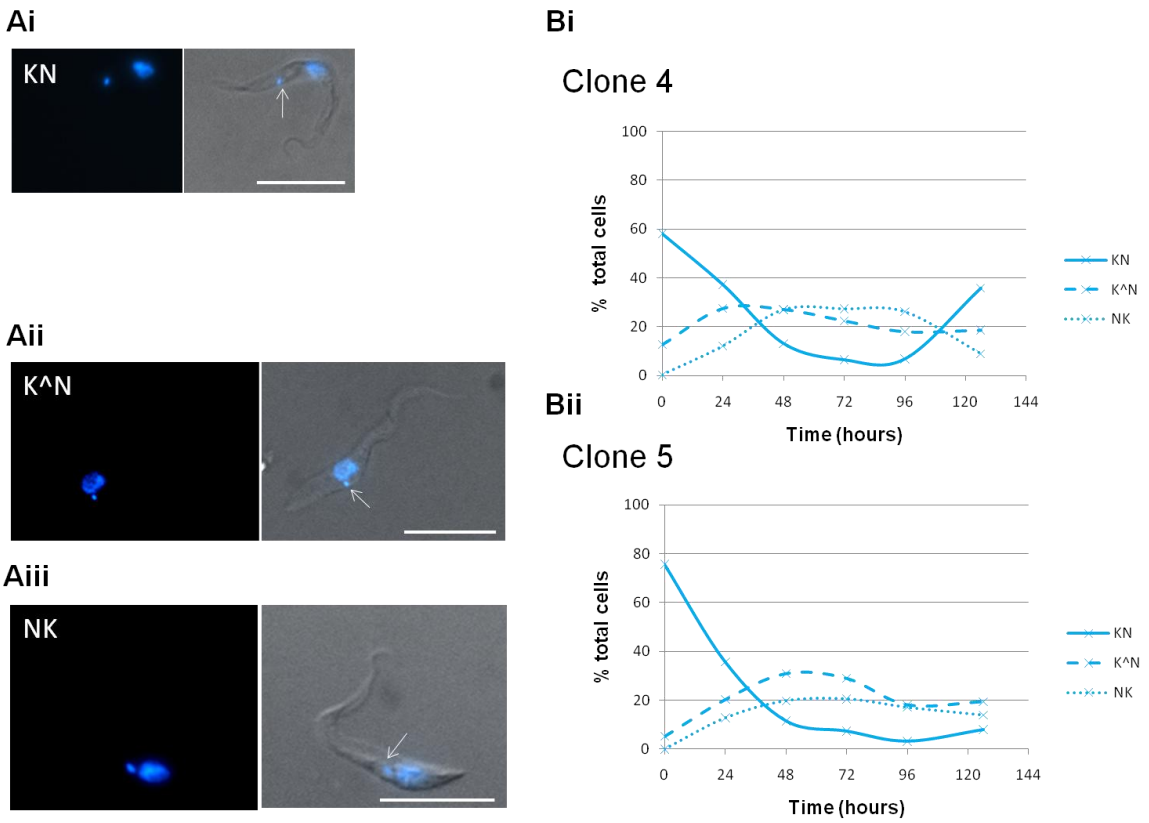

Figure 5-16 -Organelle positioning defects observed in 1N1K cells following induction of *AIR9* RNAi in procyclic cells.
Following induction of *AIR9* RNAi, cells were stained with DAPI and the relative positions of the nucleus (N) and kinetoplast (K, arrows) in 1N1K cells were examined. A: examples of the three types of 1N1K cells (Ai: normal organelle positioning (KN); Aii: kinetoplast lateral to nucleus (K^N); Aiii: kinetoplasts anterior to nucleus (NK)). Left panels: DAPI images; right panels DIC/DAPI merge. Scale bars: 10 µm. Bi and Bii: graphs indicating the proportions of the different 1N1K types within whole populations over time for clones 4 and 5, respectively.

1N2K cells displayed a variety of positioning defects, ranging in severity according to how anterior the kinetoplast positioning was relative to the nucleus. Examples of abnormal 1N2K cells are shown in Figure 5-17. A minor positioning defect where the nucleus and one kinetoplast were located at similar distances from the anterior of the cell (i.e. this kinetoplast was lateral to the nucleus) was referred to as 'KK^N'; an example of this cell type is shown in Figure 5-17A. Cells with a 'KNK' organelle arrangement were the most prevalent, where the nucleus was straddled by two kinetoplasts (Figure 5-17B). Cells with this arrangement comprised 13 % or 8 % of the whole population at 72 hours post-induction for clones 4 and 5, respectively. More severe phenotypes included 'K^NK' cells, where one kinetoplast was lateral to the nucleus and the second kinetoplast was anterior to the nucleus (shown in Figure 5-17C), and 'NKK' cells, where both kinetoplasts were located at anterior positions relative to the nucleus.

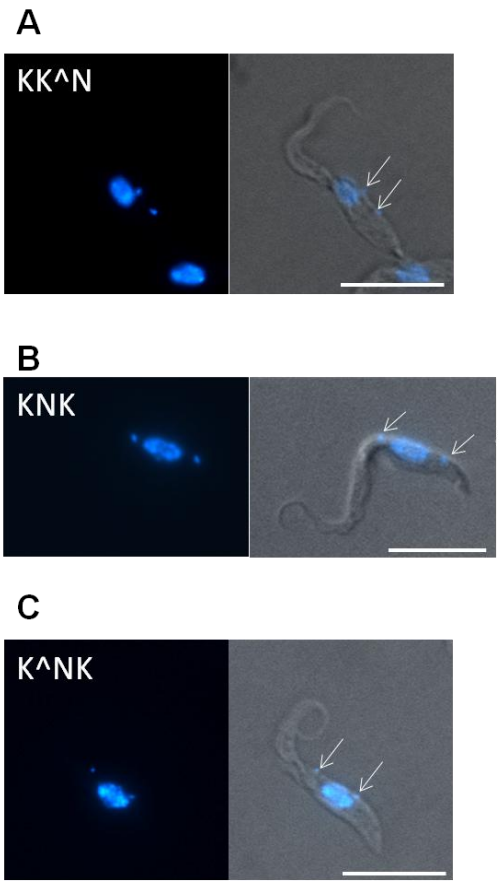

Figure 5-17 -Organelle positioning defects observed in 1N2K cells following induction of *AIR9* RNAi in procyclic cells.
Following induction of *AIR9* RNAi, cells were stained with DAPI and the relative positions of the nucleus (N) and kinetoplasts (K, arrows) in 1N2K cells were examined. A-C: 1N2K cells with organelle positions 'KK^N', 'KNK' and 'K^NK', respectively. Left panels: DAPI images; right panels: DIC/DAPI merge. Scale bars: 10 µm.

2N2K cells possessed the largest number of nucleus and kinetoplast positioning defects, probably due to the increased number of organelles and therefore possible positional combinations. As described above, the usual arrangement of the nuclei and kinetoplasts in procyclic 2N2K cells is KNKN (posterior to anterior), with the organelles arranged in a linear fashion following the axis of the cell (see Figure 5-12C). Cells displaying the organelle configuration 'K^NK^N' (describing a cell where the nuclei and kinetoplasts have segregated, but each kinetoplast is positioned lateral to the appropriate nucleus) were the most numerous of the abnormal post-mitotic cells (Figure 5-18Ai). At 96 hours post-induction, 'K^NK^N' cells comprised 1.7 or 5.3 % of the whole population for clones 4 and 5, respectively. Other abnormalities were represented by tiny proportions of cells in the context of the whole population; these rarer organelle positioning defects included cells with a 'KKNN' organelle configuration (describing cells where the kinetoplasts appear not to have segregated fully), and cells with the organelle configurations 'NKKN', 'KNNK' K^NKN', and 'KNK^N'

(where the position of only one kinetoplast was abnormal). Examples of some of these rare organelle positioning defects are shown in Figure 5-18Aii-iii. Malpositioning of organelles did not prevent furrow ingression. Examples of cells with both abnormally positioned organelles and visible cleavage furrows are shown in Figure 5-18B. Cells with abnormal organelle positioning were also observed at the abscission stage of cytokinesis, implying that they were capable of completing furrow ingression (Figure 5-18C). Occasionally, nascent daughter cell bodies did not appear to possess an equal quota of organelles, thus identifying these abnormal 2N2K parents as a potential source of 2N1K and 0N1K siblings (Figure 5-18Ci and iii).

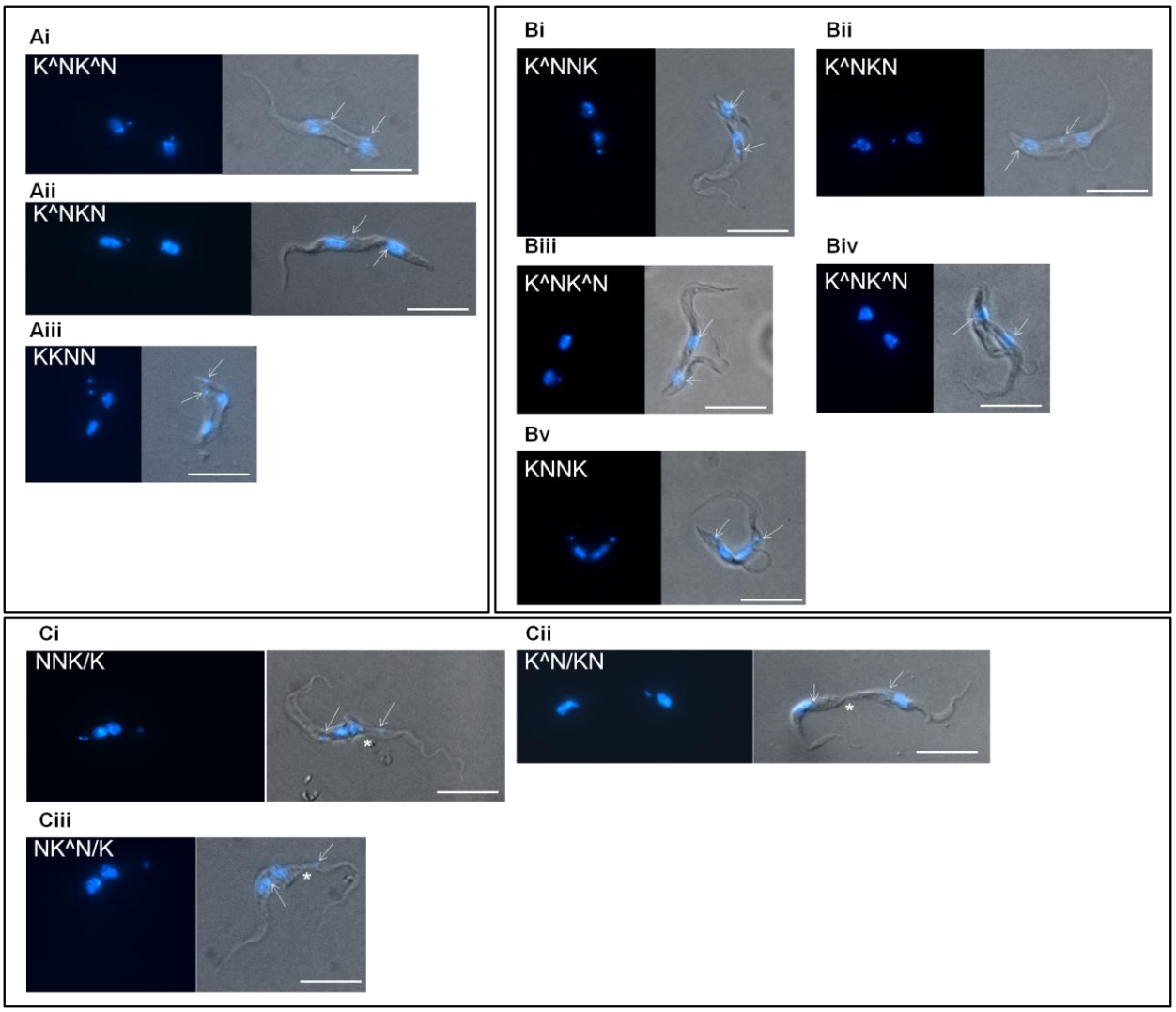

Figure 5-18 -Organelle positioning defects observed in 2N2K cells following induction of *AIR9* RNAi in procyclic cells.
2N2K cells were classified according to both organelle positioning and cytokinesis stage. A-C: cells at the pre-cytokinesis, furrow ingression and abscission stages of cytokinesis, respectively. Left panels: DAPI images; right panels: DIC/DAPI merge. The N-K positioning designations are shown. For cells at the furrow ingression or abscission stages, the N-K distribution for daughter cells is not certain, but probable outcomes for the quota of nuclei (N) and kinetoplasts (K, arrows) in each cell are indicated by '/'. Scale bars: 10 µm. Asterisks indicate the point of abscission.

Cells displaying abnormal organelle positioning were present in very large numbers at 24 hours post-induction, at which point AIR9 levels were reduced but still detectable (Figure 5-7), implying that organelle positioning is sensitive to decreased levels of AIR9. This also suggests that the cytokinesis defects observed could be a downstream effect of aberrant organelle positioning.

It was of interest to determine at which stage(s) of the cell cycle, the N-K positioning defects first appeared, but due to the relatively small numbers of 1N2K and 2N2K cells present within the 200 or so cells analysed per time point, it was not possible to investigate the chronology of the organelle positioning defect from the whole population data. Therefore, more than 200 cells of each N-K configuration (1N1K, 1N2K and 2N2K) were classified at 0, 12 and 24 hours post-induction in order to address this question. Figure 5-19 shows the percentage of abnormal cell types at the selected time points for each N-K configuration. A certain degree of abnormal organelle positioning was observed for all N-K configurations at the start of the induction (probably due to leaky expression from the T7 promoter of the RNAi construct), but by 12 hours post-induction an increase in abnormal organelle positioning for all N-K configurations was observed. At 24 hours post-induction, the percentage of cells with positioning defects for each N-K configuration was similar. Given the reduced growth rate of parasites depleted of AIR9, it is likely that only one cell cycle is completed at 24 hours (the doubling time over the first 24 hours of the time course was 19 hours for both clones in the presence of tetracycline). In light of the slow growth rate, the similar increases in the proportion of abnormal cells for all cell cycle stages suggests that abnormal organelle positioning arises simultaneously in all cell types, and is therefore independent of cell cycle stage.

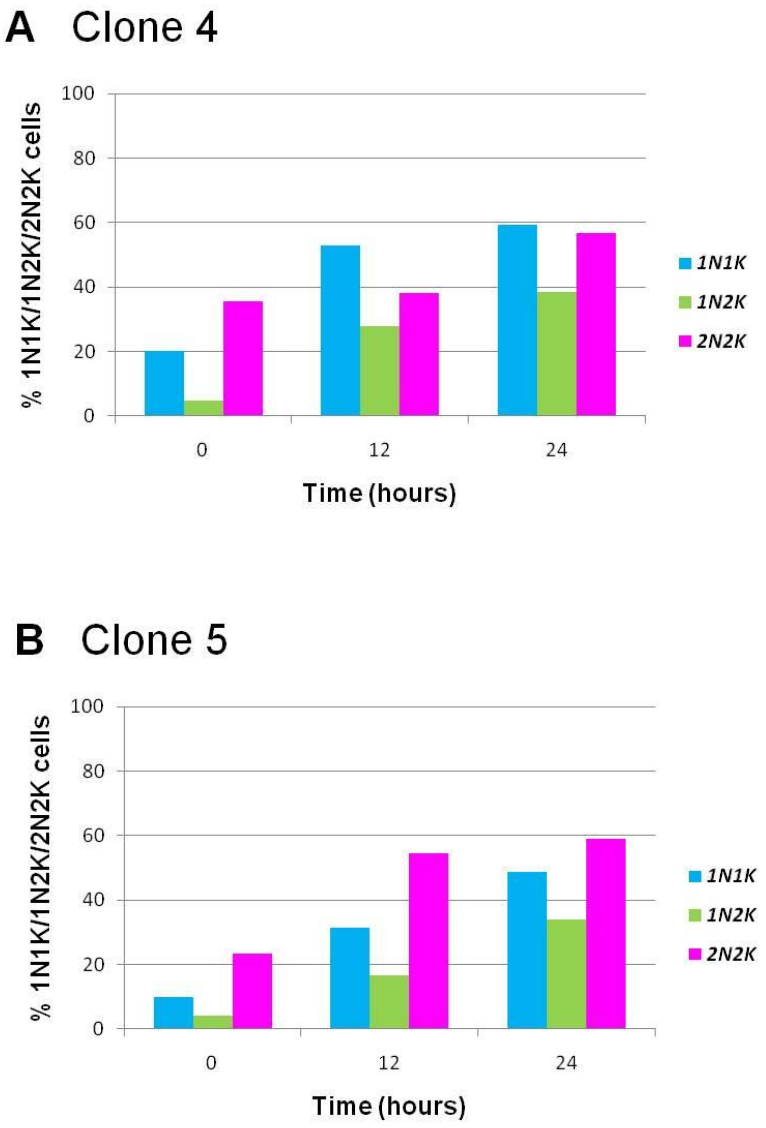

Figure 5-19 -Emergence of organelle positioning defects in different cell types following induction of *AIR9* RNAi in procyclic cells.
Procyclic *AIR9* RNAi cells (A: clone 4; B: clone 5) were induced with tetracycline and >200 DAPI-stained 1N1K, 1N2K and 2N2K cell types were analysed at 0, 12 and 24 hours post-induction. The bars show the proportions of abnormal cells for each cell type.

A more in-depth analysis of the relative positions of the nuclei and kinetoplasts in 1N1K, 1N2K and 2N2K cells revealed that the position of the kinetoplast in 1N1K cells becomes increasingly anterior over the 24 hour induction period (Figure 5-20A). This is demonstrated by the increased prevalence of the K^N and, with slightly slower kinetics, NK, cell types over time. A similar pattern was also observed in 1N2K cells, where cells displaying the KK^N arrangement and later, cells displaying the KNK arrangement, increased in abundance over the induction period (Figure 5-20B). For the 2N2K population, a large proportion of cells displaying abnormal organelle positioning were observed (Figure 5-20C). At 12 hours post-induction the predominant abnormality comprised cells with the

most posterior kinetoplast being positioned abnormally anterior (K^NKN) and these cells comprised 61.9 % or 71.8 % of the 2N2K cells with organelle positioning defects (for clones 4 and 5, respectively). At 24 hours post-induction, K^NKN cells only comprised 35.1 % and 54. 9 % of abnormal cells (for clones 4 and 5, respectively), as more severe abnormalities became more prevalent. An increasing number of cells with organelle positioning defects also appeared to be undergoing cytokinesis (Figure 5-20C), and a larger proportion of these cells were undergoing furrow ingression rather than abscission. At 24 hours post-induction, 2N2K cells with abnormal organelle positioning that were undergoing furrow ingression comprised 14.1 % and 9.1% of the 2N2K cell population, while those undergoing abscission comprised just 3.1 % and 1.2 % of 2N2K cells (for clones 4 and 5, respectively). Prediction of the eventual outcome of cleavage for cells at the furrow ingression stage was deemed too speculative; therefore, only those at the abscission stage were categorised according to organelle distribution between the nascent daughter cell bodies. At 24 hours post-induction, of the 2N2K cells with apparently normal organelle positioning that were undergoing abscission, approximately half displayed malpositioned cleavage planes. It is probable that 0N1K and 2N1K cells can arise from these cells, but it is also highly likely that some 2N2K cells with abnormal organelle positioning also eventually divide abnormally to produce 0N1K and 2N1K cells (see Figure 5-18C), and given that 2N2K cells with aberrant organelle positioning quickly outnumber those with normal organelle positions, these seem a more probable origin of the 0N1K and 2N1K cells.

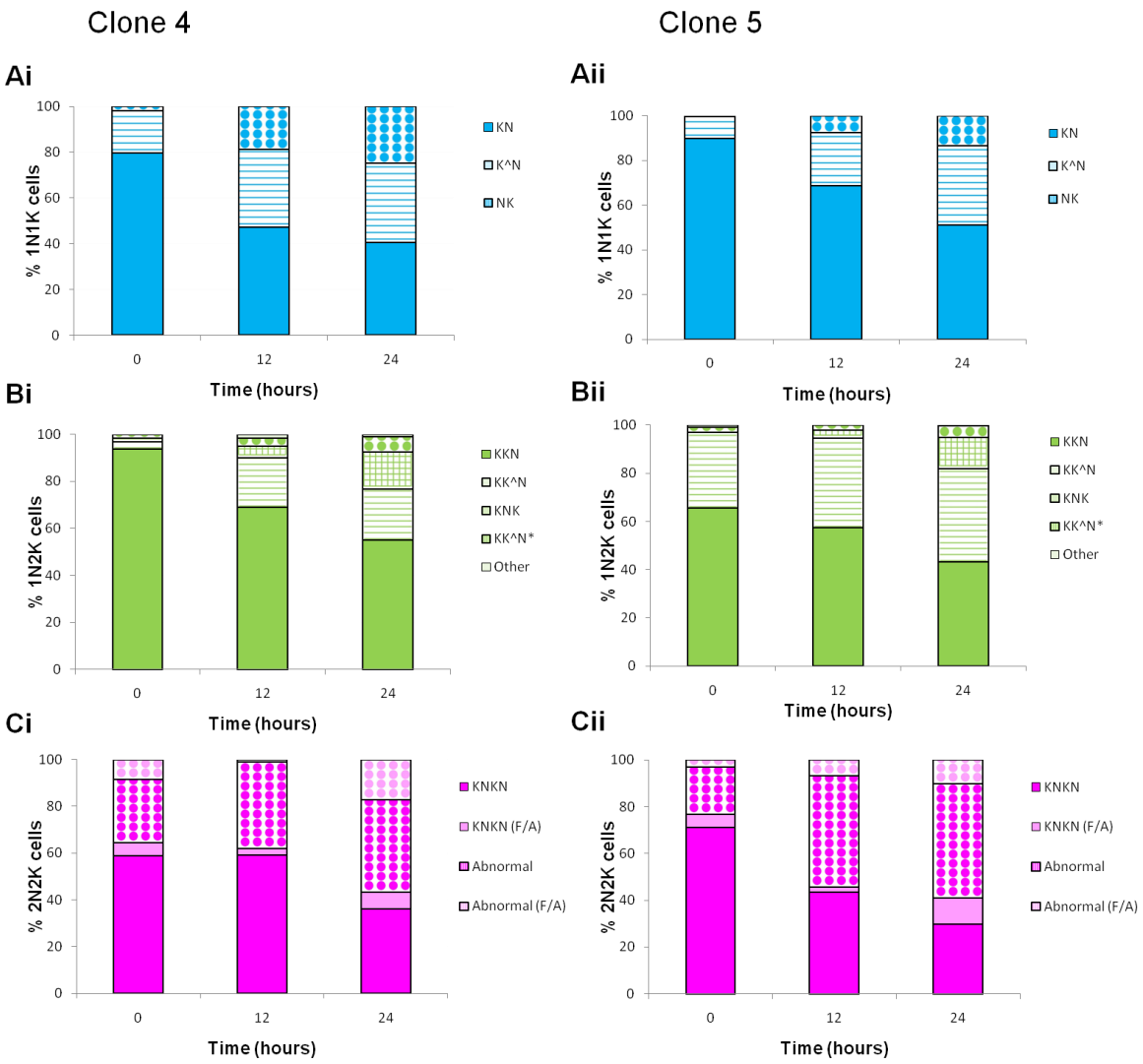

Figure 5-20 –Chronological analysis of organelle positioning defects for different N-K configurations following induction of *AIR9* RNAi in procyclic form cells.
Following induction of *AIR9* RNAi, DAPI stained cells (*n* > 200 for each N-K configuration) were classified according to organelle positioning. Normal organelle positioning: solid bars; abnormal organelle positioning: patterned bars. A: 1N1K cells (solid bars: KN; striped: K^N; circles: NK); B: 1N2K cells (solid bars: KKN; striped: KK^N; checked: KNK; circles: KK^N*); C: 2N2K cells (solid bars: KNKN; circles: other abnormal organelle positions; either non-dividing (dark pink) or dividing (light pink)); for clones 4 (i) and 5 (ii). F/A: furrow ingression/abscission.

5.3.2.6 Nuclear positioning and cell length were affected by AIR9 downregulation

Abnormal positioning of either the kinetoplast, or the nucleus, or of both of these organelles, could have resulted in the aberrant positioning of these organelles relative to each other that was observed following depletion of AIR9. In order to differentiate between these two possibilities, the position of each of these organelles relative to the posterior pole of the cell was quantified (Figure 5-21 and Figure 5-22). For simplicity, only 1N1K cells were measured, and to increase the accuracy of the measurements, cells were stained with the anti-ß-

tubulin antibody, KMX (Section 4.11.2), resulting in bright staining of the cell body and flagellum. In order to ensure sufficient numbers of abnormal cells, *AIR9* RNAi was induced for 72 hours before analysis; as a comparison, cells with normal organelle positioning from uninduced cultures grown over the same period were examined. More than 100 cells were measured for analysis.

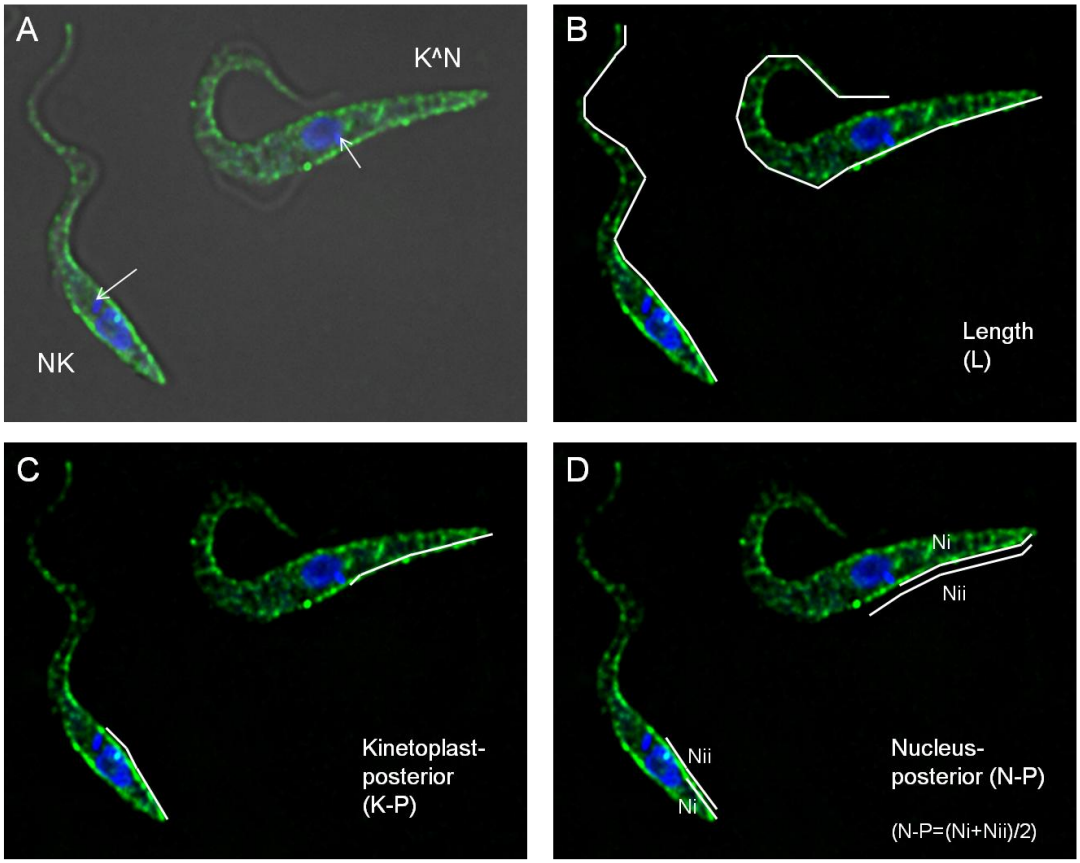

Figure 5-21 -Schematic showing measurements of nucleus and kinetoplast positions in abnormal 1N1K cells.
Procyclic *AIR9* RNAi cells were induced with tetracycline for 72 hours and stained with DAPI (blue) and anti-β-tubulin antibody (green) to allow measurement of the position of the nucleus (N) and kinetoplast (K) relative to the posterior (P) end of 1N1K cells. A: DAPI/FITC/DIC merge of abnormal 1N1K cells, with N-K positioning indicated. B-D: measurements taken (cell length (L), kinetoplast to posterior end (K-P) and nucleus to posterior end (N-P)) are indicated with white lines overlaid on the DAPI/FITC merges. Organelle measurements were taken from the centre of the organelle; for the nucleus, this was measured by averaging the shortest and greatest distance to the posterior end (Ni and Nii, respectively), while the centre of the kinetoplast was estimated by eye. The images shown in this figure are deconvolved and, as it was subsequently found that non-deconvolved images were suitable for this analysis, these do not represent the actual images used.

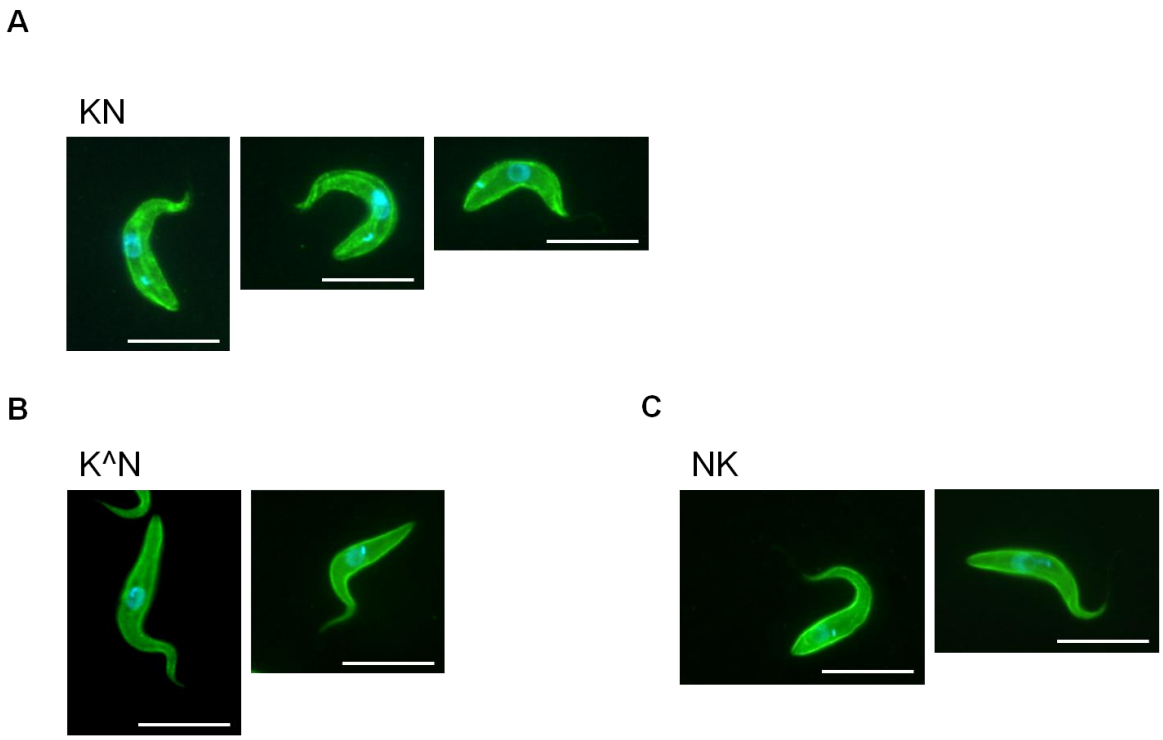

Figure 5-22 -Immunofluorescence of KMX-stained 1N1K cells.
Procyclic *AIR9* RNAi cells were induced with tetracycline for 72 hours and stained with DAPI (blue) and anti-β-tubulin antibody (green) to allow measurement of the position of the nucleus (N) and kinetoplast (K) relative to the posterior end of 1N1K cells. Examples of actual (non-deconvolved) images used for measurements are shown. A: 1N1K cells from uninduced cell population, with normal 'KN' positioning; B and C: 1N1K cells from induced populations with abnormal 'K^N' and 'NK' organelle positioning, respectively. Scale bars: 10 μm.

The parameters measured (see Figure 5-21) comprised cell length (posterior end of the cell to the anterior tip of the flagellum), the distance from the centre of the kinetoplast to the posterior end, and the distance from the centre of the nucleus to posterior end, which was calculated as the average of the distances from the most posterior and most anterior points of the nucleus to the posterior end of the cell. Kinetoplast to posterior end and nucleus to posterior end distances were then expressed as a ratio of cell length. The measurements obtained are represented graphically in Figure 5-23. Following AIR9 depletion, there was a significant increase in the K-P/L ratio and conversely, a significant decrease in the N-P/L ratio for both clones (Table 5-3).

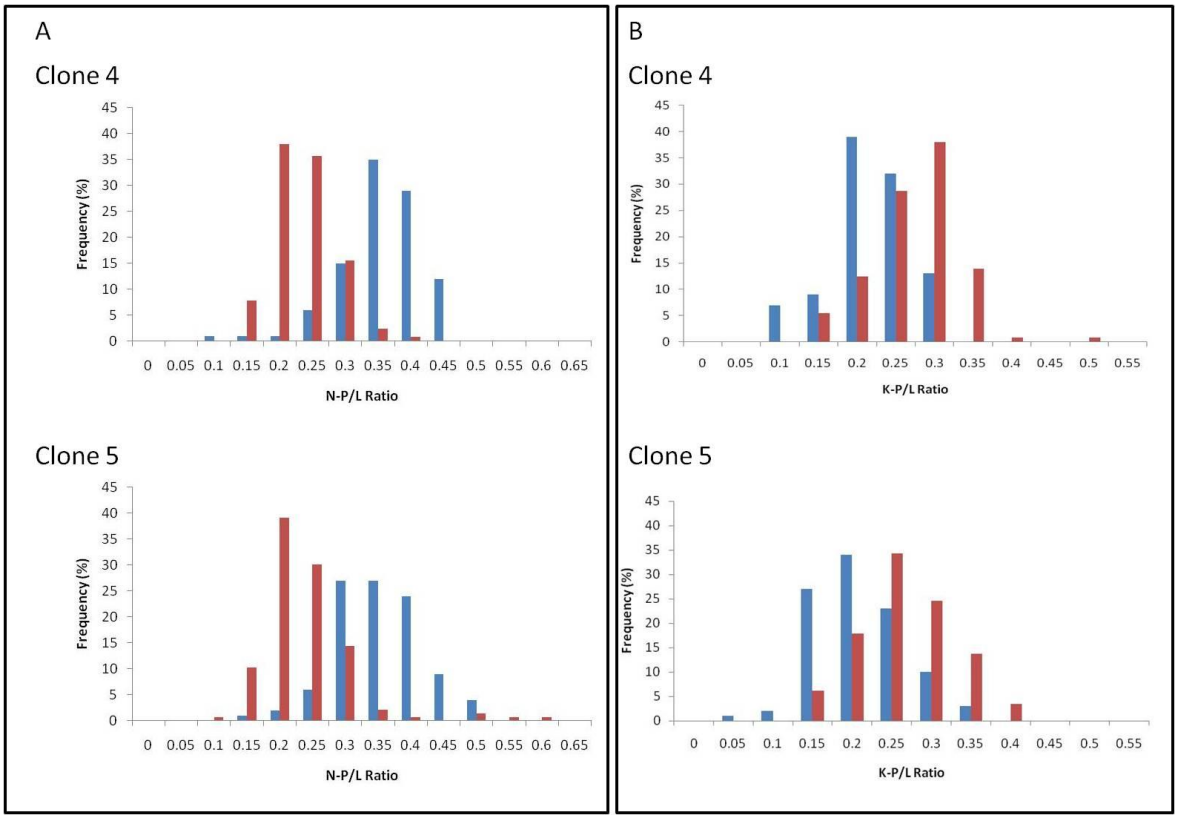

Figure 5-23-Histograms to show distribution of cell dimensions in AIR9 RNAi cell lines. Procyclic *AIR9* RNAi cells were cultured in the presence (Tet +, red bars) or absence (Tet -, blue bars) of tetracycline for 72 hours, and stained with DAPI and for β-tubulin to allow measurement of cellular dimensions (n=>100). A: ratio of nucleus to posterior/cell length (K-P/L); B: ratio of kinetoplast to posterior/cell length (N-P/L).

Surprisingly, there was also a significant increase in cell length upon AIR9 downregulation (Table 5-3) with average cell lengths increasing from 21.2 µm to 23.5 µm (clone 4) and from 19.1 µm to 22 µm (clone 5), possibly as a result of either an increase in flagellum length or posterior end extension. Whilst these two scenarios could affect relative organelle positions (exaggerated posterior extension in the absence of organelle movements would increase the K-P/L and N-P/L ratios, while flagellum extension in the absence of organelle movements would decrease these ratios), it is unlikely that increases in cell length alone directly impacted the organelle positions, as the organelles were displaced relative to the cell posterior in opposite directions (Figure 5-23).

Clone 4

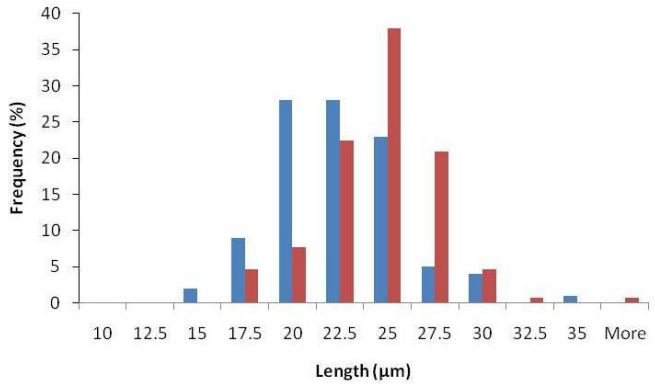

Clone 5

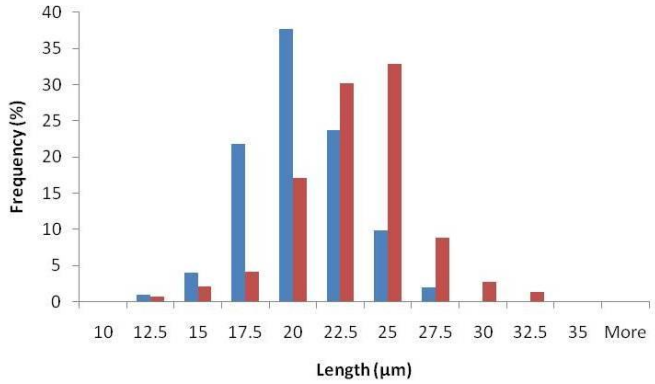

Figure 5-24-Histograms to show distribution of cell length in *AIR9* RNAi procyclic cell lines. Procyclic *AIR9* RNAi cells were cultured in the presence (Tet +, red bars) or absence (Tet -, blue bars) of tetracycline for 72 hours, and stained with DAPI and for β-tubulin to allow measurement of cell length (n=>100).

Through comparisons of organelle to posterior and organelle to anterior distances it was possible to gain a greater insight into the nature of the positioning defect. Analysis of N-P and N-A distances (Figure 5-25 A and C) revealed a significant decrease or increase in these parameters respectively for both clones (Table 5-3) whilst analysis of K-P and K-A distances indicated an increase in both parameters (Figure 5-25 B and D). Further, the increase in K-A distance was only significant for clone 5 (Table 5-3). These results imply that the increase in cell length could occur at the posterior end of the cell, perhaps encompassing the region surrounding the kinetoplast (which could explain the significant increase in K-A distance for clone 5). Importantly, the decrease in N-P and increase in N-A distances implies that the position of the nucleus moves in induced populations. It is therefore likely that AIR9 depletion causes both an increase in posterior extension and posterior movement of the nucleus.

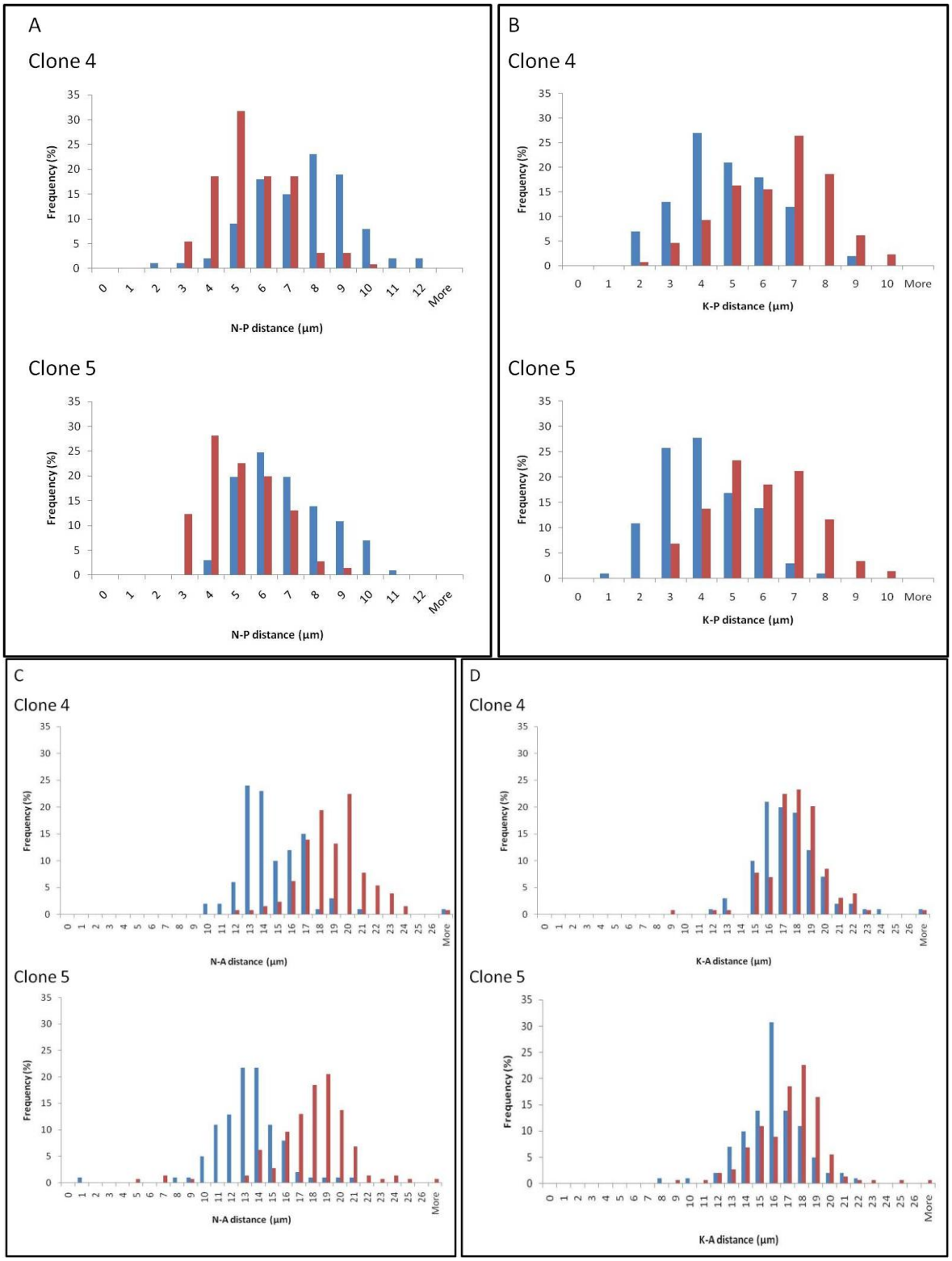

Figure 5-25 -Histograms to show distribution of cell dimensions in *AIR9* RNAi procyclic form cell lines.
Procyclic *AIR9* RNAi cells were cultured in the presence (Tet +, red bars) or absence (Tet -, blue bars) of tetracycline for 72 hours, and stained with DAPI and for β-tubulin to allow measurement of cellular dimensions (n=>100). A-D show the distribution of the measurements corresponding to parameters N-P, K-P, N-A and K-A respectively.

Table 5-3- P values obtained from statistical analysis of cell dimensions using an unpaired t-test (two-tail).
The significance of differences in cell dimensions in 1N1K cells from AIR9 RNAi procyclic form cell lines grown in the presence or absence of 1µgml^{-1} tetracycline at 72 hours was

determined by statistical analysis (Section 4.13). More than 100 cells were analysed for each clone for both induced and uninduced populations. P=0.05.

Parameter	P (T<=t)	
	Clone 4	Clone 5
N-P/L	2.48E-41	1.19E-29
K-P/L	1.67E-12	9.95E-14
Length	3.53E-07	1.28E-12
N-P	8.75E-19	2.66E-16
N-A	2.2E-29	2.96E-31
K-P	3.12E-14	2.82E-17
K-A	0.075138	0.000337

5.3.2.7 Conclusions

In procyclic form parasites, AIR9 can be effectively depleted by RNAi, such that AIR9 protein is undetectable after three days of induction. Reduction in AIR9 results in a rapid emergence of nucleus and kinetoplast positioning defects in cells at all stages of the cell cycle, and this effect is probably caused by a problem with cell polarity rather than cell cycle regulation. Relative nuclear and kinetoplast positions were affected in 1N1K populations: the kinetoplast appearing too anterior and the nucleus too posterior. Further analysis of cell dimensions revealed that a coincident increase in cell length from the posterior end of the cell and posterior movement of the nucleus are likely to cause the dramatic and opposite change in organelle positions relative to the posterior end of the cell. This supports the hypothesis that AIR9 is important for cell polarity.

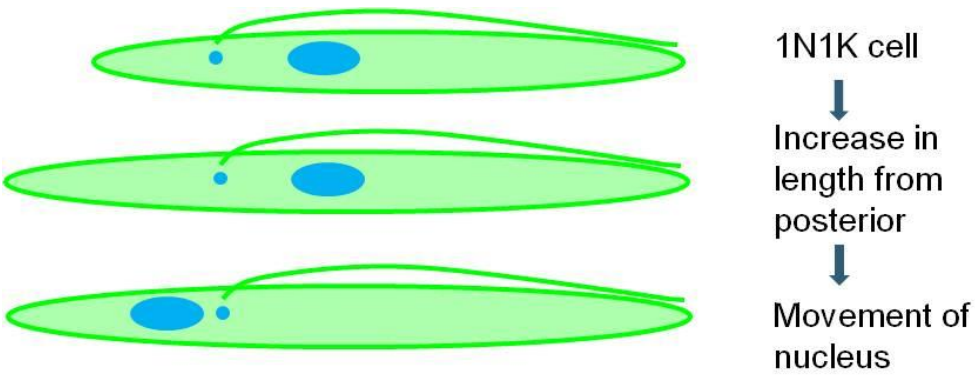

Figure 5-26 –Diagram to show the events that occur following AIR9 depletion to generate 1N1K cells with altered cell dimensions.

Following AIR9 depletion in procyclic AIR9 RNAi cell lines, 1N1K cells displayed abnormal positioning of the nucleus and kinetoplast relative the posterior end of the cell (Section 5.3.2.5). This was found to be a result of increased cell length and posterior movement of the nucleus (Section 5.3.2.6).

AIR9 depletion had an indirect effect on cytokinesis. Post-mitotic cells displaying abnormal organelle positioning accumulated at the furrow ingression stage of cytokinesis, but 2N2K cells did not increase in the context of the whole population, suggesting that AIR9 depletion led to altered kinetics of cytokinesis; it is possible that earlier initiation of cytokinesis might have compensated for delays in furrowing caused by organelle malpositioning. 2N2K cells with organelle positioning defects are the most likely source of 2N1K and 0N1K siblings, and this asymmetric cell division could be responsible for the growth defect which was characterised by a decrease but not arrest of cell proliferation. Uncoupling of organelle replication and cytokinesis resulted in the production of multinucleate cells; this is probably a downstream effect of the multitude of positioning defects, which preceded the emergence of this phenotype.

5.3.3 Downregulation of AIR9 in the bloodstream form life cycle stage of T. brucei

5.3.3.1 Generation of *T. brucei* bloodstream form RNAi cell lines

The *AIR9* RNAi plasmid, pHG27, described in Section 5.3.1 was linearised by restriction digest (Section 4.3.2.1) and transfected into bloodstream form 427 pLew13 pLew90 cells (Wirtz et al., 1999) (Section 4.3.2.2). Clones were selected by limiting dilution in medium supplemented with hygromycin, G418 and phleomycin (the latter to select for the RNAi plasmid). Two independent clones were generated and these are subsequently referred to clones 1 and 2.

To verify targeted AIR9 downregulation, additional cell lines were generated expressing tyGFP:AIR9 from the endogenous locus. Construction of this expression construct is described in Section 5.4.1). The expression plasmid (pHG172; Table 4-4) was transfected into the two *AIR9* RNAi clonal cell lines generated. Clones were selected by limiting dilution in medium supplemented with hygromycin, G418, phleomycin and blasticidin (the latter to select for the

expression construct). Transfection of RNAi clones 1 and 2 with pHG172, yielded 3 and 4 independent clones, respectively. The clones were screened by Western blotting of cell lysates with anti-GFP or anti-TY antibody (Section 4.6.3), which revealed that one clone derived from each RNAi cell line expressed tyGFP:AIR9 (Figure 5-27). Subsequent experiments refer to bloodstream form 427 pLew13 pLew90 pHG27 clone 1 pHG172 clone 2, and bloodstream form 427 pLew13 pLew90 pHG27 clone 2 pHG172 clone 1.

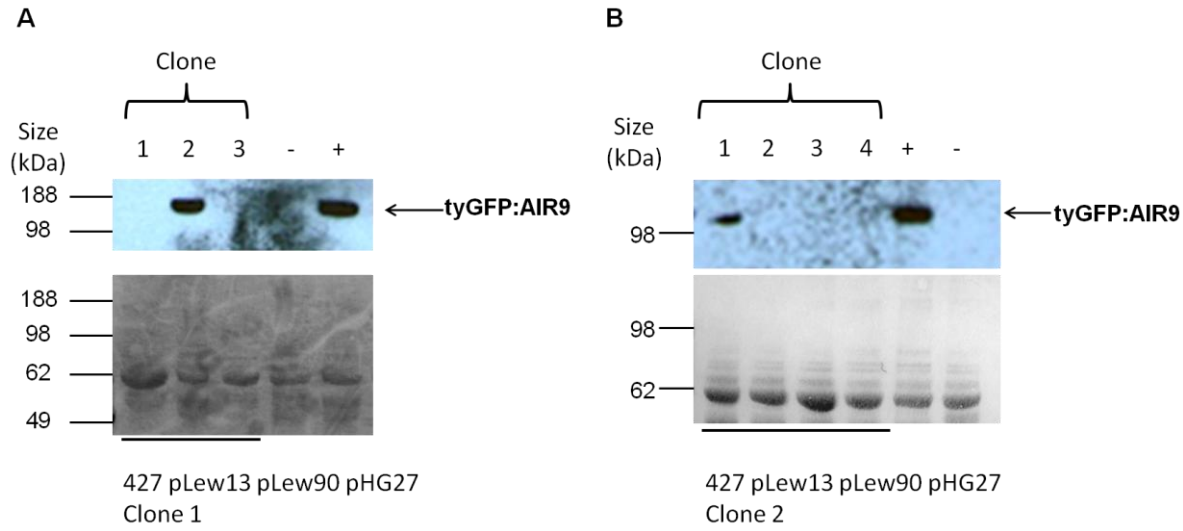

Figure 5-27- Western blot analysis of cell lysates from bloodstream form *AIR9* RNAi cell lines transfected with pHG172 for endogenous expression of tyGFP:AIR9.
Cell lysates were prepared for SDS PAGE and Western blotting (upper panels) with anti-GFP antibody. A and B: clones derived from parental cell lines 427 pLew13 pLew90 pHG27 clone 1 and clone 2, respectively. The identity of the clones derived from the transfection of the parental cell lines with pHG172 are indicated at the top. Negative control (-): uninduced bloodstream form 427 pHD449 pHG130 clone 1 (a cell line for inducible expression of ty:AIR9 (data not shown)); positive control (+): bloodstream form 427 tyGFP:AIR9 clone 15 (A) or clone 1 (B). To control for loading, the Western blots were stained with Ponceau reagent (lower panels). The signal for tyGFP:AIR9 (upper panels) was observed at its predicted size of 137 kDa.

5.3.3.2 Kinetics of AIR9 downregulation in bloodstream form *AIR9* RNAi cell lines expressing tyGFP:AIR9

Two independent bloodstream form *AIR9* RNAi cell lines expressing tyGFP:AIR9 from the endogenous locus were grown in the presence or absence of tetracycline for 24 hours (Section 4.2.2.2), and samples taken and prepared for Western blotting (Section 4.6.3) at 12 and 24 hours. Western blots of cell lysates with anti-GFP antibody (Section 4.6.3.2) revealed levels of tyGFP:AIR9 were reduced by 12 hours post-induction, and by 24 hours post-induction, tyGFP:AIR9 was barely detectable (Figure 5-28). These results show that in this system, AIR9 can be efficiently downregulated at the protein level, to the extent that AIR9

expression is almost completely depleted by 24 hours post-induction. Unlike procyclic form cells (see Figure 5-7), AIR9 expression did not vary in uninduced cells, suggesting tight regulation of the T7 promoter in the RNAi construct in these cell lines.

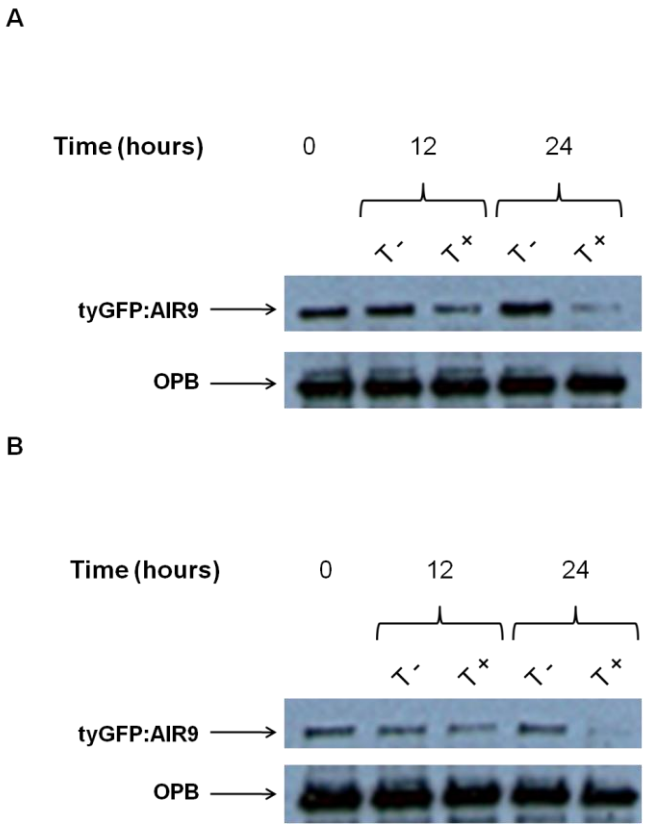

Figure 5-28- Downregulation of tyGFP:AIR9 in bloodstream form *AIR9* RNAi cell lines. Cells expressing tyGFP:AIR9 derived from bloodstream form *AIR9* RNAi cell lines: 427 pLew13 pLew90 pHG27 clone 1 pHG172 clone 2 (panel A), 427 pLew13 pLew90 pHG27 clone 2 pHG172 clone 1 (panel B); were grown in the presence (T +) or absence (T -) of 1 μgml^{-1} tetracycline for 24 hours, and cell lysates were prepared at 12 hour intervals for analysis by SDS PAGE and Western blotting with anti-GFP antibody (to detect tyGFP:AIR9), and anti-OPB antibody (to control for loading).

5.3.3.3 The effect of AIR9 downregulation on growth and DNA content in bloodstream form parasites

Growth of the *AIR9* RNAi bloodstream form parasites was arrested 18 hours post-induction, and parasite numbers then declined over the next 30 hours (Figure 5-29). At 48 hours post-induction, the parasites recovered from the growth defect, and began to proliferate at a rate comparable to uninduced cells. This recovery implies an escape from the RNAi, which is commonly observed in RNAi experiments, particularly for bloodstream form parasites (Chen et al., 2003). Potential mechanisms for reversion include loss of the RNAi fragment and mutations at the tetracycline operator or T7 promoter (Chen et al., 2003);

defects in the RNAi machinery or epigenetic phenomena have also been suggested as mechanisms for recovery from RNAi (Motyka and Englund, 2004). The exact mechanism responsible for reversion in these independent *AIR9* RNAi cell lines was not investigated in this study. However, the rapid reduction in cell proliferation coincides with reduction in AIR9 protein, and indicates that AIR9 is essential for viability in this developmental stage.

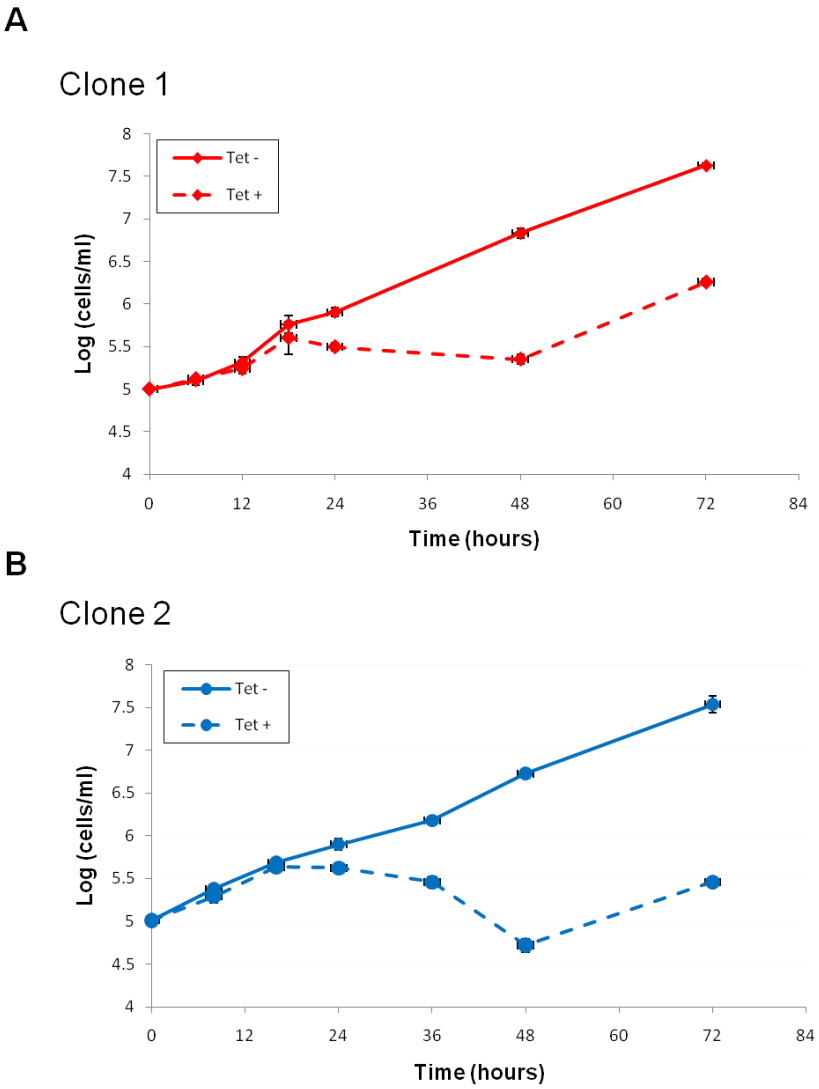

Figure 5-29 -Cumulative growth curves of bloodstream form *AIR9* RNAi cell lines. Triplicate cultures of two independent bloodstream form *AIR9* RNAi cell lines (A: clone 1; B: clone 2) were grown in the absence (Tet-) or presence (Tet +) of 1 µgml^{-1} tetracycline; growth was analysed by determining the cell density at regular intervals (shown) over a period of 72 hours.

To investigate whether the observed growth defect occurred as a result of cell cycle defects, both RNAi cell lines were analysed by flow cytometry (Section 4.10). Uninduced and induced cells were sampled at 0, 12 and 24 hours post-induction, and methanol-fixed cells were stained with propidium iodide before being analysed by flow cytometry.

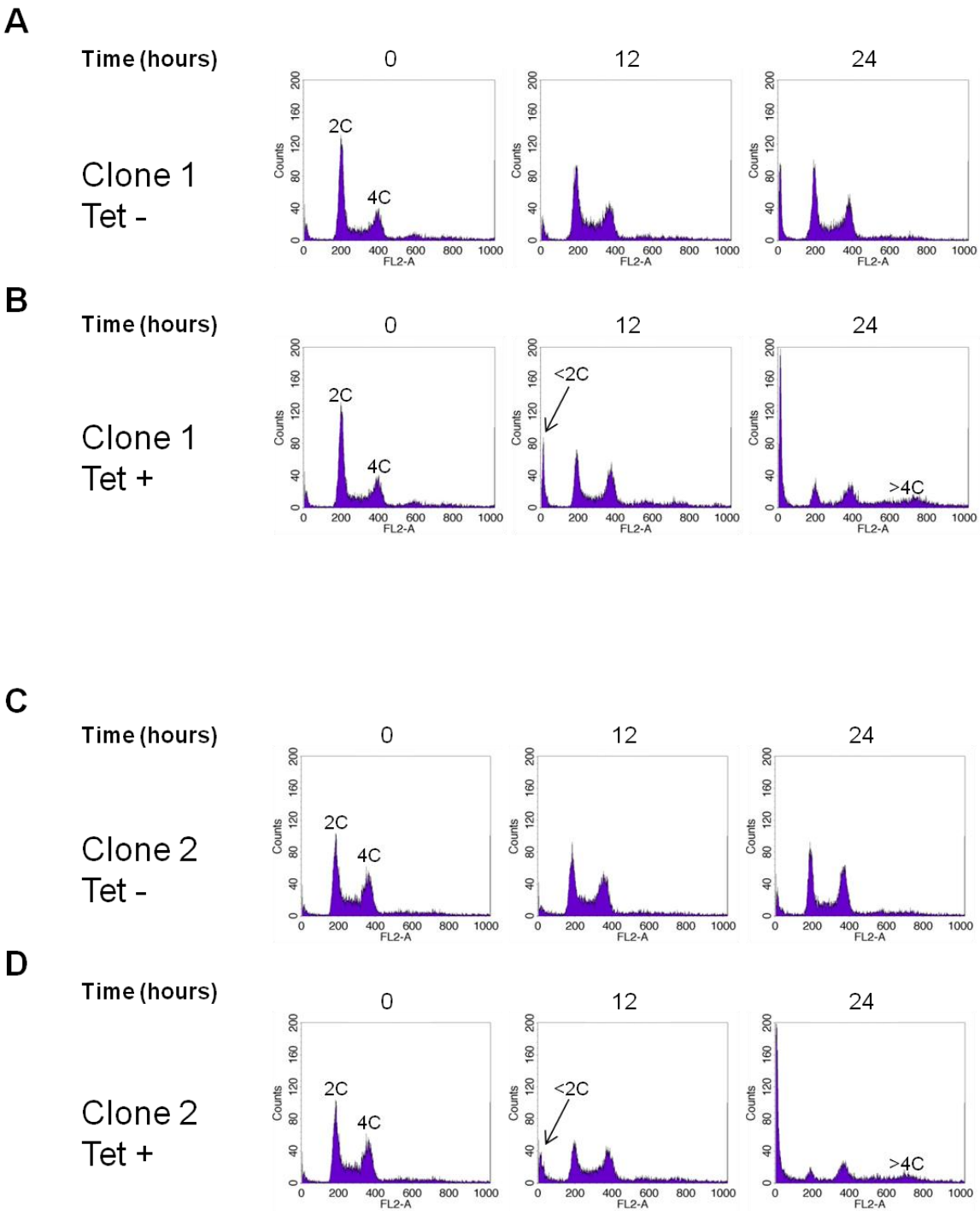

Figure 5-30 -Flow cytometry analysis of bloodstream form *AIR9* RNAi cell lines. Two independent bloodstream *AIR9* RNAi clones (A-B: clone 1; C-D: clone 2) grown in the absence Tet-) or presence (Tet+) of tetracycline were analysed by flow cytometry. Time points of sampling, and ploidy are shown.

The resultant profiles (Figure 5-30) show that both RNAi clones had the normal expected DNA content profile (as described above in Section 5.3.2.3) at the start of the induction. At 12 hours post-induction, there were significant changes to the DNA profiles for both clones; the sizes of the 2C and 4C peaks were considerably reduced and another peak appeared, corresponding to a DNA content of less than 2C, which could represent the accumulation of cell debris,

or anucleate cells. At 24 hours post-induction, further reduction of the 2C and 4C peaks was observed, the peak corresponding <2C DNA content grew dramatically, and cells with DNA content of >4C were also visible. Other experiments (not shown here) performed with additional samples taken at earlier time points (6 and 9 hours post-induction) revealed a normal DNA profile at these times, implying that abnormalities in the DNA profile first occur between 9 and 12 hours post-induction. The appearance of < 2C and >4C peaks implies that cytokinesis is impaired in these cell lines. The early abnormality in DNA profiles coincides with a slight reduction in AIR9 protein, but precedes the initiation of the growth defect. This implies that a small depletion of AIR9 can affect the DNA profile without immediately inhibiting growth. It is likely that parasites are still able to divide at 12 hours post-induction (thereby not affecting the growth rate), but the flow cytometry profiles indicate that cell division is abnormal.

5.3.3.4 Downregulation of AIR9 causes cytokinesis defects in bloodstream form parasites

To further investigate cell cycle progression following AIR9 depletion, cells grown in the presence or absence of tetracycline were sampled at 6 hour intervals over a 24 hour period, fixed with methanol and stained with DAPI for analysis by fluorescence microscopy (Section 4.11.1). Cells (>200 per time point) were classified according to the number of kinetoplasts and nuclei they contained and if relevant, the cytokinesis stage. Relative organelle positions and cell morphology were also recorded.

As expected, uninduced cell populations consisted of around 70-80% 1N1K cells, 10-15% 1N2K cells and 5-10% 2N2K cells with <5% abnormal cell types (Figure 5-31) and example images of cells with normal N-K configurations are presented in Figure 5-33. Organelle positioning in post-mitotic bloodstream cells (KKNN, posterior to anterior) differs from that observed in procyclic form parasites (KNKN), which arises from a reduced basal body segregation in bloodstream form parasites, which results in an inter-basal body distance of just 2.5 µm (Tyler et al., 2001b) that is reduced prior to cytokinesis when basal bodies are parallel to each other. Typical 2N2K cells are shown in Figure 5-33C-D. Bloodstream parasites undergo furrowing more rapidly than procyclic form cells but appear to

spend longer at the abscission stage of cytokinesis, and nascent daughter cells attached at their posterior ends are frequently observed in culture.

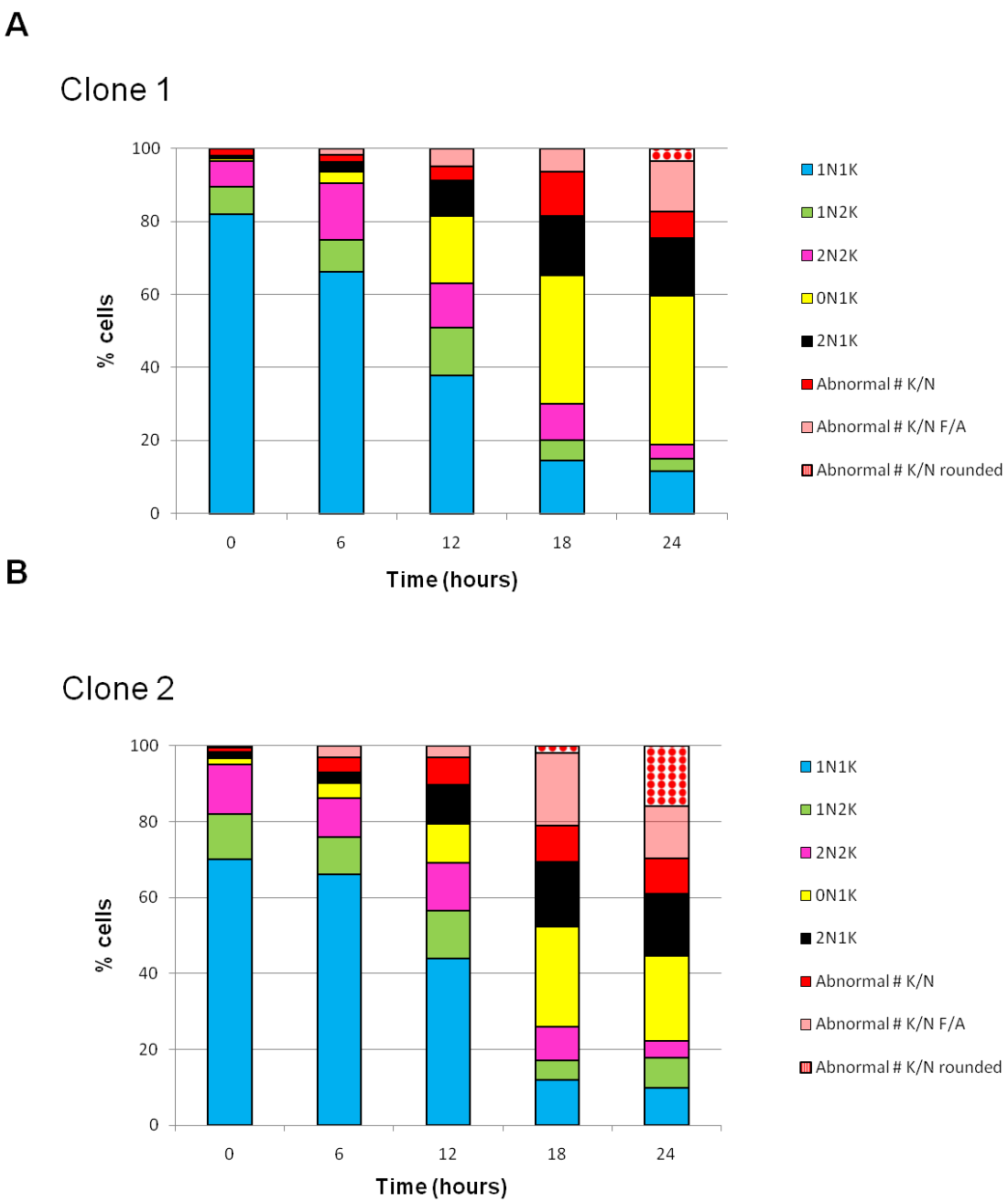

Figure 5-31 -DAPI staining of bloodstream form *AIR9* RNAi cell lines.
Bloodstream form *AIR9* RNAi cell lines (A: clone 1; B: clone 2) were induced with tetracycline and stained with DAPI at the time points indicated. More than 200 cells per time point were classified according to the number of nuclei (N) and kinetoplasts (K) per cell. F/A: furrow ingression/abscission.

Over the first 12 hours of *AIR9* RNAi induction, a rapid reduction in 1N1K cells occurred, but the size of the 1N2K and 2N2K populations remained essentially unaltered (Figure 5-31), although by 18 hours post-induction, 1N1K, 1N2K and 2N2K cell populations all declined. From 6 hours post-induction, abnormal cell types began to appear (Figure 5-31). The most abundant abnormal cell types

were 0N1K and 2N1K cells (Figure 5-34A), which appeared initially in equal numbers, and were significantly greater than in uninduced populations by 24 hours (Figure 5-32 and Table 5-4). The equal numbers of each cell type suggests that these are sibling cells resulting from the asymmetric cell division of 2N2K cells (see Figure 5-34Aiii), and probably accounts for the observed decline in 1N1K cells. 0N1K cells outnumbered 2N1K cells at later time points (particular for clone 1), and these 'extra' 0N1K cells are probably the products of abnormally dividing multinucleate cells (see later).

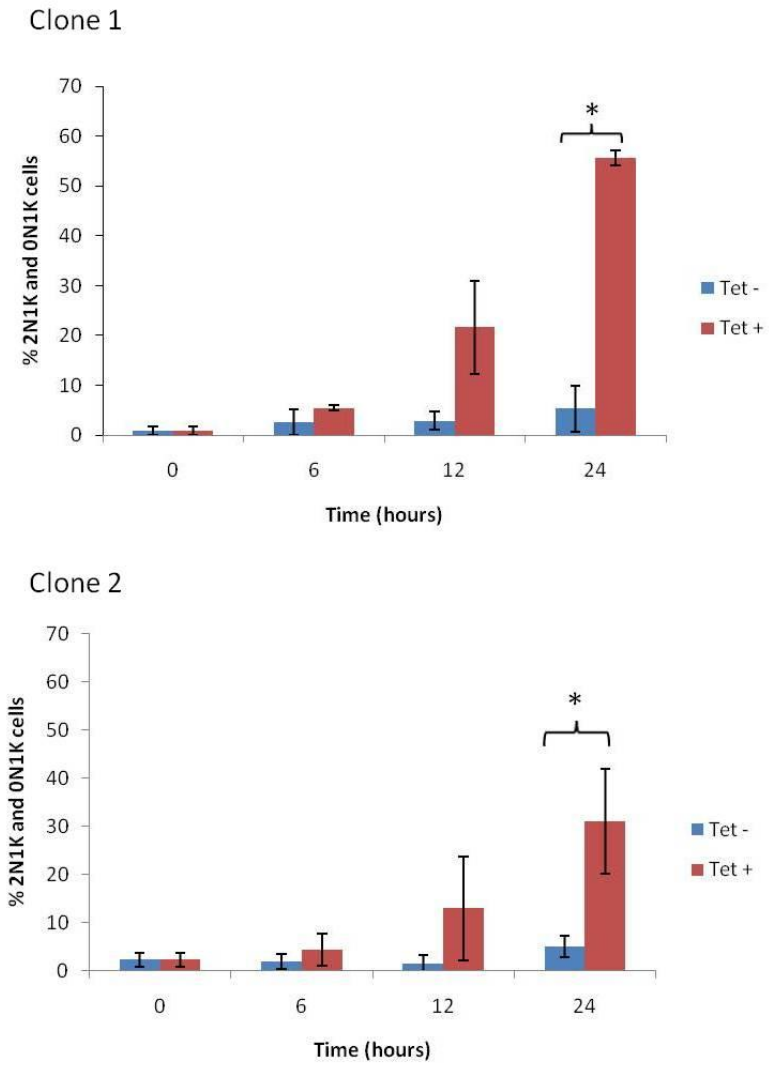

Figure 5-32- Stastical analysis of 0N1K and 2N1K cells in *AIR9* RNAi bloodstream form cell lines.
Bloodstream form *AIR9* RNAi cells grown in the absence or presence of 1 µgml^{-1} tetracycline ('Tet –' or 'Tet +', respectively) were analysed by DAPI staining and scored according to the whether cells contained two nuclei an one kinetoplast (2N1K) or were anucleate (0N1K). The results from two experiments were used to generate a mean, with values ±SEM. '*' indicates P=0.05 by an unpaired t-test (one-tail).

Table 5-4- P values from unpaired t-tests assuming equal variance (one-tail) to determine the significance of the appearance of abnormal cell types in induced *AIR9* RNAi bloodstream form lines.
The statistical significance of the appearance of 0N1K and 2N1K cells in AIR9 RNAi bloodstream form cell lines grown in the presence of 1µgml^{-1} tetracycline was determined by statistical analysis (Section 4.13) The results represent data from two separate experiments. P=0.05.

Phenotype	Time (Hours)	P (T<=t)	
		Clone 1	Clone 2
% 0N1K and 2N1K cells	6	0.137279	0.221819
	12	0.054454	0.138871
	24	0.00228	0.039642

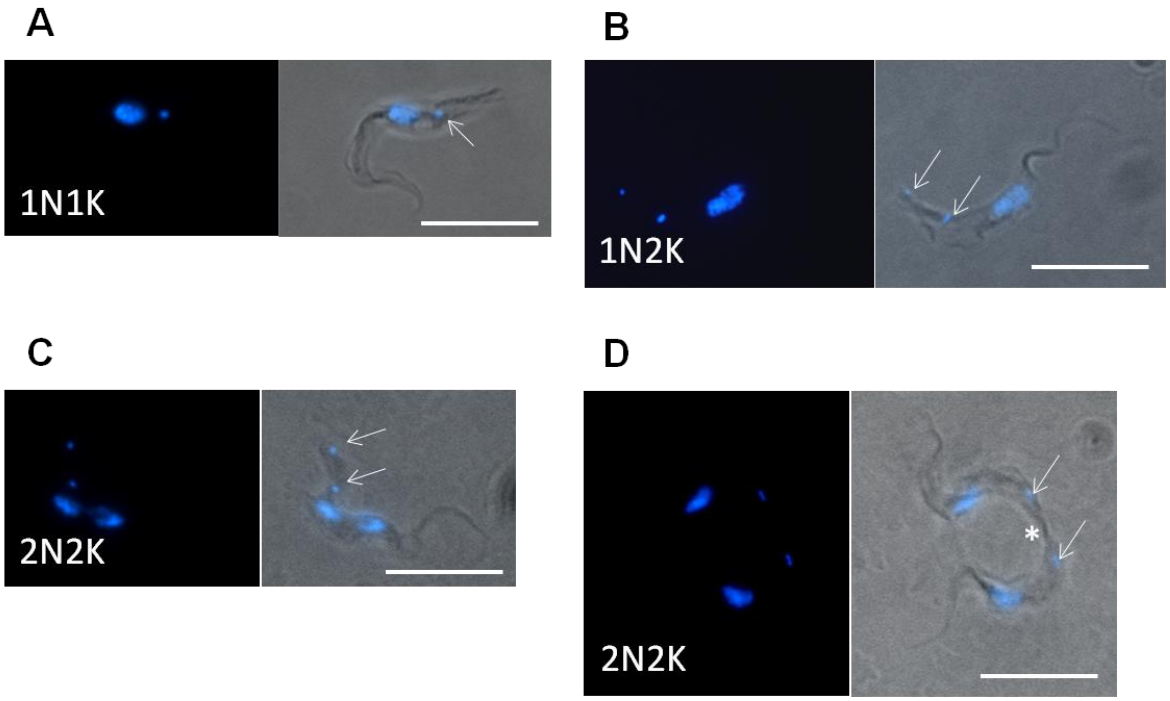

Figure 5-33 –Nucleus–kinetoplast (N-K) configurations in normal bloodstream form cells. Cells from uninduced bloodstream form *AIR9* RNAi cell lines were stained with DAPI and analysed by microscopy. Left panels: DAPI images; right panels: DAPI/DIC merge. A-D: example images of 1N1K, 1N2K, 2N2N (pre-cytokinesis) and 2N2K (abscission) cells, respectively. Scale bar: 10 µm. Arrows indicate the positions of the kinetoplasts, and the point of abscission for the 2N2K cell in D is indicated by an asterisk.

The appearance of 2N1K and 0N1K cells coincided with the emergence of multinucleate cells (Figure 5-31). These were initially vermiform in shape (Figure 5-34B), and at later time points were frequently observed to be undergoing furrow ingression or to be in abscission (Figure 5-31 and Figure 5-34C). This suggests that cytokinesis was not blocked, but delayed, although it is also possible that multinucleate cells undergoing furrow ingression were underrepresented at these early time points due to stochastic variation. At 24

hours post-induction, some multinucleate cells appeared to have lost cell polarity, and displayed a rounded morphology (Figure 5-31 and Figure 5-34D). The number of nuclei and kinetoplasts observed per cell was highly variable and up to 8 nuclei were recorded for one cell, although in many cases, it was impossible to count the actual number of these organelles.

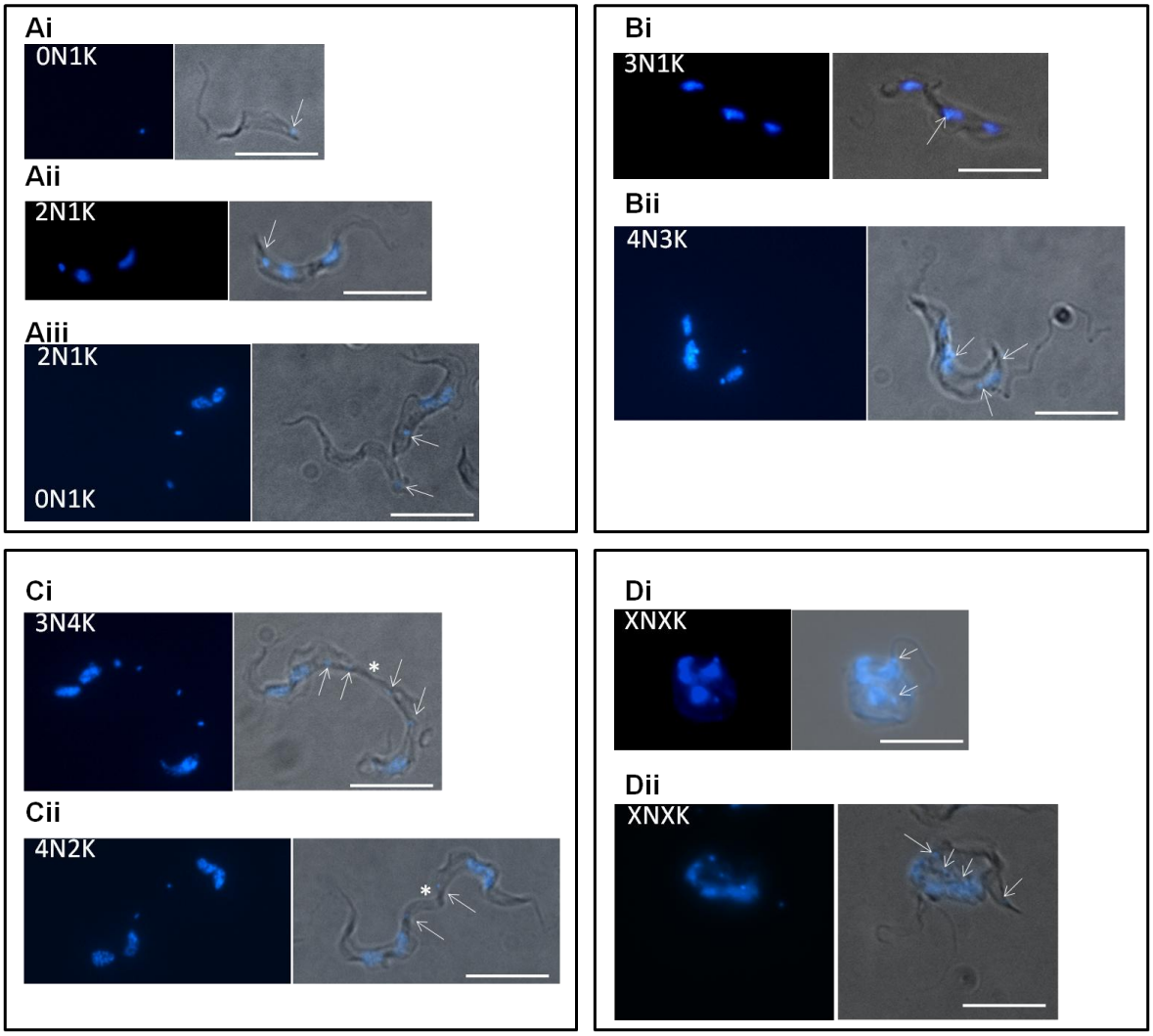

Figure 5-34 – Cells with abnormal N-K configurations observed following induction of *AIR9* RNAi in bloodstream form cells.
Bloodstream form *AIR9* RNAi cells were induced and stained with DAPI to determine the number of nuclei (N) and kinetoplasts (K, arrows) per cell, which revealed the presence of abnormal cell types. Ai-iii: 0N1K and 2N1K cells; Bi-ii: multinucleate cells without signs of cytokinesis intiation; Ci-ii: multinucleate cells undergoing abscission (sites indicated by asterisks); Di-ii: multinucleate cells with rounded morphology. Scale bars: 10 µm.

It appears that AIR9 depletion in bloodstream form trypanosomes resulted in two different cytokinesis defects; initially cleavage plane positioning was affected, resulting in asymmetric cell division, and later the coupling of cytokinesis and organelle replication was disrupted resulting in multinucleate cells. The rapid effect of AIR9 depletion on cleavage plane positioning without increasing the abundance of 2N2K cells implies that the dynamics of cytokinesis were not

affected. Similarly, the decoupling of organelle replication and cytokinesis, such that cells re-replicated their organelles without having undergone cell division, must also have occurred rapidly. Such a rapid effect is unusual; knockdown of cytokinesis regulators PK50 and PK53 resulted in the production of similar multinucleate cells (Ma et al., 2010), but in this case, 2N2K cell numbers increased from 10% to 20% or 25% of the whole population (for *PK50* and *PK53* RNAi cell lines, respectively) prior to the emergence of these cell types.

To determine whether the 2N1K and 0N1K cells were indeed sibling cells of a parental 2N2K cell, >200 2N2K cells were examined at 0, 6 and 12 hours post-induction (Figure 5-35).

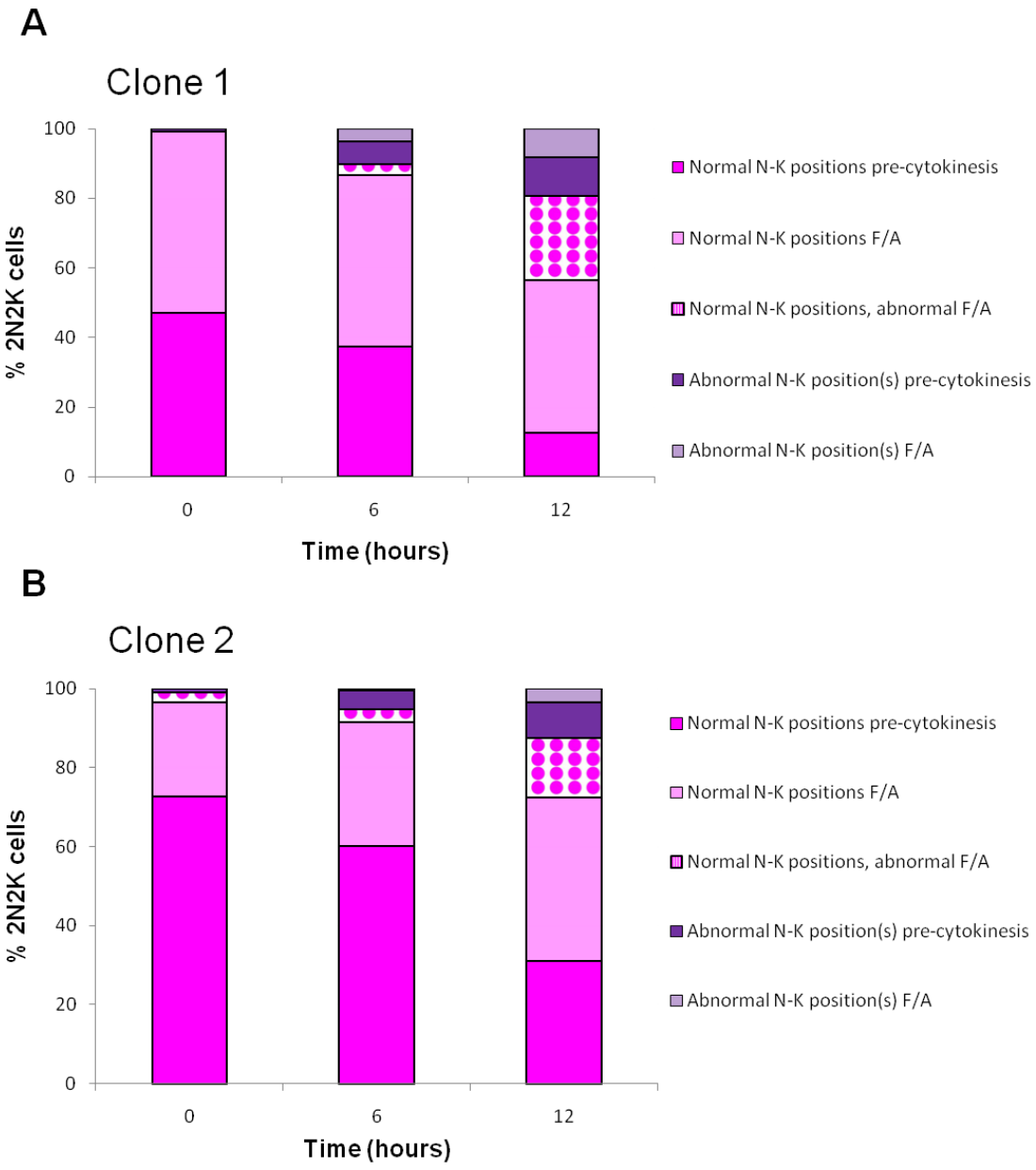

Figure 5-35 -Analysis of 2N2K cells in bloodstream form *AIR9* RNAi cell lines.

Bloodstream form *AIR9* RNAi cells (A: clone 1; B: clone 2) were induced and stained with DAPI and >200 2N2K cells were analysed at the time points indicated. Cells were classified according to the positions of nuclei (N) and kinetoplasts (K) in addition to cytokinesis stage, as indicated in the key. F/A: furrow ingression/abscission.

For both RNAi clones, an increase in cells undergoing abscission was observed over time. At the start of the induction, 42% or 16% of 2N2K cells displaying a typical 'KKNN' arrangement were undergoing abscission, and this rose to 62% or 52% at 12 hours post-induction for clones 1 and 2, respectively. However, many of the cells in abscission (23% and 15% for clones 1 and 2, respectively) displayed malpositioned cleavage furrows such that the two nascent daughter cells had 0N1K and 2N1K organelle quotas, respectively (Figure 5-36A). Furthermore, a small proportion (approximately 5%) of 2N2K cells displayed N-K positioning defects at 6 hours post-induction, and by 12 hours post-induction, 2N2K cells with abnormal N-K positioning were also observed to be undergoing cytokinesis leading to non-equivalent daughter cell progeny (Figure 5-36B-C). This experiment determined the main source of 0N1K and 2N1K cells to be 2N2K cells with typical N-K positions but abnormally positioned cleavage furrows, but also implied that 2N2K cells displaying abnormal organelle positioning may have contributed to the generation of these abnormal cells.

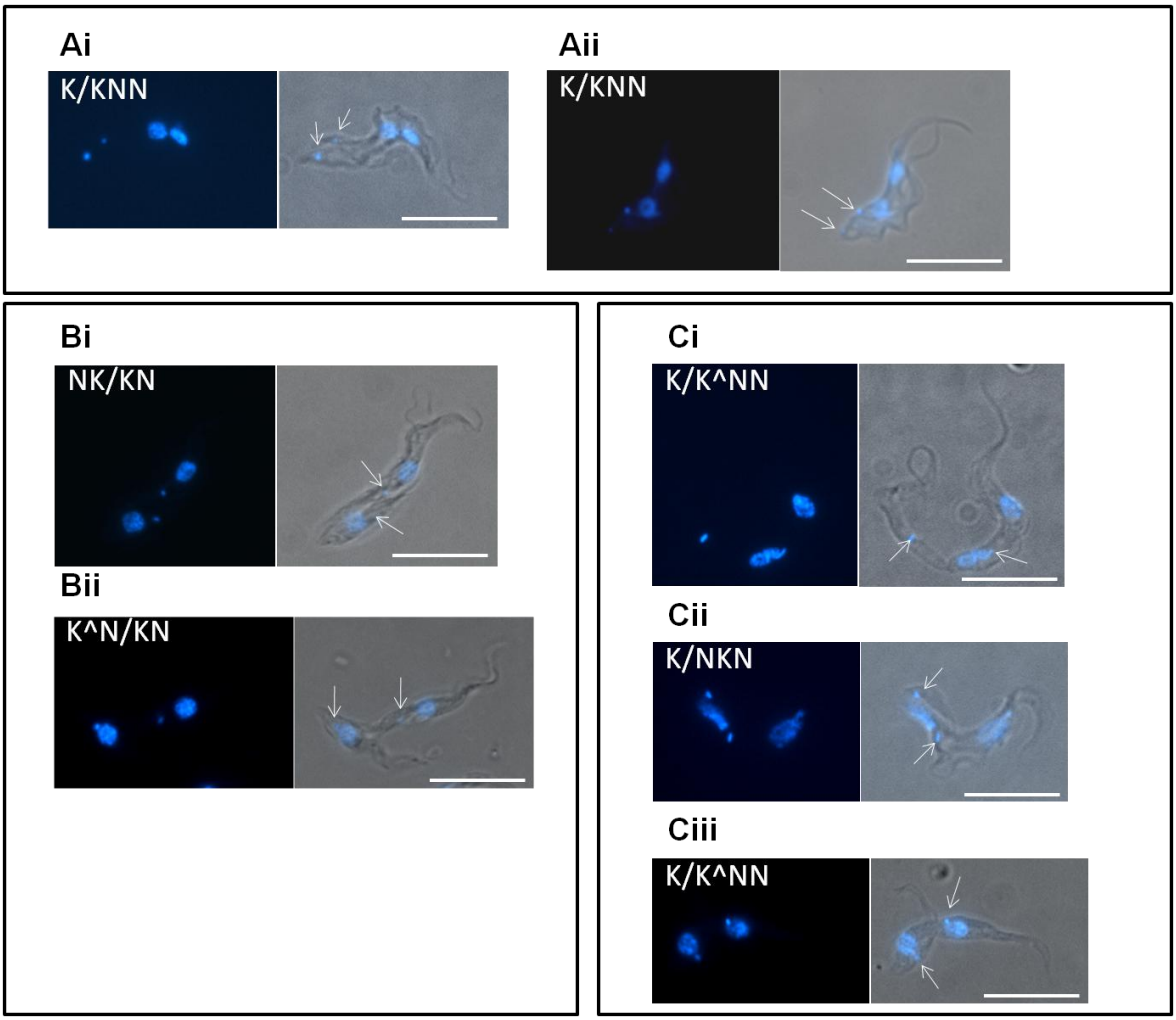

Figure 5-36 -2N2K cells displaying cytokinesis defects following induction of *AIR9* RNAi in bloodstream form trypanosomes.
Bloodstream form *AIR9* RNAi cells were induced with tetracycline and stained with DAPI, revealing 2N2K cells with cytokinesis defects. Ai-ii: cells with normal kinetoplast and nuclei positions but abnormal furrow placement; Bi-ii; cells with abnormal organelle positions undergoing furrow ingression; Ci-iii; cells with abnormal organelle positions undergoing abscission. The predicted organelle quota and arrangement for each nascent daughter cell is indicated. Scale bars: 10 μm.

To determine whether N-K positioning defects observed in 2N2K cells were also present at other cell cycle stages, >200 cells of each cell cycle stage (1N1K, 1N2K, 2N2K) were analysed at 15 hours post-induction (Figure 5-37).

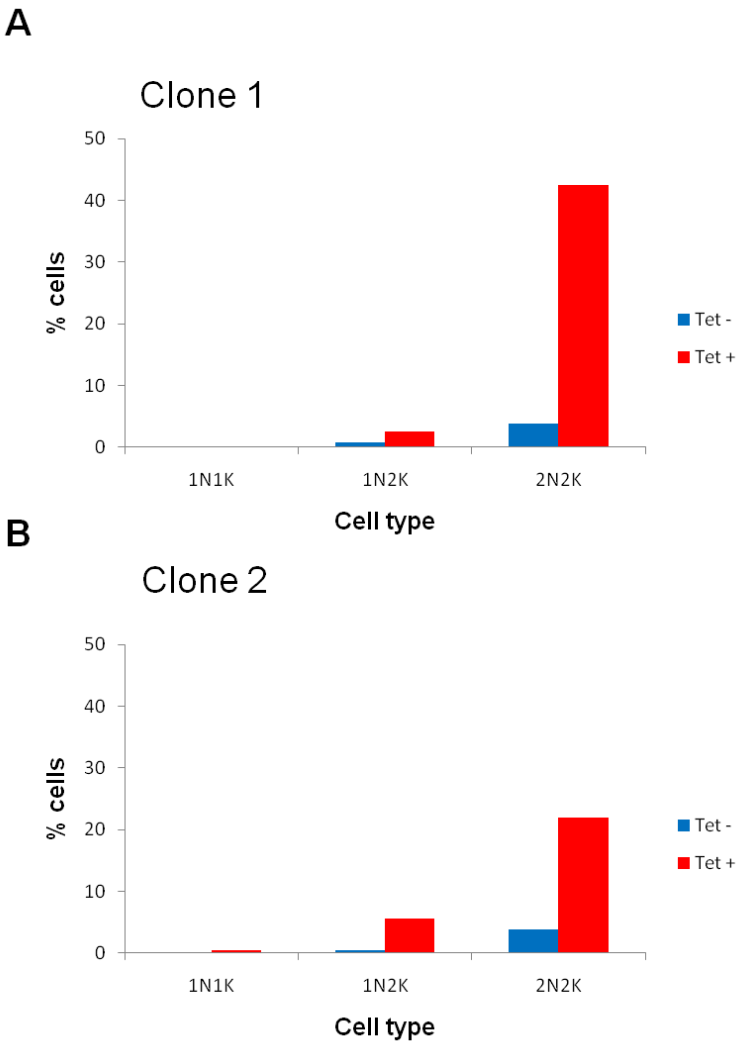

Figure 5-37 -Lineage analysis to investigate the chronology of organelle positioning defects in bloodstream form *AIR9* RNAi cell lines.
Bloodstream form *AIR9* RNAi cells (A: clone 1; B: clone 2) were induced with tetracycline (Tet) for 15 hours and stained with DAPI. The proportions of cells with abnormal organelle positioning (*n*>200 cells) for 1N1K, 1N2K, and 2N2K configurations are indicated.

As a control, similar numbers of uninduced cells were also analysed at this time point, but few displayed abnormalities in organelle positioning. Amongst the induced cell populations, no abnormal N-K positioning was observed in 1N1K cells, and only a few 1N2K cells possessed N-K positioning defects (2.5 % or 5.6 % for clones 1 and 2, respectively). However, much large proportions of 2N2K cells displayed aberrant N-K positioning (42.6 % or 22 % for clones 1 and 2, respectively). This implies that these organelle positioning defects are primarily a feature of post-mitotic cells (Figure 5-37).

5.3.3.5 Conclusions

In bloodstream form parasites AIR9 depletion was rapidly induced in the system described, such that AIR9 protein was barely detectable 24 hours after induction of the RNAi. Reduction of AIR9 protein directly affected the accuracy of cleavage furrow positioning, resulting in the production of 2N1K and 0N1K cells. In addition, organelle replication and cytokinesis became uncoupled resulting in the production of multinucleate cells that were capable of initiating cytokinesis, but that frequently did not complete cell division and instead formed clumps of attached cells. The dynamics of asymmetric cell division were not noticeably different from normal cell division, and abnormalities in N-K configurations and DNA profile preceded a decrease in cell proliferation. Unlike procyclic form cells, organelle positioning defects were not a dominant feature of the RNAi phenotype; however, abnormal organelle positioning was found to occur to an extent in post-mitotic cells, possibly suggesting a cell cycle-specific loss of cell polarity.

5.4 Localisation of AIR9 in *Trypanosoma brucei*

In order to shed further light on the function of AIR9, its cellular localisation was investigated. Since antibodies have not yet been raised to *T. brucei* AIR9, its localisation was investigated by epitope tagging AIR9 and performing (immuno) fluorescence and subcellular fractionation, using anti-tag antibodies to detect tagged AIR9. Two different tagging strategies were used, with different tags being inserted at opposite ends of the protein, in order to increase the robustness of the results, since tagging a protein may interfere with its folding or trafficking in the cell. AIR9 was therefore tagged at the N-terminus with tyGFP and at the C-terminus with a 6xHA tag. To further minimise artefacts, the tagged proteins were expressed from the endogenous locus and hence were likely to be expressed at near native levels.

5.4.1 Construction of plasmids 'pHG172' and 'pHG182' for epitope tagging of AIR9 at the endogenous locus

The vector 'pENT-6-Blast eGFP-TY' (Kelly et al., 2007) was used to add a tyGFP epitope tag to the N-terminus of AIR9. A 269 bp fragment corresponding to the 3` end of the 5` untranslated region (UTR) and a 355 bp fragment of the 5` end of the open reading frame (ORF) minus the start codon of *AIR9* were PCR-amplified (Section 4.5.4) from *T. brucei* 427 genomic DNA (Section 4.4.2) using oligonucleotides PR94 and PR95, and PR96 and PR97, respectively (Table 4-9). The UTR and ORF fragments were ligated into the pSC-A vector (Strataclone, Section 4.5.6) generating pHG108 and pHG109 (Table 4-4), respectively, and sequenced (Section 4.5.8). The UTR and ORF fragments were excised from pHG108 and pHG109 by restriction digest (Section 4.5.2) with NheI/BclI and NheI/XbaI, respectively, purified and ligated in a three-way ligation (Section 4.5.7) with BamHI/XbaI-cut pENT-6-Blast-tyGFPty generating pHG172 (Figure 5-38 and Table 4-4).

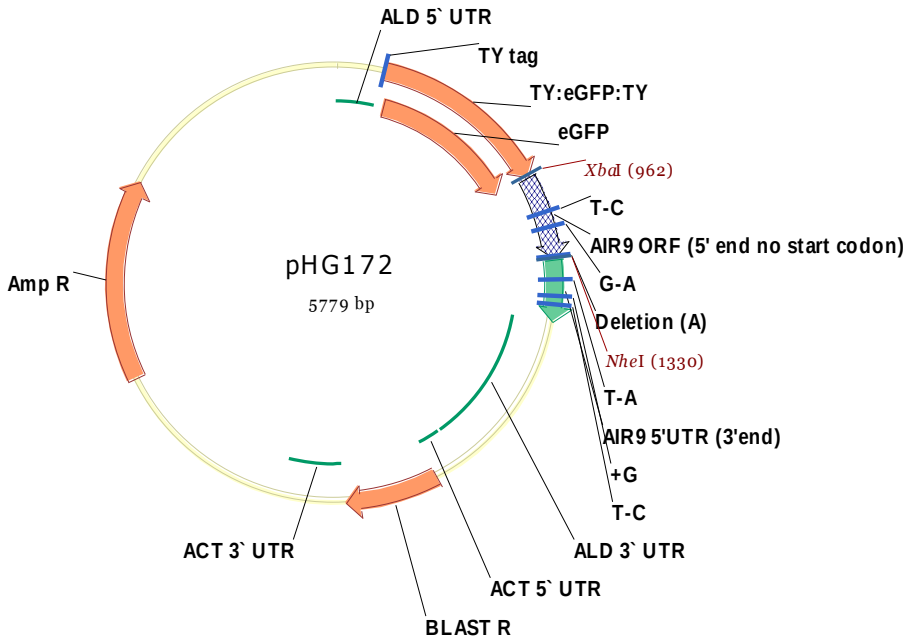

Figure 5-38 -Plasmid map of pHG172.
pHG172 was generated to add a tyGFP epitope tag to the N-terminus of AIR9. Important features of pHG172 include: *AIR9 5' UTR* (269 bases upstream from the start codon) and ORF (bases 4-358) fragments separated by a unique NheI site for linearization of the plasmid to allow integration at the endogenous locus; a tyGFP epitope tag situated upstream from and in frame with the ORF fragment, and a *blasticidin* resistance gene (BLAST R) for selection of genetically modified parasites.

The vector Orc-_6XHA_Ble was used to add six haemagluttinin epitopes (6XHA) to the C-terminus of AIR9. Orc-_6XHA_Ble is a modified version of pNAT^{6Myc}X (Alsford and Horn, 2008) where the blasticidin resistance marker has been replaced by a bleomycin resistance marker and the 6xMyc epitope tag coding sequence has been replaced with 6XHA (Calvin Tiengwe, personal communication). A 724 base fragment corresponding to the 3` end of the AIR9 ORF containing a unique AspI restriction site was PCR-amplified (Section 4.5.4) from 427 genomic DNA (Section 4.4.2) using oligonucleotides PR228 and PR229 (Table 4-9). The amplified gene fragment was ligated into pSC-B (Strataclone, Section 4.5.6), generating pHG184 (Table 4-4) and sequenced (Section 4.5.8). The AIR9 fragment was then excised from pHG184 by restriction digestion (Section 4.5.2) with HindIII and XbaI, purified (Section 4.5.3) and ligated (Section 4.5.7) into HindIII/XbaI-cut Orc-_6XHA_Ble, generating pHG182 (Figure 5-39 and Table 4-4).

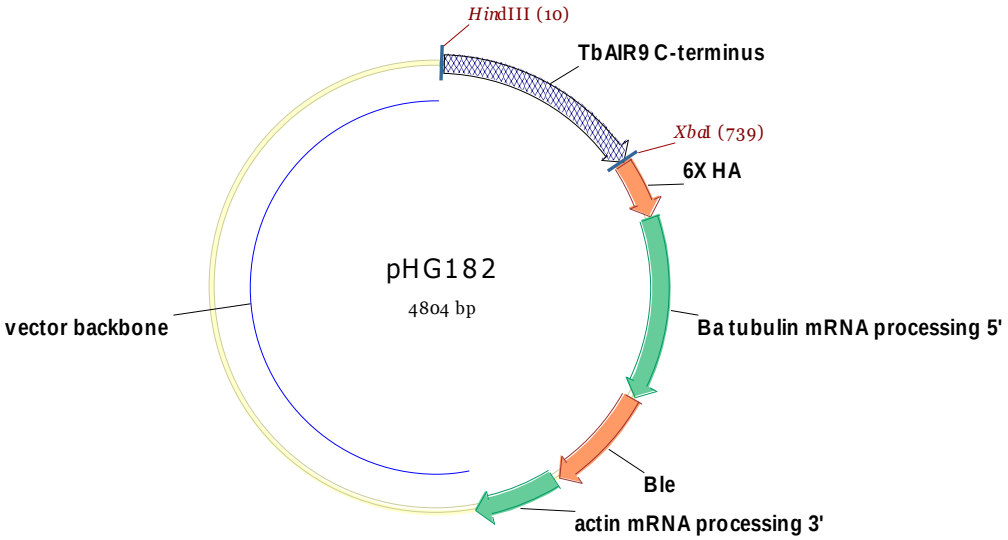

Figure 5-39 -Plasmid map of pHG182.
pHG182 was generated to add a C-terminal 6XHA tag to *AIR9*. Important features of pHG182 include a fragment (724 bp) of the 3' end of the *AIR9* ORF, minus the stop codon, inserted in frame with the 6XHA tag; a unique AspI restriction site at position 383 inside the ORF fragment to allow linearization of the plasmid for transfection and integration into the *AIR9* locus and a *bleomycin* resistance gene (Ble) for selection of genetically modified parasites.

5.4.2 Generation of parasites expressing epitope-tagged AIR9

The plasmids pHG172 and pHG182 were linearised by restriction digestion (Sections 4.5.2 and 4.3.2.1) with NheI or AspI, respectively, and transfected into 427 bloodstream and procyclic form *T. brucei* parasites (Section 4.3.2.2). Clones were selected by limiting dilution in medium supplemented with the appropriate antibiotics (Table 4-7). To verify expression of epitope tagged AIR9 protein, cell extracts from parasite clones were prepared for PAGE (Section 4.6.1) and Western blotting (Section 4.6.3) with the appropriate antibodies. Analysis of nine out of seventeen independent clones obtained from the transfection of *T. brucei* 427 bloodstream form parasites with pHG172 with anti-GFP antibody identified three clones that expressed a protein of the predicted size for tyGFP:AIR9 of 137 kDa (Figure 5-40A). Five independent clones were obtained from the transfection of bloodstream parasites with pHG182 and Western blotting with an anti-HA antibody detected a protein of the predicted size for AIR9:6XHA (117 kDa) in cell lysates of all five clones (Figure 5-40B). By similar means, four out of eight procyclic clones obtained from the transfection with pHG172 and two out of three procyclic clones obtained from the transfection with pHG182 appeared to express tyGFP:AIR9 or AIR9:6XHA, respectively (Figure 5-41).

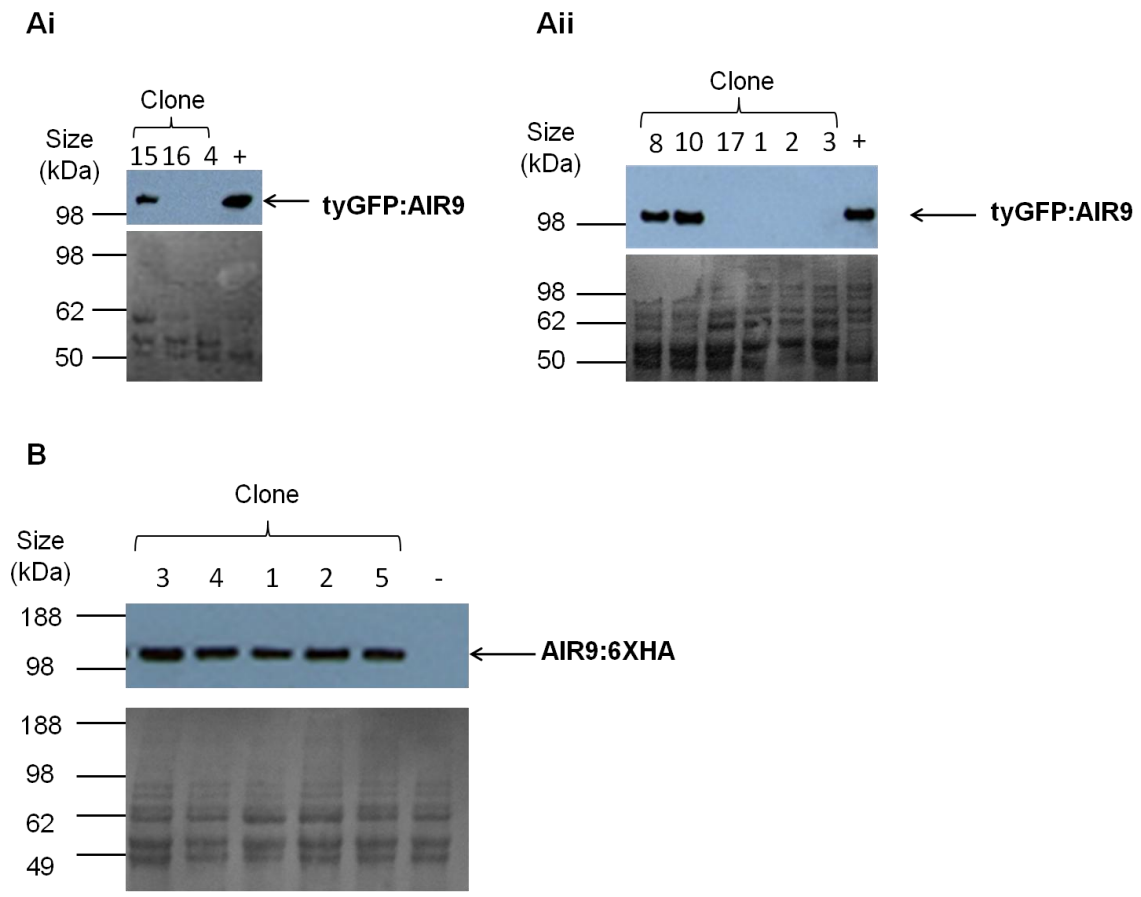

Figure 5-40 -Western blot analysis of bloodstream form parasites transfected with pHG172 and pHG182 for expression of tyGFP:AIR9 and AIR9:6XHA respectively, from the endogenous locus.
To verify expression of recombinant AIR9, cell lysates were analysed by SDS PAGE and Western blotting (upper panels) with anti-GFP antibody (Ai-ii) or anti-HA antibody (B). To control for loading, Western blots were stained with Ponceau reagent (lower panels). The numbers of clones derived from transfection of bloodstream form 427 cells are given; '+': positive control lysate (procyclic form 427 pHG172 clone 7 (see Figure 5-41A); '-': negative control lysate (bloodstream form 427).

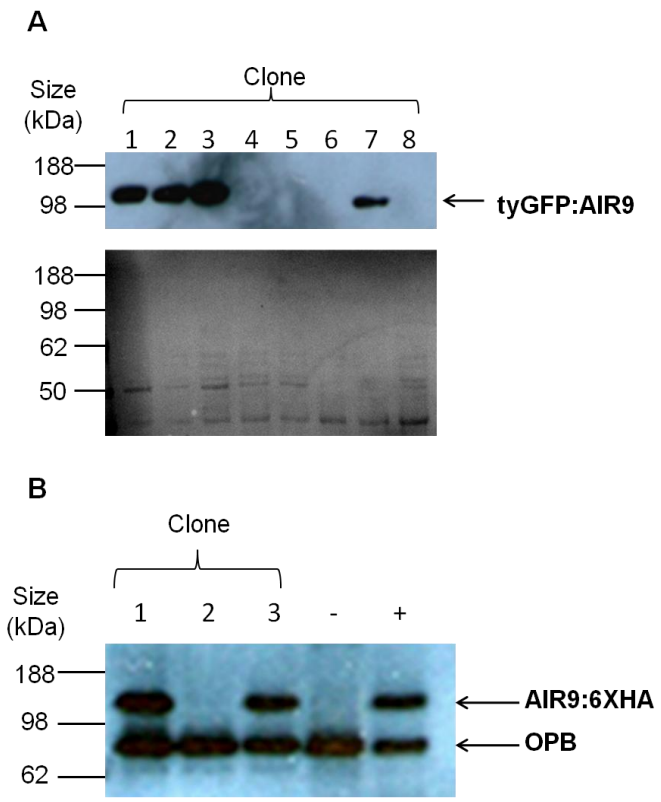

Figure 5-41 -Western blot analysis of procyclic form parasites transfected with pHG172 and pHG182 for the expression of tyGFP:AIR9 and AIR9:6XHA, respectively, from the endogenous locus.
To verify expression of recombinant AIR9, cell lysates were analysed by SDS PAGE and Western blotting with anti-GFP antibody (A, upper panel) or anti-HA antibody (B). To control for loading, Western blots were stained with Ponceau reagent (A, lower panel) or treated with anti-OPB antibody (B). The numbers of the clones derived from transfection of procyclic form 427 cells are given; '+': positive control lysate (bloodstream form 427 pHG182 clone 1 (Figure 5-40B); '-': negative control lysate (427 procyclic form).

5.4.3 Localisation of epitope tagged AIR9

Selected epitope tagged AIR9 clones were analysed by fluorescence microscopy (tyGFP:AIR9) or immunofluorescence microscopy with anti-HA antibody (AIR9:6XHA) (Section 4.11) to determine the localisation of AIR9. Cells were co-stained with DAPI (Section 4.11.1), and the pattern of fluorescence obtained was examined in cells of all cell cycle stages (Figure 5-42 and Figure 5-43).

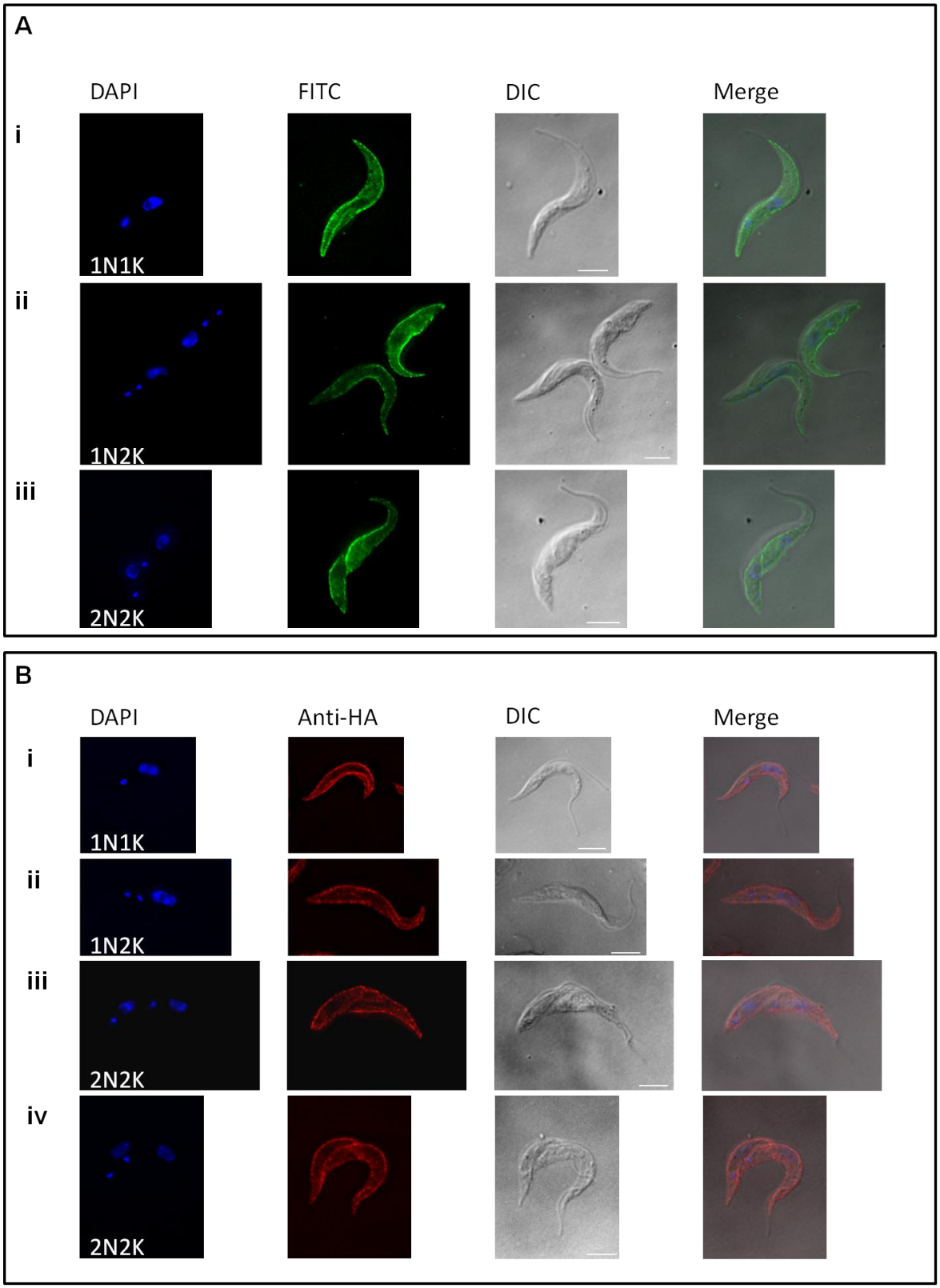

Figure 5-42 -Localisation of tyGFP:AIR9 and AIR9:6XHA in procyclic form parasites. Procyclic form clones shown to express tagged AIR9 proteins by Western blotting were examined by (immuno)fluorescence microscopy. A: cells expressing tyGFP:AIR9 (green, FITC); B: cells expressing AIR9:6XHA (red, anti-HA). Fluorescent images were deconvolved. DNA was stained with DAPI (blue) and the number of nuclei (N) and kinetoplasts (K) per cell is indicated. Cell morphology is shown in the DIC and merge (DAPI/GFP or anti-HA/DIC) panels. Scale bars: 5μm.

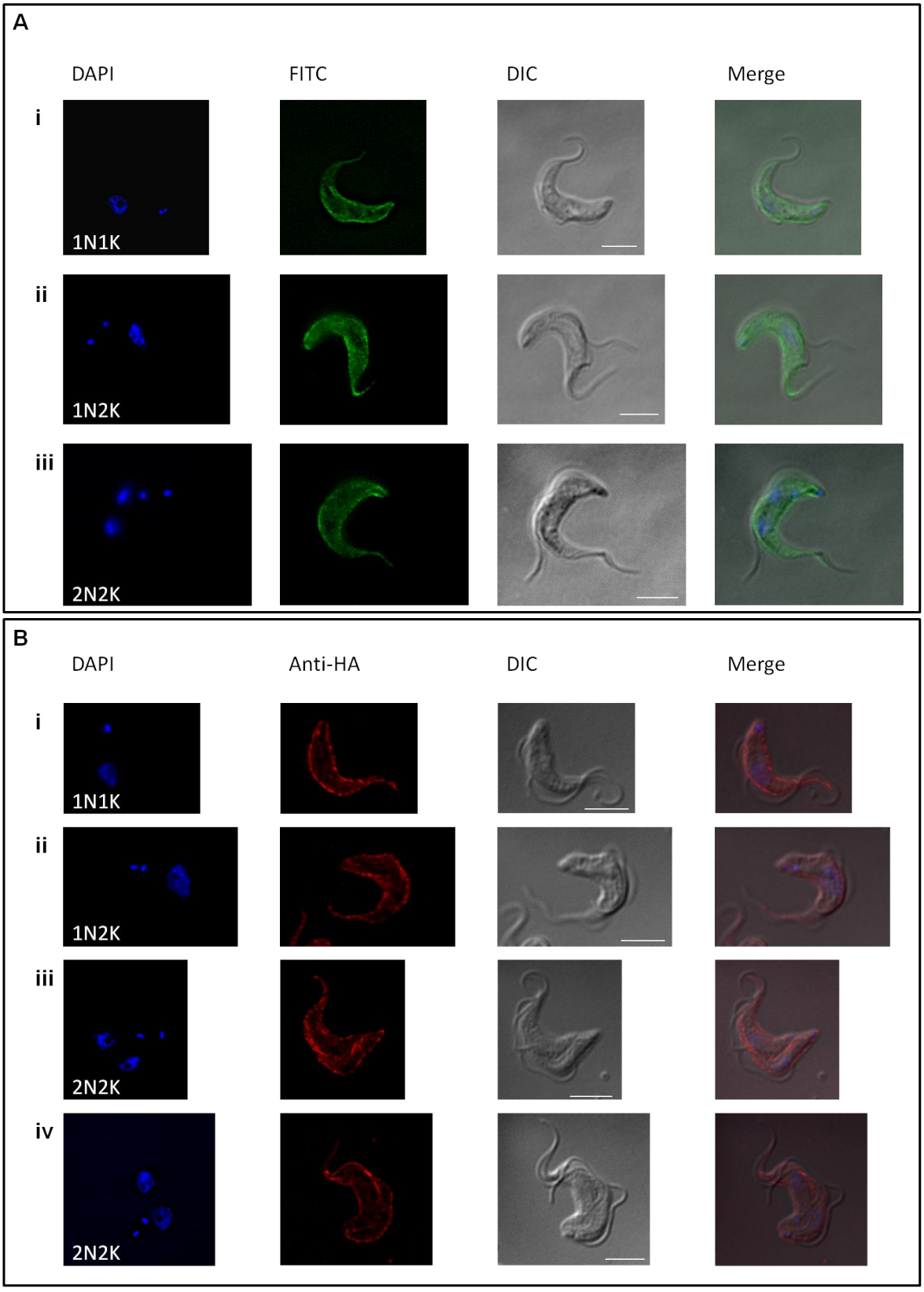

Figure 5-43 -Localisation of tyGFP:AIR9 and AIR9:6XHA in bloodstream form *T. brucei* parasites.
Bloodstream form clones shown to express tagged AIR9 proteins by Western blotting were examined by (immuno)fluorescence microscopy. A: cells expressing tyGFP:AIR9 (green, FITC); B: cells expressing AIR9:6XHA (red, anti-HA). Fluorescent images were deconvolved. DNA was stained with DAPI (blue) and the number of nuclei (N) and kinetoplasts (K) per cell is indicated. Cell morphology is shown in the DIC and merge (DAPI/GFP or anti-HA/DIC) panels. Scale bars: 5µm.

Cells at different cell cycle stages displayed similar levels of fluorescence and all exhibited bright staining of the cell body. This staining did not extend beyond the cell bodies to the flagella tips. The pronounced staining of the cell outline resembled staining of the cell surface (Engstler et al., 2007) or subpellicular cytoskeleton (Sherwin and Gull, 1989b; Woods et al., 1989). In addition, post-mitotic cells displayed particularly bright staining at the midline of the cell, which seemed to correspond to regions where invaginations of the cell body occurred, possibly localising to the site of furrow ingression (Figure 5-42Aiii and Biii-iv, and Figure 5-43Aiii and Biii-iv) although, given the cell contours at this point, it is perhaps more likely to represent AIR9 beginning to localise to the edge of the newly forming daughter cell body as can clearly be seen in Figure 5-42Biv and Figure 5-43Biii.

In order to determine whether AIR9 localises to the cytoskeleton or cell membrane of *T. brucei*, cytoskeletons of cells expressing tyGFP:AIR9 were prepared (Section 4.11.3) and analysed by fluorescence microscopy (Section 4.11.1). For both procyclic and bloodstream form cells, the intensity of fluorescence of the cytoskeletons was comparable to that observed with whole cells (compare Figure 5-42A and Figure 5-43A with Figure 5-44), indicating that tyGFP:AIR9 was not detergent extracted to any significant extent, and is therefore likely to localise to the cytoskeleton. Cytoskeletons of cells at all cell cycle stages exhibited similar, bright staining around the outline of the cell body. The flagella were more visible in the cytoskeleton preparations compared to fluorescence microscopy of whole cells, and clearly were not fluorescent, indicating that tyGFP:AIR9 does not localise to the flagellum to any significant extent. The almost identical localisation patterns obtained with the two different epitope tags inserted at opposite ends of the protein suggests that neither tag is having an aberrant effect on the localisation of AIR9.

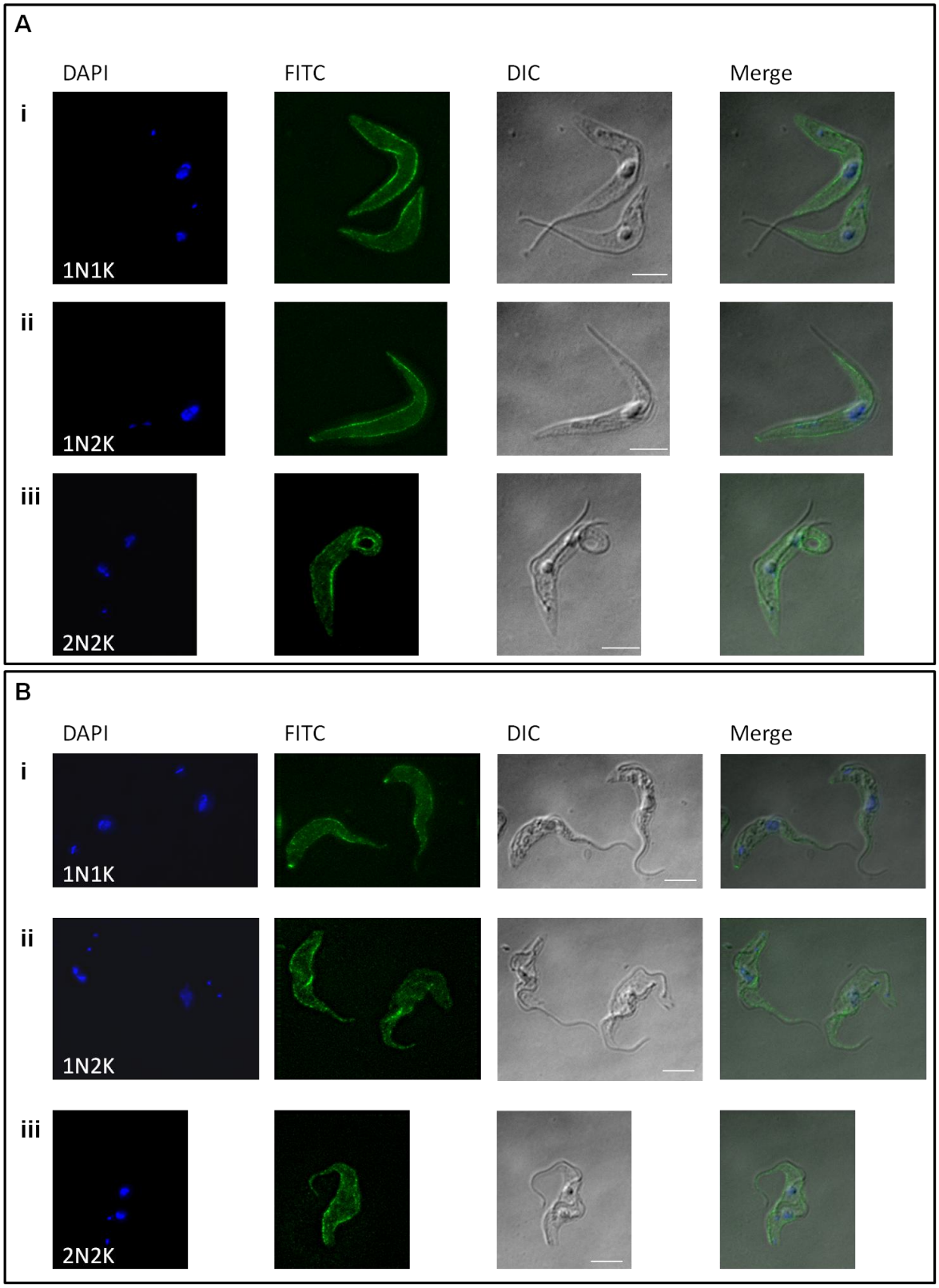

Figure 5-44 -Cytoskeletons of procyclic and bloodstream form *T. brucei* expressing tyGFP:AIR9.
Cytoskeletons were prepared from procyclic (A) and bloodstream (B) form parasites expressing tyGFP:AIR9 (green, FITC) and analysed by fluorescence microscopy. Fluorescent images were deconvolved. DNA was stained with DAPI (blue) and the number of nuclei (N) and kinetoplasts (K) per cell is indicated. Cell morphology is shown in the DIC and merge (DAPI/GFP/DIC) panels. Scale bars: 5µm.

5.4.4 Subcellular fractionation of epitope tagged AIR9

In order to more precisely examine the subcellular localisation of AIR9, biochemical fractionation of procyclic cells expressing tyGFP:AIR9 and both procyclic and bloodstream cells expressing AIR9:6XHA into cytoskeletal and flagellar fractions was carried out by a series of detergent extraction and high salt treatments (Section 4.6.10 and (Broadhead et al., 2006)). Cells treated with PEME buffer (Section 4.6.10) supplemented with the detergent NP-40 become permeablised and cytoplasmic proteins are able to diffuse out of the cells, to leave intact cytoskeletons. Application of 1 M NaCl to these cytoskeletons causes depolymerisation of subpellicular microtubules and releases microtubule-associated proteins, without affecting the stability of the flagellum or the associated microtubule quartet. Following treatment, fractions were prepared and analysed by NuPAGE (Section 4.6.1.2) and Western blotting (Section 4.6.3). Epitope tagged AIR9 was detected with anti-GFP or anti-HA antibodies, while antibodies against cytoplasmic (OPB or EF1-α), cytoskeletal (β-tubulin) and paraflagellar rod (PFRA and C) markers were used to control for the efficiency of the biochemical fractionation (Section 4.6.3.2, Table 4-14 and Figure 5-45).

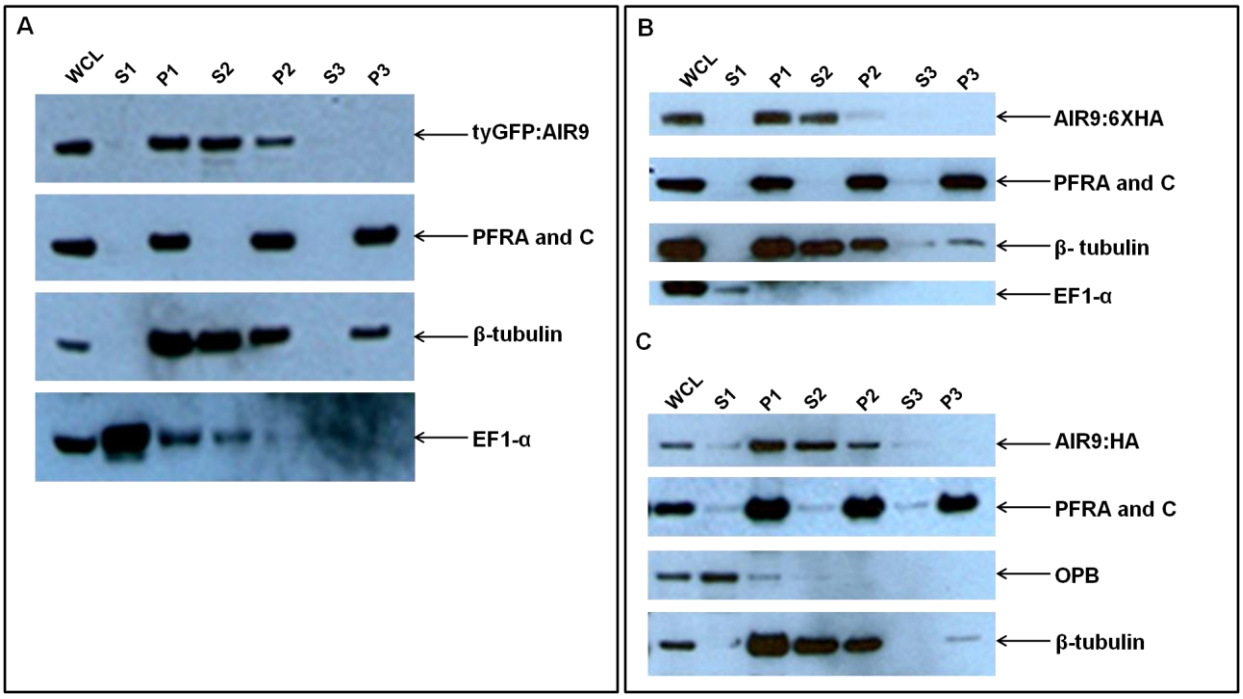

Figure 5-45 - Analysis of subcellular fractions of *T. brucei* expressing tyGFP:AIR9 and AIR9:6XHA by Western blotting.
Subcellular fractions from procyclic form cells expressing tyGFP:AIR9 (A: 427 pHG172 clone 2), and AIR9:6XHA (B: 427 pHG182 clone 1), and bloodstream form cells expressing AIR9:6XHA (C: 427 pHG182 clone 3), were prepared for NuPAGE and Western blotting with anti-GFP antibody or anti-HA antibody (as appropriate) to detect epitope tagged AIR9; anti-

β-tubulin antibody and anti-PFRA and C antibody to detect markers of the cytoskeleton and flagellum, respectively, and anti-EF1-α antibody (A and B) or anti-OPB (C) antibody to detect markers of the cytoplasm. WCL: whole cell lysate; S: supernatant; P: pellet; S1, cytoplasmic fraction; S2 and S3; depolymerised cytoskeletal fractions; P1 and P2: cytoskeletal fractions; P3: flagellar fraction. 10^6 cell equivalents were loaded per lane with the exception of the supernatant fractions in panel A, for which 5 x 10^5 cell equivalents were loaded.

The control markers showed the subcellular fractionation to have worked efficiently. EF1-α and OPB were detected in the whole cell lysates and cytoplasmic fractions, with little contaminating the cytoskeletal fractions, although problems with the degradation of EF1-α were encountered, despite the use of protease inhibitors, resulting in a reduced abundance of this protein in the cytoplasmic fractions. ß-tubulin was detected in the whole cell lysates and in the P1 cytoskeleton fractions. It was also present in the S2 depolymerised cytoskeleton fractions, showing the salt treatment was effective at depolymerising subpellicular microtubules, and some ß-tubulin remained, as expected, in the P2 cytoskeleton and flagella fractions. PFRA and C predominantly remained present in the pellet fractions to a similar extent throughout the fractionation and were present in the flagella fraction at the end, indicating that the flagellar microtubules, unlike the subpellicular microtubules, were not depolymerised by the salt treatment. tyGFP:AIR9 and AIR9:6XHA were detected to similar extents in whole cell lysates and cytoskeleton fractions, and to a lesser extent in partial cytoskeleton fractions (P2). In addition, tyGFP:AIR9 and AIR9:6XHA were detected in the supernatants obtained from the first salt treatment of the cytoskeletons. The relative quantities of tagged AIR9 and ß-tubulin detected in the cytoskeletal fractions and salt extracts of the cytoskeletons were similar, which implies that AIR9:6XHA behaves like a component of the subpellicular corset and is likely to be associated with polymerised microtubules. Very little, if any, AIR9 was detected in either the cytoplasmic or flagellar fractions, consistent with microscopy data discussed above (Section 5.4.3).

5.4.5 Microscopical analysis of procyclic tyGFP:AIR9 subcellular fractions

Analysis of subcellular fractions by microscopy (Section 4.11.3) was performed to further investigate the localisation of tyGFP:AIR9 in a cellular context. As observed previously (Figure 5-42, Figure 5-43 and Figure 5-44), both whole cells

and cytoskeletons exhibited bright staining of the whole cell body but not the flagella (Figure 5-46A and B). Salt treatment produced a curious effect whereby the majority of the staining was removed, but some protein remained adhered to the slide creating a 'ghost cell' imprint (Figure 5-46C). In addition, groups of more stable microtubules were observed which were frequently splayed out as cytoskeletons disintegrated. These microtubules appeared to be components of the subpellicular corset as opposed to the microtubule quartet (inferred from comparing the localisation of the brightly stained microtubules and the kinetoplast, which is where the microtubule quartet originates from). No staining of the flagella or basal bodies could be detected (Figure 5-46B-D).

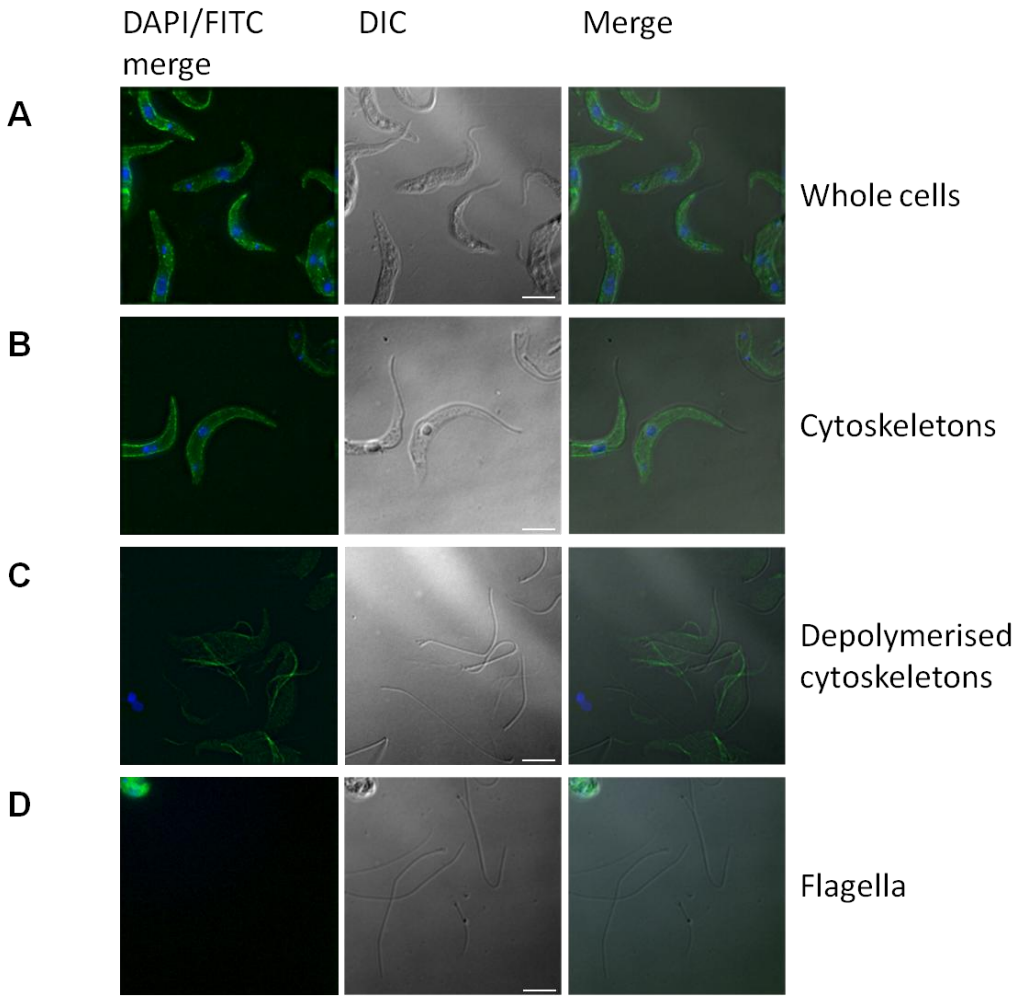

Figure 5-46 –Localisation of tyGFP:AIR9 in procyclic form cells, cytoskeletons and cytoskeletal fractions.
Whole cells, cytoskeletons and cytoskeletal fractions for procyclic form parasites expressing tyGFP:AIR9 (green) were prepared, stained with DAPI, and analysed by fluorescence microscopy. DAPI/FITC merges, DIC and DAPI/FITC/DIC merges are shown above; the fluorescence images are deconvolved. Scale bars: 5 µm.

5.4.6 Co-localisation of AIR9:6XHA and β-tubulin in procyclic form cells

To further investigate the localisation of AIR9, cytoskeletons (Section 4.11.3) prepared from procyclic form cells expressing AIR9:6XHA were co-stained with anti-HA and anti ß-tubulin antibodies (Table 4-16) and analysed by immunofluorescence microscopy (Section 4.11.2) revealing that while the staining patterns of these antibodies co-localised within the subpellicular corset, only anti-ß-tubulin stained the flagella (Figure 5-47). This was particularly noticeable at the region of the flagellum tip (Figure 5-47C). Interestingly, cytoskeletons of post-mitotic cells undergoing furrow ingression displayed bright staining outlining the nascent daughter subpellicular corset that was observed with both anti-HA and anti ß-tubulin antibodies (Figure 5-47B), implying that this pattern of staining can occur as a result of increased microtubule density at the furrow. The similarity between the staining patterns obtained with anti-HA and anti-ß-tubulin antibodies provides further evidence that AIR9:6XHA localises to the subpellicular microtubules.

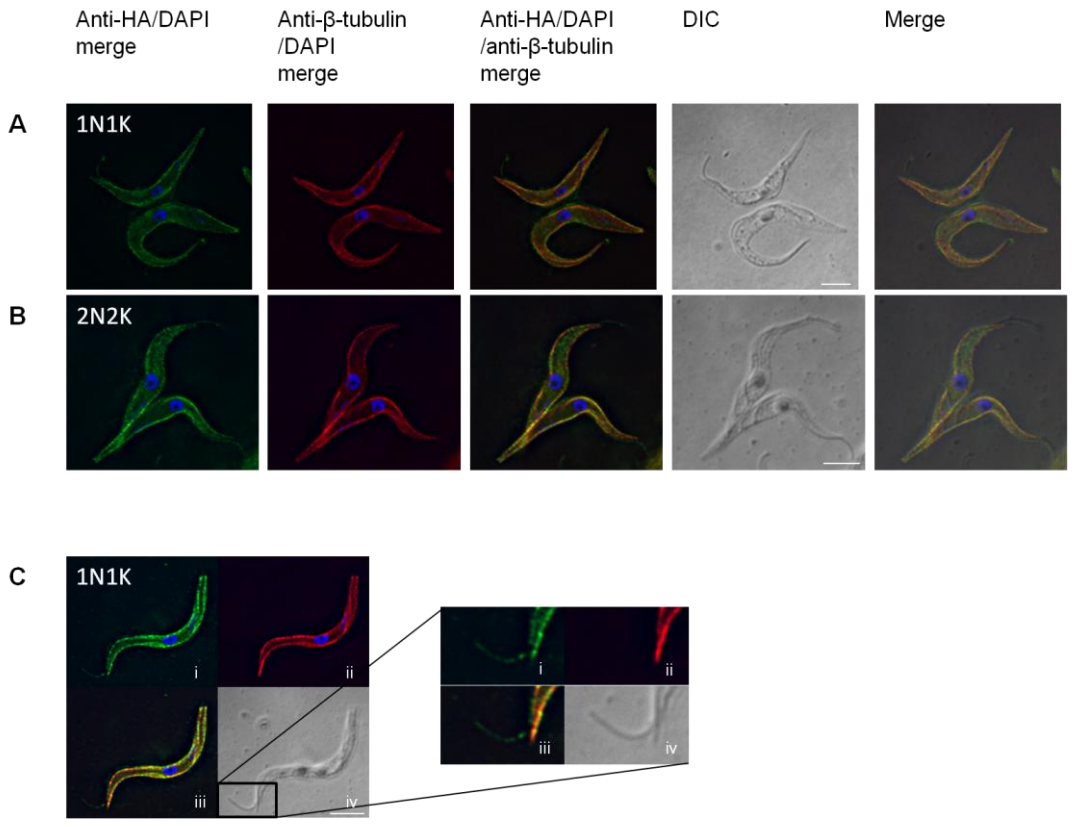

Figure 5-47 –Immunofluorescence analysis of AIR9 and β-tubulin in cytoskeleton preparations of procyclic form *T. brucei* expressing AIR9:6XHA.
Cytoskeletons of procyclic form 427 pHG182 clone 3 cells (Section 5.4.2) were analysed by immunofluorescence using anti-β-tubulin (green) and anti-HA (red) antibodies. DNA was

stained with DAPI (blue) and the number of nuclei (N) and kinetoplasts (K) per cell are indicated (A: 1N1K; B: 2N2K). C: two fold enlargement of the anterior of a 1N1K cell to show staining at the flagellar tip. Fluorescenc images are deconvolved and the identity of each panel is indicated in A and B; in C, i: anti-β-tubulin; ii: anti-HA; iii: anti-β-tubulin/HA merge; iv: DIC. Scale bars: 5 μm.

5.4.7 Dynamics of tyGFP:AIR9 depletion following AIR9 RNAi induction

Depletion of several *T. brucei* MAPs by RNAi has shown them to be depleted preferentially from the posterior end of the parasite (Baines and Gull, 2008; Olego-Fernandez et al., 2009). It was therefore of interest to investigate the dynamics of AIR9 depletion in AIR9 RNAi cells. To this end, procyclic and bloodstream form AIR9 RNAi cell lines expressing tyGFP:AIR9 from the endogenous locus (described in Sections 5.3.2.1 and 5.3.3.1) were analysed by fluorescence microscopy (Section 4.11.1) at 24 and 48 hours (procyclic form) or 12 and 24 hours post-induction (bloodstream form).

As expected, in uninduced cells or at time 0, tyGFP:AIR9 was detected at the outline of the cell body, but not in the flagellum (Figure 5-48Ai and Bi and Figure 5-49Ai).

In procyclic cell lines, induced cells were markedly less bright at their posterior ends (Figure 5-48Aii-iii, Bii-iii and Bv-vi), which was true for cells with and without organelle positioning defects (compare Figure 5-48Aii-iv with Figure 5-48Bii-iii); the emergence of cells with organelle positioning defects in procyclic form RNAi cell lines is described in section 5.3.2.5. This depletion of fluorescence extended for up to half of the cell length in some cases (Figure 5-48Biii), and a few cells were also observed with virtually no fluorescence at all (Figure 5-48iv). In addition, a bright region of fluorescence was observed in the vicinity of the kinetoplast (Figure 5-48Aiv and Bvi), which could potentially represent tyGFP:AIR9 entering the lysosome prior to degradation.

In bloodstream form cells, induction of AIR9 RNAi also resulted in the depletion of tyGFP:AIR9 preferentially from the posterior end (Figure 5-49Aii and Bi). Some cells were also observed to be completely devoid of tyGFP:AIR9 fluorescence (Figure 5-49Biii). However, some abnormal cells, particularly

multinucleate cells, were still strongly fluorescent even after 24 hours' induction and displayed bright lines of staining within the cell (Figure 5-49Bvi).

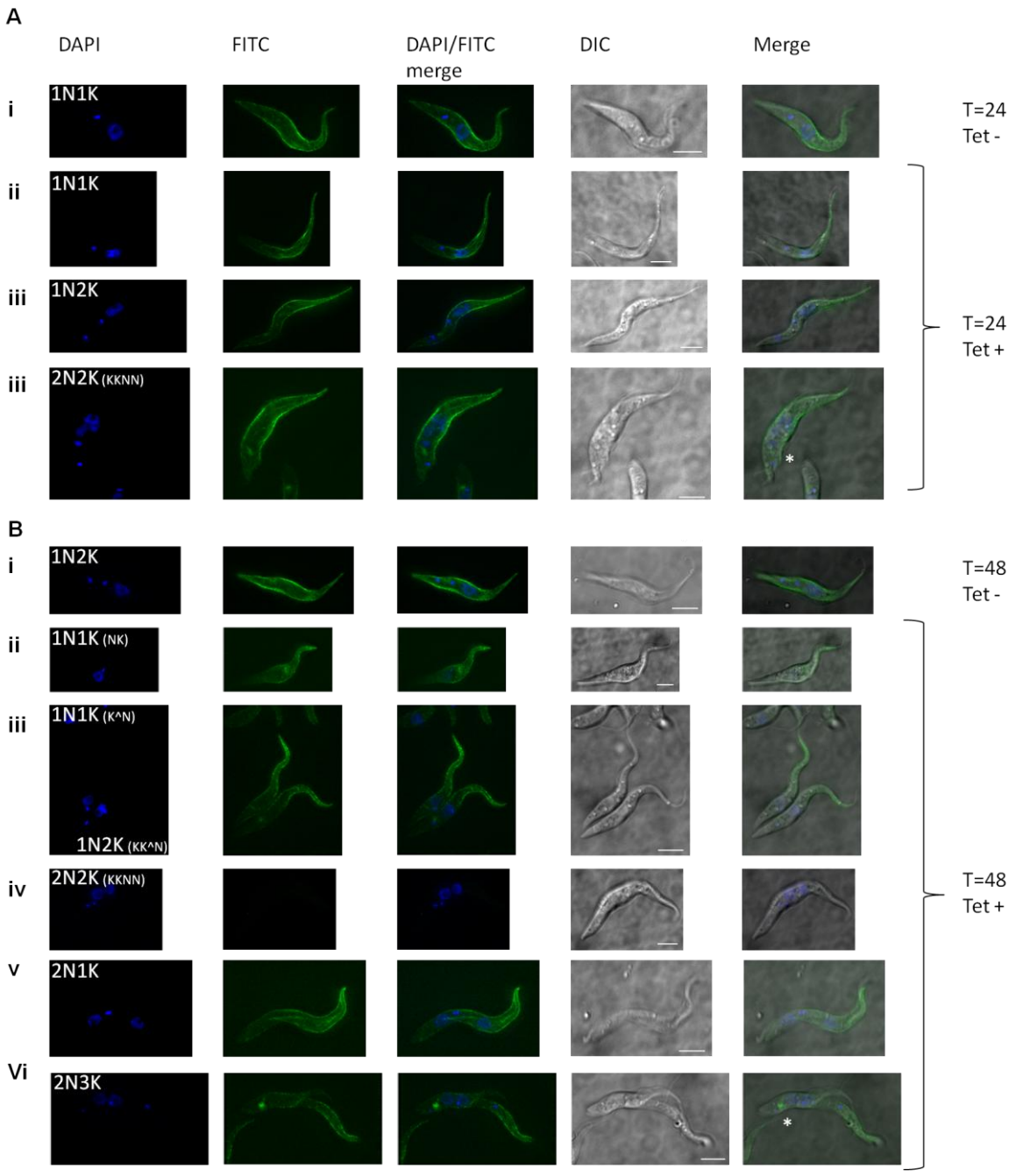

Figure 5-48 –Dynamics of tyGFP:AIR9 depletion in procyclic form *AIR9* RNAi cell lines. RNAi cell lines expressing tyGFP:AIR9 (described in Section 5.3.2.1) were grown in the presence (Tet +) or absence (Tet -) of tetracycline for 24 (A) or 48 (B) hours. Cells were stained with DAPI (blue) and analysed by fluorescence microscopy (tyGFP:AIR9, green, FITC). The number of nuclei (N) and kinetoplasts (K) per cell are indicated, and, where appropriate, the positions of these organelles are noted as described in Section 5.3.2.5. Fluorescence images are deconvolved. DAPI, FITC, DAPI/FITC merge, DIC and merged panels are indicated. Asterisks in Aiv and Bvi indicate a region of more concentrated staining anterior to the posterior most kinetoplast. Scale bars: 5 µm.

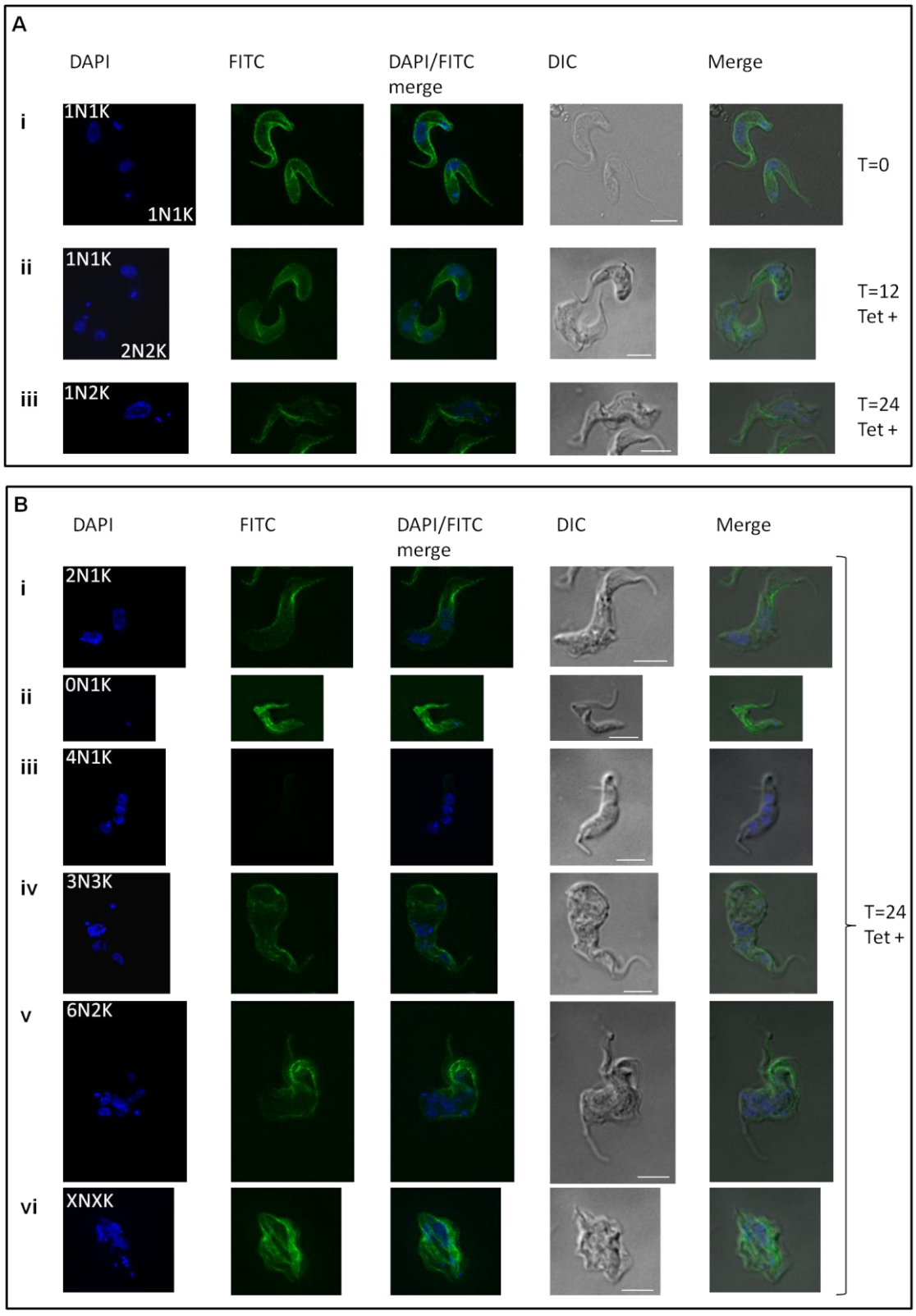

Figure 5-49 –Dynamics of tyGFP:AIR9 depletion in bloodstream form *AIR9* RNAi cell lines. RNAi cell lines expressing tyGFP:AIR9 (described in Section 5.3.2.1) were grown in the presence of tetracycline (Tet +) for 0-24 hours, as indicated. Cells were stained with DAPI (blue) and analysed by fluorescence microscopy (tyGFP:AIR9, green, FITC). Example images of cells with normal (A) and abnormal (B) nuclei (N)-kinetoplast (K) configurations, as indicated, are shown. Fluorescence images are deconvolved. DAPI, FITC, DAPI/FITC merge, DIC and merged panels are indicated. Scale bars: 5 µm.

The preferential depletion of AIR9 from the posterior end of the cell is consistent with a MAP-like role for AIR9. At this region, the subpellicular microtubules are more dynamic, which could explain the more rapid loss of protein from this location. The lines of bright fluorescence observed in some multinucleate cells are harder to interpret, but could represent ingressions of the cell body analogous to those observed normally in post-mitotic cells. If this is the case, the irregular localisation of this staining would provide another indicator of disrupted cell polarity.

5.4.8 Organisation of subpellicular microtubules in procyclic form AIR9 RNAi cell lines

To investigate the effect on microtubule structure following depletion of AIR9 by RNAi, the procyclic form AIR9 RNAi cell lines (clones 4 and 5; Section 5.3.2.1) were cultured in the presence or absence of tetracycline for 72 hours (Section 4.2.2.2) prior to fixation and analysis by Transmission Electron Microscopy (Section 4.11.4). The organisation of the subpellicular microtubules appeared to be unaffected by depletion of AIR9 (Figure 5-50A-B). Basal body transition zones displayed normal quota and arrangement of doublet microtubules (Figure 5-50D), flagellar axonemes displayed the typical '9 + 2' organisation (Figure 5-50C) and the position of flagella and basal bodies relative to the kinetoplast and flagellar pocket appeared to be comparable between uninduced and induced cells (Figure 5-50E-F). These results demonstrate that despite the dramatic effect on organelle positioning, AIR9 depletion did not cause dramatic alterations to the cytoskeleton, and this implies that whilst AIR9 is localised to the cytoskeleton, it does not play a role in maintaining the structural integrity of subpellicular microtubules.

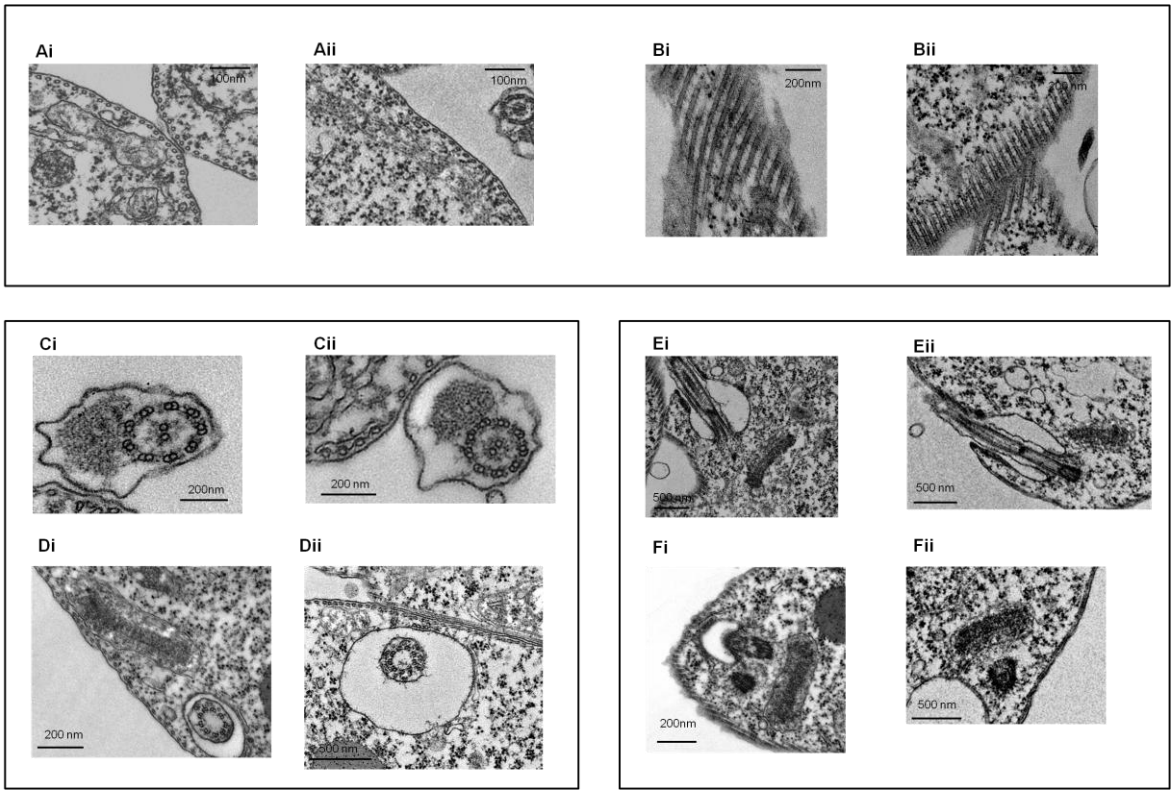

Figure 5-50 -Analysis of cytoskeletal structures in procyclic form *AIR9* RNAi cells by transmission electron microscopy.
Procyclic form *AIR9* RNAi cells (427 pLew13 pLew 29 pHG27 clone 4 (Section 5.3.2.1)) were grown in the presence or absence of tetracycline for 72 hours and analysed by transmission electron microscopy (TEM). TEM images are shown for uninduced ('i') and induced ('ii') cells. Images show: transverse (A) and glancing (B) sections of subpellicular microtubules; transverse section of flagellum (C); transverse (D) and longitudinal (E) sections of transition zone of flagellum; basal bodies and kinetoplast (F). Scale bars are indicated for each image.

5.4.9 Expression of tyGFP:AIR9 in T. brucei epimastigote parasites

The organelle positioning defect observed in procyclic form cells depleted of AIR9 was reminiscent of the 'NK' arrangement of organelles in salivary gland epimastigote parasites (Sharma et al., 2007). This may imply that AIR9 has a role in the changes in organelle positioning that occur during differentiation. As organelle positioning was affected when AIR9 depletion occurred, it was hypothesised that a decrease in AIR9 in the epimastigote stage could mediate this change in N-K positioning. In order to investigate whether AIR9 is absent or expressed at lower levels during this life cycle stage, tsetse fly transmissible procyclic form parasites were transfected with pHG172 (Table 4-4, Section 5.4.1), and transfectants were fed to tsetse flies which were later dissected to obtain salivary gland epimastigotes. These epimastigotes were analysed by fluorescence microscopy to detect expression of tyGFP:AIR9. (With the

exception of preparation of the pHG172 plasmid, this work was carried out by Wendy Gibson and Lori Peacock, University of Bristol).

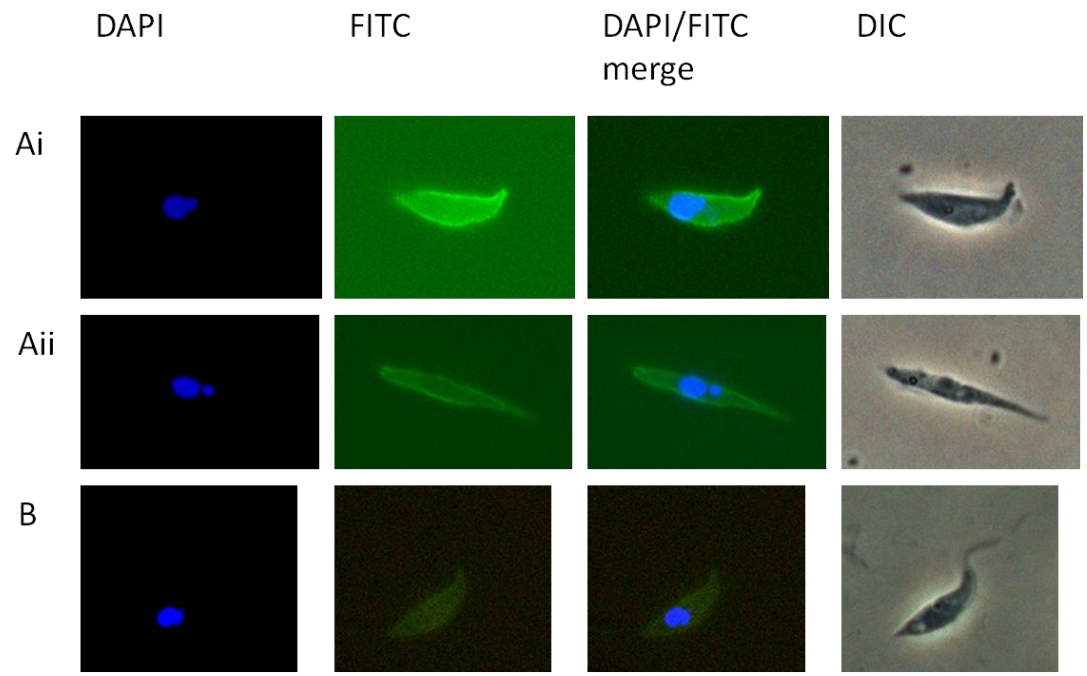

Figure 5-51 -Localisaton of tyGFP:AIR9 in epimastigotes.
Procyclic form 427 variant 3 parasites were transfected with pHG172 (section 5.4.1), and clones which were found to express tyGFP:AIR9 were fed to tsetse flies as a blood meal. Epimastigotes from the salivary glands of dissected tsetse flies were dissected, stained with DAPI and analysed by fluorescence microscopy at 19 (Ai-ii) and 20 days (B) post-infection. DAPI, FITC, DAPI/FITC merge and DIC images are shown. These data were generated by Prof. Wendy Gibson and Dr Lori Peacock at the University of Bristol.

Contrary to the hypothesis, tyGFP:AIR9 was expressed in epimastigotes (Figure 5-51) with a comparable localisation to that observed in procyclic and bloodstream form parasites cultured *in vitro*. Hence, AIR9 depletion does not appear to be required in epimastigote parasites to maintain the distinctive 'NK' organelle arrangement at this life cycle stage.

5.4.10 Summary

AIR9 displayed a cytoskeletal localisation in both bloodstream and procyclic form life cycle stages, which was indiscriminate of whether cells expressed AIR9 with a tyGFP tag at the N terminus or a 6XHA tag at the C terminus (Section 5.4.3). Staining of whole cell bodies but not flagella indicated localisation to the subpellicular corset, which was confirmed by analysis of cytoskeletons by microscopy, subcellular fractionation, and co-immunofluorescence of cytoskeletons using antibodies against ß-tubulin and the AIR9 epitope tag

(Section 5.4.3 and Section 5.4.6). All cell cycle stages in both procyclic and bloodstream form cells displayed similar staining patterns, although post-mitotic cells displayed additional staining along the midline of the cell which was believed to represent staining at the edge of the nascent daughter cell. Analysis of cells depleted of AIR9 by RNAi revealed that downregulation of AIR9 occurs at the posterior end more rapidly than the rest of the cell body (Section 5.4.7), which is in agreement with its localisation to the subpellicular microtubules. Depletion of AIR9 did not result in obvious changes to the organisation of subpellicular microtubules as observed by TEM (Section 5.4.8) and therefore, the organelle and cleavage furrow positioning defects observed upon depletion of AIR9 are not likely to be due to loss of microtubule structural integrity. In addition, the expression of AIR9 in epimastigotes suggested that depletion of AIR9 is not required for maintaining the 'NK' organisation of organelles (Figure 5-51).

The localisation of AIR9 may explain the functional roles of this protein in organelle and cleavage plane orientation. The presence of Ig-like folds in the structure of this protein (Section 5.1) suggest that it is capable of interacting with other proteins, and recruitment of cytoplasmic proteins to the cytoskeleton could be important for communicating information regarding cell polarity. It is possible that AIR9 could form a scaffold for the association of proteins involved in spatial organisation of organelles or cleavage plane orientation.

6 Microtubule dynamics

6.1 Inhibitors of microtubule dynamics

Small molecules, which inhibit the stability of microtubules are readily available, due to their pharmacological applications as herbicides, anthelmintics and antineoplastic agents. Paclitaxel (‘taxol’), vinca alkaloids and colchicine are natural inhibitors of microtubule dynamics, and were isolated from the pacific yew (*Taxus brevifolia*), the pink periwinkle plant (*Catharanthus roseus*) and the autumn crocus (*Colchicum autumnale*), respectively (Hait et al., 2007). In contrast, the anthelmintic benzimidazoles and dinitroanaline herbicides are synthetic heterocyclic aromatic compounds. The inhibitors bind to different sites within microtubules. Taxol (Figure 6-1) binds to microtubules at the taxol-binding pocket, a hydrophobic pocket on the ß-tubulin subunit, causing microtubule shortening and stabilisation. The effect of the drug is dependent on its concentration, and higher concentrations can also induce bundling of microtubules. Vinca alkaloids, including vinblastine and vincristine (Figure 6-1), bind to a separate binding site located between tubulin heterodimers, and binding of these compounds to the positive ends of microtubules inhibits their polymerisation. This effect is observed when low concentrations of inhibitor are applied, and at higher drug concentrations, binding can also occur at low affinity but high capacity binding sites, resulting in disintegration of microtubules. Due to their effect on mitotic spindle assembly, these drugs are used as anti-neoplastic agents, and much is known about the both the mechanisms of action for these compounds and their off-target effects. In addition to their effects on mitosis, low concentrations of these compounds have been shown to causes changes in the phosphorylation of proteins involved in various signalling pathways including the immune response to lipopolysaccharides, and apoptosis. Colchicine and benzamidazoles bind to a high affinity site near the monomer/monomer interface of the ß-tubulin subunit (Fennell et al., 2008), which is the region where α-tubulin binds to ß-tubulin. The binding site of dinitroanaline herbicides is not known.

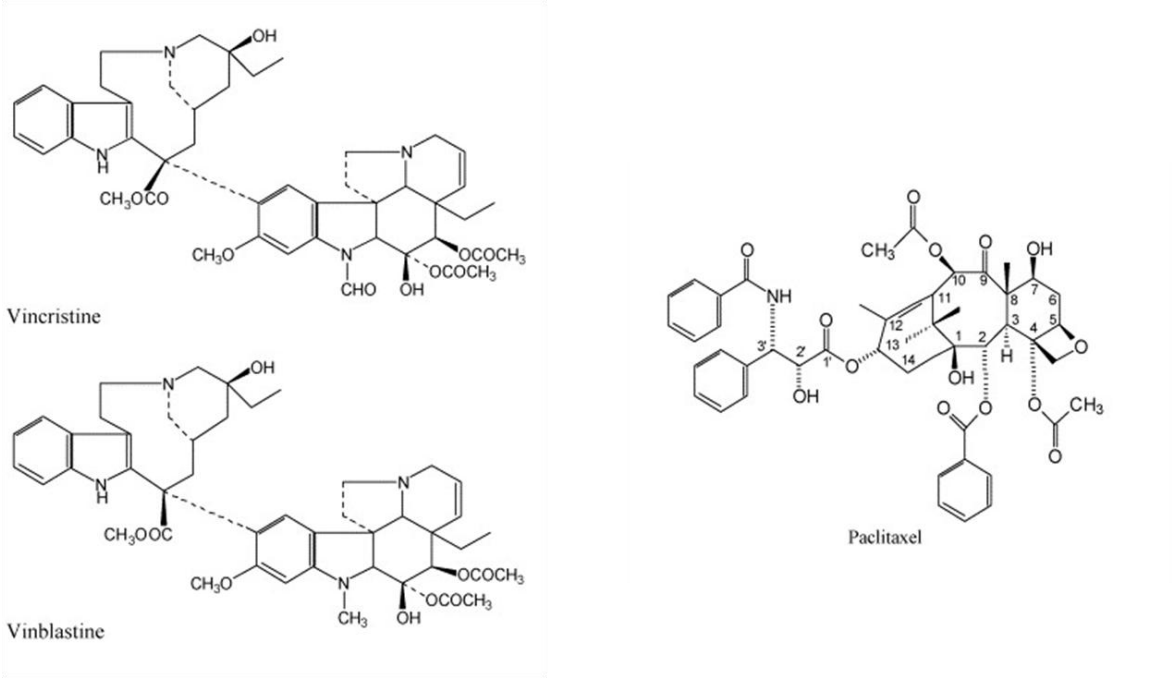

Figure 6-1 -Chemical structures of inhibitors of microtubule dynamics.
The chemical structures for the vinca alkaoids vincristine, vinblastine and paclitaxol (taxol) are shown. Adapted with permission from (Hait et al., 2007).

6.2 Treatment of trypanosomes with microtubule inhibitors

Although microtubule inhibitors were not developed to target trypanosome tubulin, purification of tubulin and microtubule polymerisation assays have been developed and used to verify binding and the effects of microtubule inhibitors on microtubule stability *in vitro,* as well as the effects of microtubule inhibitors on cell viability and cell cycle progression in several Trypanosomatids. Taxol stimulated polymerisation of *T. brucei* tubulin and led to the formation of bundled microtubules, while vinblastine inhibited microtubule assembly (Macrae and Gull, 1990). Studies in *Leishmania* and *T. cruzi* imply that there are direct interactions between these inhibitors and microtubules *in vivo*. For example, vinblastine-resistant *Leishmania* possess mutations in the tubulin gene (Borges et al., 2005). Taxol treatment of *Leishmania* parasites caused a decrease in the levels of tyrosinated tubulin at the cell posterior where microtubules are more dynamic, implying stabilisation of this subpopulation of microtubules (Chavan et al., 2007). Aggregation of tubulin in the cytosol of *Leishmania* parasites treated with taxol has also been reported (Havens et al., 2000). Treatment of *T. cruzi* with vinblastine led to a reduction in cell length (Baum et al., 1981), and in a separate study (Grellier et al., 1999) inhibited furrow initiation, yielding giant,

rounded, multinucleated cells. Taxol treatment of *T. cruzi* also affected cytokinesis, by arresting furrow ingression at a specific point along the cell body, and the authors inferred that altered microtubule dynamics at the furrow were responsible for this phenotype (Baum et al., 1981). Treatment of *T. brucei* with vinca alkaloids is known to be lethal (Ochola et al., 2002) although the effect of these inhibitors on cytokinesis in this organism has not yet been explored.

Other compounds have been shown to preferentially target mitotic microtubules in trypanosomes, for example, the sulphanilamides (Bhattacharya et al., 2004). Dinitroaniline herbicides have also been shown to bind to *Leishmania* tubulin (Chan and Fong, 1990), and to produce drastic effects on the morphology and viability of *T. brucei* parasites *in vivo* (Chan et al., 1993), which may reflect the fact that tubulin in trypanosomes is more similar to plant tubulin than to mammalian tubulin (Chan and Fong, 1994).

In view of the effects of taxol and vinca alkaloids on the cytoskeletons and cell cycle progression in other Trypanosomatids, their effect on *T. brucei* was investigated here. Procyclic and bloodstream form 427 *T. brucei* were cultured *in vitro* in the presence of taxol, vincristine or vinblastine, and the effects on proliferation, morphology and cell cycle progression monitored.

6.3 Treatment of *T. brucei* with taxol

6.3.1 The effect of taxol on the growth of T. brucei

Bloodstream and procyclic form 427 parasites were grown in the presence of a range of different concentrations of taxol (or the equivalent volume of solvent) for 24 or 35 hours, respectively (Section 4.12 and Figure 6-2). Bloodstream form parasites were more sensitive to the effects of taxol compared to procyclic form parasites and incubation with 1 μM taxol proved to be lethal (Figure 6-2A). Procyclic form parasites became immobile and swollen after application of the drug, but although growth was severely impaired (Figure 6-2B), treatment with the concentrations described was not lethal within the 35 hour test period. Bloodstream form parasites clearly demonstrated a dose-dependent

susceptibility to the drug, whereas a dose-dependent effect was not obvious for procyclic form parasites. Growth for both life cycle stages was unaffected by the addition of DMSO solvent.

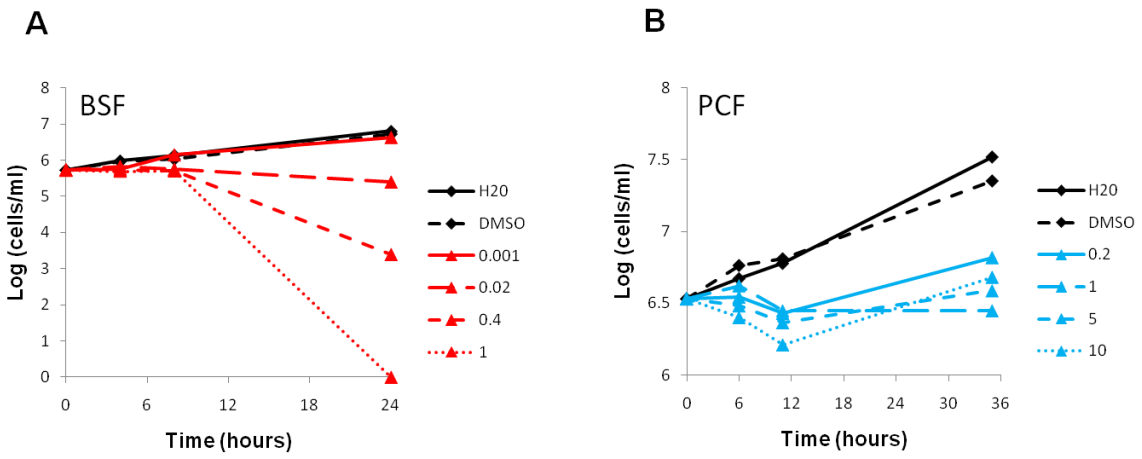

Figure 6-2 -Cumulative growth curves for taxol-treated bloodstream and procyclic form *T. brucei* strain 427.
Bloodstream (BSF, A) and procyclic (PCF, B) form parasites were incubated with taxol at the concentrations (μM) indicated, or equivalent volumes of DMSO solvent or sterile water, and cell density monitored over time.

6.3.2 *The effects of taxol on the cell cycle and morphology of* T. brucei

To investigate morphology and cell cycle progression of parasites incubated with taxol, cells were stained with DAPI (Section 4.11.1) and >200 cells analysed by fluorescence microscopy at 0, 3, 6 and 9 hours (bloodstream form, Figure 6-3) or at 2.5, 5, 7.5 and 10 hours (procyclic form, Figure 6-5) post-treatment. For control cultures (incubated without taxol or with DMSO solvent), the proportions of 1N1K, 1N2K and 2N2K cells remained constant over the 9 or 10 hour test period (Figure 6-3Ai-ii and Figure 6-5Ai-ii), and changes in morphology were not evident by microscopy.

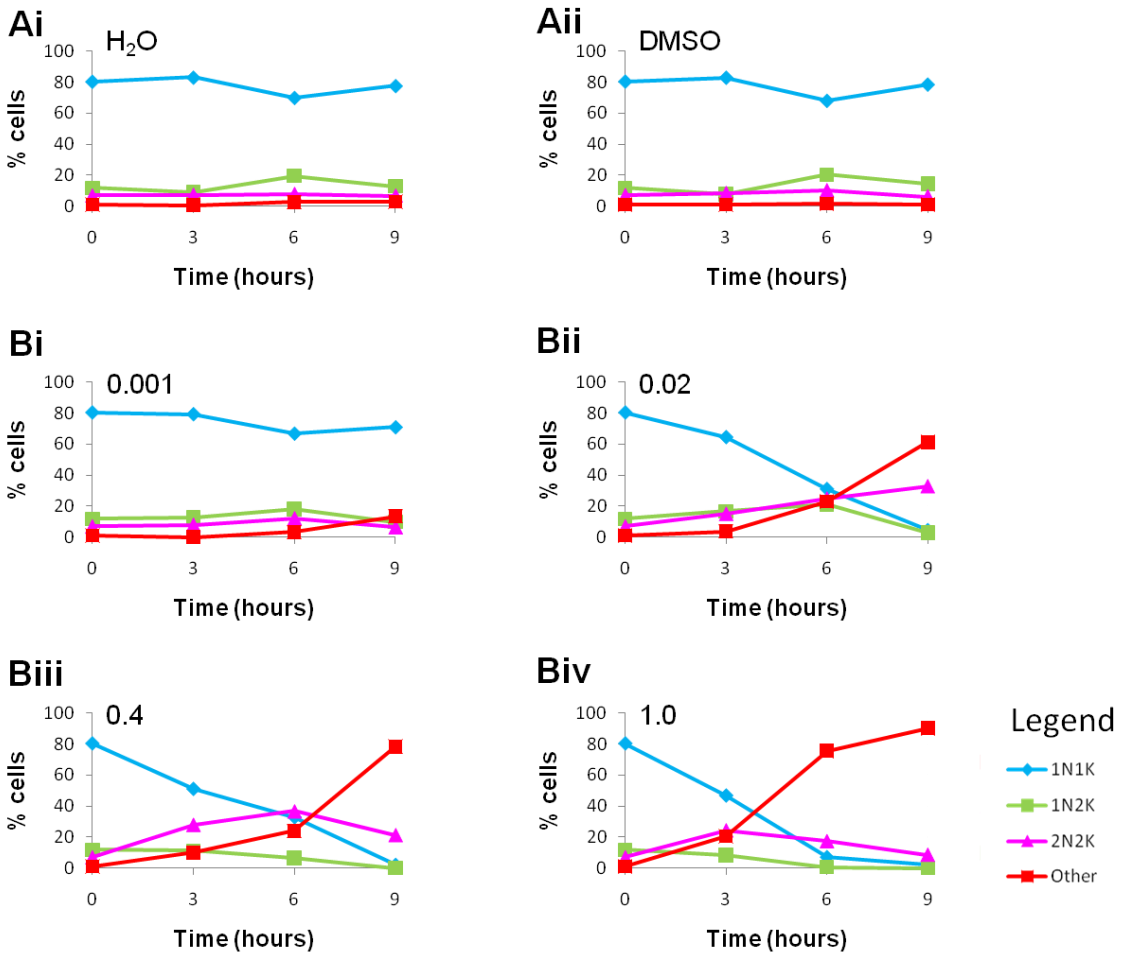

Figure 6-3 -DAPI staining of taxol-treated bloodstream form cells.
Bloodstream form cells treated with taxol (at the concentrations (μM) indicated in Bi-iv), or equivalent volumes of sterile water (Ai) or DMSO solvent (Aii) were sampled at the time points indicated, stained with DAPI and classified according to the number of nuclei (N) and kinetoplasts (K) in each cell (*n*>200).

In bloodstream form parasites, the addition of 0.001 μM taxol also had little effect on cell cycle progression over this time period (Figure 6-3Bi). However, incubation of bloodstream form parasites with between 0.02 μM and 1 μM taxol caused a dramatic increase in the number of post-mitotic (2N2K) cells (Figure 6-3Bii-iv) which was coincident with a decrease in cells at other stages of the cell cycle. Following the rise in post-mitotic cells, abnormal cells with multiple nuclei and kinetoplasts appeared, suggesting that post-mitotic cells underwent extra rounds of organelle replication in the absence of cell division, and that therefore taxol inhibits cytokinesis in this life cycle stage. Occasionally anucleate cells (0N1K) and cells lacking a kinetoplast (1N0K) were also observed (Figure 6-4Bi). Cells treated with 1 μM taxol, rapidly began to show severe morphological defects, including a loss of DNA integrity and swelling of the cell body (Figure 6-4A-B).

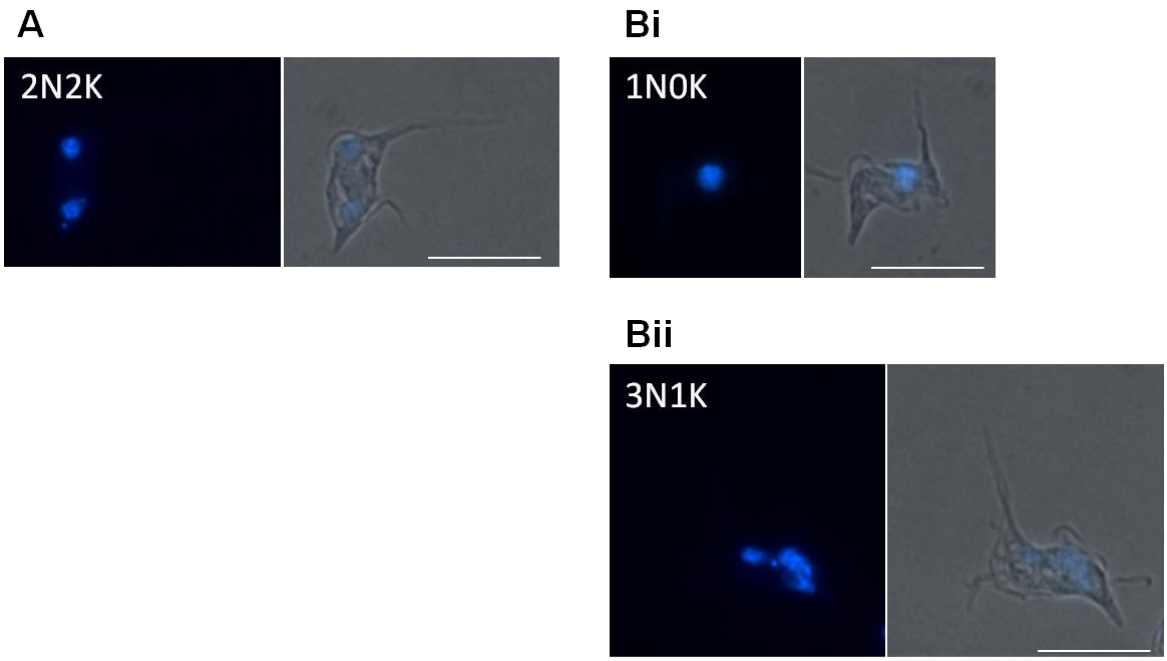

Figure 6-4 -Abnormal cell types observed following treatment of bloodstream form cells with taxol.
Example images of DAPI-stained bloodstream form parasites treated with >0.001 µM taxol. Abnormal cells with rounded morphology are shown. A: 2N2K cell with abnormal organelle positioning; Bi-ii: cells with abnormal N-K configurations. Left panels: DAPI; right panels: DAPI/DIC merge N: nucleus; K: kinetoplast. Scale bar: 10 µm.

Since taxol appeared to only affect cytokinesis and not mitosis as evident from both the rise in 2N2K cells and increase in abnormal multinucleate cell types, it seems taxol does not inhibit spindle dynamics in bloodstream form *T. brucei* parasites as it does in mammalian cells.

Procyclic form cultures also accumulated post-mitotic (2N2K) cells post-taxol treatment (Figure 6-5), and there were few differences in phenotype between parasites treated with differing taxol concentrations.

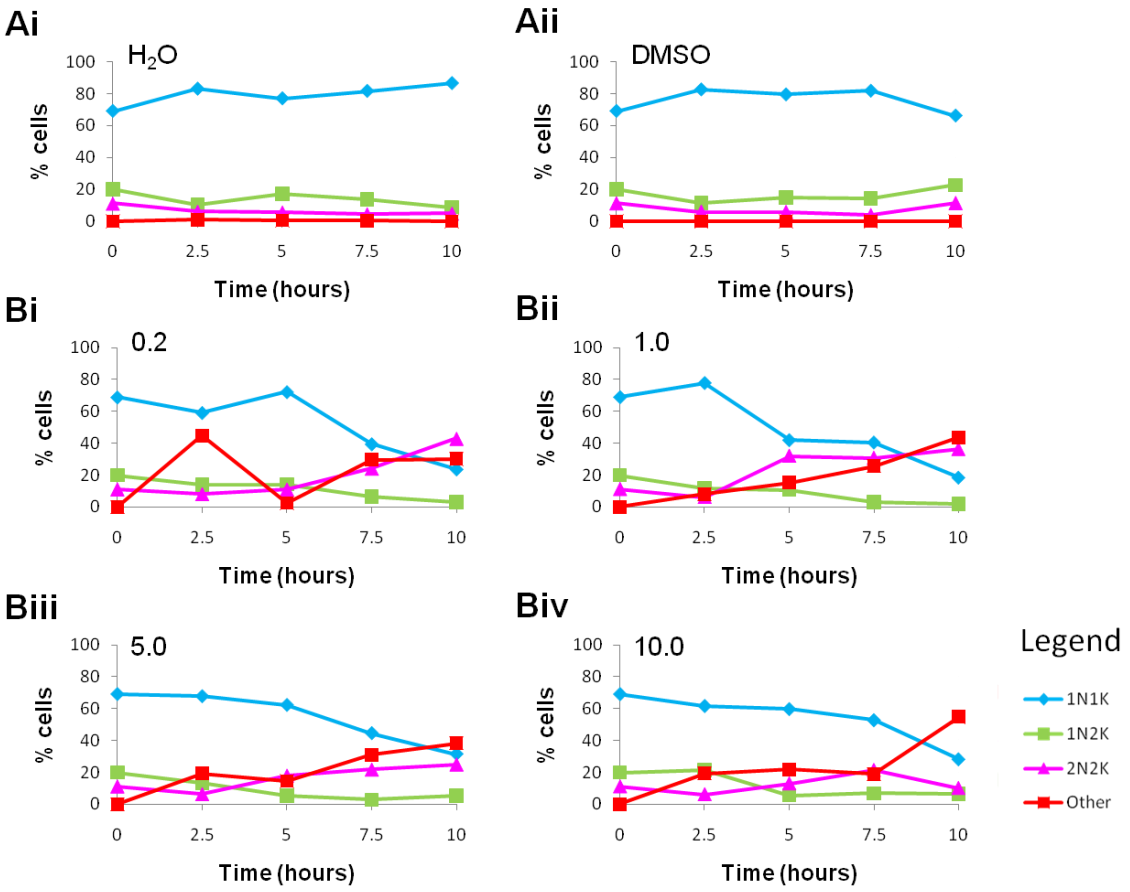

Figure 6-5 –DAPI staining of taxol-treated procyclic form cells.
Procyclic form cells treated with taxol (at the concentrations (μM) indicated in Bi-iv), or equivalent volumes of sterile water (Ai) or DMSO solvent (Aii) were sampled at the time points indicated, stained with DAPI and classified according to the number of nuclei (N) and kinetoplasts (K) in each cell (n>200).

2N2K cells were observed at various stages of cytokinesis (Figure 6-6Ai-iii), and quantification showed that the majority had not initiated furrow ingression (Figure 6-7Bi-ii). However, abnormal cytokinesis phenotypes were also common, and following 10 hours of drug treatment, approximately 10 % of cells treated with 0.2, 1 or 5 μM taxol displayed abnormal cleavage plane positioning, whereby organelles were unequally distributed between nascent daughter cells (shown in Figure 6-6Bi-ii), resulting in 0N1K and 2N1K daughter cells (Figure 6-6Biii-iv). In addition to cleavage plane positioning defects, aberrant organelle positioning was observed (Figure 6-7Bi-iv), which was only noticed in the post-mitotic cell population.

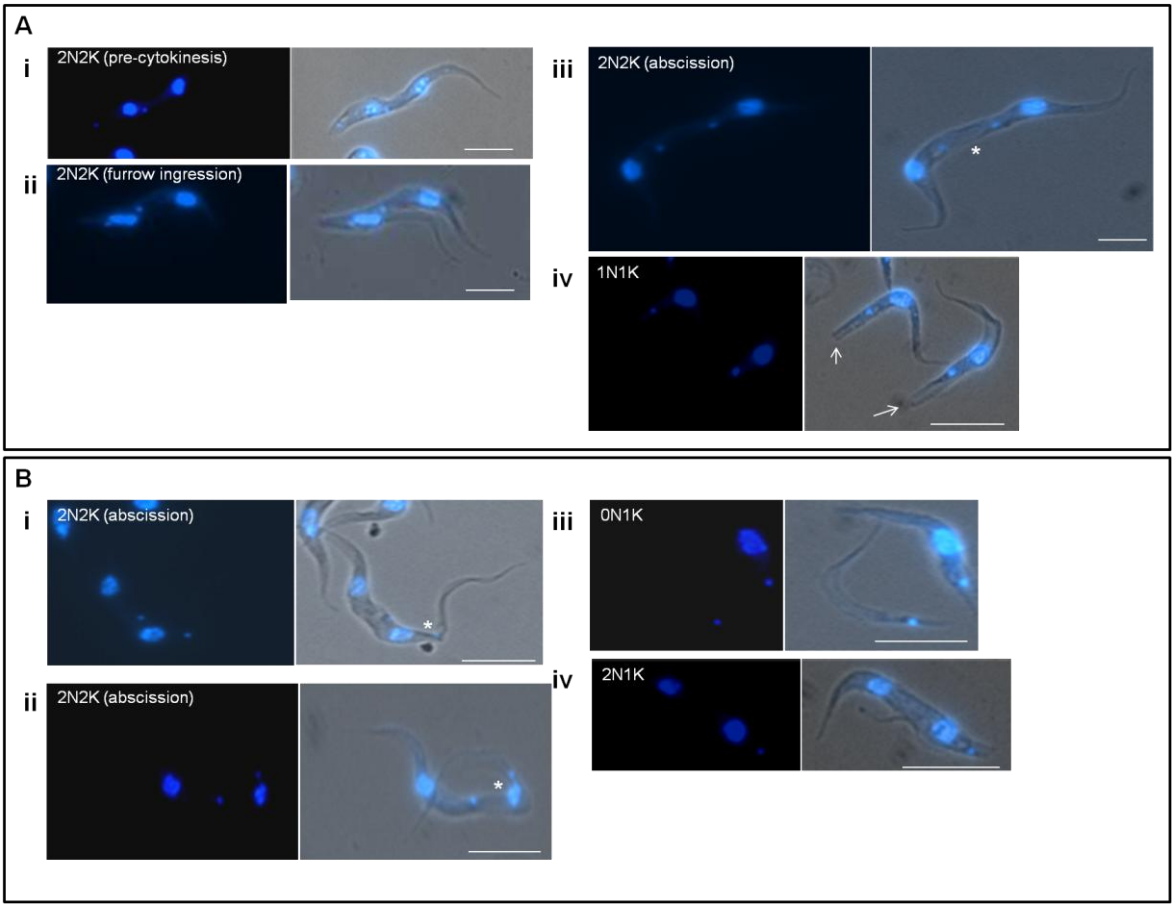

Figure 6-6 –Images of taxol-treated procyclic form *T. brucei*.
Procyclic form 427 cells were incubated with 0.2-10 μM taxol, stained with DAPI and analysed by fluorescence microscopy. Ai-iii: example images of 2N2K cells at different cytokinesis stages (indicated); daughter 1N1K cells with abnormal (blunt) posterior end morphology (arrows). Bi-ii: 2N2K cells undergoing abscission (asterisks) with abnormal furrow placement; Biii-iv: abnormal daughter cells resulting from malpositioned cleavage furrow. Left panels: DAPI; right panels: DAPI/DIC merge. N: nucleus; K: kinetoplast. Scale bar: 10 μM.

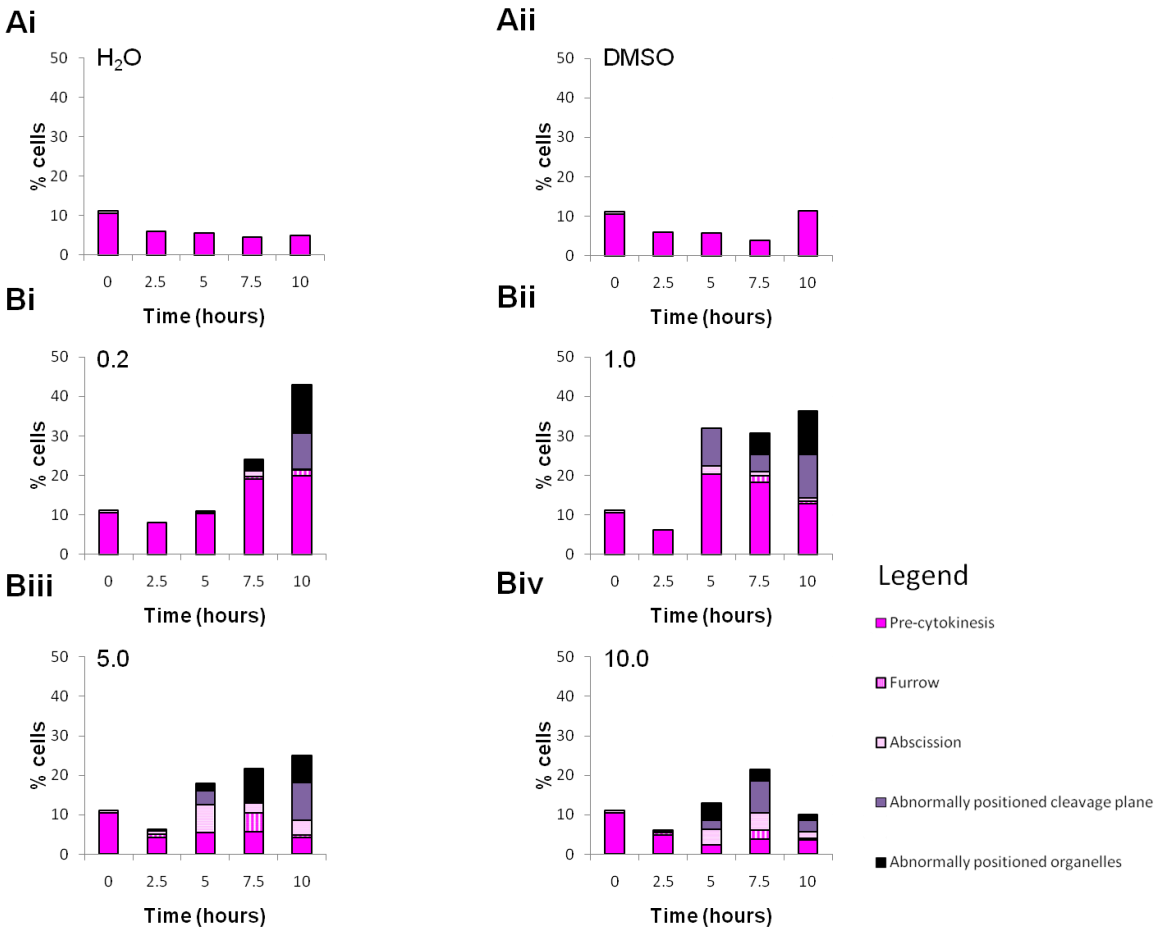

Figure 6-7 -Analysis of 2N2K cells observed in populations of procyclic form parasites treated with taxol.
Procyclic form 427 *T. brucei* were treated with the concentrations (μM) indicated of taxol (Bi-iv) or equivalent volumes of sterile water (Ai) or DMSO (Aii) and stained with DAPI. Cells with 2 nuclei and 2 kinetoplasts (2N2K, see Figure 6-5) were further classified according to their cytokinesis stage, and also, where appropriate according to cleavage plane orientation and relative positions of nuclei and kinetoplasts as indicated in the key. Numbers of 2N2K cells of each type are expressed as a proportion of the total cells in the population.

At later time points, multinucleate cells with up to four nuclei were observed, and these possessed varying numbers of kinetoplasts and were sometimes observed undergoing (abnormal) cytokinesis. Cells with severe morphological defects were also observed and were likely to be dying cells since they displayed problems with nuclear integrity and possessed very abnormal swollen cell bodies. Interestingly, other more minor morphological abnormalities were observed, comprising a thickening and change in shape to the posterior end of cells (Figure 6-6Aiv), implying that these cells either derived from an abnormal abscission, or that the drug directly affected the structure of the posterior end of the cell.

Hence, the application of taxol to procyclic form parasites inhibited the initiation of furrow ingression and lead to abnormal placement of the cleavage furrow, resulting in deregulation of the cell cycle. Whilst these appear to be direct effects, accumulation of more severe morphological defects and the presence of apparently dying cells implied that other processes were also being affected. Taxol may interfere with various signalling pathways, as implicated by studies in mammalian cells, and accumulation of different problems could result in the more severe phenotypes observed. It is also worth noting that the motility of taxol-treated parasites was affected, and it is possible that this may have contributed to the accumulation of cells at the abscission stage of cytokinesis.

6.4 Treatment of *T. brucei* with vincristine

6.4.1 The effect of vincristine on growth of T. brucei

Bloodstream and procyclic form 427 parasites were cultured in the presence of a range of concentrations of vincristine (Section 4.12) for 24 or 32 hours, respectively (Figure 6-8). Bloodstream form parasites treated with 0.05 µM vincristine exhibited slightly reduced growth, but concentrations ≥0.2 µM vincristine, severely impaired growth (Figure 6-8A). Growth of procyclic form parasites was inhibited in the presence of all drug concentrations tested, and the effect on cell proliferation was not dose-dependent (Figure 6-8B).

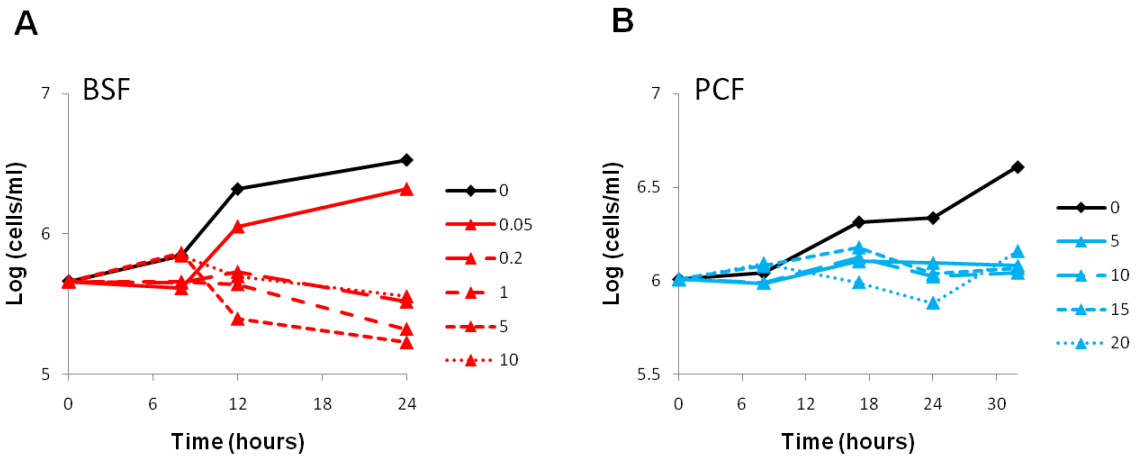

Figure 6-8 -Cumulative growth curves for vincristine-treated bloodstream and procyclic form *T. brucei* strain 427.
Bloodstream (BSF, A) and procyclic (PCF, B) form parasites were incubated with vincristine at the concentrations (µM) indicated, and cell density monitored over time.

6.4.2 The effects of vincristine on the cell cycle and morphology of *T. brucei*

DAPI staining (Section 4.11.1) of vincristine-treated bloodstream form cells (0.05, 0.2 and 1 μM) revealed a dramatic increase in post-mitotic (2N2K) cells at 6 hours post-treatment (Figure 6-9Bii-iii) (with these cells comprising more than 50 % of the population for 0.2 μM and 1 μM vincristine) that was not observed in control populations. At later time points, multinucleate cells accumulated, probably due to an uncoupling of cytokinesis and cell cycle progression. At the higher drug concentrations of 5 μM and 10 μM vincristine, cells at all cell cycle stages rapidly began to display severe phenotypes whereby the nuclear integrity was affected, and morphology became drastically rounded and abnormal, and it is likely that this was due to vincristine toxicity at these concentrations.

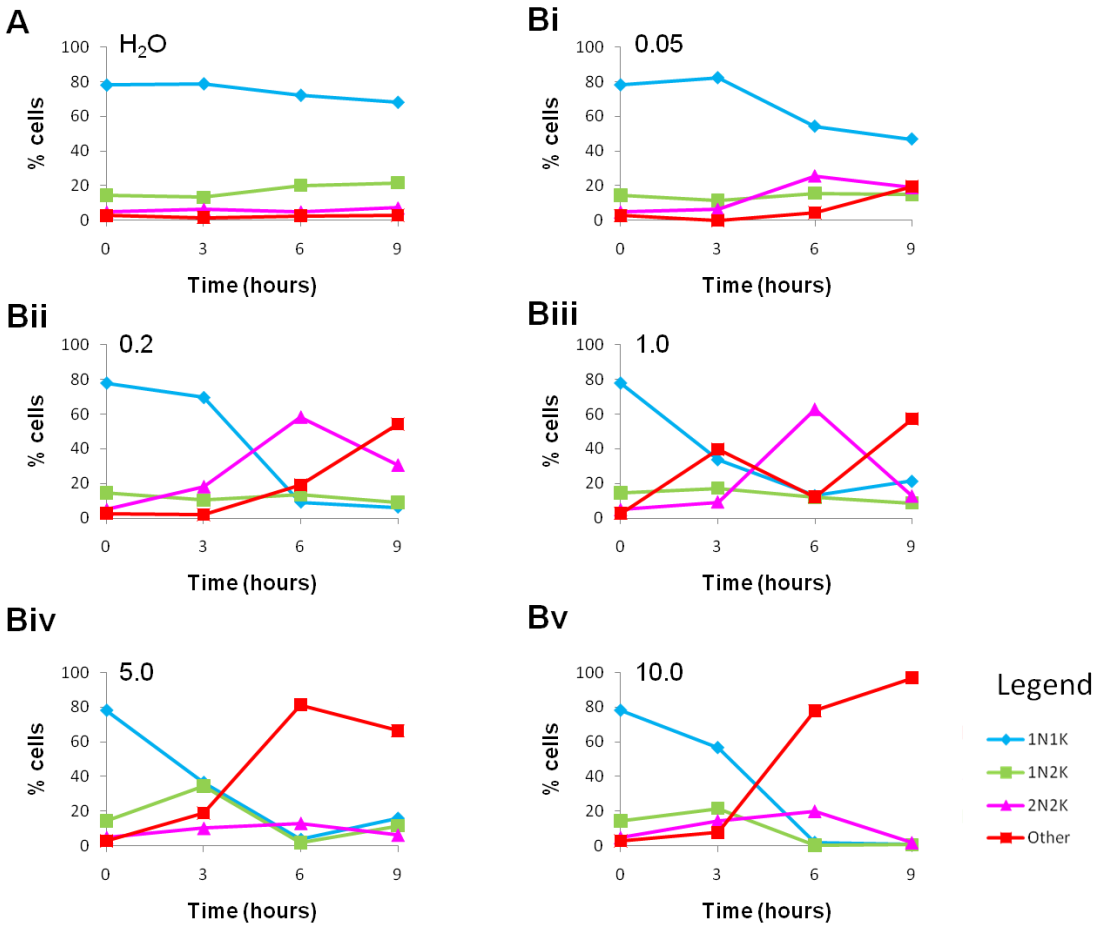

Figure 6-9 -DAPI staining of vincristine-treated bloodstream form cells.
Bloodstream form cells treated with vincristine (at the concentrations (μM) indicated in Bi-v), or an equivalent volume of sterile water (A) were sampled at the time points indicated, stained with DAPI and classified according to the number of nuclei (N) and kinetoplasts (K) in each cell (*n*>200).

The 2N2K cells were classified according to cytokinesis stage (Figure 6-10), and at 6 hours post-treatment with 1 μM vincristine, post-mitotic cells undergoing furrow ingression comprised 36 % of the whole population (Figure 6-10Biii). These parasites appeared to be stalled at a similar stage of furrow ingression (Figure 6-10C), and this was investigated in more detail using Scanning Electron Microscopy (Section 4.11.5) to obtain more detailed images of these cells (Figure 6-11). However, due to the undulating topology of the cell body, it was not possible to accurately determine the extent of furrow ingression, although qualitative analysis indicated that the furrow had ingressed approximately 75 % of the whole cell length.

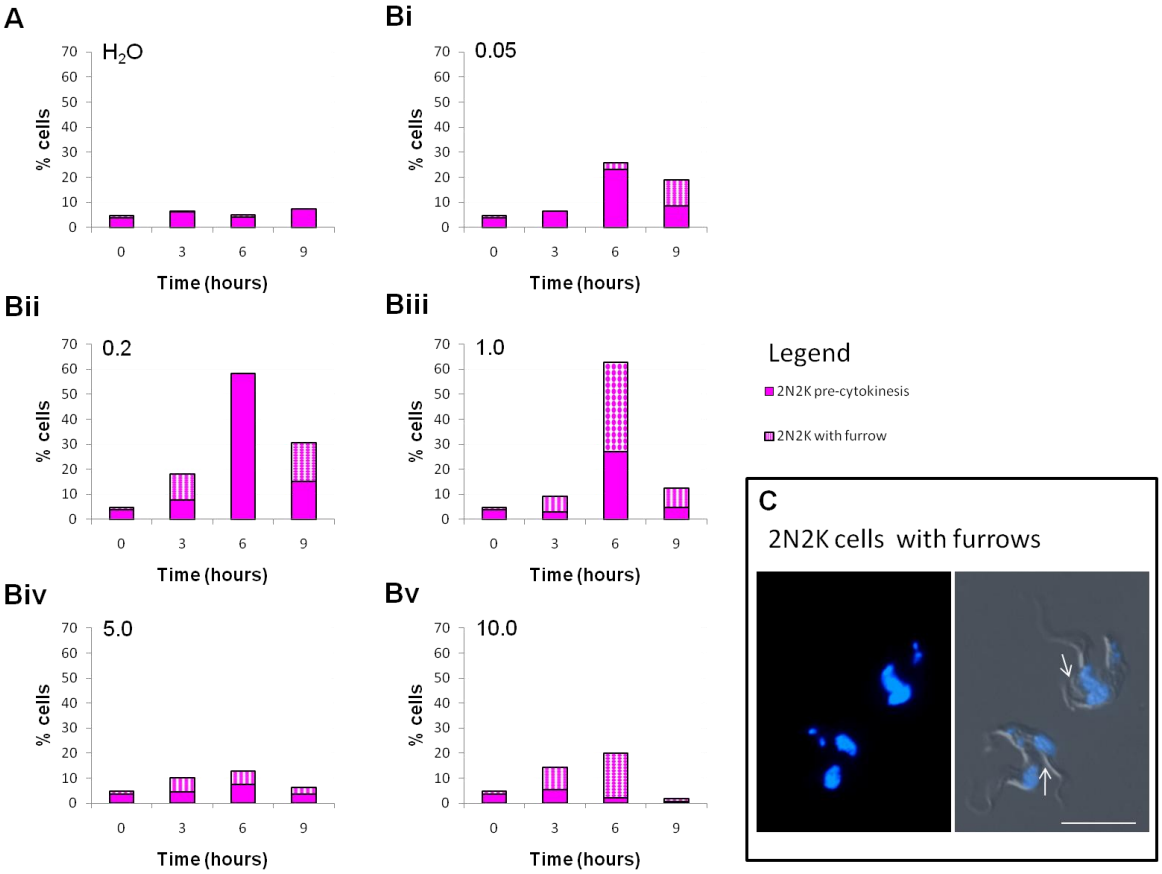

Figure 6-10 –Analysis of cytokinesis stages for vincristine-treated bloodstream form 2N2K cells.
Bloodstream form 427 *T. brucei* were treated with the concentrations (μM) indicated of vincristine (Bi-v) or an equivalent volume of sterile water (A) and stained with DAPI. Cells with 2 nuclei and 2 kinetoplasts (2N2K, see Figure 6-9) were further classified according to their cytokinesis stage, as indicated in the key. C: example images of 2N2K cells with furrows (arrows). Left panel: DAPI; right panel: DAPI/DIC merge. Scale bar: 10 μM. Numbers of 2N2K cells of each type are expressed as a proportion of the total cells in the population.

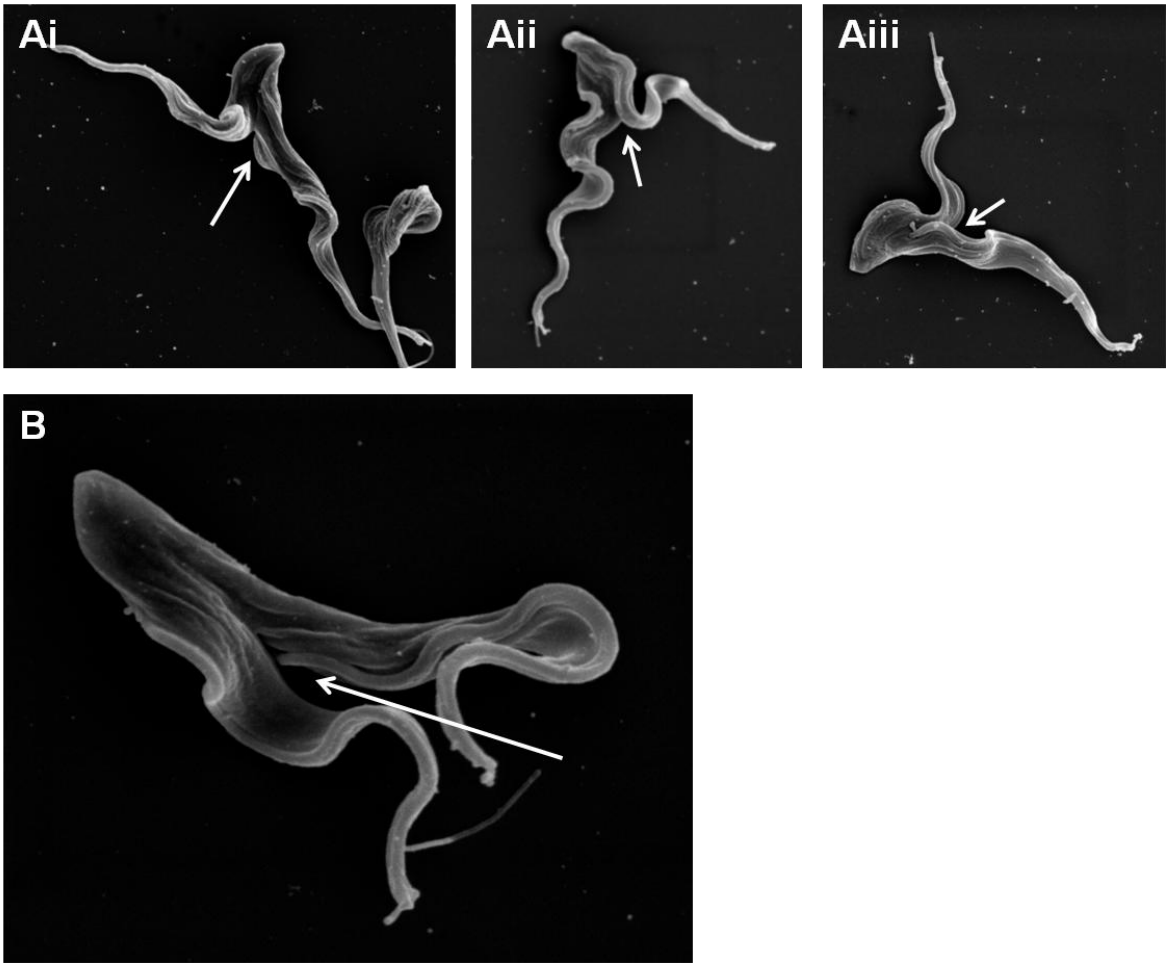

Figure 6-11 -Scanning electron microscopy images of furrowing 2N2K cells following vincristine treatment of bloodstream form *T. brucei*.
Bloodstream form parasites were grown for 6 hours in the presence of 1 µM vincristine prior to analysis by scanning electron microscopy. Typical examples of cells displaying furrows are shown in A-B. Arrows indicate the direction of furrow ingression. B is enlarged to better see the ingressing furrow.

Hence, the effect of vincristine on bloodstream form parasites differed according to the concentration of drug administered. For concentrations of 0.05 - 1 µM, dramatic cytokinesis defects were observed comprising inhibition of cytokinesis prior to, and part way through, furrow ingression. Cells which did not initiate cytokinesis were likely to become multinucleate, which implied that downstream of the initial cytokinesis block, cell cycle deregulation had occurred. Higher concentrations of drug were clearly lethal to the parasites, as exhibited by the defects in cell morphology and nuclear integrity.

In contrast, procyclic form parasites were observed to lose nuclear integrity and display abnormal morphology very rapidly following incubation with all concentrations of vincristine tested (Figure 6-12), compared to cells grown in the absence of drug, which were normal in appearance. This suggested that

vincristine treatment at this range of concentrations is toxic and the drug probably affects multiple targets when applied in these quantities.

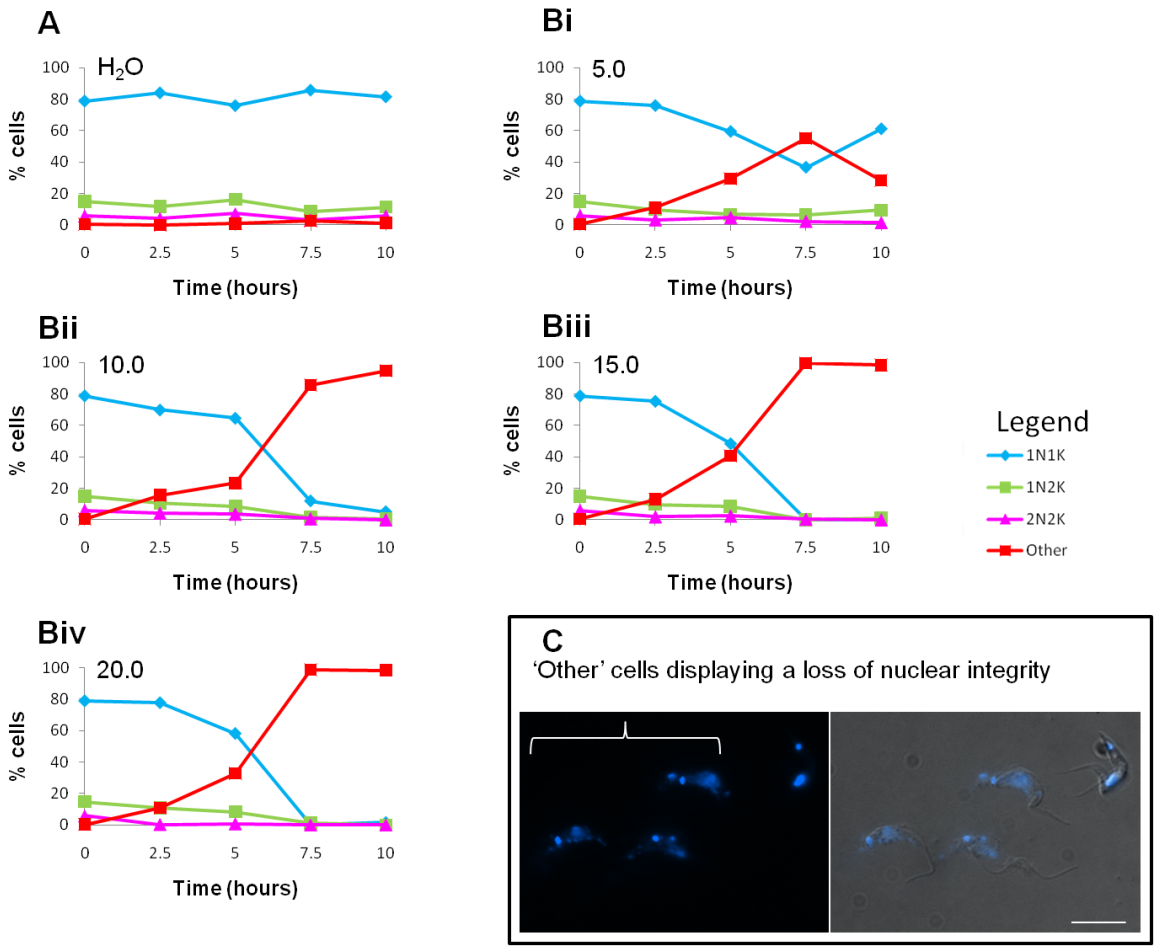

Figure 6-12 -DAPI staining of vincristine-treated procyclic form cells.

Procyclic form cells treated with vincristine (at the concentrations (μM) indicated in Bi-iv), or an equivalent volume of sterile water (A) were sampled at the time points indicated, stained with DAPI and classified according to the number of nuclei (N) and kinetoplasts (K) in each cell (*n*>200). C: images of cells displaying 'other' configurations (bracket), with diffuse DAPI staining of the nucleus. Left panel: DAPI; right panel: DAPI/DIC merge. Scale bar: 10 μm.

6.5 Treatment of *T. brucei* with vinblastine

6.5.1 The effect of vinblastine on growth of T. brucei

Bloodstream and procyclic form 427 parasites were cultured in the presence of a range of concentrations of vinblastine (or the equivalent volume of solvent) for 25 hours (Section 4.12 and Figure 6-13). Incubation of bloodstream form parasites with 0.05 μM or 0.2 μM vinblastine had only a minor inhibitory effect on proliferation but for concentrations ≥1 μM vinblastine, growth was severely

impaired in a dose-dependent fashion (Figure 6-13A), and 25 hours of treatment with 10 μM vinblastine proved lethal. Growth of procyclic form parasites was inhibited in the presence of all vinblastine concentrations tested (Figure 6-13B), and whilst parasites did continue to proliferate to a small extent in the presence of 5 and 10 μM vinblastine, higher concentrations arrested growth. Growth of parasites of both life cycle stages was unaffected by the presence of an equivalent volume of methanol solvent.

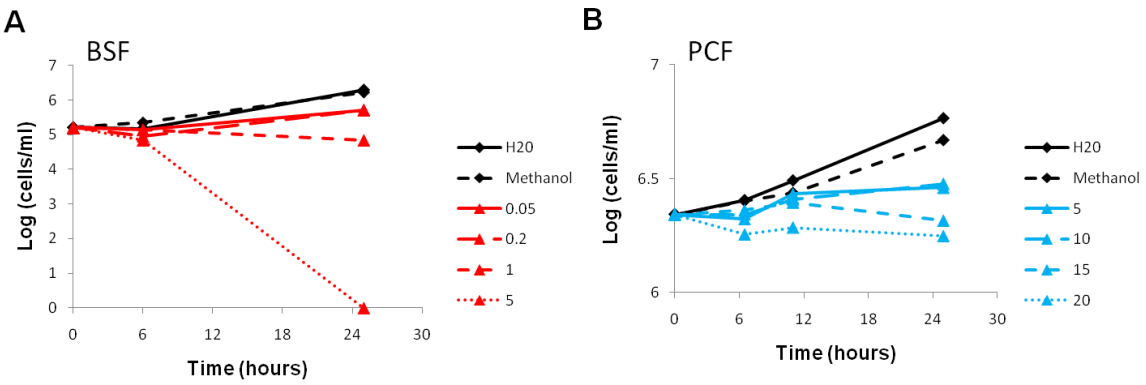

Figure 6-13 -Cumulative growth curves for vinblastine-treated bloodstream and procyclic form *T. brucei* strain 427.
Bloodstream (BSF, A) and procyclic (PCF, B) form parasites were incubated with vinblastine at the concentrations (μM) indicated, or equivalent volumes of methanol solvent or sterile water, and cell density monitored over time.

6.5.2 The effects of vinblastine on the cell cycle and morphology of T. brucei

As above, DAPI staining (Section 4.11.1) was performed for drug treated parasites. Similarly to vincristine treatment, vinblastine caused an accumulation of post-mitotic cells in bloodstream form parasites (Figure 6-14). This effect was most dramatic when cells were treated with 1 μM vinblastine, and for this concentration at 6 hours post-treatment, 2N2K cells comprised 68 % of the whole population (Figure 6-14Biii).

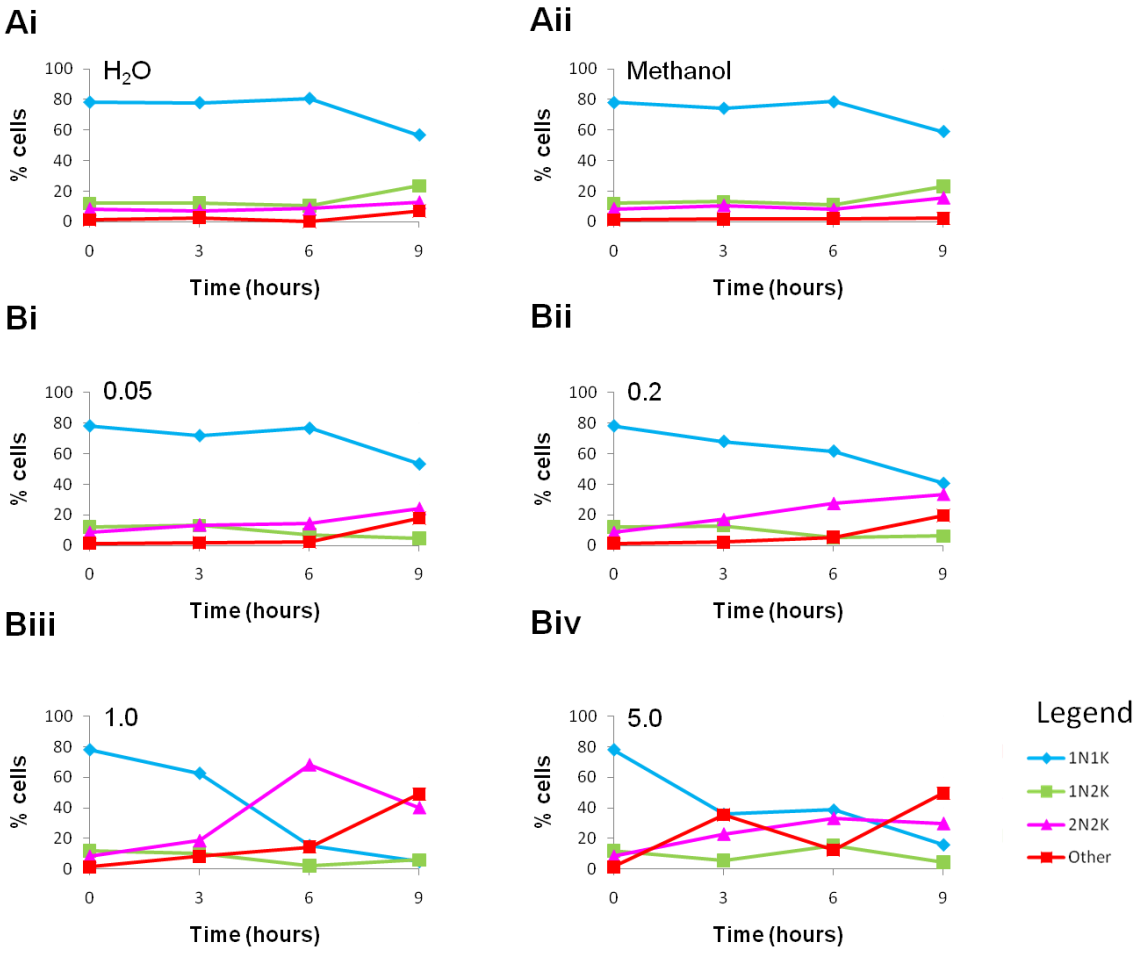

Figure 6-14 -DAPI staining of vinblastine-treated bloodstream form cells. Bloodstream form cells treated with vinblastine (at the concentrations (μM) indicated in Bi-iv), or equivalent volumes of sterile water (Ai) or methanol solvent (Aii) were sampled at the time points indicated, stained with DAPI and classified according to the number of nuclei (N) and kinetoplasts (K) in each cell (*n*>200).

Over time, these post-mitotic cells comprised increasing numbers of cells undergoing furrow ingression (Figure 6-15). Cells that were inhibited at initiation or completion of cytokinesis proceeded to replicate their organelles in the absence of cell division. This was apparent from the coincident drop in 2N2K cells and dramatic increase in multinucleate cells observed at 9 hours post treatment with 1 μM vinblastine (Figure 6-14 Biii).

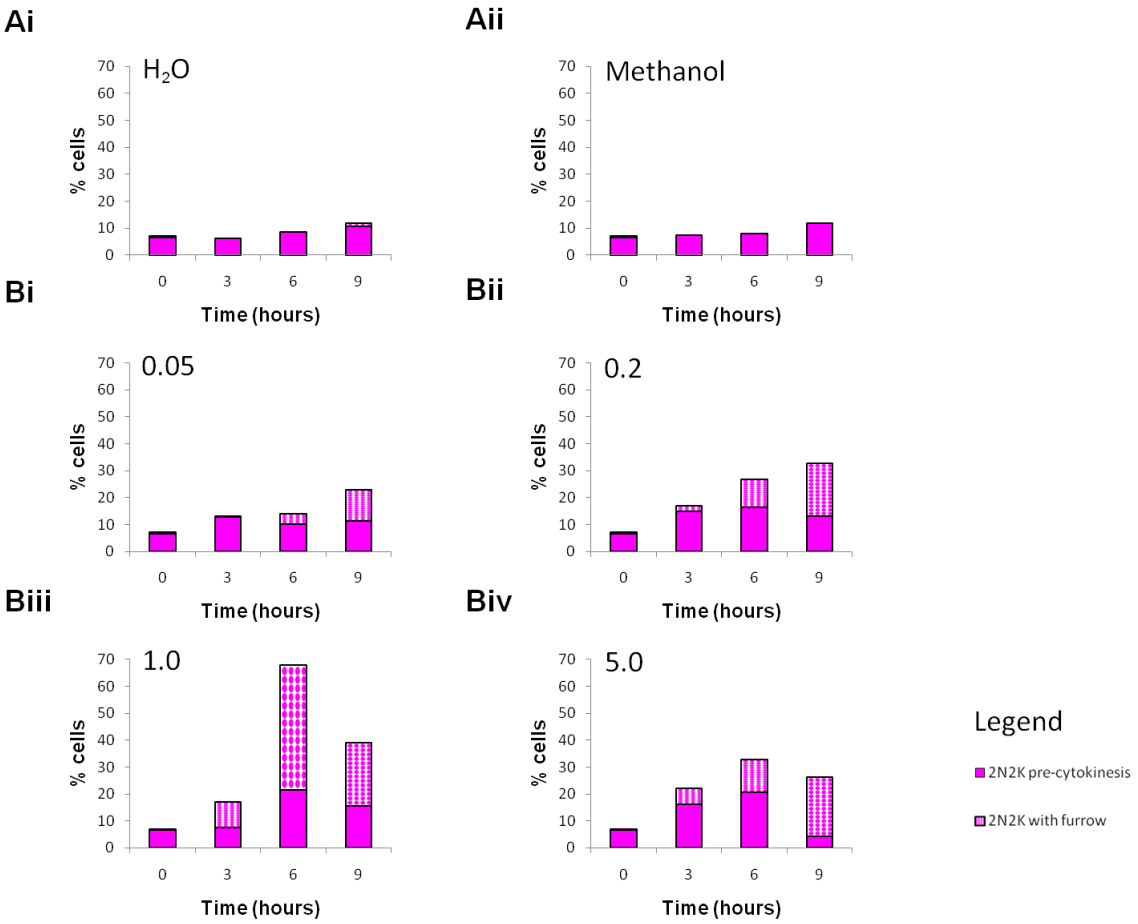

Figure 6-15 –Analysis of 2N2K cells observed in populations of bloodstream form parasites treated with vinblastine.
Bloodstream form 427 *T. brucei* were treated with the concentrations (μM) indicated of vinblastine (Bi-iv) or equivalent volumes of sterile water (Ai) or methanol (Aii) and stained with DAPI. Cells with 2 nuclei and 2 kinetoplasts (2N2K, see Figure 6-14) were further classified according to their cytokinesis stage. Numbers of 2N2K cells of each type are expressed as a proportion of the total cells in the population.

In contrast, treatment of procyclic form parasites with 5-20 μM vinblastine (Figure 6-16) did not cause any dramatic changes to the relative proportions of cells at different cell cycle stages (Figure 6-16Bi-iv), although defects associated with mitosis and organelle segregation were observed (Figure 6-17). These abnormal phenotypes comprised cells with unequally sized nuclei positioned extremely close together, and occasionally nuclear segregation was totally inhibited such that it was not possible to determine whether a cell possessed one large nucleus or two separate nuclei. A more thorough analysis of G2/M cells would be required to determine the extent of the nuclear segregation defect, and to provide insights into whether kinetoplast segregation is also affected. At later time points, cells with severe abnormalities were observed and these comprised cells with defects in nuclear and structural integrity, and to a lesser

extent, multinucleate cells were observed, which frequently displayed clear defects in nuclear segregation (Figure 6-17).

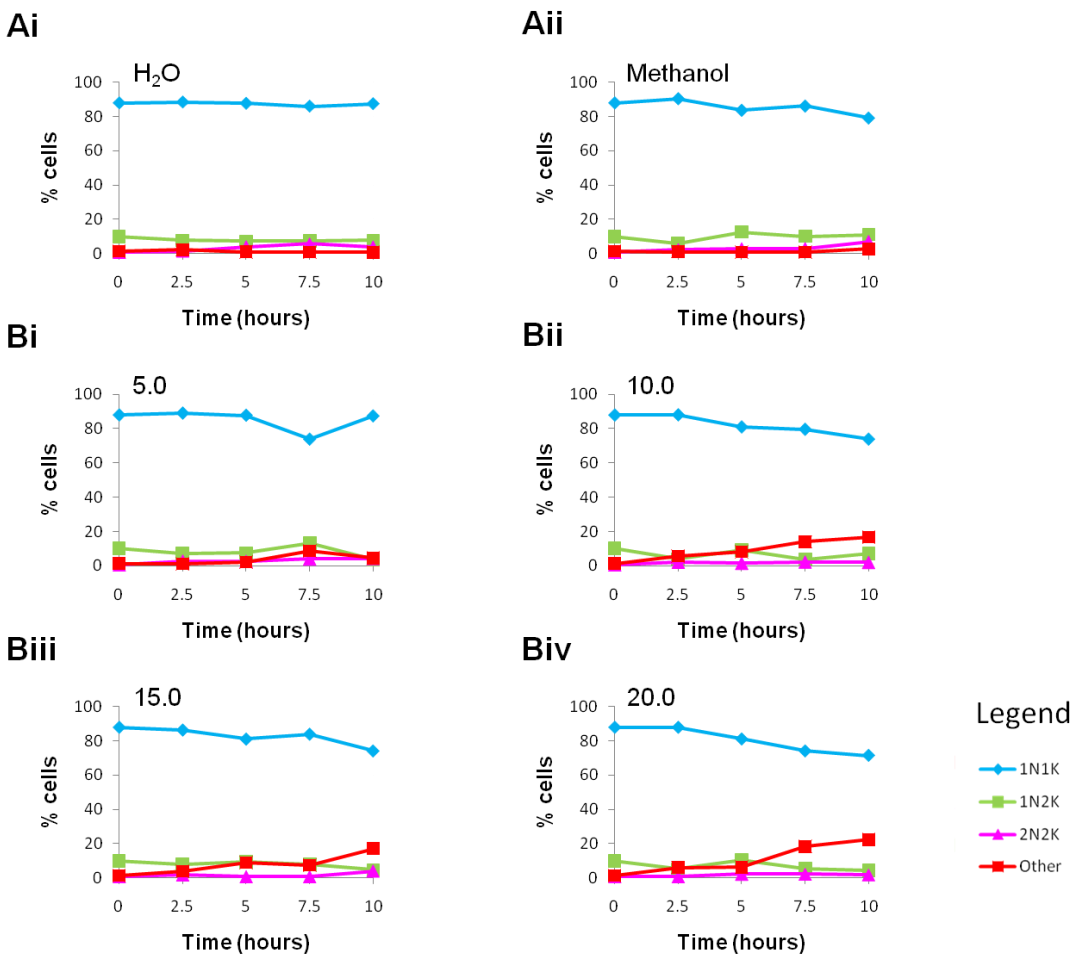

Figure 6-16 -DAPI staining of vinblastine-treated procyclic form cells.
Procyclic form cells treated with vinblastine (at the concentrations (μM) indicated in Bi-iv), or equivalent volumes of sterile water (Ai) or methanol solvent (Aii) were sampled at the time points indicated, stained with DAPI and classified according to the number of nuclei (N) and kinetoplasts (K) in each cell (*n*>200).

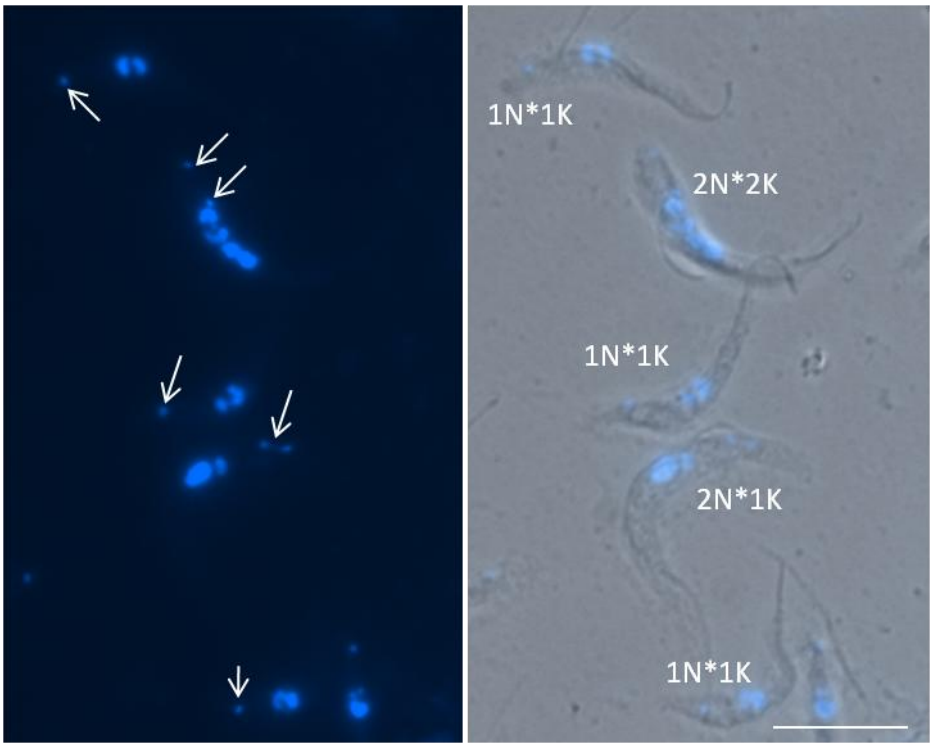

Figure 6-17 –Abnormal cell types observed following treatment of procyclic form cells with vinblastine.
Example images of DAPI-stained procyclic form parasites treated with 5-20 µM vinblastine. Abnormal cells displaying nuclear segregation (N*) defects are shown. Kinetoplasts (K) are indicated by arrows. Left panel: DAPI; right panel: DAPI/DIC merge. Scale bar: 10 µm.

Vinblastine treatment of procyclic form parasites therefore appeared to cause inhibition of nuclear segregation, although the nature of this segregation defect was not investigated in detail. Vinblastine also affected cell morphology at later time points, which may be due to non-specific effects.

6.6 Conclusions

Microtubule inhibitors universally inhibited the growth of *T. brucei* parasites to varying extents. The degree of growth inhibition was associated with the concentration of inhibitor and was also dependent on life cycle stage. Bloodstream form parasites were more susceptible to all of these inhibitors, as inferred from the lethal effect of taxol and vinblastine and severe growth inhibition induced by vincristine treatment that was observed at lower concentrations of the drugs compared to procyclic parasites.

Both procyclic and bloodstream form parasites exhibited cytokinesis defects following treatment with the microtubule stabilising agent taxol. In both life cycle stages, an accumulation of 2N2K cells was observed, although in

bloodstream form cells, inhibition of cytokinesis rapidly led to the accumulation of multinucleate cells. This phenotype is usually associated with the absence or over-riding of a cytokinesis checkpoint, which would ordinarily inhibit organelle re-replication. Procyclic form cells also underwent re-replication of organelles, but appeared to do so less readily. This may reflect the fact that procyclic parasites were able to undergo furrow ingression, albeit inaccurately. The rapid inhibition of cytokinesis in both life cycle stages is highly indicative that this phenotype represents a direct effect on the processes involved in cytokinesis initiation, and one intriguing possibility is that the taxol binding pocket on microtubules could be the site for interaction with MAPs associated with signalling pathways that regulate cytokinesis.

Treatment of bloodstream form cells with either vinca alkaloid produced similar phenotypes at similar concentrations and resulted in a dramatic effect on cytokinesis leading to an accumulation of post-mitotic cells, a large proportion of which had initiated furrow ingression but were apparently stalled before completing cell division. Qualitatively, these cells appeared to be inhibited at a similar stage of furrow ingression, which could imply that there are cytokinesis specific checkpoints that monitor furrow ingression.

In contrast, vincristine and vinblastine caused differing effects on procyclic form parasites, whereby vincristine appeared to be far more toxic. This may be due to the slight difference in the molecular composition of vincristine, which could have increased the potency of this compound relative to vinblastine against procyclic form parasites. This suggests the molecular target(s) of the drugs is different according to parasite life cycle stage, which could, for example, be explained by post-translational modifications of tubulin. This is not without precedence, since vinca alkaloids are known to exhibit differences in their levels of toxicity for neoplastic cells according to the specific neoplasma being treated (Hait et al., 2007). It was difficult to determine whether any effect on cytokinesis occurred in procyclic form cells treated with vincristine as they quickly developed severe problems with nuclear and structural integrity implying that the drug had multiple targets and was generally very toxic to these parasites. Procyclic form cells treated with vinblastine to some extent displayed problems with organelle segregation; however, they also went on to exhibit similar severe defects. The absence of an effect on cytokinesis prior to the

appearance of severely abnormal cells in procyclic parasites treated with vinblastine could add to the evidence that bloodstream form and procyclic form cells regulate cytokinesis in differerent ways. Alternatively, these differences in phenotypes may reflect the presence of stage-specific MAPs present at the vinca alkaloid binding site causing changes in the interactions of vinca alkaloids with microtubules.

The effect of these inhibitors on microtubule dynamics *in vitro* (Macrae and Gull, 1990) and the observation of morphological changes that are consistent with effects on microtubule stability, indicate that tubulin is their main target *in vivo* and, together with the evidence from other Trypanosomatid species, these data suggest that microtubule dynamics are important during cytokinesis.

6.7 Effect of alterations in microtubule dynamics on AIR9 in procyclic *T. brucei*

Given that data presented in Chapter 5 indicate that AIR9 is a MAP with key roles in cell polarity and cytokinesis, it was of interest to determine the effects of microtubule inhibitors on the localisation of AIR9. To facilitate visualisation of AIR9, 427 procyclic cells expressing tyGFP:AIR9 (Section 5.4.2) were used and were treated with taxol or vinblastine (Section 4.12) before being analysed by fluorescence microscopy (Section 4.11.1 and Figure 6-18).

Treatment of tyGFP:AIR9 427 procyclic form cells with 20 μM taxol or 40 μM vinblastine for 5 hours (equivalent to concentrations that affected microtubule dynamics *in vitro* (Macrae and Gull, 1990) seemed to strike a good balance between producing a morphological defect without also resulting in an accumulation of multinucleate cells. A morphological defect in multinucleate cells is highly likely to be a result of loss of cell polarity due to the multinucleate phenotype, rather than as a direct result of the effect of microtubule inhibitors on microtubule dynamics, and interpretation of the effect on localisation of a specific protein is subsequently open to misinterpretation. Taxol treatment of the procyclic cells, as expected from data described above (Section 6.3.2), resulted in a large accumulation of 2N2K cells undergoing abscission with aberrant cleavage furrow positioning (Figure 6-18Bi-ii). Small

numbers of 0N1K and 2N1K cells, and some cells displaying abnormal organelle positioning were also observed. In general, tyGFP:AIR9 staining appeared normal following taxol treatment (Figure 6-18Bi), although in post-mitotic cells undergoing abscission, the smaller daughter cell (typically containing just a single kinetoplast) possessed a region of brighter fluorescence intensity at the anterior tip of the cell body (Figure 6-18Bii). Cells undergoing abscission are rarely observed in procyclic form populations, and in order to draw an informed conclusion as to whether tyGFP:AIR9 is usually enriched at this region, it would be necessary to analyse more parasites at this stage of cytokinesis in untreated cells.

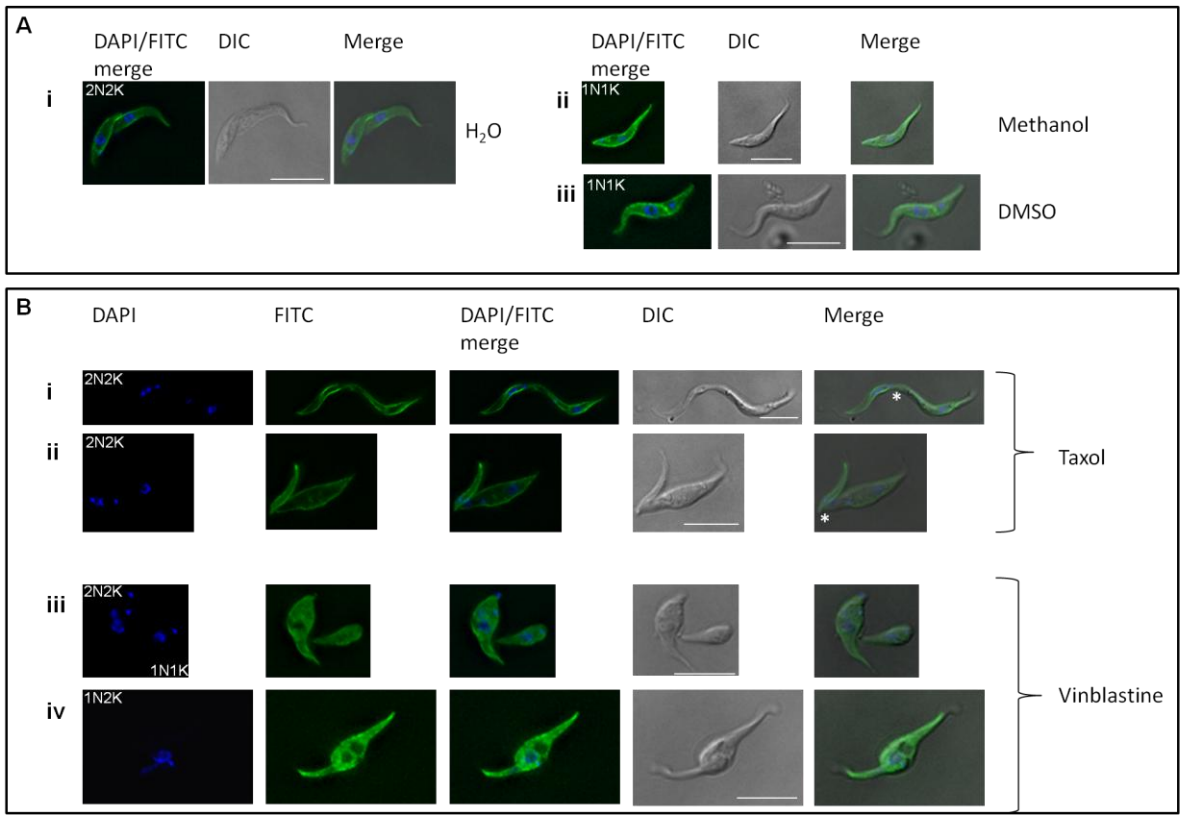

Figure 6-18 –The effect of microtubule inhibitors on the localisation of tyGFP:AIR9 in procyclic form parasites.
Procyclic form parasites expressing tyGFP:AIR9 (427 pHG172 clone 3 (section 5.4.2)) were grown in the presence of 20 µM taxol or 40 µM vinblastine (B); or equivalent volumes of solvent (DMSO and methanol, respectively), or sterile water (A) for 5 hours before being stained with DAPI and analysed by fluorescence microscopy. DAPI, FITC (tyGFP:AIR9, green), DAPI/FITC merge, DIC and DAPI/FITC/DIC ('merge') images are indicated. Nucleus (N) and kinetoplast (K) configurations for each cell are indicated, and where appropriate, the point of abscission is marked by an asterisk. Scale bars: 5 µm.

Treatment of the procyclic cells with vinblastine resulted in organelle segregation and positioning defects, as described in Section 6.5.2. The morphology of treated cells was dramatically altered, and cells developed

pointed posterior ends and became bulbous at the nuclear region (Figure 6-18Biii-iv). These parasites exhibited a bright but diffuse fluorescence, with reduced signal intensity at the cell outline implying that tyGFP:AIR9 had, to some extent, become localised to the cytoplasm (although this was not verified by other means). The binding site for vinblastine sulphate is thought to be conserved in *T. brucei* ß-tubulin (due to the presence of an asparagine residue at position 100, and evidence from *in vitro* studies (Gull, 1999)), and hence, the apparent change in tyGFP:AIR9 localisation following vinblastine treatment could indicate that tyGFP:AIR9 (or a binding partner) and vinblastine sulphate bind to the same region of microtubules.

6.7.1 Conclusions

Taxol and vinblastine sulphate treatment caused alterations in the morphology of procyclic form parasites. These morphological changes comprised a cytokinesis phenotype whereby cells displayed stalled and asymmetric abscission, which occurred following taxol treatment, and a change in cell shape comprising a bulge at the central region and elongation of anterior and posterior ends, which occurred following vincristine treatment. The distribution of tyGFP:AIR9 was altered in vinblastine-treated cells, where the staining pattern appeared to indicate a change from cytoskeletal to cytoplasmic localisation. tyGFP:AIR9 cells treated with taxol remained brightly stained, particularly at around the cell body outline, and additionally, a region of more intense staining was observed at the anterior tip of smaller anucleate daughter cell body.

These results have several implications. Firstly, vinblastine appeared to have an inhibitory effect with regards to the localisation of tyGFP:AIR9 at the perimeter of the cell, implying that the drug and AIR9 (or a binding partner of AIR9 required to localise AIR9 to microtubules) interact with tubulin at the same site. Secondly, taxol did not have this effect so it is unlikely that AIR9 (or binding partner) binds to the taxol binding pocket. Finally, the intense staining observed at the anterior end of the anucleate daughter cells following taxol treatment could imply increased microtubule stability or polymerisation at the site of furrow ingression, resulting in increased microtubule density at this part of the furrow. As the initiation of furrow ingression occurs at the tip of the posterior

most flagellum, the effect would only be noticed at the anterior of this nascent cell. The potentially increased microtubule density may have led to an increased concentration of tyGFP:AIR9 at this region.

7 The Polo-like kinase family: function, structure and regulation

7.1 Discovery of Polo-like kinases

Mitotic defects in the *Drosophila melanogaster* mutant *polo* and subsequent identification of a serine threonine kinase at the *polo* locus led to the discovery of a large family of highly conserved Polo-like kinases (PLKs) that were found to be important for many aspects of cell cycle regulation (Llamazares et al., 1991; Sunkel and Glover, 1988). Yeasts only possess one PLK (Kitada et al., 1993; Ohkura et al., 1995), mammals possess four (reviewed in (Barr et al., 2004)); *C. elegans* and *X. laevis*, three (Chase et al., 2000a; Chase et al., 2000b; Descombes and Nigg, 1998; Duncan et al., 2001); and *D. melanogaster*, two (Bettencourt-Dias et al., 2005; Sunkel and Glover, 1988). Whilst the roles of metazoan PLK family members: PLK1 (mammals), Plx1 (*X. laevis*) and polo (*D. melanogaster*); and those of the yeast PLKs: Cdc5 (*S.cerevisiae*) and Plo1 (*S. pombe*) are well studied, there is much to be discovered concerning the roles of these 'extra' PLKs including the divergent family members – SAK (also known as PLK4) and PLK4, which are found in mammals and *D. melanogaster,* respectively. SAK and PLK4 possess just a single, yet unusual, polo-box motif (Leung et al., 2002); and as yet have only one well established role, which is in centriole duplication (Bettencourt-Dias et al., 2005). Human PLK2 and PLK3 have similar structures to PLK1, and have also been shown to have cell cycle roles, although these are less well understood (reviewed in (Archambault and Glover, 2009)). This introduction will focus on human PLK1 and the yeast PLKs.

7.2 Cell cycle regulation by Polo-like kinases

Phenotypic analysis of *polo* mutant *D. melanogaster* larvae revealed mitotic defects including circular and random arrangements of chromosomes, multiple centrioles, lack of spindle asters and abnormal mitotic spindle arrangement (Sunkel and Glover, 1988), and subsequent studies involving other PLK family members revealed that the mitotic function of PLK is largely conserved. An additional role for PLK in the spatial coordination and regulation of cytokinesis

was first identified in fission yeast through the analysis of temperature sensitive Plo1p mutants (Bahler et al., 1998; Ohkura et al., 1995), and although the precise mechanisms of cytokinesis regulation vary according to organism, the outcome of PLK involvement is similar in different systems.

PLK1 has roles in mitotic entry, centrosomal separation and maturation, spindle assembly, the DNA damage response, the spindle attachment checkpoint, and mitotic exit; some of these functions are highly conserved, for example, the roles in mitotic entry and mitotic exit, which involve PLK1 homologues in other metazoans, and in yeasts (reviewed in (Archambault and Glover, 2009; Petronczki et al., 2008; Takaki et al., 2008; van Vugt and Medema, 2005)). A brief summary of how PLK1 is involved in these processes is given below.

Entry into M phase involves the cyclin-dependent kinase 1-cyclin B complex (CDK1/CYCB). The activity of this complex is affected by the phosphorylation state of CDK1, which is determined by the relative activities of the inhibitory kinases, Wee1 and MYT1, and an antagonising phosphatase CDC25. Through phosphorylation of these regulators of CDK1 activity (causing inactivation of Wee1 and MYT1, and activation of CDC25), PLK1 is involved in a positive feedback pathway culminating in mitotic entry (Inoue and Sagata, 2005; Kumagai and Dunphy, 1996; Watanabe et al., 2004). In addition, PLK1 has a role in the breakdown of the nuclear envelope, as it can phosphorylate the major component of the dynein/dynactin motor protein complex: $p150^{Glued}$, positively regulating its accumulation to the nuclear envelope during prophase (Li et al., 2010a).

Spindle pole bodies (yeast), and centrioles (mammalian cells) are important in the production of a nuclear spindle. These microtubule-organising centres (MTOCs) are the location for multiple MAPs, microtubule nucleators (including the γ-tubulin ring complex), motor proteins and other structural proteins and cell cycle regulators. Spindle generation, positioning and regulation of spindle dynamics are complex processes which require both PLK and Aurora kinase A. Recruitment and/or activation of several important nucleators and regulators has been shown to require PLK, including the γ-tubulin ring complex, the negative regulators of tubulin nucleation, Ninein-like protein and Stathmin, the microtubule stabilising factor, Centrobin (Budde et al., 2001; Casenghi et al.,

2003; Lane and Nigg, 1996; Lee et al., 2010), and Aurora kinase A (De Luca et al., 2006).

Attachment of kinetochores to microtubules is regulated by the spindle attachment checkpoint (SAC) and progression through this checkpoint is essential for the separation of sister chromatids during anaphase. Localisation of PLK to kinetochores and the contribution of PLK to these early and late mitotic processes varies according to the organism (Archambault and Glover, 2009; Lee et al., 2005). Phosphorylation of the SAC component BUBR1 by PLK1/Plx1 is important for stable attachment of kinetochores to the spindle microtubules in human cells (Elowe et al., 2007) and for the SAC in *X. laevis* respectively (Wong and Fang, 2007). Another protein regulated by PLK1 with roles in kintechore/ spindle attachment is CLIP-170; a protein which binds to dynactin, and localises to kinetochores at prometaphase. Phosphorylation of CLIP-170 by PLK1 enhances its association with casein kinase 2 (CK2), an event necessary for CK2 mediated phosphorylation and subsequent association with dynein/dynactin at the kinetochores (Li et al., 2010a). Phosphorylation of cohesin components by PLK1 is thought to cause dissociation of these components from the chromatid arms leaving only residual cohesin at the kinetochore which is later removed by separase-mediated cleavage of SCC1 as a result of APC activation (Sumara et al., 2002). In budding yeast, cohesin dissociation does not occur in early mitosis, although Cdc5 mediated phosphorylation of SCC1 is thought to promote the cleavage of this protein by separase at metaphase (Alexandru et al., 2001). Dissociation of cohesin allows chromatid separation during anaphase.

The inactivation of the CDK1-mitotic cyclin complex through degradation of the mitotic cyclins or inactivation of CDK1 is essential for mitotic exit. In mammalian cells, Cyclin B degradation is mediated by the APC, a process indirectly controlled by PLK1 through phosphorylation of the early mitotic inhibitor 1 protein (EMI1) whose role is to inhibit the APC (Hansen et al., 2004; Moshe et al., 2004). Yeasts lack EMI1-like APC inhibitors, and instead mitotic exit is regulated by the septation intiation network (fission yeast) or the mitotic exit network and FEAR pathway (budding yeast). In both cases, these kinase cascades are initiated by Plo1 and Cdc5 in fission and budding yeast respectively, and lead to the cytoplasmic retention of the phosphatase CDC14, triggering events which ultimately cause inhibition of CDK1 (Section 1.9.1.2.1).

Cytokinesis involves several complex processes: determination of the cleavage site, construction of the contractile apparatus, coordination of mitosis and cytokinesis, constriction of the contractile ring and abscission (reviewed in (Balasubramanian et al., 2004; Barr and Gruneberg, 2007; Guertin et al., 2002)).

In yeasts the cleavage site is selected early in the cell cycle. The future cleavage plane is referred to as the bud selection site or the cortical band in budding or fission yeast, respectively. Predetermination of the cleavage axis in this way constrains the localisation of the mitotic nucleus, which must be positioned accordingly, and in fission yeast, this involves trafficking one daughter nucleus through the bud neck. By contrast, the position of the cleavage site in mammalian cells is determined during the anaphase to metaphase transition when the central spindle is assembled. The contractile apparatus which is positioned at the cleavage site is largely comprised of actin and myosin forming a contractile ring. In yeasts, septin deposition occurs at either side of the actomyosin contractile ring, forming septin rings which are believed to stabilise the contractile ring and restrict spreading of the cleavage furrow. Abscission in yeasts and mammalian cells involves different processes. Septum formation involving the activity of chitin synthase is important in yeasts, whilst abscission in mammalian cells requires targeted vesicle delivery at the midbody (reviewed in (Bi, 2001; McCollum, 2005)).

In yeasts, Plo1 and Cdc5 have dual roles in cytokinesis, both as components of mitotic exit pathways, and independently. Direct roles for Plo1 and Cdc5 in cytokinesis were established through the analysis of temperature sensitive mutants which failed to septate producing a ‘chain’ phenotype which describes cells that have undergone mitosis but remain attached by a thread of cytoplasm (Bahler et al., 1998; Ohkura et al., 1995; Park et al., 2003; Tanaka et al., 2001). Also, overexpression of Plo1 or expression of PLK1 (the human homologue of Cdc5) in budding yeast resulted in prolific septation (Lee and Erikson, 1997; Ohkura et al., 1995). In mammalian cells, a separate role for PLK1 in cytokinesis has only recently been elucidated, due to the mitotic arrest caused by activation of the SAC which occurs when PLK1 is downregulated (Sumara et al., 2004), or when dominant negative versions are expressed (Seong et al., 2002). Recently, the generation and application of PLK1 inhibitors (Brennan et al., 2007; Petronczki et al., 2007; Santamaria et al., 2007), and an analogue sensitive

mutant PLK1 (Burkard et al., 2007) has allowed investigations into the post-mitotic functions of this kinase. The post-anaphase inhibition of PLK1 achieved in these studies inhibited furrow ingression, which was found to be a result of failure to construct a contractile ring. The recruitment and regulation of actin and myosin to form the contractile ring requires the small GTPase RhoA, which is in turn activated by the Rho GTPase-exchange factor (GEF) Ect2. PLK1 inhibition prevented recruitment of Ect2 to the central spindle, and prevented Rho A accumulation (Brennan et al., 2007; Burkard et al., 2007; Petronczki et al., 2007; Santamaria et al., 2007), and it has been proposed that phosphorylation of Ect2 by PLK1 allows interaction of this protein with the centralspindlin complex (comprised of two Rho GTPase-activating protein (GAP) molecules and two kinesin molecules), leading to recruitment and activation of RhoA, thus linking the anaphase spindle with the cortical cleavage furrow, promoting timely furrow ingression (reviewed in (Petronczki et al., 2008).

The diverse array of cell cycle functions involving PLKs are accompanied by dynamic patterns of localisation, which vary according to the organism studied (reviewed in (Archambault and Glover, 2009)). In human cells at prophase through to metaphase, PLK1 is found at the mitotic centrosomes, centromeres, and kinetochores, and at anaphase, PLK1 is additionally located at the spindle midzone. Following telophase, PLK1 is only found at the spindle midbody. In budding yeast, Cdc5 can be found at the spindle pole bodies at all stages of the cell cycle, and additionally at the mother bud neck during mitosis and cytokinesis. In fission yeast, Plo1 appears at the spindle pole bodies at prophase through to anaphase, and can be found at the spindle during mitosis. In addition, Plo1 marks the future site of septation during anaphase.

The changes in PLK localisation facilitate interactions with different substrates according to cell cycle stage, and combined with multiple regulatory mechanisms controlling activity and substrate specificity, PLKs are able to function as versatile regulators of many cell cycle processes.

7.3 PLK structure

All PLK family members contain an N-terminal serine/threonine kinase domain and a C-terminal polo-box domain (PBD) comprised of one (PLK4 and SAK) or two polo-box motifs. The crystal structures of the polo-box domains of SAK and PLK1, and the kinase domain of PLK1 have been solved (Bandeiras et al., 2008; Cheng et al., 2003; Kothe et al., 2007; Leung et al., 2002). However, the structure of the full length kinase has yet to be elucidated. The crystal structure of the PLK1 kinase domain was obtained for both a mutant form of the kinase (T210V) which was crystallised in the presence a non hydrolyzable ATP analogue (Kothe et al., 2007), and the wild type kinase crystallised in the presence of a selective designed ankyrin repeat protein, DARPin 3H10 (Bandeiras et al., 2008) and both forms of the kinase domain resulted in the generation of largely identical crystal structures. The crystal structure of the human PLK1 kinase domain is shown in Figure 7-1.

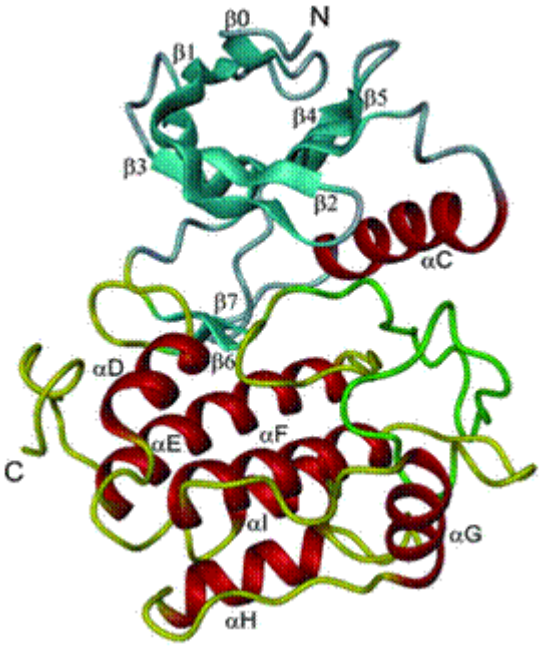

Figure 7-1 –Ribbon diagram of the kinase domain of human PLK1.
The diagram shows the crystal structure of the human PLK1 kinase domain, solved in complex with DARPin 3H10 (Bandeiras et al., 2008). The β-sheet structures are coloured cyan; α-helices, red; the activation loop, green; and the C^{α} chains of the N-terminal and C-terminal lobes are shown in grey and yellow, respectively. Adapted with permission from (Bandeiras et al., 2008).

The kinase domain was found to exhibit a classical kinase fold consisting of N- and C-terminal lobes, with an ATP binding site positioned at a cleft between these regions. The N-terminal lobe comprised an antiparallel ß-sheet and a

single α-helix, and the C-terminal lobe was found to be primarily α-helical. Kinase activation involves the rotation of the single α-helix in the N-terminal lobe, breaking the salt bridge between Lys82 and Glu101 which allows the lysine residue in the ATP binding site to interact with the phosphate of ATP in a catalytically productive manner. Other conserved residues involved in kinase activity are the DFG motif, which interacts with magnesium ions, and the activation segment (T-loop), which when inactivated, can block the ATP binding groove, an action that is reversed by phosphorylation of various T-loop residues. Intriguingly, both crystal structures implicated that the kinase domains crystallised in the active state despite the lack of detectable phosphorylation within the kinase domain (as determined by mass spectrometry (Kothe et al., 2007), and it was speculated that this active form may be the default conformation of the PLK1 kinase domain, and that auto-regulation of PLK1 activity by the PBD could override the importance for strict regulation at the level of T-loop phosphorylation.

The generation of a soluble and active kinase domain truncated protein was difficult to achieve, partly due to underestimation of the size of the core kinase domain through bioinformatic approaches. The final proteins for both structures contained an additional N-terminal ß-strand termed ß0, and a C-terminal loop which has an ordered structure. Both of these regions were essential for solubility. To purify the kinase domain proteins, either a 6XHis or GST epitope was added at the N-terminus (Bandeiras et al., 2008; Kothe et al., 2007); in both cases, a eukaryotic insect cell expression system was employed as expression in *E. coli* resulted in co-purification with the chaperone GroEL, indicating incorrect folding (Bandeiras et al., 2008).

The crystal structure of the PLK1 PBD was solved for a complex comprising the PBD and an optimal phosphopeptide binding partner (Cheng et al., 2003). The polo-box motifs in the PBD of PLK family members share only around 20-25 % sequence identity (Elia et al., 2003b), and for human PLK1 the polo box motifs share just 12 % sequence identity. Surprisingly, both motifs exhibit very similar structures comprising identical folds, each based on a six stranded ß-sheet and an α-helix (Figure 7-2). The motifs are associated by a linker region which forms an exposed loop, and tethered together by a region called the polo-box cap (PC) which wraps around the two polo-box motifs and consists of an alpha helical

segment, loop and 3_{10} helix. The two polo-box motifs are arranged such that the α-helical regions flank the twelve ß-sheets, forming a shallow positively charged grove surrounded by a hydrophobic surface. Solving the crystal structure of the PBD has greatly facilitated the understanding of how the full length PLK interacts with binding partners to control localisation and substrate recognition.

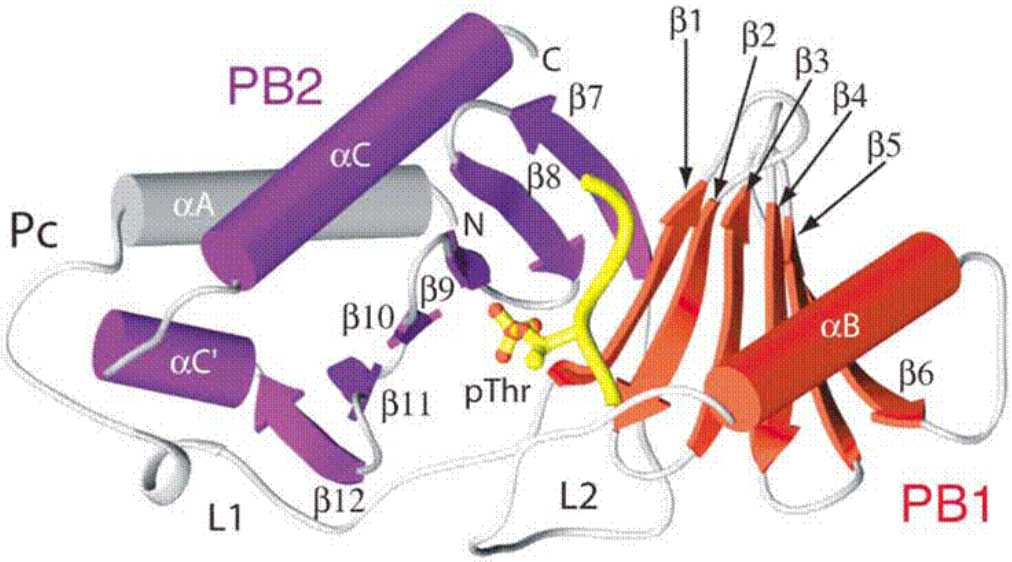

Figure 7-2 –Ribbon diagram of the Polo-box domain of human PLK1 in complex with a pThr-containing peptide.
The Polo-box motifs (PB) 1 and 2 are coloured red and purple, respectively, and the Polo-box cap (Pc) is coloured grey. The pThr-containing peptide positioned at the PBD binding cleft is shown as a ball and stick representation, coloured in yellow. Adapted with permission from (Elia et al., 2003b).

The PBD was found to be capable of binding to phosphorylated substrates independently from the kinase domain through the screening of a degenerate phosphopeptide library with an *in vitro* expression HeLa cell cDNA library (Elia et al., 2003a). The PLK clone identified in this screen encoded a protein which lacked crucial residues of the kinase domain, and the production of a series of truncated proteins revealed that the minimum binding domain comprises the whole PBD (including both of the polo-box motifs and the PC), which binds to a consensus binding motif of [Pro/Phe}-[Φ/Pro]-[Φ]-[Thr/Gln/His/Met]-Ser-[pThr/pSer]-[Pro/X], where Φ represents hydrophobic residues and X is any residue (Elia et al., 2003a; Elia et al., 2003b). Analysis of the crystal structure of the PBD in association with the phosphopeptide revealed that alternating residues from both polo-box motifs contribute to binding, forming a zipper-like interaction. The residues which interact with the negatively-charged phosphate group were referred to as the 'His-Lys pincer' (residues His538 and Lys540), and

those which form non-polar interactions with the phosphopeptide and select for Ser at the pThr-1 position included Try414 and Leu490. Selectivity for Ser at the pThr-1 position is thought to be important for targeting binding to specific substrates, and mutation of this residue to Ala within a minimal phosphopeptide abolished interaction with the PBD (Yun et al., 2009). These important residues were found to be highly conserved amongst different PLK1 proteins.

The 'His-Lys' pincer residues, and Try414 are important for *in vivo* localisation and function. Mutations of the 'His-Lys pincer' residues (Archambault et al., 2008; Elia et al., 2003b; Hanisch et al., 2006), Try414 residue (Garcia-Alvarez et al., 2007; Lee et al., 1998; Song et al., 2000), or all three conserved residues (Archambault et al., 2008; Seong et al., 2002) affected the localisation of PLK, and where the effect on cell cycle was investigated, cell cycle arrest at the spindle assembly checkpoint was reported (Elia et al., 2003b). Whilst the residues described are important for phospho-dependent localisation, other studies have shown that phospho-independent PBD-mediated interactions also contribute to localisation (Archambault et al., 2008), and even PBD-independent localisation can occur (Garcia-Alvarez et al., 2007). This suggests that PBD/binding partner interactions could be quite divergent, and not just restricted to phosphorylated proteins.

7.4 Substrates of PLK

A large number of *in vivo* phosphopeptide substrates have now been identified as binding partners of the PBD (reviewed in (Park et al., 2010), and through a screen to isolate novel binding partners, it was demonstrated that the PBD (but not a 'His-Lys pincer' mutant) was capable of binding proteins from mitotic but not G1/S cell lysates. These interacting proteins could be phosphorylated by full length PLK1 (Lowery et al., 2007), and several of these binding partners have also been shown to act as substrates for the mitotic kinase CDK1 (reviewed in (Park et al., 2010), indicating that CDK1 could prime substrates for PLK1 interaction and PLK1-mediated phosphorylation. Intriguingly, it has been suggested that whilst CDK1 phosphorylation could target PLK to binding partners at prometaphase and metaphase, CDK1 phosphorylation could also inhibit recruitment of PLK to binding partners during anaphase. This suggests that upon

anaphase entry, cyclin B degradation and decreased CDK1 activity would lead to dephosphorylation of these proteins, allowing PLK to prime its own substrates stimulating mitotic exit and cytokinesis (Neef et al., 2007). Self priming as a mechanism for binding has been demonstrated in several independent studies (Kang et al., 2006; Neef et al., 2003; Neef et al., 2007b; Wolfe et al., 2009), supporting the hypothesis that PLK binding can occur through both self and non-self priming. This mechanism for activity would allow temporal and spatial control of PLK activity and control over cell cycle events.

7.5 Regulation of PLK activity

7.5.1 Mechanisms for the activation of PLK

In addition to substrate targeting, control of PLK activity is also regulated through autophosphorylation and phosphorylation by upstream kinases. It has been demonstrated that PLK from mitotic cell extracts migrates more slowly by SDS PAGE than its interphase counterpart, and this was attributed to phosphorylation predominantly at serine but also at threonine residues (Hamanaka et al., 1995; Lee et al., 1995; Mundt et al., 1997). Mitotic PLK was more active against an α-casein substrate, and exhibited higher levels of autophosphorylation. Dephosphorylation of mitotic PLK through incubation with a protein phosphatase has been shown to reduce PLK activity to interphase levels (Hamanaka et al., 1995; Mundt et al., 1997). Phosphorylation of the T-loop of protein kinases is a common means of activation, and phosphorylation of the Thr210 residue has been observed for mitotic PLK1 *in vivo*, suggesting that this mechanism for activation may be conserved in PLK1 (Jang et al., 2002b). Mutation of the conserved Thr210 (or Plx1 Thr201) residue to aspartic acid to mimic phosphorylation resulted in increased activity against an α-casein substrate, and also increased autophosphorylation, whilst the opposite effect was observed when this residue was mutated to valine (Jang et al., 2002b; Lee and Erikson, 1997; Qian et al., 1999). These effects equated to a four fold increase or three fold decrease in activity against an α-casein substrate for PLK1 T210D and PLK1 T210V, respectively (Lee and Erikson, 1997). A second potential regulatory residue at the kinase domain was identified as Ser137 (Jang et al., 2002b). This residue is highly conserved and is surrounded by a similar amino

acid sequence to Thr210. Mutation of this residue to aspartic acid resulted in increased activity of PLK1 against α-casein, although a protein with the equivalent residue mutated to valine displayed a similar level of activity compared to the wild type protein. This residue was not identified as a phosphorylation site *in vivo*, and is therefore unlikely to be a target for upstream kinases, particularly given that Ser137 forms part of the hinge region connecting the N and C-terminal lobes and is at a site likely to be inaccessible to other proteins.

Several protein kinases capable of phosphorylating the Thr210 residue of the PLK T-loop have now been identified. These include members of the Ste 20-like kinase family and Aurora kinase A (Aur-A). Additionally a phosphatase has been identified which can remove this phosphate group, potentially acting as an antagonist to upstream kinases (Yamashiro et al., 2008).

Xenopus polo-like kinase kinase (xPLKK1), a member of the Ste-20 kinase family, purified from mitotic *X. laevis* oocytes was found to phosphorylate Plx1 at Thr201, causing activation (Qian et al., 1998). In addition, xPLKK1 was found to display similar kinetics of activation to Plx1 during the cell cycle. Other homologues of xPLKK1 have been identified including murine lymphocyte orientated kinase or LOK (Ellinger-Ziegelbauer et al., 2000) and its human homologue Stk10 (Walter et al., 2003), human Ste-20 like kinase or SLK (Ellinger-Ziegelbauer et al., 2000), and *Drosophila* dPLKK (Alves et al., 2006). All of these kinases have been shown to phosphorylate and activate PLK *in vitro*, and the target phosphorylation site for human SLK has been confirmed as PLK1 Thr210 (Johnson et al., 2008). The activity levels of SLK and Stk10 were found to remain relatively stable during the cell cycle in contrast to what was observed for xPLKK (Ellinger-Ziegelbauer et al., 2000; Walter et al., 2003). A direct role for the Ste 20-like family members in PLK activation has not yet been demonstrated, and for several reasons there is some speculation as to the role of these kinases *in vivo*. Firstly, murine LOK is only expressed in lymphatic tissues (although this does not apply to the human homologue), and secondly, a further study investigating the activation of Plx1 by xPLKK, reported that xPLKK phosphorylation did not occur at the Thr201 residue (equivalent to Thr210) but at Thr10, and that this phosphorylation event did not increase Plx1 activity (Kelm et al., 2002). Finally, depletion of xPLKK does not inhibit activation of

Plx1, and xPLKK1 has been shown to act as a substrate of Plx1 (Erikson et al., 2004), suggesting that xPLKK1 participates in a positive feed back loop for Plx1 activation, rather than acting as a *bona fide* upstream kinase.

Other kinases which have been shown to phosphorylate PLK *in vitro* but are unlikely to have physiological roles in activation of this kinase *in vivo* include protein kinase A and the CDK1/ CYCB complex, which phosphorylated xPLK1 residues Thre201 and Ser340 respectively (Kelm et al., 2002).

Phosphorylation of PLK1 at Thr210 by Aur-A has been found to involve interaction with an Aur-A coactivator, BORA (Macurek et al., 2008; Seki et al., 2008). Depletion of BORA or Aur-A (or chemical inhibition of Aur-A) prevented phosphorylation of PLK1 at Thr210, inhibited activation of PLK1 and led to cell cycle arrest suggesting that these two proteins could act in the same pathway. The observations that Aur-A activation preceded activation of PLK1 during the cell cycle, and that the temporal localisation of both proteins at the centrosomes coincided with the detection of Thr210 phosphorylation of PLK1, suggested that AUR-A acts upstream of PLK1. BORA could interact with non-phosphorylated PLK1 through association with both the kinase domain and PBD, and this interaction greatly stimulated Aur-A-mediated phosphorylation of the PLK1 Thr210 residue. Neither Aur-A nor BORA could stimulate PLK1 activity alone. Whilst this would suggest that PLK1, BORA and Aur-A interact as a complex, an association of Aur-A and BORA could not be demonstrated when these kinases were expressed at endogenous levels, suggesting that prior association of PLK1 with BORA is required for Aur-A activity against PLK1. Crucially, phosphorylated PLK1 was not further activated by Aur-A, and expression of PLK T210D partially compensated for the cell cycle arrest caused by Aur-A downregulation, implying that phosphorylation at Thr210 by Aur-A is sufficient for PLK1 activation.

Together these studies provided substantial and physiological evidence sufficient to construct a model for PLK1 activation, whereby during G2, interaction of PLK1 with BORA prevents PLK1 from targeting other substrates, until Aur-A becomes activated and localised to the centrosomes during the G2/M transition. Interaction of active Aur-A with the PLK1/BORA complex leads to phosphorylation and activation of PLK1, and upon degradation of BORA (which is

targeted for degradation at mitosis) activated PLK1 is released and able to localise to and target other substrates.

7.5.2 Autoinhibition by the PBD as an important mechanism for PLK regulation

A further mechanism for PLK regulation involves interaction of the kinase domain with the PBD. The PBD of PLK1 has been found to interact with the full length kinase (which was not a consequence of dimerisation, as no association of wild type PLK1 could be demonstrated), and this association was shown to be independent of the 'His-Lys pincer', suggesting that interaction between the PBD and the kinase domain involves a different association from the interaction of the PBD and its binding partners (Elia et al., 2003b; Jang et al., 2002a).

Association of the PBD with PLK1 inhibited activity of this protein against α-casein. This effect was exacerbated for a truncated form of PLK1 which lacked the PBD. This effect was not due to competitive inhibition as the PBD was not a substrate for PLK1 (Jang et al., 2002a). In addition, the activities of truncated forms of Cdc5 and PLK1 lacking the PBD were shown to be between 3 and 5 times greater than those demonstrated by the full length kinases (Jang et al., 2002a; Lee and Erikson, 1997). These data suggested that PLK can self regulate activity through an inhibitory *trans* interaction between the PBD and the kinase domain. Experiments which showed that autoinhibition of full length PLK1 could be relieved by the provision of an optimal phosphopeptide motif (which binds to the PBD truncation with a greater affinity than the full length protein), implied that self regulation inhibits kinase activity in the absence of a suitable substrate (Elia et al., 2003b). It was also found that autoinhibition only occurs in the absence of activation, as incubation of the PBD with mitotically-activated PLK1, or with a truncated PLK1 containing the T210D mutation, failed to inhibit the activity of these proteins (Jang et al., 2002a).

7.5.3 Models for PLK activity

The activation of PLK has been explained by self and non self-priming models, and the activity of the activated kinase domain can involve processive or

distributive mechanisms (Figure 7-3). These models are not mutually exclusive, and it is likely that a combination of different mechanisms occur *in vivo*. Self and non-self priming describe the phosphorylation of a target substrate allowing interaction of the PBD with the phosphoepitope and relieving autoinhibition of the kinase domain. Self priming defines PLK mediated phosphorylation of its own target substrate (Lee et al., 2008). This could be a means of recruiting PLK to specific regions of the cell, for instance, phosphorylation of centrosomal or central spindle proteins by a partially active PLK would stimulate the activity of bound PLK, creating more docking sites, which would lead to increased PLK recruitment. This model necessitates that PLK recruitment is controlled by the levels of PLK and/or availability of the binding partner. Non-self priming describes the generation of a PLK docking site through the action of another kinase, for example the CDK1/CYCB complex. This mechanism would allow regulation of PLK binding through phosphorylation of the substrate (and activation of the kinase responsible), rather than substrate availability. The processive and distributive phosphorylation models describe how PLK could target substrates (Lowery et al., 2004). In the first model, the PBD binding partner and the substrate would be one and the same, linking spatial and temporal regulation of kinase activity. In the second model, the binding partner would bring PLK to the vicinity of a separate protein which could be associated in a complex with this binding partner. This mechanism of activity could potentially lead to phosphorylation of different substrates or timely phosphorylation of substrate (s) without requiring a change in binding partner.

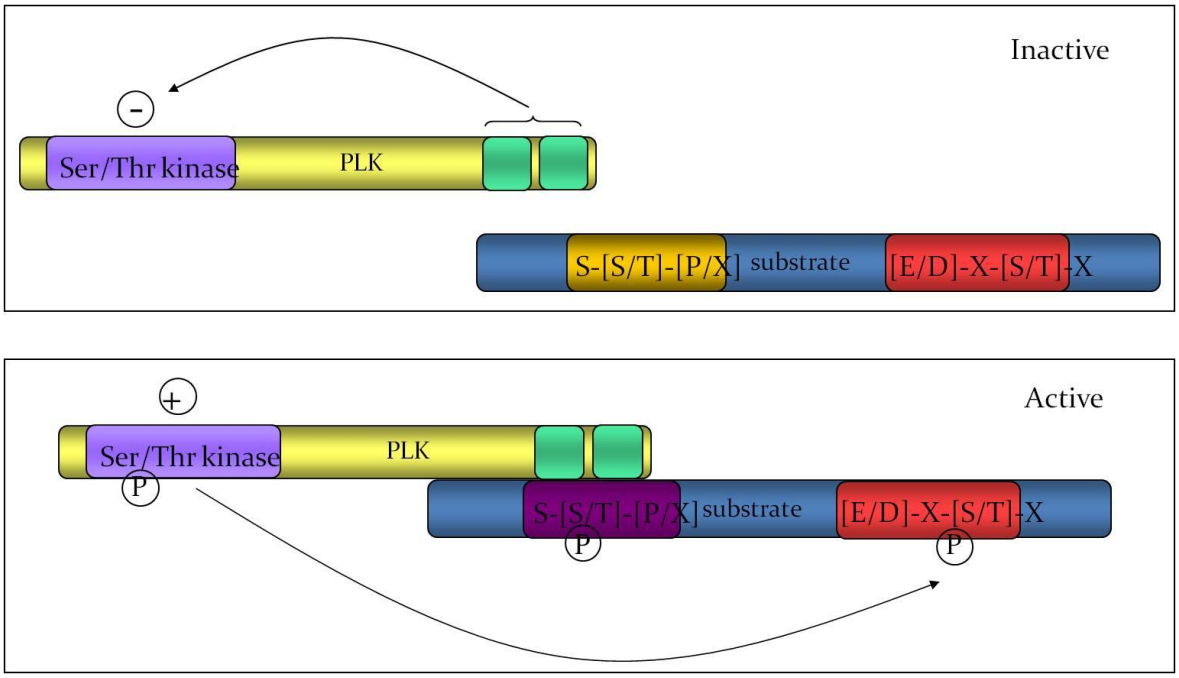

Figure 7-3 –Schematic illustrating non-self priming and processive models for PLK activity. Inactive PLK is shown above, where autoinhibition by the PBD) is indicated ('-'). Active PLK is shown below ('+'), where 'P' indicates phosphorylation of the kinase domain either as a result of autophosphorylation, or phosphorylation by an upstream kinase. The PBD is shown here binding to a consensus phospho-epitope within the target substrate (processive model) as oppose to a non-substrate protein (distributive model), where phosphorylation has occurred at the PBD binding site as a result of non-self priming by another kinase. Phosphorylation of the target substrate by PLK is indicated by the arrow and 'P'. Colours: green = polo-box; purple = kinase domain; dark purple= PBD binding site; red= target PLK phosphorylation site.

7.6 *T. brucei* PLK

T. brucei possesses a single *PLK* gene which is found on chromosome 7 (Tb07.2F2.640) and closely aligns with *S. cerevisiae* Cdc5 (Graham et al., 1998). The levels of sequence identity between Cdc5 and TbPLK were found to be 29.6 % and 54.1 % for the full length protein and kinase domain, respectively, where the kinase domain was defined as comprising residues 47-291(Graham et al., 1998). The level of sequence identity between human PLK1 and TbPLK was found to be 25 % for the full length kinase, and 47.5 % for the kinase domain, described here as comprising residues 43-297 (Kumar and Wang, 2006). TbPLK contains the conserved serine/threonine kinase active site signature at residues 160-172, and the kinase ATP binding site signature at residues 49-70; the PBD comprises two polo-box motifs at residues 564-642 and 690-756, respectively (Kumar and Wang, 2006). In addition, TbPLK was found to display a poly-asparagine insertion between the kinase domain and PBD, which was of variable length according to the *T. brucei* strain. This length polymorphism was speculated to be a result of

unequal crossing-over events or polymerase slippage (Graham et al., 1998). TbPLK was capable of complementing an *S. cerevisiae* Cdc5 mutant suggesting that this enzyme can perform the functions of a typical PLK protein (Kumar and Wang, 2006). A model of the kinase domain of TbPLK is shown in Figure 7-4, which was generated using Phyre software (http://www.sbg.bio.ic.ac.uk/~phyre/), and viewed using the molecular viewing tool Pymol.

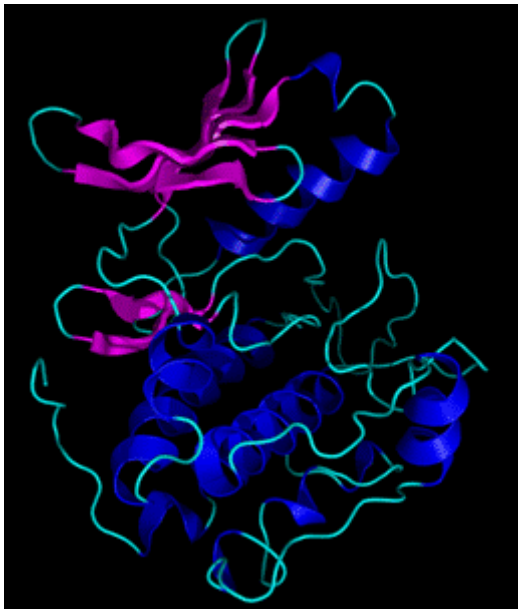

Figure 7-4 -The predicted structure for the kinase domain of *T. brucei* PLK.
The structure for the kinase domain of *T. brucei* PLK was predicted using Phyre software and viewed using Pymol. The β-sheet structures are shown in pink, and the α-helices in blue and C^{α} helices in cyan.

The localisation and functions of TbPLK have previously been investigated and are discussed in context in Section 1.9.1.2.2. Briefly, RNAi of *TbPLK* in procyclic form parasites did not affect mitosis but inhibited cytokinesis (Graffenried et al., 2008; Hammarton et al., 2007; Kumar and Wang, 2006). In addition, treatment of hydroxyurea-synchronised procyclic form cells with an inhibitor of TbPLK, or RNAi of *TbPLK* followed by synchronisation of procyclic form cells led to cell cycle arrest at cytokinesis (Li et al., 2010b). RNAi of *TbPLK* in bloodstream form parasites also inhibited cytokinesis, although in this case, initiation of furrow ingression occurred and parasites accumulated partway through cleavage; again no problems with mitosis were observed (Hammarton et al., 2007). Overexpression or depletion of *TbPLK* in procyclic form cells inhibited cytokinesis, and additionally inhibited basal body duplication, kDNA synthesis and kinetoplast segregation. RNAi of *TbPLK* in bloodstream form cells was also

found to inhibit kinetoplast segregation (Hammarton et al., 2007). RNAi of *TbPLK* in a separate study identified problems with Golgi bilobe biogenesis and Golgi duplication (Graffenried et al., 2008).

The localisation of TbPLK is dynamic and cell cycle related. Consistent with an inability to detect a mitotic function for TbPLK, no nuclear localisation has been observed, and instead TbPLK can be found at the basal bodies, Golgi bilobe and flagellum attachment zone (Graffenried et al., 2008; Kumar and Wang, 2006; Umeyama and Wang, 2008). At the flagellum attachment zone, TbPLK localises to a discrete spot which migrates along the cell coincident with extension of the FAZ, before disappearing at anaphase (Li et al., 2010c; Umeyama and Wang, 2008). The pattern for TbPLK localisation is consistent with the functional roles of this protein. Whilst TbPLK has been shown to phosphorylate Centrin 2 *in vitro* (Graffenried et al., 2008), further supporting a role for PLK in Golgi bilobe duplication (Section 2.1.2), no other physiological PLK substrates are known. The apparent lack of a mitotic role for TbPLK in *T. brucei* indicates that, despite it being able to complement Cdc5 in yeast (Kumar and Wang, 2006), this is a divergent polo-like kinase, and hence activation of TbPLK may also differ from other organisms. Indeed, conserved residues associated with PLK regulation in other organisms are absent from TbPLK. These include the human PLK1 residues W414 and L490 (F561 and R652 in TbPLK strain TREU 927 GUTat.10.1) which are required for substrate specificity and localisation to the mitotic spindle, and also the 'His-Lys pincer' required for association with phosphorylated peptides which comprises residues H538 and K540 in human PLK1, and K712 and E714 in TbPLK (strain TREU 927 GUTat.10.1). However, it is possible that the nearby H710 and K712 may perform the same role in TbPLK (Figure 7-6). The Thr210 residue (Figure 7-5) required for activation of human PLK1 is conserved in TbPLK (Thr198) and the second putative target for upstream kinases, Ser137 is a threonine residue (Thr125) in TbPLK.

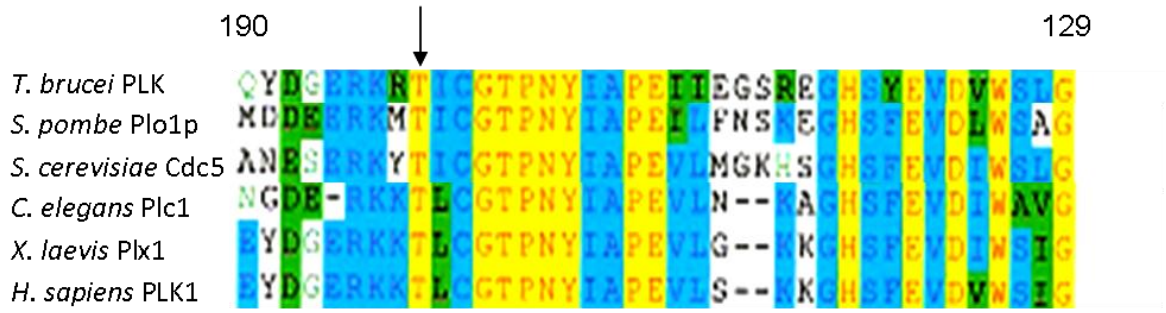

Figure 7-5 -Conservation of the T-loop residue Thr210
Alignment of PLKs from the organisms indicated was carried out using AlignX software (Invitrogen). The *T. brucei* PLK sequence is for the genome strain, TREU 927 GUTat.10.1. The conserved T-loop residue is indicated by the arrow.

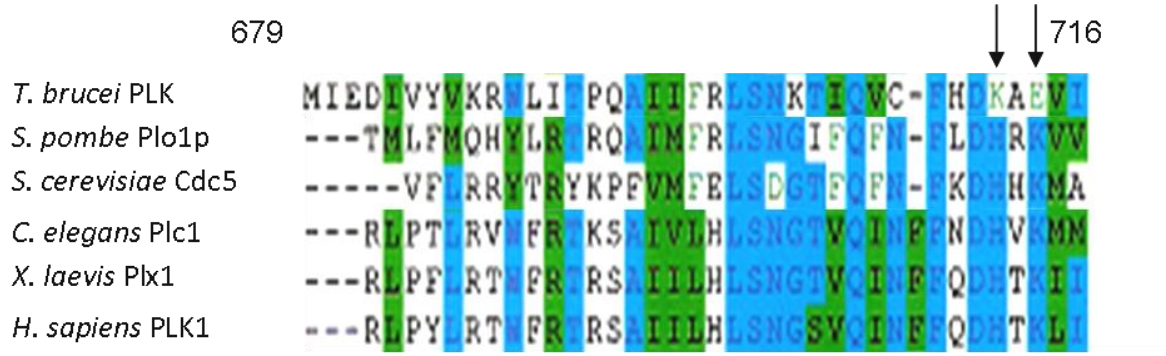

Figure 7-6 -Conservation of the 'His-Lys pincer'.
Alignment of PLKs from the organisms indicated was carried out using AlignX software (Invitrogen). The *T. brucei* PLK sequence is for the genome strain, TREU 927 GUTat.10.1. The conserved His and Lys residues are indicated by the arrows. Nearby histidine and lysine residues that could function as a potential 'His-Lys pincer' in TbPLK are shown at residues 710 and 712.

7.7 Project aims

The aim of this study was to investigate how the activity of TbPLK is regulated. Soluble, active recombinant PLK was generated, and through the use of a series of mutant/truncated PLKs, key residues required for the activity of PLK *in vitro* were determined (Section 7.8) and the role of the PBD in modulating the activity of the full length kinase investigated (Section 7.10). Based on the *in vitro* data obtained, selected mutations were also examined in an *in vivo* setting (Section 7.9).

7.8 Regulation of *in vitro* activity of recombinant *T. brucei* PLK

7.8.1 Generation of plasmids for the production of recombinant PLK proteins in E. coli

To enable the activity of recombinant PLK to be studied *in vitro*, *E. coli* expression plasmids allowing the expression and purification of full length PLK with various mutations were generated (Table 4-4). Previously it has been shown that introducing a mutation at residue N169 (N169A) abolishes the activity of PLK ((Hammarton et al., 2007). This mutation was therefore used to generate a recombinant dead kinase, which was necessary to act as a control for activity assays and other experiments. The role of the conserved T-loop residue, T198, was investigated by mutating it to either a non-polar alanine or valine residue to prevent phosphorylation at this position, or to a negatively charged aspartic acid residue to mimic the presence of a phosphate group in an attempt to generate a constitutively active kinase. A further mutant was generated to investigate the role of residues H705 and K707, which may potentially act as a 'His-Lys pincer' motif, which has been found in PLKs in other organisms to interact with phosphorylated proteins mediating substrate binding (Section 7.3). In addition to these full length mutant PLKs, plasmids allowing the expression of truncated proteins corresponding to the PBD and kinase domains (both wildtype (WT) and N169A versions) of PLK were generated in order to allow investigation of the role of the PBD in regulating the activity of the kinase domain. To facilitate purification of these PLK variants, the proteins were expressed as N-terminal glutathione-S-transferase (GST) or 6 x histidine (6XHis) fusion proteins in *E. coli* (see Figure 7-7).

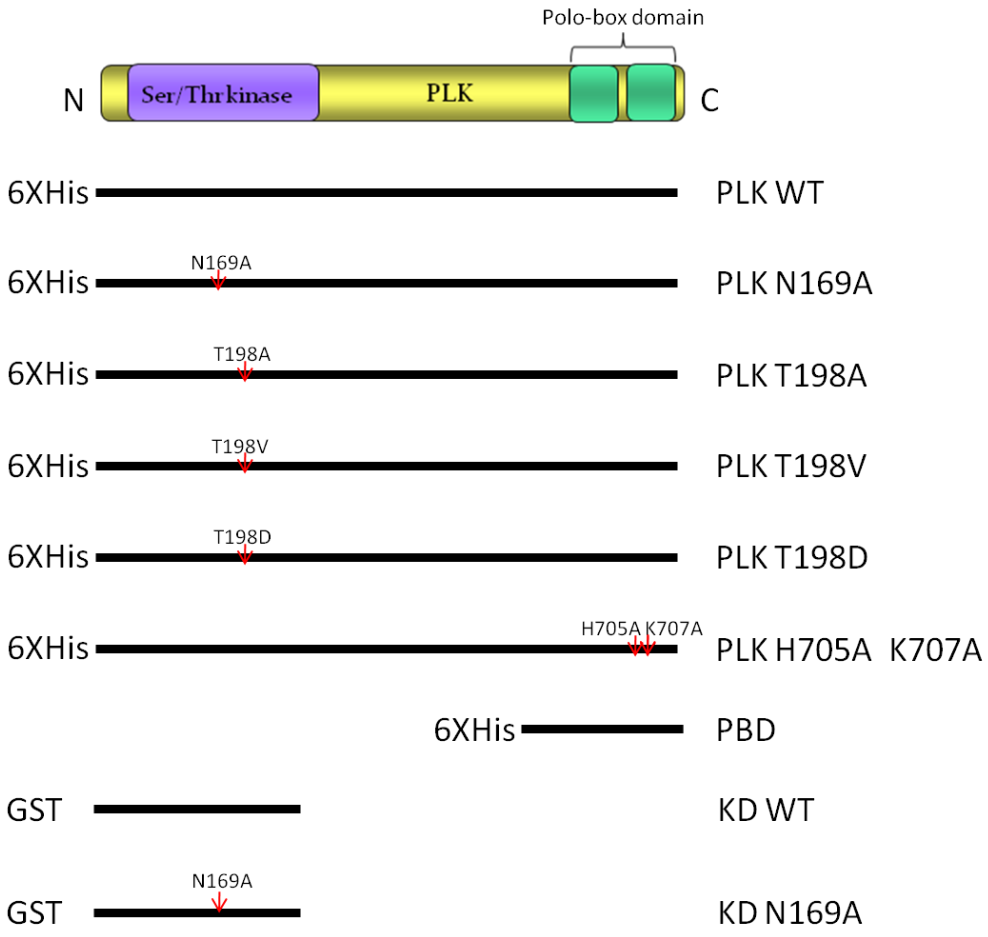

Figure 7-7 -Schematic of recombinant PLK proteins purified in this study.
The recombinant proteins generated in this study are shown with the appropriate epitope tag indicated (left).The location and nature of introduced amino acid mutations are indicated by red arrows. The PBD core with the polo-box cap (PBD) comprises residues 430-763 while the kinase domain (KD) comprises residues 2-294 of PLK. The corresponding plasmids are: PLK WT, pHG3; PLK N169A, pHG4; PLK T198A, pHG157; PLK T198V, pHG123; PLK198D, pHG163; PLK H705A K707A, pHG169; PBD, pHG148; KD WT, pGL1530; KD N169A, pGL1531 (Table 4-4).

Tetracycline-inducible *T. brucei* expression constructs for wildtype and kinase dead (N169A) PLK (pGL1278 and pGL1279, respectively) were previously generated (Hammarton et al., 2007). In order to generate His-tagged versions of wild type and kinase dead PLK, oligonucleotides OL2138 and OL2139 (incorporating the restriction sites, NheI and XhoI, respectively (Table 4-10)) were used to amplify the coding sequence for PLK WT and PLK N169A from pGL1278 or pGL1279,respectively (Section 4.5.4). The resultant PCR products were ligated into the cloning vector pCR4-TOPO (Invitrogen; Section 4.5.6) generating plasmids pGL1780 and pGL1781 (corresponding to PLK WT and PLK N169A, respectively, see Table 4-4). These plasmids were sequenced (Section 4.5.8) before the *PLK* genes were subcloned as NheI/XhoI fragments into similarly digested pET-28a(+) (Novagen) (Section 4.5.7), generating pHG3 (6XHis:PLK WT) and pHG4 (6XHis:PLK N169A) (Table 4-4). T-loop mutations to

replace T198 with alanine, valine or aspartic acid were generated by site directed mutagenesis (Section 4.5.5) using oligonucleotides PR124 and PR125 (T198A), PR126 and PR127 (T198V), or PR168 and PR169 (T198D) (Table 4-10) using pHG3 as a template. The final plasmids pHG157 (6XHis:PLK T198A), pHG123 (6XHis:PLK T198V), and pHG163 (6XHis:PLK T198D) (Table 4-4) were sequenced (Section 4.5.8) to verify the presence of the mutation and the absence of any other mutations in the *PLK* sequence.

To generate the H705A K707A mutant, oligonucleotide pairs PR170 and OL2139, and PR171 and OL2138 (Table 4-10) were used to amplify two overlapping fragments each containing the desired mutations and either the upstream or downstream region of *PLK WT*. These PCR products were purified and used as templates in a Gene SOEing PCR reaction (Section 4.5.4) with oligonucleotides OL2138 and OL2139 (containing NheI and XhoI restriction sites, respectively; Table 4-10). This PCR reaction generated full length *PLK H705A K707A,* which was ligated into pSC-B (Stratagene; Section 4.5.6) generating pHG152 (Table 4-4) and sequenced (Section 4.5.8). *PLK H705A K707A* was subcloned as a NheI and XhoI digested fragment into the same sites in pET-28a(+), generating pHG169 (Table 4-4).

To generate a truncated PLK protein comprising the PBD, oligonucleotides were designed to incorporate a region of the *PLK* gene encoding the polo-box domain with an additional N-terminal extension to account for the possibility that, like human PLK1, an alpha helix (the Polo-box cap or PBC) precedes the polo-box motifs, and acts as a tether. JPred software (http://www.compbio.dundee.ac.uk) was used to determine whether an alpha helix was predicted at this region (Kelley and Sternberg, 2009). An alpha helix was predicted with the highest possible level of confidence, comprising residues 484-502 (Figure 7-8).

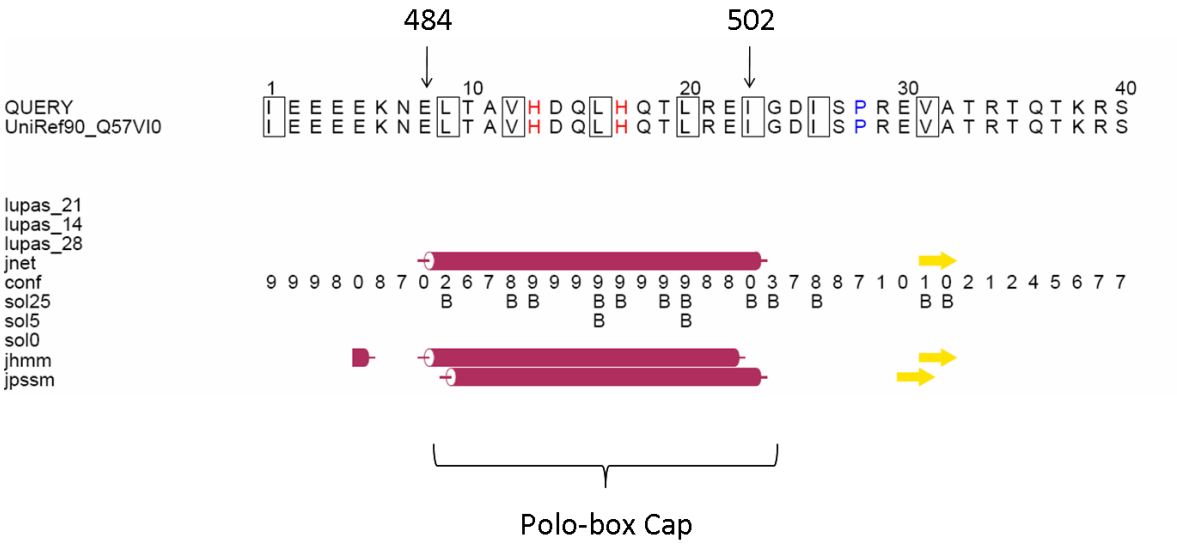

Figure 7-8 -Schematic showing the predicted Polo-box cap for *T. brucei* PLK.
The red cylinders indicate predicted alpha helices, and yellow arrows indicate predicted beta sheets. The numbers below indicate the confidence of the prediction from 0 (low confidence) to 9 (high confidence).'Sol' predictions are predicted solvent accessibility for 25 %, 5 % and 0 % cut offs (as indicated), 'B' indicates buried residues. 'Jnet' refers to the final secondary structure prediction, 'Jhmm' and 'jpssm' represent position-specific scorring matrix and hidden Markov profiles, respectively. 'Lupas' refers to the Lupas Coil prediction (window size of 14, 21 and 28). The boxes and red/blue text shown in the amino acid sequence indicate aliphatic residues, histidine residues and proline residues, respectively. The numbers and arrows at the top of the figure indicate the start and end residues of the predicted Polo-box cap.

Oligonucleotides PR172 and OL2139 (incorporating NheI and XhoI restriction sites, respectively; Table 4-10) were therefore used to PCR-amplify (Section 4.5.4) a region of *PLK* encoding amino acids 430-763, using pHG3 (Table 4-4) as template. The fragment amplified incorporated the PBD and upstream PBC and also some of the conserved sequence downstream from the poly-asparagine insertion (located at the central region). The PCR product was ligated into pSC-B (Section 4.5.6) producing pHG148 (Table 4-4) and sequenced (Section 4.5.8), before the *PLK* fragment was subcloned (Section 4.5.7) as an NheI/XhoI fragment into the same sites of pET-28a(+), generating pHG153 (Table 4-4).

Kinase domain truncations were generated using oligonucleotides OL2142 and OL2141 (incorporating BamHI and XhoI restriction sites, respectively; Table 4-10) to PCR-amplify a *PLK* fragment corresponding to amino acid residues 2-294 (comprising the kinase domain core, plus three extra amino acids downstream from the predicted kinase domain described in (Graham et al., 1998). In order to generate both an active and a dead version of the kinase domain (KD), plasmids pGL1278 (WT) or pGL1279 (N169A) were used as templates in the PCR reactions. The PCR products were ligated into pCR-4 TOPO (Invitrogen; Section 4.5.6)

generating plasmids pGL1525 and pGL1526 (corresponding to the KD WT and KD N169A, respectively; Table 4-4) which were sequenced (Section 4.5.8) and subcloned (Section 4.5.7) into BamHI/XhoI digested pGEX5X1 (GE Healthcare) to generate the plasmids pGL1530 and pGL1531 corresponding to GST:KD WT and GST:KD N169A, respectively (Table 4-4).

7.8.2 Purification of recombinant proteins

The expression plasmids for each of the PLK variants described above were transformed into BL21 (DE3) pLysS *E.coli* cells (Promega) to allow expression and purification of the recombinant proteins. To optimize expression (Section 4.6.4.1), transformed *E. coli* were grown at different temperatures for varying periods in the presence of different concentrations of Isopropyl ß-D-1-thiogalactopyranoside (IPTG). Samples were prepared at appropriate time points and analysed by PAGE (Section 4.6.1) in conjunction with Coomassie Blue staining (Section 4.6.2) and/or Western blotting with anti-His or anti-GST antibodies (Section 4.6.3), where appropriate, to identify conditions leading to expression of each recombinant protein. Optimal conditions were established for each of the recombinant proteins (growth at 15^{o}C for 16 hrs in the presence of 1 mM IPTG for full length PLK proteins and PBD protein; growth at 20^{o}C for 20 hrs in the presence of 0.5 mM IPTG for the kinase domain truncated proteins). Recombinant proteins were purified via affinity chromatography as appropriate for the purification tag (Section 4.6.4.2), and yields were typically 10-50 mg per 200 ml of *E. coli* cells (Figure 7-9, Figure 7-10, Figure 7-11 and Figure 7-12).

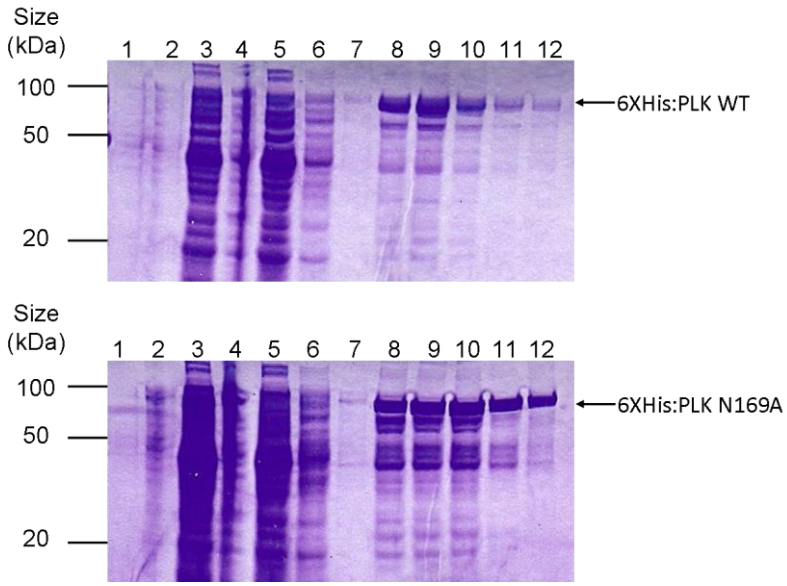

Figure 7-9 -Coomassie-stained SDS-PAGE gels of 6XHis:PLK WT and 6XHis:PLK N169A purifications.
Purified recombinant 6XHis:PLK proteins (predicted size 88 kDa) are indicated by the arrows. Lanes 1 and 2: uninduced and induced *E. coli* whole cell lysates, respectively; lanes 3 and 4: soluble and insoluble fractions of *E. coli* cell lysates, respectively; lane 5: flow through; lanes 6- 7: washes 1-2; lanes 8-11: elutions 1-4; lane 12: nickel beads following elution. Protein loading relative to the cleared lysate corresponds to the ratios: 1:25 (lanes 1-2), 1:1 (lanes 3-7), and 1:8 (lanes 8-12). The inaccurate loading of whole cell lysate fractions was due to high sample viscosity.

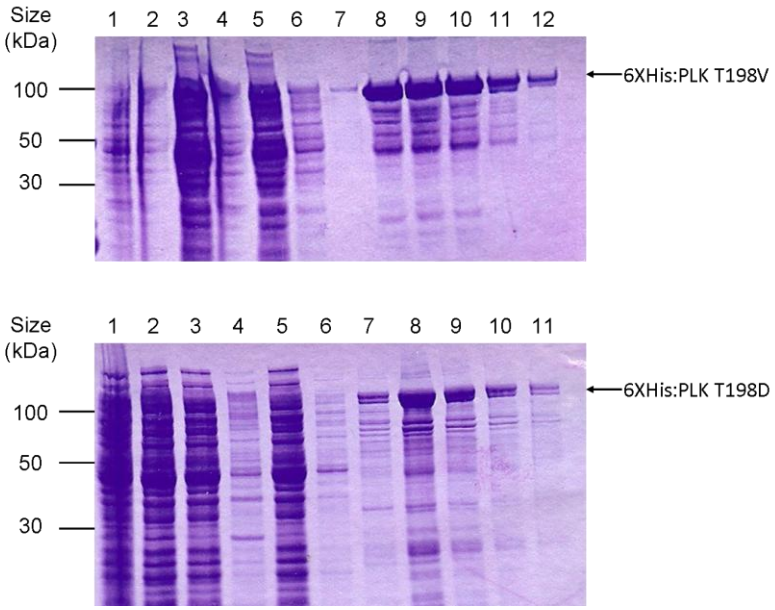

Figure 7-10 -Coomassie stained SDS PAGE gels of 6XHis:PLK T198A and 6XHis:PLK T198D purifications.
Purified recombinant 6XHis:PLK proteins (predicted size 88 kDa) are indicated by the arrows. Lanes 1 and 2: uninduced and induced *E. coli* whole cell lysates, respectively; lanes 3 and 4: soluble and insoluble fractions of *E. coli* cell lysates, respectively, lane 5: flow through; lanes 6-7 (upper gel) and lane 6 (lower gel): washes 1-2 for 6XHisPLK T198V or pooled washes 1-2 for 6XHis:PLK T198D, respectively; lanes 8-11 (upper gel) or 7-10 (lower gel): elutions 1-4 for 6XHisPLK T198V and 6XHis:PLK T198D, respectively; lane 12 (uppder gel) or 11 (lower gel): nickel beads following elution for 6XHisPLK T198V and 6XHis:PLK T198D, respectively. Protein loading relative to the cleared lysate corresponds to the ratios:

1:25 (lanes 1-2), 1:1 (lanes 3-7), and 1:8 (lanes 8-12). The inaccurate loading of whole cell lysate fractions was due to high sample viscosity.

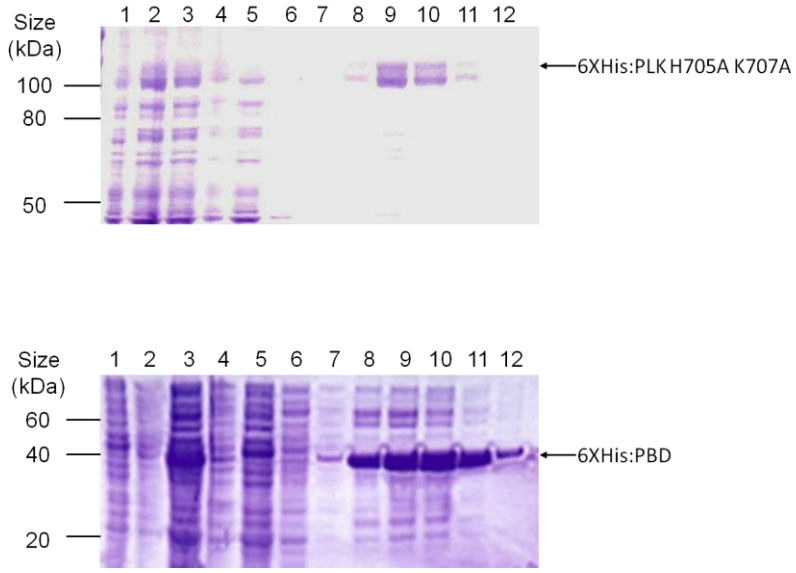

Figure 7-11 -Coomassie stained SDS PAGE gels of 6XHisPLK H705A K707A and 6XHis:PBD purifications.
Purified recombinant 6XHisPLK proteins (predicted size 88 and 39 kDa, respectively) are indicated by the arrows. Lanes 1 and 2: uninduced and induced *E. coli* whole cell lysates, respectively; lanes 3 and 4: soluble and insoluble fractions of *E. coli* cell lysates, respectively; lane 5: flow through; lanes 6-7: washes 1-2; lanes 8-11: elutions 1-4; lane 12: nickel beads following elution. Protein loading relative to the cleared lysate corresponds to the ratios: 1:25 (lanes 1-2), 1:1 (lanes 3-7), and 1:8 (lanes 8-12). The inaccurate loading of whole cell lysate fractions was due to high sample viscosity.

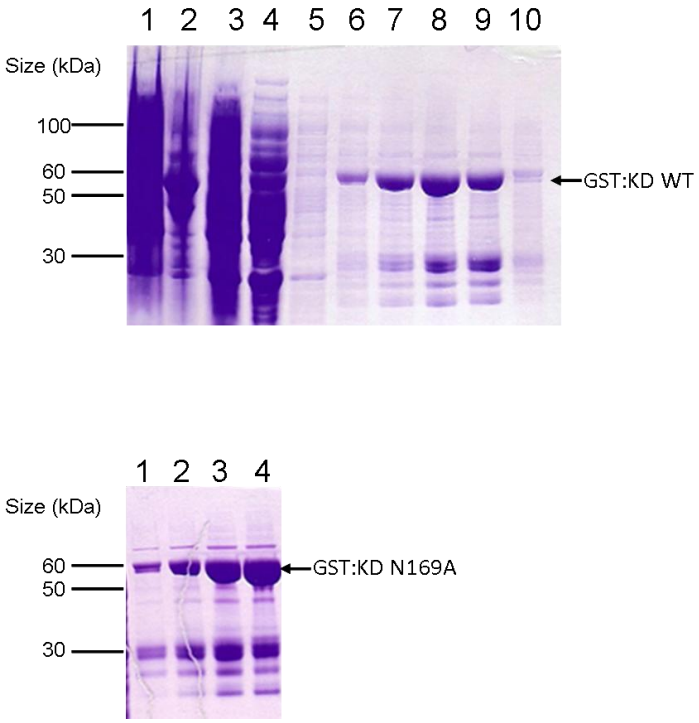

Figure 7-12 -Coomassie stained SDS PAGE gels of GST:KD WT purification and elution fractions of purified GST:KD N169A.

Purified recombinant GST:PLK proteins (predicted size 60 kDa) are indicated by the arrows. Top gel (purification of GST:KD WT): lane 1:induced *E. coli* whole cell lysate; lanes 2 and 3: insoluble and soluble fractions of *E. coli* cell lysates, respectively; lane 4: flow through; lane 5: pooled wash fractions (washes 1-3); lanes 6-9: elutions 1-4; lane 10: glutathione-sepharose beads following elution. Protein loading relative to the original culture corresponds to the ratios: 1:10 (lane 1), 1:1 (lanes 2-4), 1:10 (lane 5) and 1:100 (lanes 6-10). Bottom gel: eluted fractions (1-4) from the purification of GST:KD N169A.

7.8.3 Assessing activity of recombinant PLK against generic kinase substrates

To investigate the activity of 6XHis:PLK WT, fresh protein was dialysed into an appropriate buffer (Section 4.6.6) and kinase assays were carried out using ^{32}P γ ATP to detect phosphorylation of substrates, and also to detect autophosphorylation (Section 4.7). 6XHis:PLK WT was active against the generic kinase substrates α-casein, histone H1 and myelin basic protein (Figure 7-13), and the preferred substrate was found to be α-casein. Autophosphorylation was also readily detected for 6XHis:PLK WT. No autophosphorylation or phosphorylation of substrates could be detected for 6XHisPLK: N169A.

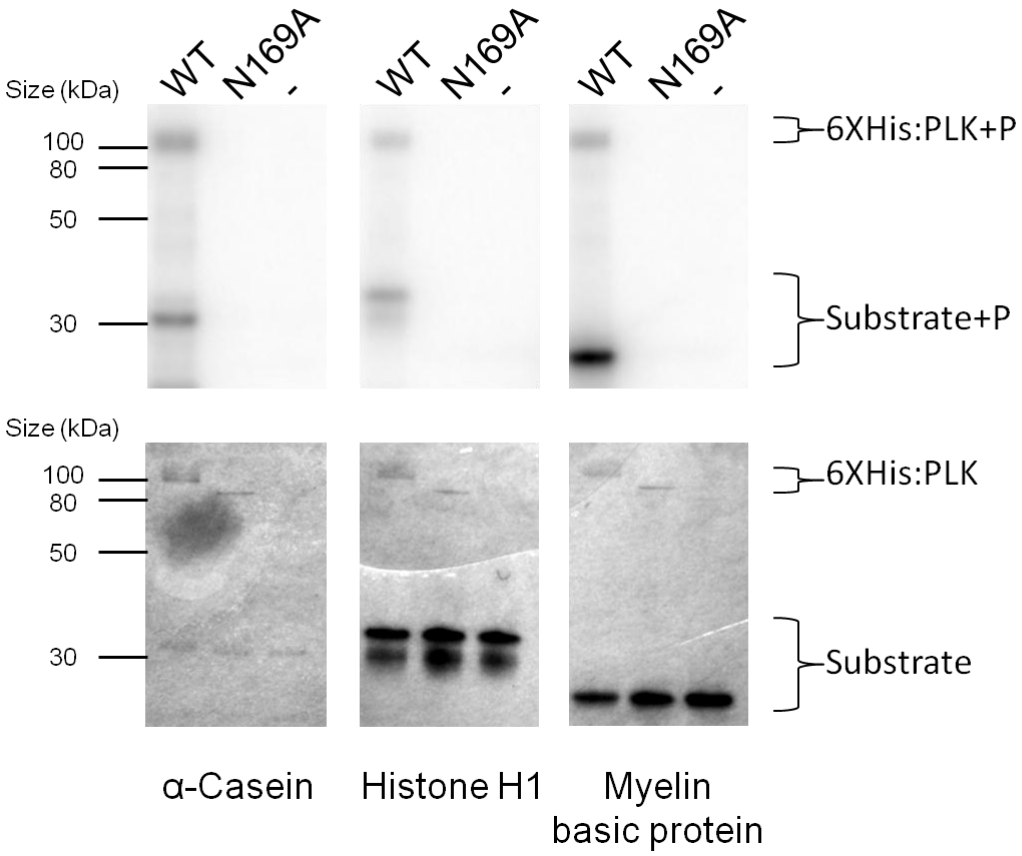

Figure 7-13 -The activity of recombinant PLK against generic kinase substrates.

6XHis:PLK WT (WT), 6XHis:PLK N169A (N169A) or a buffer control (-) were used in kinase assays to determine the activity of recombinant PLK against generic kinase substrates. Top panels: autoradiographs; bottom panels: the corresponding Coomassie gels acting as loading controls. PLK proteins (predicted size: 88 kDa), and substrates are indicated. '+P': phosphorylated proteins.

7.8.4 Autophosphorylation of recombinant 6XHis:PLK proteins

Whilst 6XHis:PLK N169A was found to migrate through an SDS PAGE gel at the predicted molecular weight of 88 kDa, migration of 6XHis:PLK WT was significantly impaired, corresponding to a molecular weight of approximately 100 kDa (Figure 7-13 and Figure 7-14). In addition, the protein appeared as a blurred band by Coomassie staining. Both of these phenomena were suggestive of protein phosphorylation.

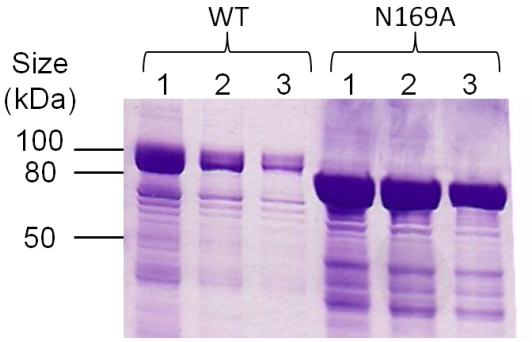

Figure 7-14 -Electrophoretic mobility of 6XHis:PLK WT and 6XHis:PLK N169A. Different elutions (1-3) from the purification of recombinant PLK proteins were prepared for SDS PAGE, and Coomassie staining to compare differences in the electrophoretic mobility of 6XHis:PLK WT and 6XHis:PLK N169A. The predicted size for both proteins was 88 kDa.

To investigate whether phosphorylation could account for the apparent differences in electrophoretic mobility of 6XHis:PLK WT and 6XHis:PLK N169A, Western blotting of these proteins with anti-phosphoserine and anti-phosphothreonine antibodies (Section 4.6.3) was carried out. 6XHis:PLK WT was found to be phosphorylated at both serine (Figure 7-15A) and threonine residues (Figure 7-15B), whilst phosphorylation of 6XHis:PLK N169A at these residues was barely detectable.

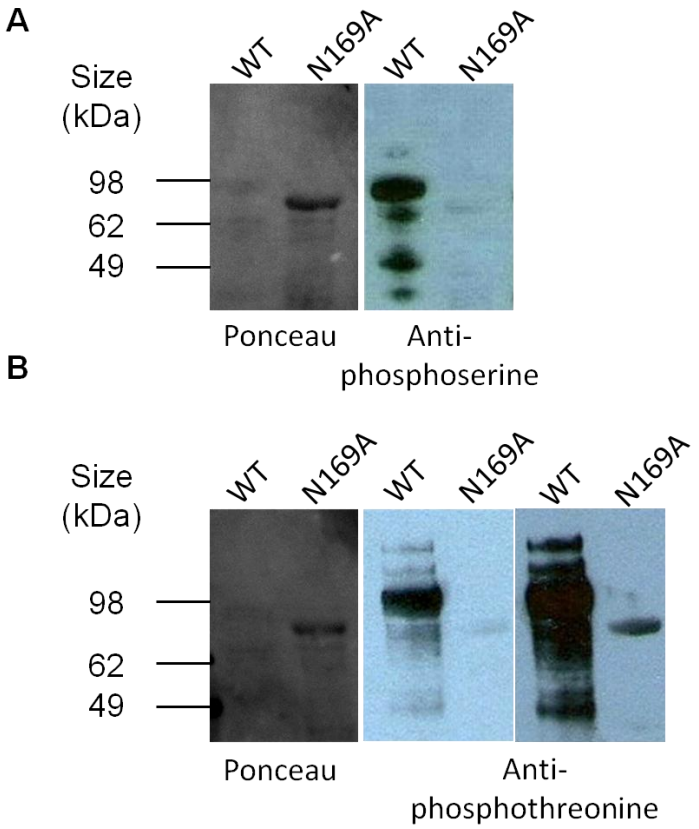

Figure 7-15 -Phosphorylation status of recombinant PLKs.
6XHis:PLK WT and 6XHis:PLK N169A were prepared for SDS PAGE and Western blotting with anti-phosphoserine (A) or anti-phosphothreonine (B) antibodies at the appropriate concentrations. The Western blot membranes were stained with Ponceau reagent to control for loading (left panels) prior to blocking and incubating with antibody. Different length exposures (shorter exposure in middle panel) are shown for the detection of anti-phosphothreonine antibody in order to show the low level of phosphorylation detected for 6XHis:PLK N169A.

In order to identify specific phosphorylated residues, these proteins were analysed by Mass Spectrometry (Section 4.6.8). No phosphorylated residues were detected for 6XHisPLK N169A through this method, while multiple phosphorylated residues were detected for 6XHis:PLK WT (Table 7-1). A number of detected phosphorylated peptides contained one phosphosite but more than one threonine or serine residue within their length, and it was not possible to determine which of the serine or threonine residues was phosphorylated ('ambiguous' phosphosites,Table 7-1). The majority of phosphorylated residues were detected within the central region of the PLK protein; however, phosphorylation sites were also found within the kinase and polo-box domains. The phosphorylation sites identified did not correspond to sites identified for *in vivo* expressed PLK where mass spectrometry analysis was performed on phosphopeptide enriched cytosolic cell lysates extracted from bloodstream form trypanosomes (five ambiguous phosphorylation sites were detected at the

central region of PLK: S457, T460, T461, T463, T464 (Nett et al., 2009)); or those residues at sites predicted to be targeted by upstream kinases (Thr198 or Thr125, equivalent to human PLK1 Thr210 and Ser137, respectively). The difference between phosphorylation sites detected in *in vivo* and *in vitro* studies may imply that phosphorylation of these sites were an *in vitro* artefact; whilst the inclusion of 6XHis:PLK N198A in these analyses should control for possible phosphorylation by *E. coli* Ser/Thr kinases (Macek et al., 2008), it is possible that 6XHis:PLK exhibits aberrant autophosphorylation in the environment of the *E. coli* cytoplasm. Alternatively, at least some of these phosphosites may be present *in vivo* but may have eluded detection. Attempts to further investigate phosphorylation sites for *in vivo* expressed PLK have to date proved unsuccessful.

Table 7-1 -Phosphorylation sites for recombinant 6XHis:PLK WT identified by mass spectrometry analysis.
6XHis:PLK WT and 6XHis:PLK N169A were analysed by mass spectrometry. This approach failed to reveal any phosphorylated residues for 6XHis:PLK N169A, although multiple residues were identified for 6XHis:PLK WT. The numbers of phosphorylation sites identified at different regions of PLK are shown above, where 'ambiguous' describes those residues identified in a trypsin digested peptide which contained more than one serine or threonine residue, and 'unambiguous' describes those residues identified in peptides with only one serine or threonine residue such that there could be no doubt as to the exact phosphorylation site.

Region	Ambiguous	Unambiguous
N-terminus	S28, T29	
Kinase domain		S88, S91, T107
Centre	T304, T305, T308, T309, S313, S314, S382, T383, S396, S402, T507, T509, T511	S338, S357, S361, T484, T493, S501
Polo-box 1	S628, S630, S641, S644	
Loop		S649, T651
Polo-box 2	S713, S714, S716, T720, T722, T725, S732, S734, S735, T738	T687, S755

7.8.5 The role of autophosphorylation in PLK activity

7.8.5.1 Dephosphorylation of recombinant 6XHis:PLK proteins

To investigate whether the observed phosphorylation of PLK could be reversed, dephosphorylation of 6XHis:PLK WT was carried out using the enzyme lambda protein phosphatase (λPPase) (Section 4.8). Analysis of λPPase treated 6XHis:PLK WT by SDS PAGE revealed that both the impaired migration through an SDS PAGE gel, and the blurred appearance of Coomassie stained 6XHis:PLK were abolished following 45 minutes of treatment (Figure 7-16A). A comparison of 6XHis:PLK WT and 6XHis:PLK N169A treated with λPPase for 1 hour revealed that this change in migration by SDS PAGE was only observed for the WT PLK protein (Figure 7-16B), and that the electrophoretic mobilities of 6XHisPLK:WT and 6XHis:PLK N169A after this incubation were identical. This evidence suggested 6XHis:PLK WT, which is able to autophosphorylate, but not 6XHis:PLK N169A, the kinase dead mutant, exhibits prolific autophosphorylation at serine and threonine residues. This autophosphorylation was responsible for the impaired migration through SDS PAGE gels, and blurred appearance of the 6XHis:PLK WT band by Coomassie staining, since these phenomena could be reversed through treatment with λPPase.

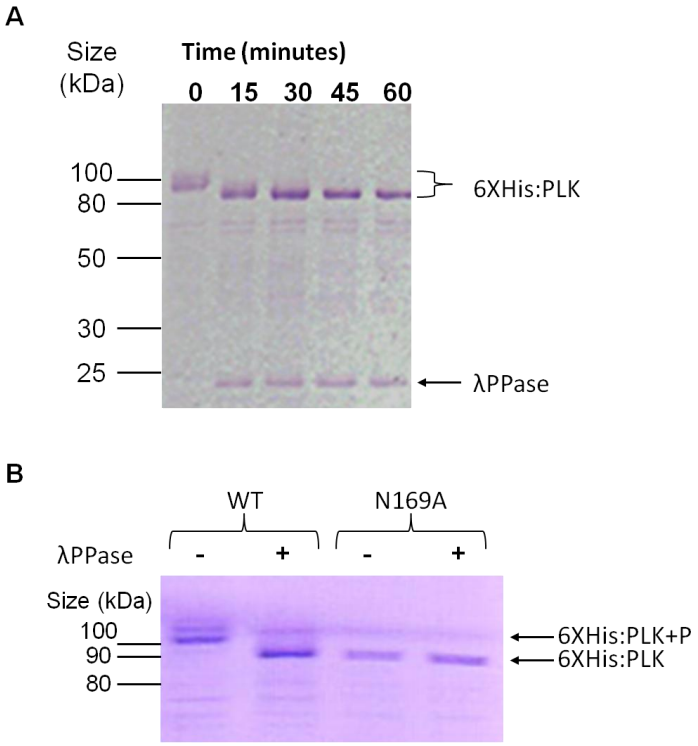

Figure 7-16 -Lambda protein phosphatase (λPPase) treatment of recombinant PLK.

A: Coomassie-stained SDS PAGE gel of a time course of λPPase treatment of 6XHis:PLK WT . Time points are indicated. B: Coomassie-stained SDS PAGE gel comparing the effect of λPPase treatment on 6XHis:PLK WT (WT) and 6XHis:PLK N169A (N169A).

7.8.5.2 Activity of dephosphorylated recombinant 6XHis:PLK

In order to investigate the effect of autophosphorylation on activity, 6XHis:PLK WT bound to nickel beads (Section 4.6.4.2.1) was treated with lambda protein phosphatase (λPPase) (Section 4.8) before being extensively washed (to remove the λPPase), and eluted as a dephosphorylated protein (Section 4.8.1). To assess the efficiency of the λPPase treatment, samples from the purification were prepared for SDS PAGE (Section 4.6.1) and Western blotting with an anti-phosphothreonine antibody (Section 4.6.3). Phosphorylation at threonine residues for untreated, but not treated 6XHis:PLK WT, was detected, implying that λPPase treatment had been efficient (Figure 7-17). The eluted proteins were filtered by centrifugation using filtration device with a 50 kDa cut off (Section 4.8.1) to further remove any remaining λPPase.

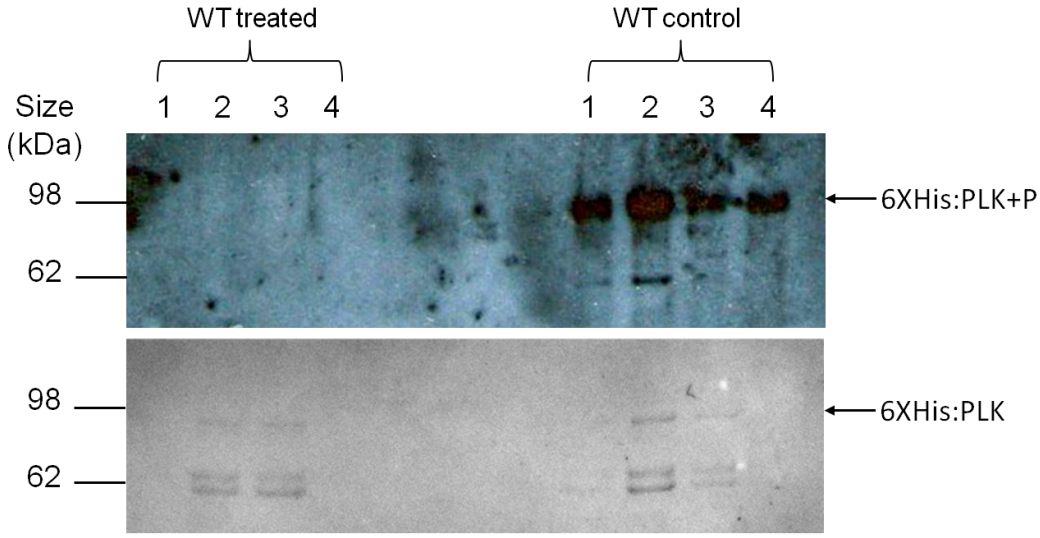

Figure 7-17 -Purification of Lambda protein phosphatase (λPPase) treated 6XHis:PLK WT. 6XHis:PLK WT immobilised on nickel beads was treated with λPPase prior to elution and preparation of eluate samples for SDS PAGE and Western blotting with anti-phosphothreonine antibody. Phosphothreonine residues were detected in control but not treated samples (top panel). To control for loading of treated and untreated proteins, the Western blot was incubated with Ponceau reagent (bottom panel).

Kinase assays (Section 4.7) using equal molar amounts (Section 4.6.5) of treated and untreated 6XHis:PLK WT (Section 4.8.1) were carried out, and to investigate whether autophosphorylation occurs prior to substrate phosphorylation, independent reactions were halted at 10 minute intervals during a 30 minute assay (Figure 7-18). Both treated and untreated 6XHis:PLK WT displayed

increasing activity towards an α-casein substrate over time; however, the activity of treated 6XHis:PLK WT was dramatically impaired. Autophosphorylation of untreated 6XHis:PLK WT was readily detectable, and this increased over time. Autophosphorylation of treated 6XHis:PLK WT was just detectable at 30 minutes post-incubation with ^{32}P γ ATP, implying that autophosphorylation may not be required for activity or that small, undetectable amounts of autophosphorylation are sufficient for activity. These results show that phosphorylation of 6XHis:PLK WT is important for its activity *in vitro*.

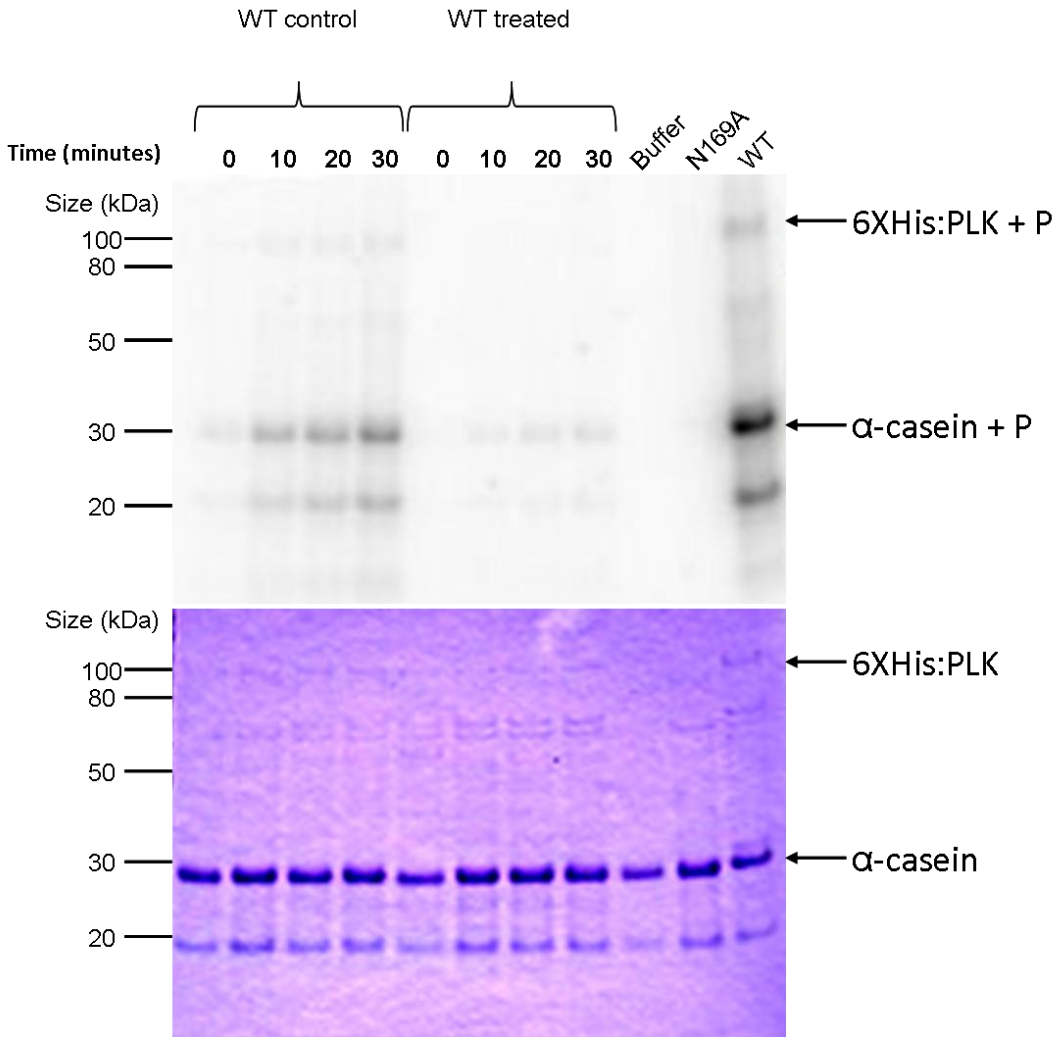

Figure 7-18 -Analysis of the importance of autophosphorylation for *in vitro* activity of PLK. The activities of λPPase treated 6XHis:PLK WT, or an untreated control (subjected to an equivalent treatment minus the λPPase enzyme) were assessed by performing kinase assays with an α-casein substrate. Four independent reactions of increasing duration (as indicated) were carried out. The positive control (6XHis:PLK WT (WT)) and negative controls (6XHis:PLK N169A (N169A) or assay buffer (buffer) are indicated. The autoradiograph (top panel) shows the detection of radiolabelled proteins, and as a loading control, the equivalent Coomassie-stained SDS PAGE gel is shown below. 6XHis:PLK proteins have a predicted size of 88 kDa.

7.8.6 Investigations into the importance of phosphorylation of T-loop residue T198 for the activity of recombinant 6XHis:PLK

7.8.6.1 Rationale

T198 is a highly conserved residue in PLK family members (Section 7.5.1), including TbPLK (Section 7.6), and is an in vivo target of upstream kinase Aur-A in humans (Section 7.5.1). The *T. brucei* Aur-A homologue, AUK1 is an important cytokinesis regulator in *T. brucei* (Section 1.9.1.1), and it is possible that these proteins are components of the same signalling pathways. Other putative upstream kinases which could target T198 include members of the Ste 20-like kinase family (TbSLK1 (Tb927.8.5730) and TbSLK2 (Tb09.211.3820) which have been identified as regulators or potential regulators of PLK in other organisms (Section 7.5.1).

Although this residue was not detected as a phosphorylation site *in vivo* (Nett et al., 2009), this does not preclude phosphorylation at T198. This study did not use synchronised cultures, which could be necessary for the detection of *in vivo* phosphorylation sites for the following reasons: firstly, PLK is expressed at S/ G2/M phases of the cell cycle (Umeyama and Wang, 2008); secondly it is possible that phosphorylation of T198 is a cell cycle specific event; finally given the observation that PLK is localised to the FAZ, it is possible that sequestration to cytoskeletal elements decreases the amount of available PLK in the cytoplasmic fraction which was used for these analyses. The latter observation concurs with my own difficulties in extracting exogenously expressed PLK from cell lysates further implying that different strategies may be required for identification of *in vivo* phosphorylation sites of PLK. Given these possibilities, it was not considered unlikely that T198 could function to regulate the activity of PLK, and mutated 6XHis:PLK T198 mutants were generated and purified as described in Section 7.8.1 and Section 7.8.2 in order to analyse the phosphorylation status and activity of 6XHis:PLK T-loop mutants T198A, T198V and T198D.

7.8.6.2 Autophosphorylation of 6XHis:PLK T-loop mutants

From analysis of Coomassie-stained SDS-PAGE gels, it was demonstrated that 6XHis:PLK WT and 6XHis:PLK T198D displayed similar electrophoretic mobility

and were present as a blurred band, indicating that 6XHis:PLK T198D, like 6XHis:PLK WT, was autophosphorylated *in vitro* (Figure 7-19). The electrophoretic mobility and appearance by Coomassie staining of 6XHis:PLK T198V was comparable to that of 6XHis:PLK N169A, indicating that autophosphorylation was absent or minimal. 6XHis:PLK T198A displayed intermediate electrophoretic mobility suggesting that mutation of the threonine T-loop residue to alanine reduced, but did not abolish, autophosphorylation (Figure 7-19).

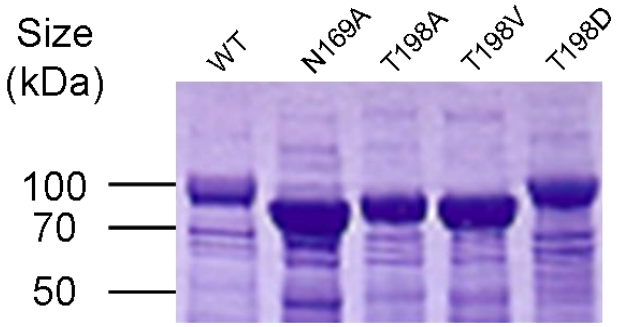

Figure 7-19 -Comparison of electophoretic mobility of 6XHis:PLK proteins. Equimolar amounts of 6XHis:PLK WT and the mutants 6XHis:PLK N169A, T198A, T198V and T198D were analysed by SDS-PAGE and Coomassie staining.

To investigate the nature of phosphorylation of the T-loop mutants, samples were prepared for SDS PAGE (Section 4.6.1) and Western blotting with anti-phosphothreonine or anti-phosphoserine antibodies (Section 4.6.3). Similar levels of phosphorylated serine and threonine residues could be detected for 6XHis:PLK WT and 6XHis:PLK T198D (Figure 7-20 and Figure 7-21). The abundance of phosphorylated threonine and serine residues detected for T-loop mutants 6XHis:PLK T198A and 6XHis:PLK T198V was much lower, although not as low as for the 6XHis:PLK N169A kinase dead mutant. These results imply that the differences in electrophoretic mobility through SDS PAGE gels are, as predicted, a consequence of different degrees of autophosphorylation.

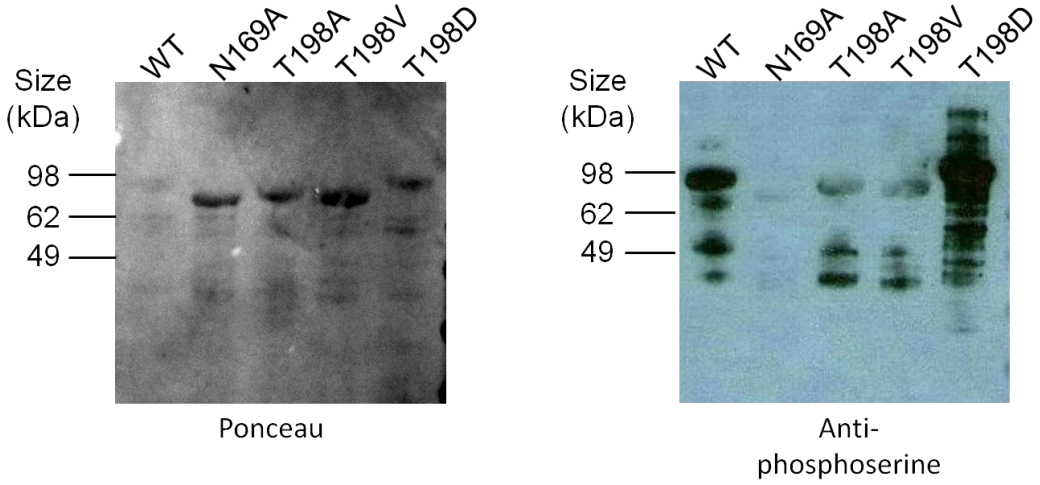

Figure 7-20 -Western blot analysis of phosphorylated serine residues in 6XHis:PLK proteins. Equivalent amounts of 6XHis:PLK WT, N169A or T198A/V/D proteins were prepared for SDS PAGE and Western blotting with anti-phosphoserine antibody (right panel). Prior to incubation with antibodies, the Western blot was stained with Ponceau reagent (left panel) to control for protein loading.

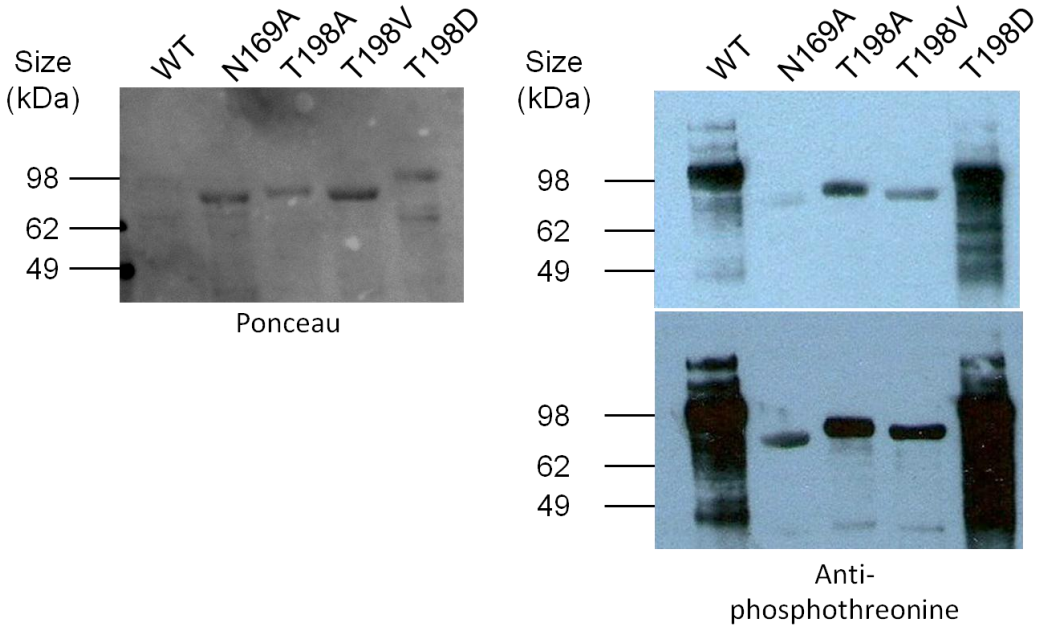

Figure 7-21 -Western blot analysis of phosphorylated threonine residues in 6XHis:PLK proteins.
Equivalent amounts of 6XHis:PLK WT, N169A or T198A/V/D proteins were prepared for SDS PAGE and Western blotting with anti-phosphothreonine antibody (right panels; top: shorter exposure; bottom: longer exposure). Prior to incubation with antibodies, the Western blot was stained with Ponceau reagent (left panel) to control for protein loading.

In order to identify specific phosphorylation sites on the T198 mutant PLK proteins, proteins were prepared for analysis by mass spectrometry (Section

4.6.8). No phosphorylation sites were detected for 6XHis:PLK T198V; however, phosphorylation sites were identified for both 6XHis:PLK T198A and 6XHis:PLK T198D, with the latter exhibiting the greatest number of detectable phosphorylated residues (Table 7-2). A comparison of the location of these phosphorylation sites (where ambiguous and unambiguous residues were analysed together) revealed that three sites were common to the WT, T198A and T198D 6XHis:PLK proteins(**Error! Reference source not found.**), and that these residues were located in the central region, between the kinase domain and first polo-box motif. There were also other residues in common between 6XHis:PLK WT and either T198A orT198V 6XHis:PLK mutants within the central region, and one phosphorylated residue was found to be common between 6XHis:PLK WT and 6XHis:PLK T198D and the second polo-box motif. The differences in detectable phosphorylation sites between the different proteins suggested that the T-loop residue T198 is important in influencing the sites of autophosphorylation.

Table 7-2 -Location of phosphorylated serine and threonine residues for recombinant PLK proteins.
The number and location of phosphorylation sites identified by mass spectrometry analysis for WT and T-loop mutated versions of 6XHis:PLK are shown below. The identification of phophorylated trypsin digested peptides containing one or more threonine or serine residue led to the classification of some phosphorylation sites as 'ambiguous', whilst when only one threonine or serine residue was present in the phosphorylated peptide residues were classified as 'unambiguous'.

	PLK WT		PLK T198A		PLK T198D	
Region	Ambiguous	Unambiguous	Ambiguous	Unambiguous	Ambiguous	Unambiguous
N-terminus	S28, T29					
Kinase domain		S88, S91, T107		S75		S75
Centre	T304, T305, T308, T309, S313, S314, S382, T383, S396, S402, T507, T509, T511	S338, S357, S361, T484, T493, S501	S382, T383, T388, S396, S402	S338, S501	T304, T305, T308, T309, S313, S314, S382, T383	S338
Polo-box 1	S628, S630, S641, S644				S628, S630	
Loop		S649, T651				
Polo-box 2	S713, S714, S716, T720, T722, T725, S732, S734, S735, T738	T687, S755		S738		S755

7.8.6.3 Activity of 6XHis:PLK T-loop mutants

To compare the relative activities of T-loop mutants with 6XHis:PLK WT, *in vitro* kinase assays were carried out (Section 4.7) using equivalent amounts (Section 4.6.5) of 6XHis:PLK proteins, and an α-casein substrate. 6XHis:PLK WT showed the highest level of activity against the substrate, which was approximately two fold (estimated) greater than the level of activity displayed by 6XHis:PLK T198D (Figure 7-22). This was unexpected, as other studies have reported increased levels of activity following substitution of the equivalent T-loop residue with aspartic acid (Section 7.5.1). Both 6XHisPLK:T198A and 6XHisPLK:T198V displayed similar and low levels of activity against the α-casein substrate (with a slightly higher level of activity displayed for 6XHis:PLK T198A), and as discussed previously (Section 7.8.3), no activity could be detected for 6XHis:PLK N169A. A reduction in PLK activity following mutation of the T-loop threonine to alanine or valine has been previously reported for mammalian PLK1 (Section 7.5.1). 6XHisPLK WT exhibited the greatest level of autophosphorylation, whilst no autophosphorylation could be detected for 6XHis:PLK N169A. 6XHis:PLK T198D exhibited slightly less autophosphorylation in comparison to 6XHis:PLK WT, whilst lower and similar levels of autophosphorylation were detected for 6XHisPLK:T198A and 6XHisPLK T198V, consistent with the data obtained by Western blotting with anti-phosphoserine/threonine antibodies (Figure 7-20 and Figure 7-21) and the abundance of phosphorylation sites detected by mass spectrometry (Table 7-2).

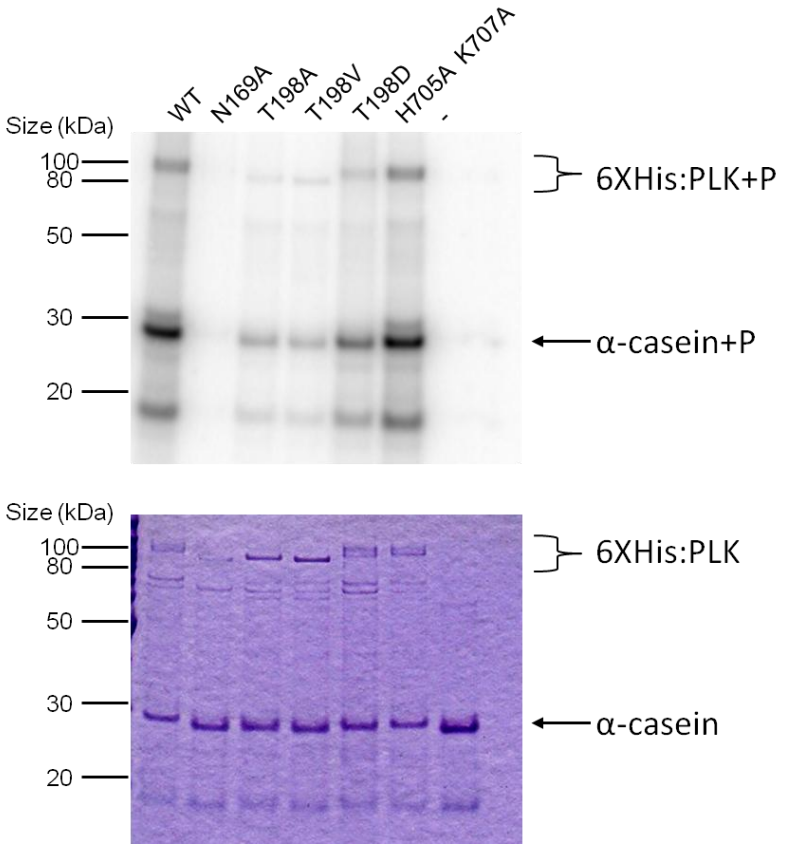

Figure 7-22 -The activities of recombinant 6XHis:PLK proteins.
The activities of equivalent amounts of WT and mutated versions of recombinant PLK proteins (as indicated at the top of the figure) were tested in a kinase assay (including a buffer control (-)) with an α-casein substrate. The autoradiograph (top panel) shows the detection of radiolabelled proteins, and to control for loading, the equivalent Coomassie-stained gel is shown (bottom panel). '+P' indicates phosphorylated proteins.

7.8.6.4 Conclusions

The studies described above demonstrate that the T-loop T198 residue is clearly important for *in vitro* activity of PLK (Figure 7-22). Interestingly, of the 42 residues identified as either putative or unambiguous phosphorylation sites for 6XHis:PLK WT, only 13 of these were common to either 6XHis:PLK T198A or 6XHis:PLK T198D, and a different pattern of autophosphorylation was detected between the T198A and T198V mutants. These sites of autophosphorylation may further contribute to the differences in activity between 6XHis recombinant proteins.

Whilst the differences in the mass spectrometry data could be attributed to variation in the detection of phosphorylated residues, it is also possible that mutations at the T-loop residue could alter the specificity of autophosphorylation. It is important to note that these data are for *in vitro* analyses; therefore, expression of T-loop-mutated PLK proteins *in vivo* was

carried out to determine whether the T-loop is important for activity under physiological conditions.

7.9 Investigation of the importance of T-loop residue T198 *in vivo*

7.9.1 Background

Since PLK is an essential enzyme in *T. brucei*, gene replacement strategies were not suitable to test the functional consequences of mutating T198 *in vivo*, and therefore an alternative strategy was required. Overexpression of ty:PLK WT in procyclic form parasites has been shown previously to inhibit basal body duplication, kDNA replication, kinetoplast segregation and cytokinesis, whilst overexpression of ty:PLK N169A produced no discernable effect on growth or cell cycle regulation over a 72 hour period (Hammarton et al., 2007). Therefore, this system was suitable for providing an *in vivo* readout of activity of the T198 PLK mutants in procyclic form parasites.

7.9.2 Generation of plasmids for inducible expression of ty:PLK with mutations at the conserved T-loop residue T198

In order to test the activity of *in vivo* expressed T198 mutants, and perform functional studies, plasmid constructs to allow the tetracycline-inducible expression of these PLK variants in *T. brucei* were generated. Previously the plasmid pGL1278 was generated (Hammarton et al., 2007) for tetracycline-inducible expression of ty:PLK in *T. brucei* cell lines which constitutively express the tetracycline repressor protein TetR (Wirtz and Clayton, 1995). To substitute the T198 residue for valine or aspartic acid, oligonucleotide pairs PR126 and PR127 or PR168 and PR169 (Table 4-10) were used for site directed mutagenesis (Section 4.5.5) of the pGL1278 plasmid and introduction of the desired T198V or T198D substitutions, respectively. This generated plasmids pHG158 (ty:PLK T198V,) and pHG164 (ty:PLK T198D) which were sequenced (Section 4.5.8) to confirm the presence of the appropriate mutations and absence of any other mutations. An additional plasmid was generated for the inducible expression of

ty:PLK T198A, although due to time constraints, clones generated from these transfections were not analysed, and this work will not be discussed.

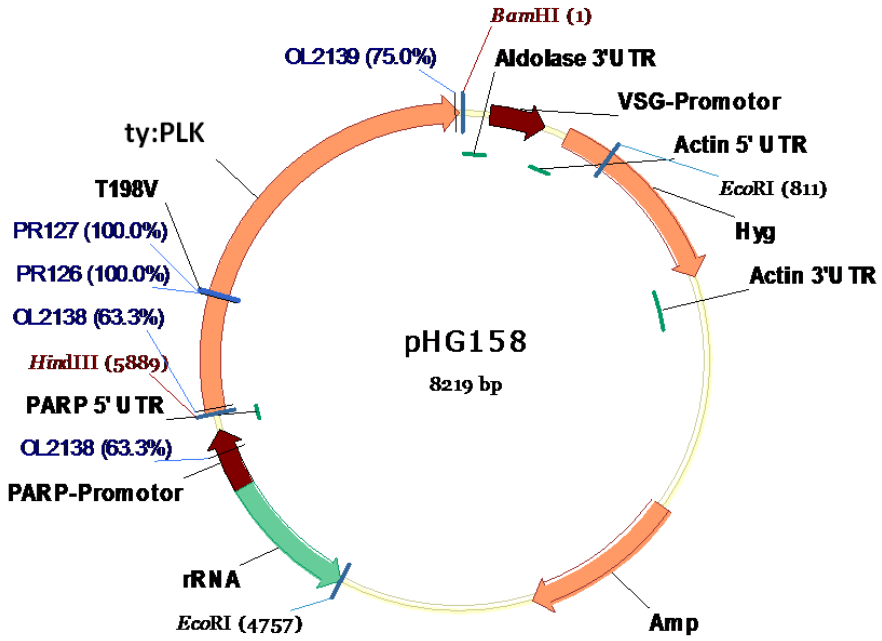

Figure 7-23 -Map of pHG158, a plasmid allowing inducible expression of ty:PLK T198V. pHG158 was generated by site directed mutagenesis of pGL1278 (Hammarton et al., 2007) using the oligonucleotides PR126 and PR127 (indicated). Note that the PARP promoter has been modified to contain two Tet operator sites to allow tetracycline-inducible expression of ty:PLK. The vector is linearised by digestion with NotI, integrates into the ribosomal RNA (rRNA) gene array, and confers hygromycin resistance.

7.9.3 Generation of cell lines for the inducible expression of ty:PLK with T-loop mutations T198V and T198D

Procyclic form 427 pHD449 parasites (Wirtz and Clayton, 1995) were transfected with NotI linearised (Section 4.3.2) pHG158 or pHG164 (Table 4-4), and clones were selected by limiting dilution in SDM79 medium supplemented with the appropriate drugs (Table 4-7). Transfection of procyclic form 427 pHD449 with pHG158 generated 18 independent clones. Twelve clones were selected for screening, and these parasites were grown for 16 hours in the presence or absence of tetracycline (1 μgml^{-1}) before cells were harvested and prepared (Section 4.2.2.2) for analysis by SDS PAGE (Section 4.6.1) and Western blotting (Section 4.6.3) with anti-TY antibody (Section 4.6.3.2). Eleven of these clones were found to express ty:PLK T198V, and clones 6 and 7 (Figure 7-24) were selected for future experiments. Transfection of procyclic form 427 pHD449 with pHG164 generated two pools and two clones, which were screened for expression of ty:PLK T198D as described for ty:PLK T198V above. All of the pools

and clones were found to express ty:PLK T198D (Figure 7-25), and clones 1 and 2 were selected for future experiments.

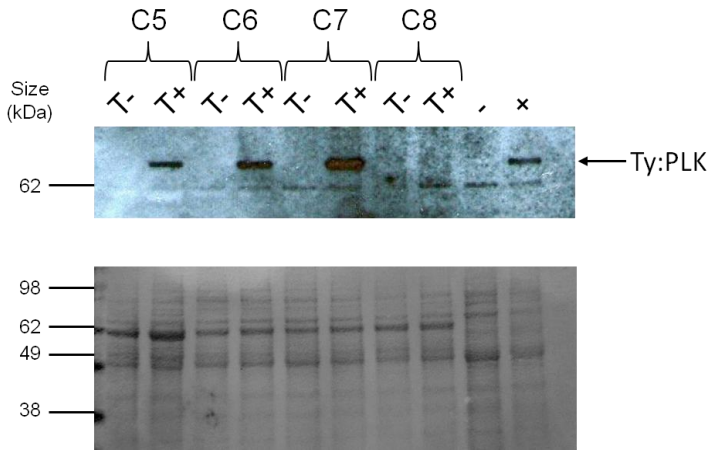

Figure 7-24 -Western blot analysis of procyclic form 427 pHD449 pHG158 clones.
427 pHD449 pHG158 clones were screened for inducible expression of ty:PLK T198V by incubating cells with or without tetracycline (T- or T+, respectively) for 16 hours prior to preparation of cell lysates for SDS PAGE and Western blotting with anti-TY antibody (top panel). C5-C8 represent lysates from clones 5-8, respectively. Procyclic 427 WT cells and procyclic 427 pHD449 pGL1278 (T+) cells acted as negative (-) and positive (+) controls, respectively. To control for loading, the Western blot was stained with Ponceau reagent prior to being incubated with antibodies (bottom panel). The predicted size for ty:PLK was 90 kDa.

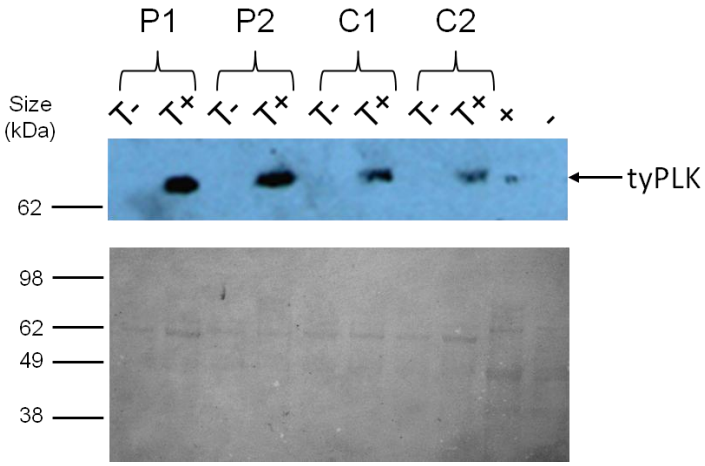

Figure 7-25 -Western blot analysis of procyclic form 427 pHD449 pHG164 clones.
427 pHD449 pHG164 clones were screened for inducible expression of ty:PLK T198D by incubating cells with or without tetracycline (T- or T+, respectively) for 16 hours prior to preparation of cell lysates for SDS PAGE and Western blotting with anti-TY antibody (top panel). P1-2 and C1-2 represent lysates from pools 1-2 and clones 1-2 respectively. Procyclic 427 WT cells and procyclic 427 pHD449 pGL1278 (T+) cells acted as negative (-) and positive (+) controls, respectively. To control for loading, the Western blot was stained with Ponceau reagent prior to being incubated with antibodies (bottom panel). The predicted size for ty:PLK was 90 kDa.

7.9.4 Comparison of inducible protein expression for cell lines expressing ty:PLK variants

In order to compare the functional consequences of overexpression of different ty:PLK variants, it was necessary to verify that equivalent levels of protein expression were induced. Cell lines expressing ty:PLK WT, tyPLK N169A, and cells from two independent clonal cell lines expressing either tyPLK:T198V or ty:PLK T198D were grown for 16 hours in the presence or absence of tetracycline (1 μgml^{-1}), before harvesting the cells and preparing cell lysates (Section 4.2.2.2). Cell lysates were analysed by SDS PAGE (Section 4.6.1) and Western blotting (Section 4.6.3) with anti-TY antibody (Section 4.6.3.2) to detect ty:PLK variants, and anti-EF1α antibody (Section 4.6.3.2) to control for loading (Figure 7-26). Whilst no ty:PLK could be detected in cell lysates obtained from uninduced parasites, equivalent levels of ty:PLK were detected for cell lysates obtained from induced cells. Interestingly, no differences in electrophoretic mobility were observed between the variants. This may indicate that phosphorylation of PLK *in vivo* involves fewer residues than *in vitro,* potentially rendering detection of these phosphorylation events by SDS PAGE impossible, or that only a small proportion of PLK is phosphorylated *in vivo*, which would not be unexpected, especially considering that asynchronous cell populations were used for this analysis.

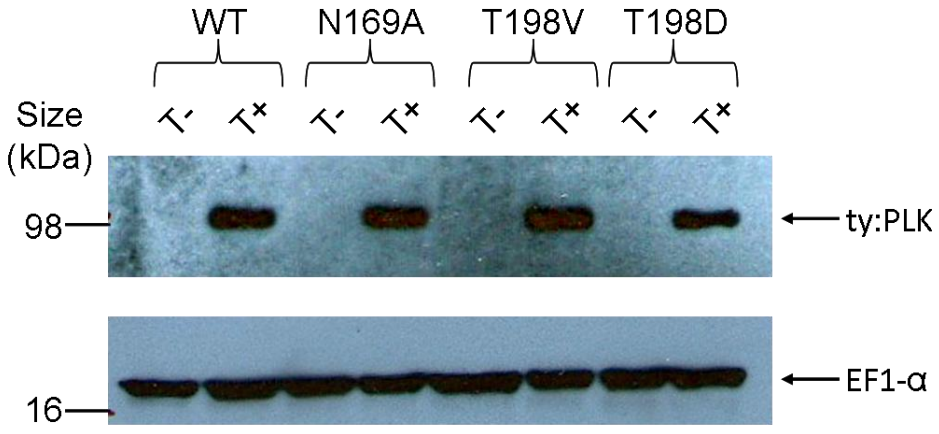

Figure 7-26 -Western blot analysis to compare expression levels of ty:PLK proteins. Expression of ty:PLK proteins was induced by the application of tetracycline (1 μgml^{-1}). Cells grown in the presence (T+) or absence (T-) of tetracycline were harvested at 16 hours post-induction. Lysates were prepared for SDS PAGE and Western blotting with anti-TY (top panel) and anti-EFI-α (bottom panel) antibodies to detect ty:PLK proteins or to act as a loading control, respectively.

7.9.5 The activity of ty:PLK variants

In order to determine whether the activity of ty:PLK proteins expressed *in vivo* was affected by mutation at T198, extracts of cells (Section 4.6.9) expressing ty:PLK variants were incubated with anti-TY antibody-conjugated beads or control beads (Section 4.6.11) and, following washing, the resulting protein/bead complexes were used to perform kinase assays with an α-casein substrate (Section 4.7). ty:PLK WT was found to exhibit the greatest level of activity against α-casein, although this was only slightly greater than the activity shown by ty:PLK T198V and ty:PLK T198D (Figure 7-27). No activity was detected for ty:PLK N169A, and in addition, it was not possible to detect autophosphorylation for any of the PLK proteins. This implied that regulation of ty:PLK activity *in vivo* does not involve phosphorylation of the Thr198 T-loop residue, and that activity is independent of phosphorylation at this site, which contrasts with what was found for the equivalent recombinant proteins expressed in *E. coli* (Section 7.8.6), and what has been found for PLK variants expressed in other organisms (Section 7.5.1); although the activity of these proteins against endogenous substrates may be quite different to what is observed with an α-casein susbtrate.

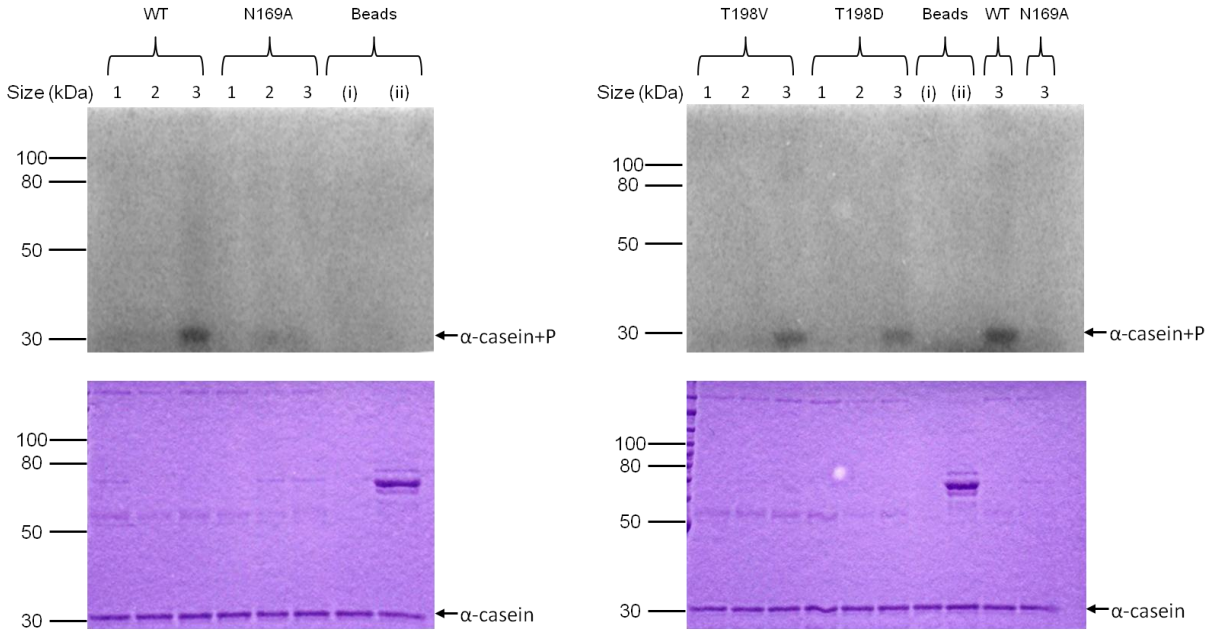

Figure 7-27 -Activity of ty:PLK proteins against an α-casein substrate.
ty;PLK proteins were immobilised on TY beads and used to perform kinase assays with an α-casein substrate. To control for the non-specific interaction of other protein kinases with TY beads, uninduced lysate controls were included in the assay, and to control for possible interactions of kinases with unconjugated beads, induced lysates were incubated with unconjugated beads. Additionally, TY beads and beads without conjugated antibody that

had not been incubated with cell lysates were included as negative controls. Lanes 1 -2: lysate controls (uninduced lysate with TY beads (1) and induced lysate with control beads (2)); lane 3: induced lysate with TY beads; lanes (i-ii) no-lysate controls (control beads and TY beads respectively). The autoradiograph shows the radiolabelled proteins that were detected (top panels), and the equivalent Coomassie-stained gels (bottom panels) are included to show equivalent loading.

7.9.6 The effect of overexpression of ty:PLK variants on T. brucei cell proliferation and DNA content

Given that kinase assays of immunoprecipitated ty:PLK WT, T198V and T198D showed them all to be active in an *in vitro* assay using the generic kinase α-casein substrate, it was of interest to investigate the functional behaviour of the T198 mutants *in vivo*. ty:PLK WT and ty:PLK N169A cell lines (Hammarton et al., 2007) and also two independent clonal ty:PLK T198V and ty:PLK T198D cell lines were grown in the presence or absence of tetracycline (1 $\mu g ml^{-1}$) for a 48 hour period (Section 4.2.2.2). To determine the proliferation of these cell lines, cell density was monitored at regular intervals (Section 4.2.2.3). Induced ty:PLK N169A cells grew normally (Figure 7-28B); however, the growth of induced ty:PLK WT cells was severely impaired (Figure 7-28A), as had been reported previously (Hammarton et al., 2007). Induced cells expressing ty:PLK T198V or ty:PLK T198D also displayed impaired growth, comprising growth inhibition but not growth arrest, over the 48 hour induction period (Figure 7-28C-D). The growth of uninduced cells was normal in all cases.

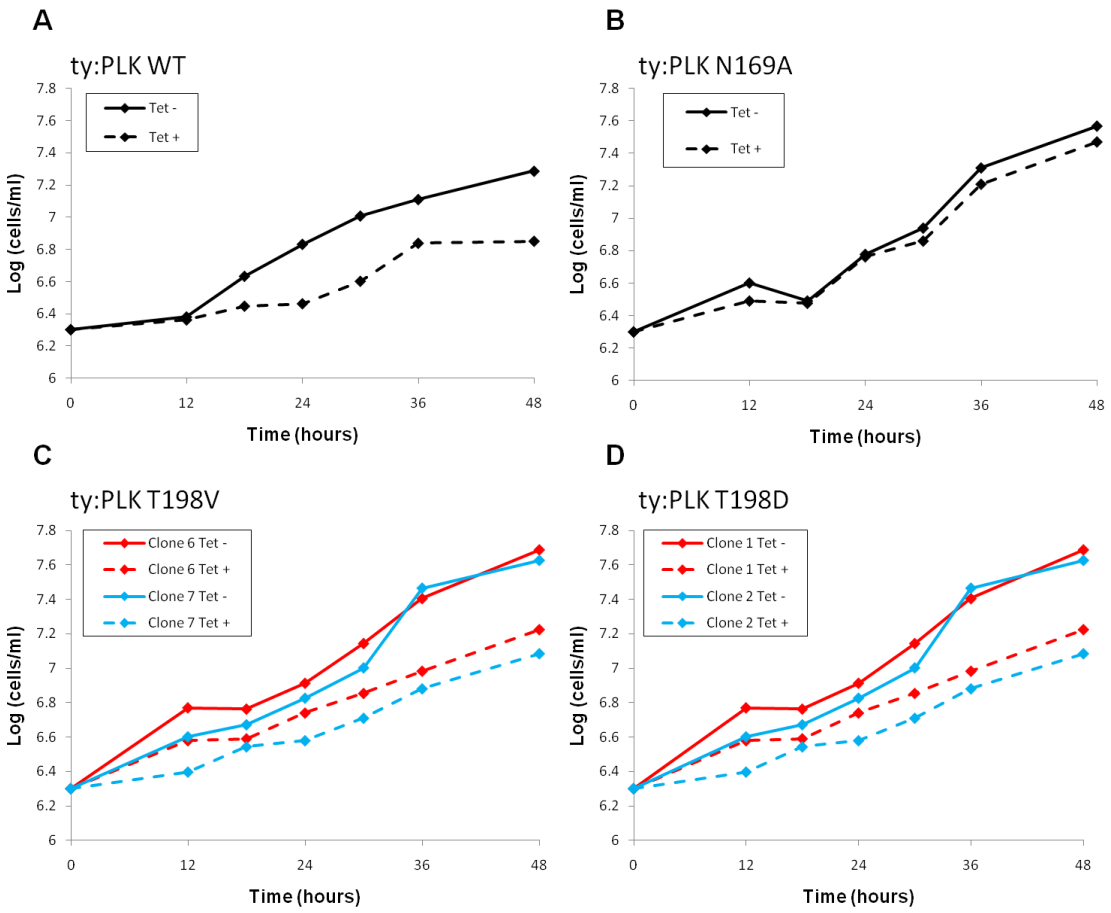

Figure 7-28 -Growth of *T. brucei* cells expressing ty:PLK proteins.
***T. brucei* ty:PLK cell lines were cultured in the presence (Tet +) or absence (Tet -) of tetracycline for 48 hours and cell density monitored at regular intervals.**

To investigate the possibility that cell cycle defects were responsible for the observed growth defects, cells were analysed by flow cytometry (Section 4.10). Uninduced and induced cells were sampled at 0 and 12 hours and thereafter at 6 hour intervals for 36 hours. Fixed cells were treated with propidium iodide to stain the DNA and the fluorescent properties of cells were analysed (Section 4.10) and compared (Figure 7-29). Prior to induction of ty:PLK expression, cells exhibited normal DNA profiles, comprising distinctive 2C and 4C peaks. Cells expressing ty:PLK N169A retained a normal DNA profile throughout the induction period (Figure 7-29B). However, for cells expressing ty:PLK WT, ty:PLK T198V, ty:PLK T198D changes in DNA profile were observed from 12 hours post-induction (Figure 7-29A, C and D respectively). The changes in DNA profile comprised a coincident decrease in the 2C peak and increase in the 4C peak, followed by the appearance of a peak corresponding to cells with >4C DNA content at 18 hours post-induction for cell lines expressing ty:PLK WT and TYPLK: T198V, and at 24 hours post-induction for cell lines expressing ty:PLK T198D. The DNA profiles for uninduced cells were normal at equivalent time points (data not shown). Both

ty:PLK T198V/D cell lines analysed exhibited very similar DNA profiles (data not shown).

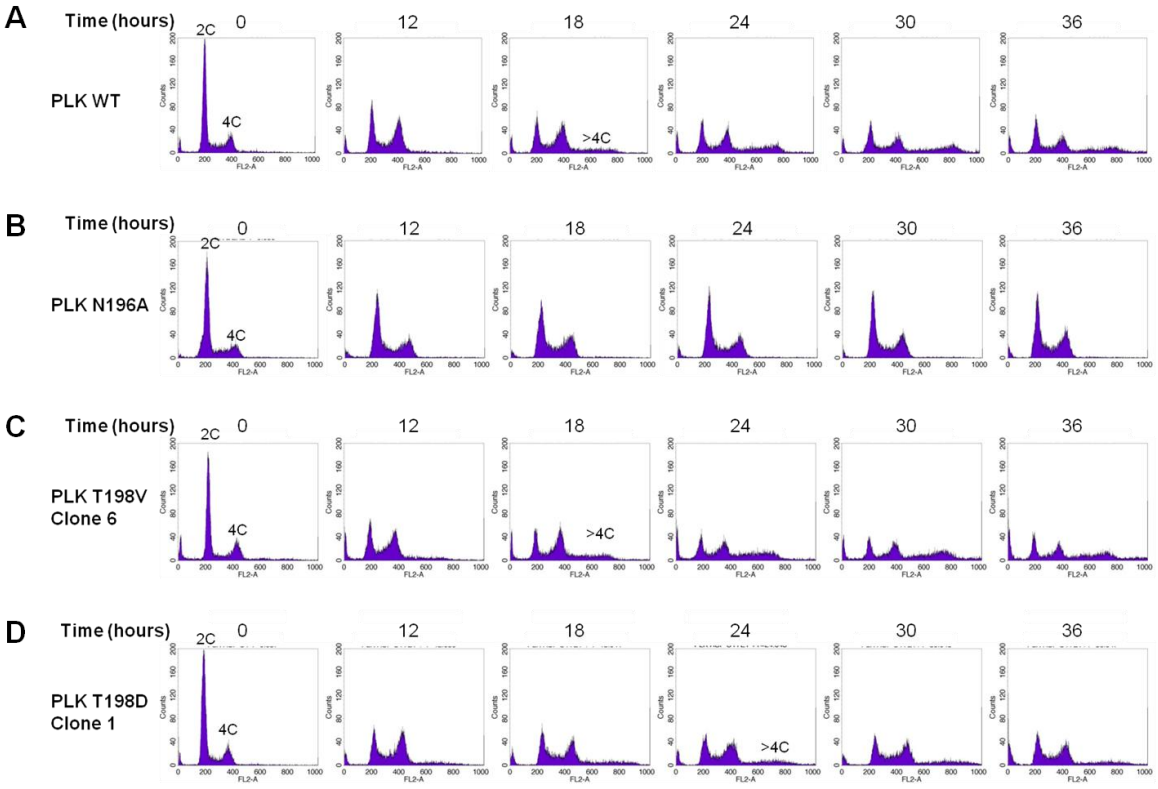

Figure 7-29 -Flow cytometry analysis of cell lines overexpressing ty:PLK variants. Cells grown in the presence of tetracycline (1 μgml^{-1}) to overexpress the ty:PLK variants indicated were sampled at regular intervals, fixed, stained with propidium iodide and analysed by flow cytometry. Histograms of frequency (counts, y-axis) against whole cell fluorescence (FL2-A, x-axis) were used to compare the effects of overexpression of different ty:PLK proteins on cell ploidy. Ploidy is indicated where appropriate. C: DNA content.

The similarity between the growth phenotypes and DNA profiles during overexpression of ty:PLK WT and ty:PLK T-loop mutants was unexpected and implied that activity of PLK *in vivo* does not involve phosphorylation at this residue.

7.9.7 The effect of overexpression of ty:PLK variants on nucleus and kinetoplast configurations

To further characterise cell cycle defects appearing following overexpression of different ty:PLK proteins, cells cultured in the presence or absence of tetracycline (1 μgml^{-1}) were sampled at 0 and 12 hours, and thereafter at 6 hour intervals, fixed and stained with DAPI for analysis by fluorescence microscopy (Section 4.11.1). Over 200 individual cells were examined at each time point. Cells were classified according to the number of kinetoplasts and nuclei

contained within them and the relative positions of these organelles. Initially the populations typically comprised 80-85 % 1N1K cells, 8 % 1N2K cells and 5 % 2N2K cells, with the rest comprising abnormal cell types (Figure 7-30). Populations of uninduced cells displayed similar proportions of these cell types throughout the experiment (data not shown). Overexpression of ty:PLK N169A had no effect on the composition of cells in the population for the duration of the induction (Figure 7-30B). However, overexpression of ty:PLK WT, ty:PLK T198V or ty:PLK T198D had similar and dramatic effects on the cell cycle (Figure 7-30A, C and D). The second clone for each of the ty:PLK T198V/D mutant cell lines displayed almost identical N-K configurations to those presented below for the first clone (data not shown).

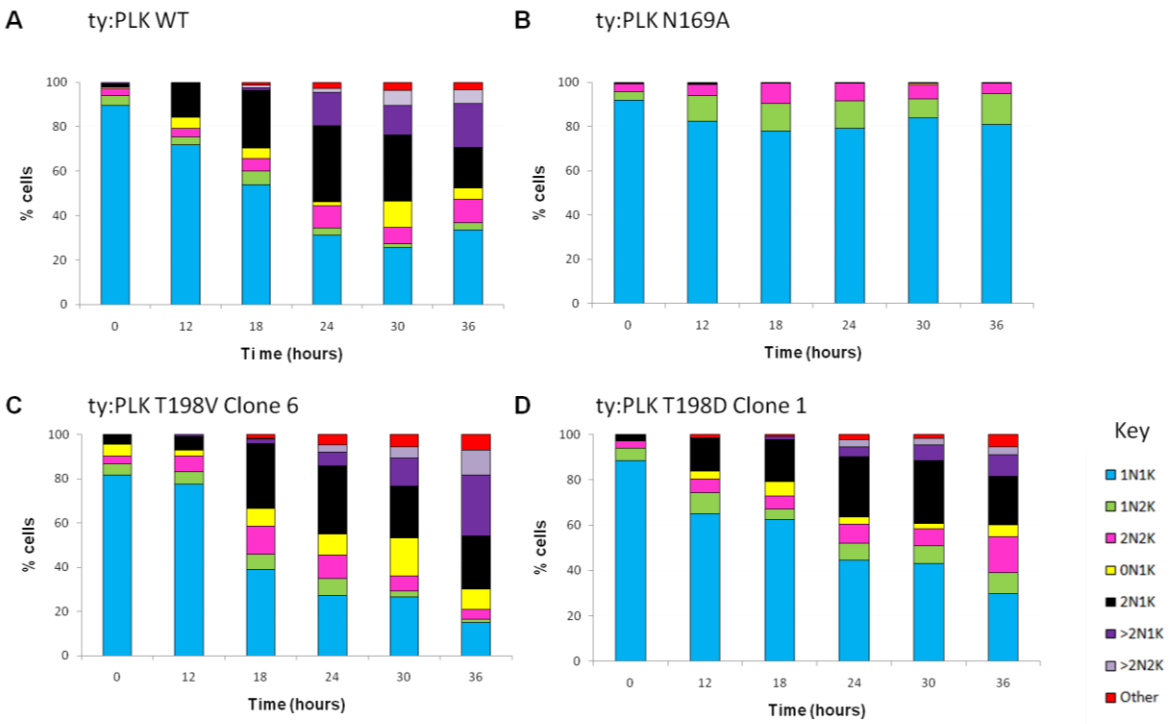

Figure 7-30 -Analysis of cells overexpressing ty:PLK variants by DAPI staining. Cells expressing ty:PLK WT or T198V/D were cultured in the presence of tetracycline (1 µgml^{-1}) and the number of nuclei (N) and kinetoplasts (K) per cell was determined by DAPI staining (*n*>200 cells/time point).

A decrease in 1N1K cells was apparent from 12 hours post-induction, which was accompanied by the appearance of 2N1K cells and these abnormal cells continued to accumulate over the next 12 hours (Figure 7-30A, C and D; and Figure 7-31). At 18 hours, 2N2K cells with abnormal organelle positioning appeared (KKNN) (Figure 7-32), and 24 hours post-induction, multinucleate cells with one kinetoplast (Figure 7-30 and Figure 7-33), which was later succeeded by the appearance of smaller numbers of multinucleate cells with two kinetoplasts

(Figure 7-30). An increase in total 2N2K cells was also observed, although since only relatively small proportions of these cells are present in the whole population, there was some stochastic variation between cell lines (Figure 7-30). The decrease in 1N1K cells, accumulation of 2N1K cells and appearance of multinucleate cells would account for the changes in DNA profile observed by flow cytometry analysis (Figure 7-29).

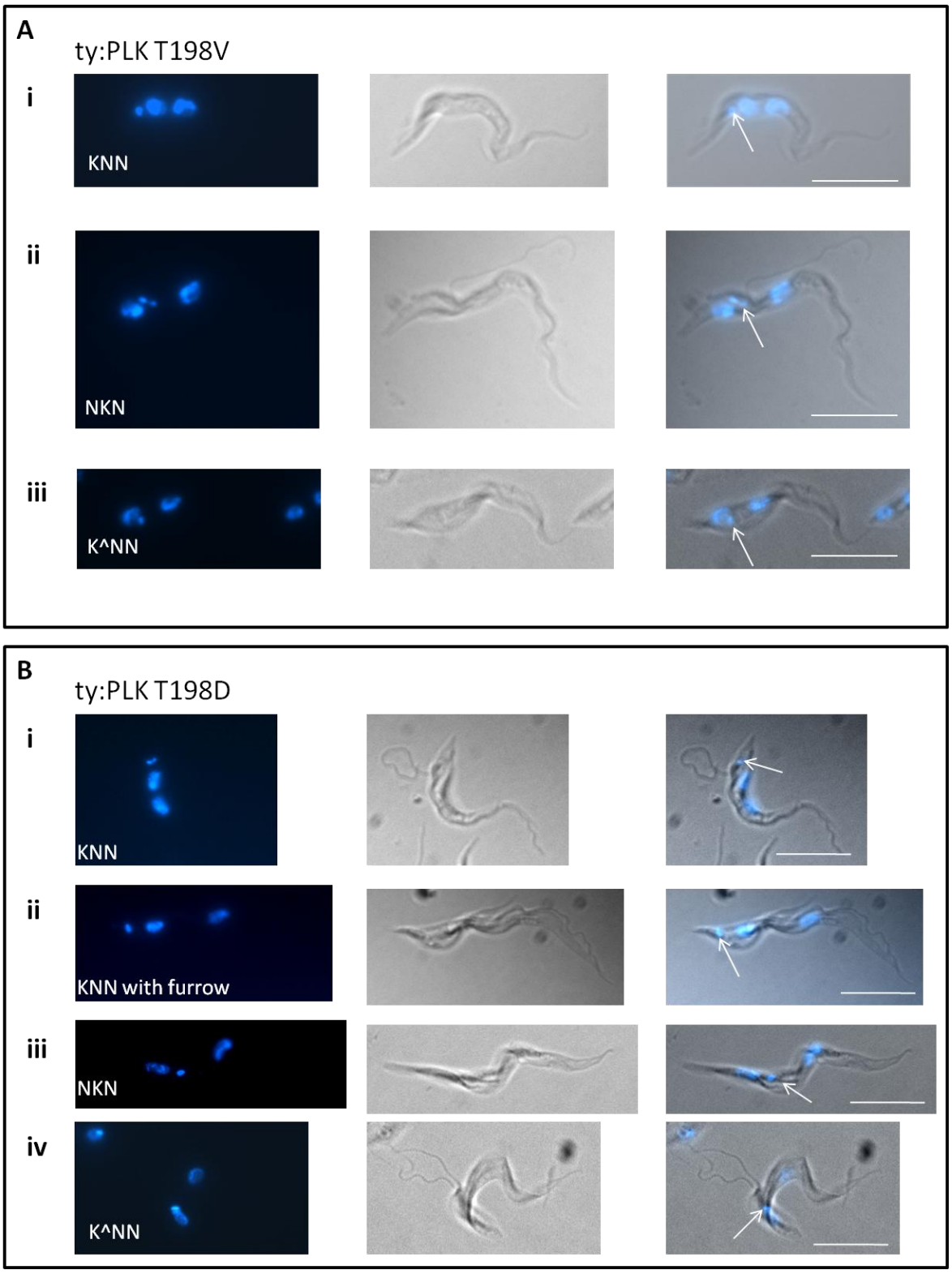

Figure 7-31 -2N1K cells observed during the overexpression of ty:PLK T198V/D. Example images of DAPI-stained 2N1K cell types for procyclic cell lines expressing ty:PLK T198V (Ai-iii) and ty:PLK T198D (Bi-iv). Left panels: DAPI; middle: DIC; right: merged image. A selection of 2N1K cells with variable organelle positioning, and furrow ingression status are presented. Organelle configurations are given and refer to the positions of these organelles relative to the posterior end of the cell; '^' indicates where the kinetoplast is positioned lateral to the nucleus. Arrows indicate the positions of kinetoplasts. Scale bar: 10 µm.

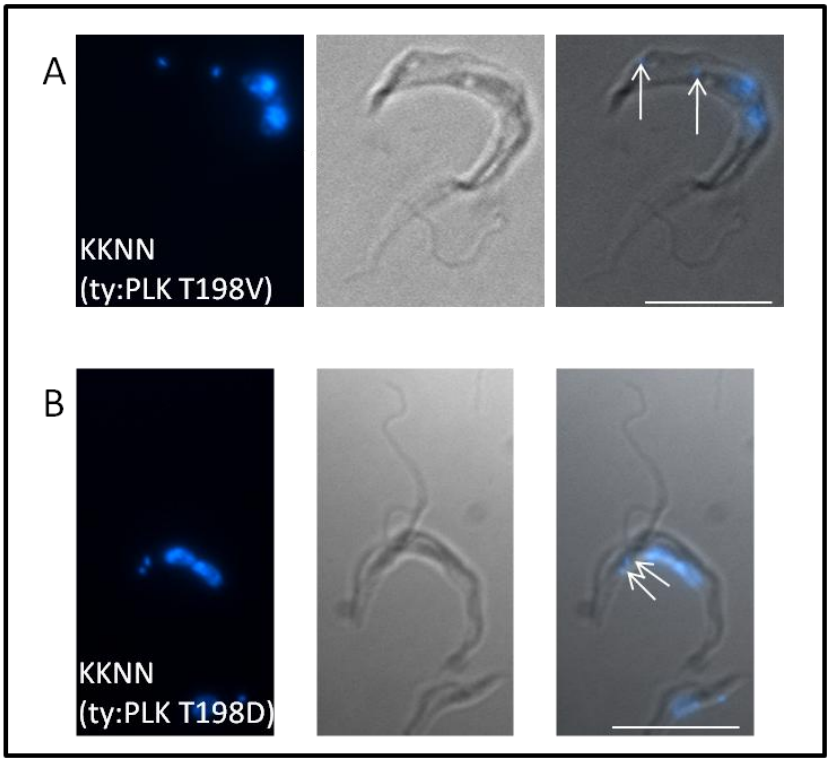

Figure 7-32 -Abnormal organelle positioning in 2N2K cells during the overexpression of mutated ty:PLK T198V/D.
Example images of 2N2K cells with abnormal organelle positions 'KKNN' observed following the overexpression of ty:PLK T198V (A) or ty:PLK T198D (B) are shown above. Arrows indicate the positions of kinetoplasts. Scale bar: 10 µm.

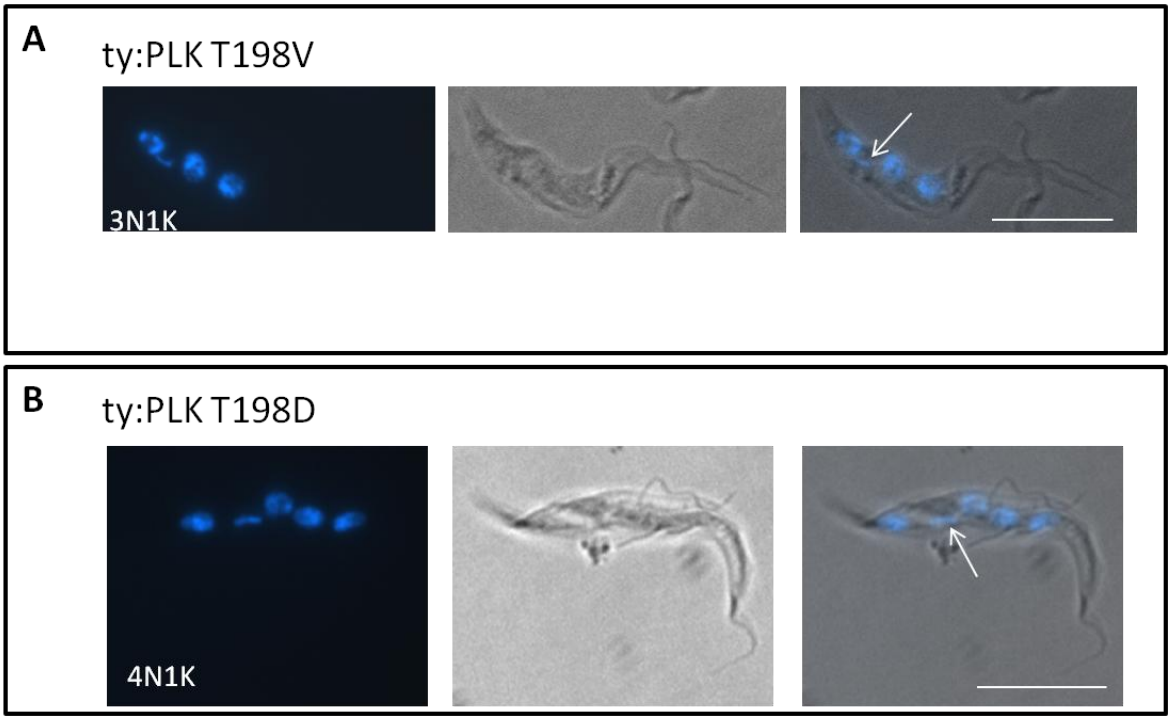

Figure 7-33 -Multinucleate cells observed during the overexpression of ty:PLK T198V/D.
Example images of DAPi-stained multinucleate cells observed following the overexpression of ty:PLK T198V (A) or ty:PLK T198D (B) are shown above. Arrows indicate the positions of kinetoplasts. Scale bar:10 µm.

The position of the single kinetoplast in 2N1K cells was variable (Figure 7-31), and 2N1K cells displayed KNN and NKN organelle configurations, and in some, the kinetoplast was positioned lateral to the most posterior nucleus (Figure 7-31Aiii and Biv). When 2N1K cells were classified according to organelle positions, KNN organelle configurations were found to be the most prevalent (Figure 7-34), and this was the case for all the cell lines analysed (with the exception of cells overexpressing ty:PLK N169A, where no 2N1K cells were observed), again consistent with previous data for ty:PLK WT (Hammarton et al., 2007).

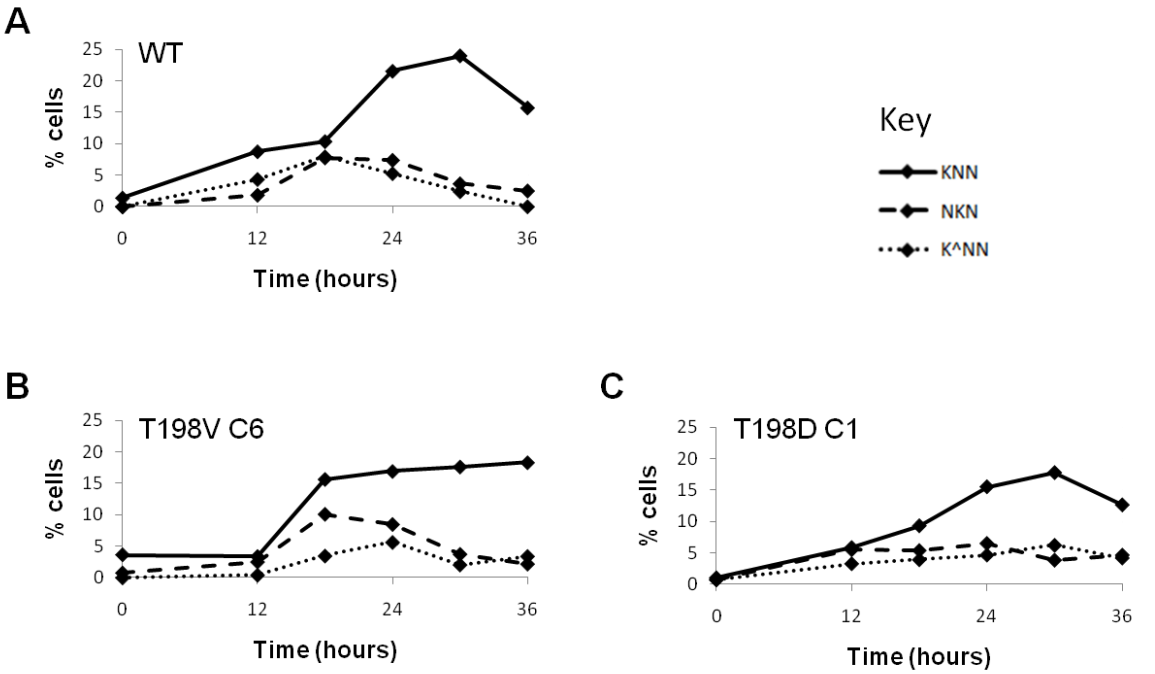

Figure 7-34 -Analysis of organelle positioning in 2N1K cells.
2N1K cells observed following the overexpression of ty:PLK WT and T198V/D were classified according to the relative positions of the nuclei (N) and kinetoplasts (K). Only the three dominant organelle positions are shown (see key and Figure 7-31), with the order of the organelles given relative to the posterior end of the cell. '^' indicates that the kinetoplast was positioned lateral to the nucleus.

2N1K cell types can arise as a consequence of abnormal cell division, or premature entry into mitosis. Abnormal cell division of 2N2K cells was not observed, and furthermore, the proportions of 2N1K cells far exceeded those of 0N1K cells (Figure 7-30) suggesting that 0N1K cells arise from the aberrant division of other cell types, although no obvious source for the 0N1K cells could be identified from analysis of whole populations. This excluded the possibility that abnormal cell division caused the accumulation of 2N1K cells in this study. The possibility that premature entry into mitosis caused these cells to arise was

also deemed unlikely as, if this was the case, a dramatic increase in 2N2K cells could be expected following the rise in 2N1K cells, and this did not occur. From the enlarged and elongated appearance of kinetoplasts in some 2N1K cells (Figure 7-31Aii and Bi), it seemed possible that in cell lines expressing ty:PLK T198V and ty:PLK T198D, impaired kinetoplast segregation rather than abnormal cell division or premature entry into mitosis, caused the accumulation of 2N1K cells and the later accumulation of multinucleate cells with one kinetoplast, as had been described previously for cells overexpressing ty:PLK WT (Hammarton et al., 2007). However, since there was a slight increase in 2N2K cells, and multinucleate cells with two kinetoplasts appeared at later time points, kinetoplast division was probably impaired but not totally inhibited following overexpression of ty:PLK WT or T198V/D variants. Eventual kinetoplast division in some of these KNN 2N1K cells may account for the appearance of KKNN 2N2K cells (Figure 7-32).

7.9.8 Summary of in vivo studies

Mutation of T198 in the T-loop of PLK was hypothesised to impair (T198V) or override (T198D) *in vivo* regulation by upstream kinases. The activities of T-loop mutants were comparable to the wild type kinase (Figure 7-27), suggesting that, in fact, regulation of PLK activity probably occurs at other residues or via other mechanisms. A comparison of expression levels confirmed that the equivalent levels of activity were not a consequence in the variation of expression levels between T-loop mutants and wild type PLK (Figure 7-26).

The evidence that ty:PLK T-loop mutants and ty:PLK WT exhibit similar levels of activity does not necessarily contradict the results obtained from recombinant assays; the activity of T-loop mutants *in vitro* (Section 7.8.6.3) may well be a result of the variable ability of these proteins to autophosphorylate (Section 7.8.6.2). It is possible that autophosphorylation is inhibited *in vivo,* which could account for the similarities in the activities of proteins when they are expressed in *T. brucei* cells. Possible mechanisms by which this could occur include regulation by phosphatases, inhibitory phosphorylation by other kinases or interaction with substrates, and the prolific autophosphorylation observed *in vitro* for 6XHis:PLK WT and 6XHis:PLK T198D may not be physiologically relevant

(Peck, 2006). Phosphorylation at sites other than the T-loop T198 residue could also account for the almost identical phenotypes observed for the overexpression of ty:PLK WT and the ty:PLK T-loop mutants. Although it was not possible to obtain sufficient quantities of ty:PLK proteins by immunoprecipitation for mass spectrometry analysis (data not shown), further knowledge of *in vivo* phosphorylation sites may help to explain these results.

Overexpression of all three proteins led to an accumulation of 2N1K cells, and multinucleate cells with one kinetoplast, most likely as a result of impaired kinetoplast segregation (Section 7.9.7). The number of basal bodies was not analysed in this study; however, previously, overexpression of tyPLK: WT inhibited basal body duplication and it would be interesting to investigate whether this was also the case for the overexpression of ty:PLK T-loop mutants. It was previously suggested that the similar effects observed through RNAi-mediated depletion of PLK, and overexpression of ty:PLK could be the result of a negative feedback pathway. As the overexpression of WT and T-loop mutated versions of ty:PLK produced the same phenotype, possible positive feedback pathways probably do not involve phosphorylation at this residue.

7.10 The role of the polo-box domain in autoregulation of PLK

The PBD has been shown to have roles in PLK localisation and substrate recognition *in vivo* (Section 7.5.3). Intriguingly, *in vitro* studies have shown that the activity of the full length kinase is regulated through interaction with this domain (Section 7.5.2).

In order to investigate whether *T. brucei* PLK is regulated by similar autoregulatory mechanisms, a truncated protein comprising the polo-box domain was generated (Sections 7.8.1 and 7.8.2). In addition to studies concerning autoregulation, the role of the residues His705 and Lys707 in the PBD was investigated. The important *in vivo* role for these residues in other organisms led to the generation of a construct for overexpression of ty:PLK H705A K707A. However, analysis of these cell lines could not be completed due to time

constraints, and only the *in vitro* work concerning the 6XHis:PLK H705A K707A recombinant protein will be discussed.

7.10.1 Interaction of the PBD with full length PLK

To investigate the possibility that the PBD can interact with full length PLK, recombinant 6XHis:PBD was immobilized on nickel beads (Section 4.6.4.2.1) and incubated with cell lysate from cells expressing ty:PLK WT (Section 4.9). Following incubation, the beads were washed before eluting 6XHis:PBD and any interacting proteins (Section 4.6.4.2.1). Appropriate fractions from the purification were analysed by SDS PAGE (Section 4.6.1) and Western blotting with an anti-TY antibody (Section 4.6.3) in order to detect ty:PLK WT (Section 7.9). ty:PLK WT was detected in the input (cell lysate fraction), but only small amounts of ty:PLK WT were apparently present in the flow through fractions (for nickel beads with and without 6XHis:PBD) (Figure 7-35). For the beads without 6XHis:PBD, significant amounts of ty:PLK WT were detected in the wash fraction, and little in the elution, although a substantial amount of ty:PLK WT remained on the beads following elution, suggesting ty:PLK WT non-specifically interacts with nickel beads. However, for nickel beads bound by 6XHis:PBD, little 6XHis:PLK WT was detected in either the flow through or the wash fractions, yet significant amounts were present in the elution fraction, arguing that in addition to interacting with the nickel beads, 6XHis:PLK WT was also able to specifically interact with 6XHis:PBD (Figure 7-35). No proteins were detected using the anti-TY antibody for a non-induced lysate used as a negative control, confirming that this antibody exclusively detected ty:PLK WT . These results show that ty:PLK WT expressed *in vivo*, is able to interact with recombinant 6XHis:PBD.

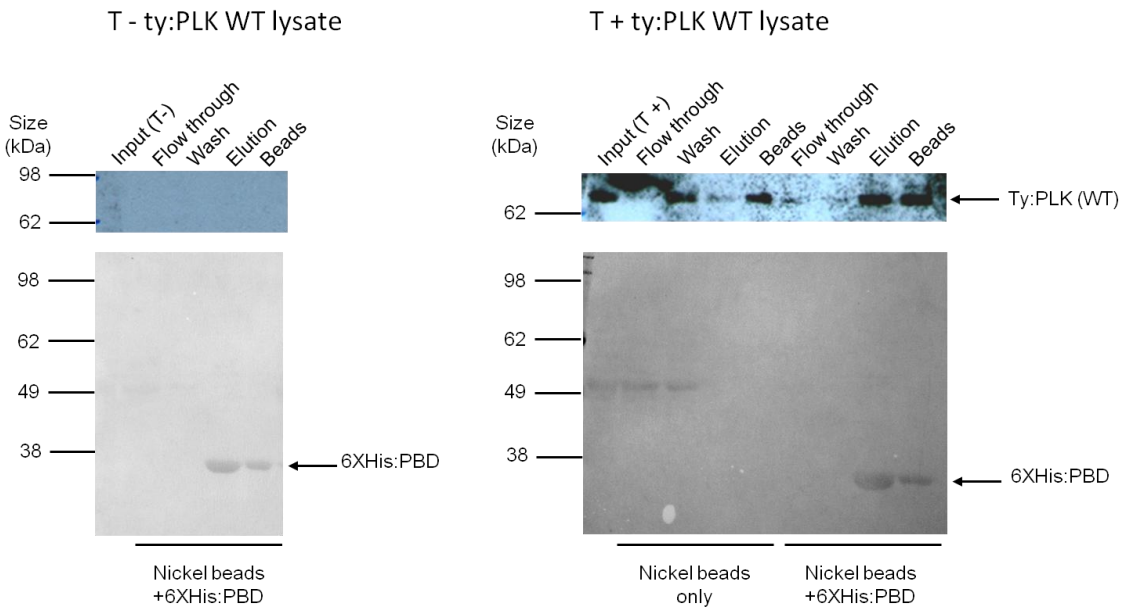

Figure 7-35 - Interaction of ty:PLK WT with 6XHis:PBD.
Potential interactions between the PBD of PLK and the full length protein were investigated through the incubation of cell lysate containing ty:PLK WT, with 6XHis:PBD immobilised on nickel beads (far right of figure). Following the incubation, unbound proteins were removed by washing the beads and both the 6XHis:PBD and any interacting proteins were eluted from the beads for analysis by SDS PAGE and Western blotting with an anti-TY antibody to detect ty:PLK WT (upper panels). To detect the 6XHis:PBD, Western blots were stained with Ponceau reagent (lower panels). To control for non-specific interactions of ty:PLK WT with the nickel beads, nickel beads without 6XHis:PBD were incubated with ty:PLK WT lysate (right of figure), and to ensure that the anti-TY antibody specifically recognised ty:PLK WT and not other proteins that could interact with 6XHis:PBD, a non-induced cell lysate control was included (left of figure).

7.10.2 6XHis:PBD does not inhibit the activity of 6XHis:PLK WT

The evidence that ty:PLK WT interacts with 6XHis:PBD gave rise to the possibility that an autoinhibitory mechanism might regulate *T. brucei* PLK. To investigate this, 6XHis:PBD was incubated with either 6XHisPLK WT (untreated) or lambda protein phosphatase (λPPase) treated 6XHisPLK WT for 30 minutes (to maximise binding) in the absence of ATP prior to performing kinase assays with an α-casein substrate. The inclusion of λPPase treated 6XHis:PLK WT was necessary to control for the possibility that autoinhibition only occurs when the protein is in its unphosphorylated state, as has been demonstrated previously in other studies of PLKs (Section 7.5.1). In addition, a time course was carried out as a precaution to avoid any potential masking effects, should autophosphorylation of dephosphorylated 6XHis:PLK WT occur which could potentially lead to or prevent its interaction with 6XHis:PBD.

Untreated 6XHis:PLK WT displayed detectable levels of autophosphorylation, while autophosphorylation of λPPase treated 6XHis:PLK WT was barely detectable over the 30 minute duration of the kinase assay (Figure 7-36). The level of autophosphorylation exhibited by untreated 6XHis:PLK WT was unaffected by the presence of the 6XHis:PBD. Phosphorylation of the α-casein substrate was greater for phosphorylated 6XHis:PLK WT than for dephosphorylated enzyme, as previously demonstrated (Section 7.8.5), and was not altered by the presence of 6XHis:PBD (Figure 7-36). Together, these results suggested that unlike in other organisms, interaction of the PBD with PLK does not inhibit the activity of full length PLK.

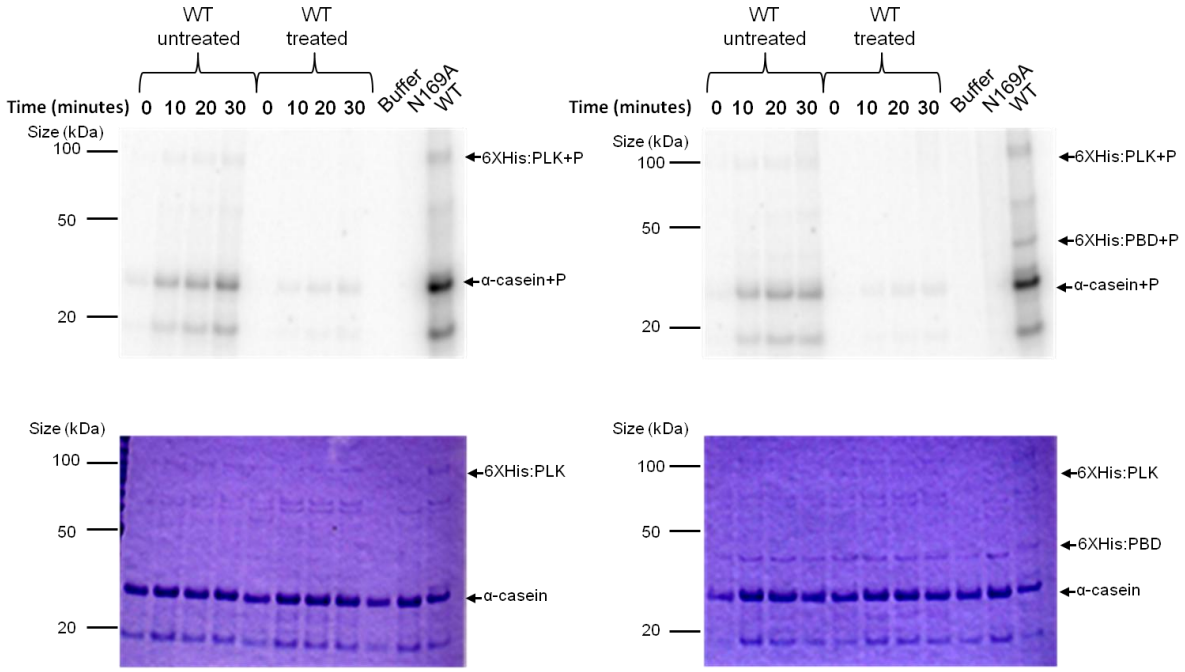

Figure 7-36 -Kinase assays to investigate autoinhibition of full length PLK by the PBD. Kinase assays of full length PLK (6XHis:PLK WT, either untreated or treated with λPPase) were performed with α-casein substrate in the presence (right panels) or absence (left panels) of 6XHis:PBD. Independent reactions were set up and halted at 10 minute intervals. To control against possible effects due to the conditions of λPPase treatment, 6XHis:PLK WT which had not been subject to these conditions was also included (far right of each gel). Negative controls were provided by the kinase dead 6XHis:PLK N169A protein ('N169A'), or an equivalent volume of kinase assay buffer ('buffer'). The autoradiographs (top panels) show the detection of radiolabelled proteins, and the equivalent Coomassie-stained gels show equal loading (bottom panels).

7.10.3 6XHis:PBD acts as a substrate for full length 6XHis PLK variants, and does not inhibit the activity of these proteins

In order to further investigate the potential for an autoinhibitory mechanism of regulation involving the PBD, and phosphorylation of the PBD by full length PLK, full length 6XHis:PLK T-loop mutants and a PBD mutant (see below) were incubated with 6XHis:PBD for 30 minutes prior to performing kinase assays in the presence or absence of an α-casein substrate.

In the absence of 6XHis:PBD, all the PLK variants exhibited autophosphorylation, with the exception of 6XHis:PLK N169A (Figure 7-37A). Addition of the 6XHis:PBD had no effect on autophosphorylation (compare Figure 7-37A and B), and 6XHis:PBD was found to be a substrate of active full length 6XHis:PLK variants. Phosphorylation of the 6XHis:PBD was readily detected due to both the impaired migration of 6XHisPBD through an SDS PAGE gel, and incorporation of radiolabelled phosphate as detected in the autoradiograph (Figure 7-37B). Activity against α-casein was not affected for any of these proteins in the presence of 6XHis:PBD (compare Figure 7-37C and D). Phosphorylation of 6XHis:PBD was slightly reduced in the presence of α-casein, suggesting that there was competitive inhibition between the substrate and 6XHis:PBD (compare Figure 7-37C with Figure 7-37D). Phosphorylation of 6XHis:PBD was not unexpected, as mass spectrometry analysis identified several autophosphorylation sites within the PBD of the full length 6XHis:PLK proteins (Sections 7.8.4 and 7.8.6.2). However, this phenomenon has not been observed for human PLK1, and for human PLK1, the PBD was found to inhibit the activity of the full length kinase (Section 7.5.2). It is possible that *T. brucei* PLK is regulated through alternative mechanisms, although differences in experimental approach could also account for these results. Due to difficulties associated with immunoprecipitation of ty:PLK, it was not possible to attempt these assays with a more physiologically relevant version of PLK.

Mutation of the residues H705 and K707 within the second polo-box motif of *T. brucei* PLK was carried out (Section 7.8.1) to determine whether a functional equivalent of the 'His-Lys pincer' is present (Section 7.5.2). These residues were

substituted with alanine residues which are non polar, and should prevent potential interactions with the negatively charged phosphate group of phosphorylated substrates. Kinase assays with an α-casein substrate revealed that 6XHis:PLK H705A K707A exhibited similar levels of autophosphorylation and substrate phosphorylation as those observed for 6XHis:PLK WT (Figure 7-13 and Figure 7-37). Further *in vitro* investigations into the role of these residues would preferably involve kinase assays with physiologically appropriate substrates, for example Centrin 2 (Graffenried et al., 2008); however, until identification of phosphorylated target proteins are identified, the scope for further *in vitro* investigation is limited.

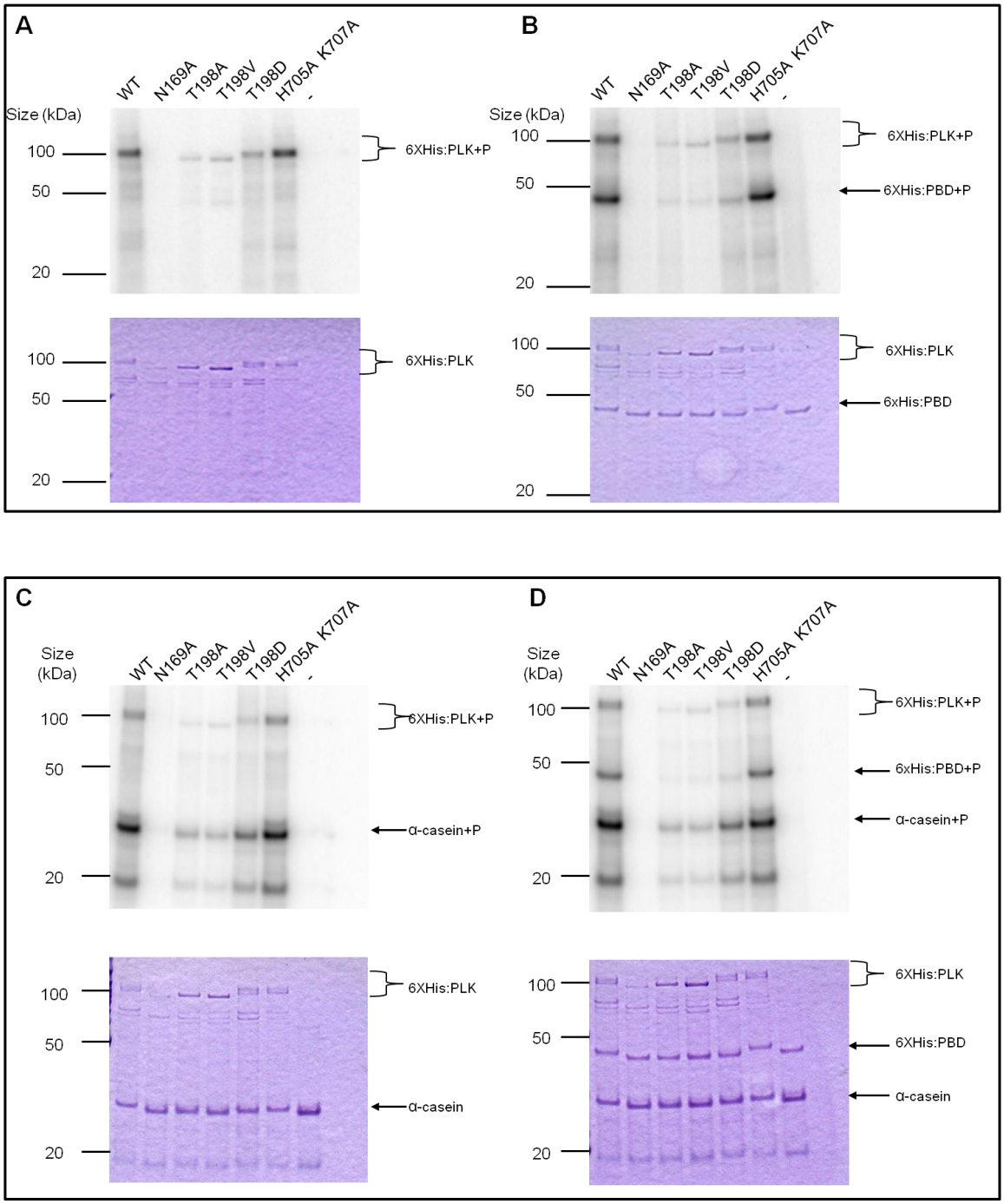

Figure 7-37 -Kinase assays investigating the PBD as a substrate of 6XHis:PLK variants. Kinase assays of 6XHis:PLK variants (WT, N169A, T198A/V/D, H710A/K712A) were performed in the absence or presence of an α-casein substrate (A-B and C-D, respectively), with (B and D) or without (A and C) the addition of 6XHis:PBD. A buffer only control (-) controlled for any contaminating kinase activity of the 6XHis:PBD or the kinase assay buffer. The autoradiographs (upper panels) show the detection of radiolabelled proteins, and the equivalent Coomassie-stained gels (lower panels) are displayed to control for protein loading.

7.10.4 Truncation of the C-terminus of PLK abolished activity

Proteins corresponding to WT and dead versions of the kinase domain (KD) of *T. brucei* PLK were generated (Sections 7.8.1 and 7.8.2) in order to determine whether deletion of the PBD could stimulate kinase activity. Whilst GST epitope tagged active and dead (N169A) recombinant proteins were extremely soluble (Figure 7-12), neither autophosphorylation nor activity against an α-casein substrate could be detected during *in vitro* kinase assays (Figure 7-38).

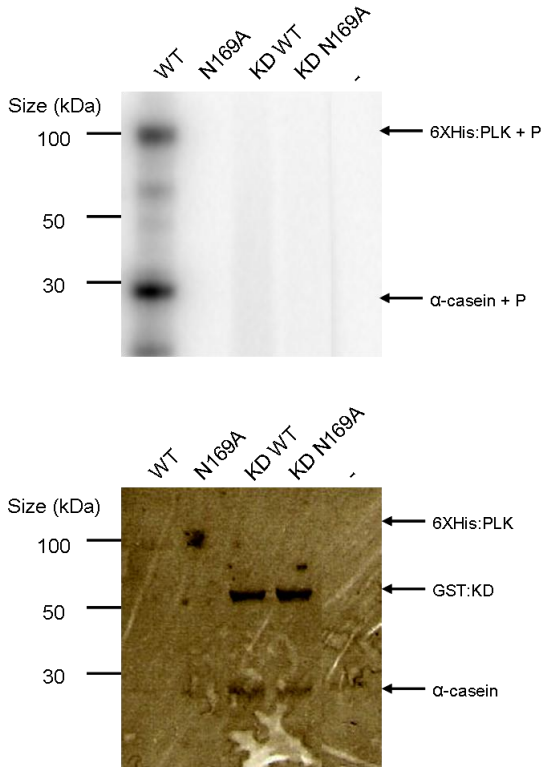

Figure 7-38 –The activity of recombinant PLK kinase domain.
6XHis:PLK WT (WT), 6XHis:PLK N169A (N169A) GST:PLK KD (WT), GST:PLK KD (N169A) or a buffer control (-) were used in kinase assays to determine the activity of recombinant PLK kinase domain against generic kinase substrates. Top panels: autoradiographs; bottom panels: the corresponding Coomassie gels acting as loading controls. PLK proteins (predicted size: 88 kDa and 60 kDa for full length and kinase domains respectively), and substrates are indicated.

It is possible that the inactivity of GST:KD WT could be explained by the presence of the relatively large GST epitope tag which may have impeded access to the active site; alternatively, the presence of a 70 kDa band observed in eluted fractions of GST:KD WT and N169A may indicate that the *E. coli* chaperone DnaK copurifed with these proteins (Figure 7-12). Should this be the case, the inactivity of GST:KD WT could be a result of inappropriate protein folding, a phenomenon which has been commonly observed for the PLK KD in

other organisms. The PLK1 KD reportedly proved difficult to purify. To achieve purification of soluble and active human PLK1 KD it was necessary to incorporate a loop downstream of the core kinase domain, and in addition expression required the utilization of eukaryotic expression systems (discussed in Section 7.3). Whilst a GST tagged version of the *T. brucei* KD incorporating amino acids residues 2-294 is inactive, it is likely that through testing a variety of truncations, a soluble and active version of the *T. brucei* KD could be obtained, which would allow investigation into the role of the PBD using this experimental approach.

7.11 Summary

Previous studies involving *T. brucei* PLK have identified potential phosphorylation sites in endogenous PLK (Nett et al., 2009), and reported activity of overexpressed PLK against generic and *T. brucei* specific substrates (Graffenried et al., 2008; Hammarton et al., 2007). In addition, a recent study has shown that a recombinant GST:PLK protein is active against α-casein *in vitro* (Li et al., 2010b). Whilst these investigations show that *T. brucei* PLK is both active and phosphorylated, no investigations into the mechanism of activity or roles of these phosphorylation sites have been published. This study aimed to investigate these unresolved issues through a combination of *in vitro* and *in vivo* approaches.

This study found that recombinant *T. brucei* PLK is extensively phosphorylated at both serine and threonine residues (Section 7.8.4), and that phosphorylation of the wild type recombinant protein is important for its activity (Section 7.8.5). In addition, it was revealed through the generation of recombinant T-loop mutants that *in vitro* activity can be influenced by mutation of the T198 residue, although a T198D mutant surprisingly showed reduced activity in comparison to the equivalent wild type equivalent (Section 7.8.6.3). *In vivo* experiments implied that this residue is not important for activity in a physiological environment, which indicated that *T. brucei* PLK may be activated by alternative upstream kinases to those identified in other organisms and at a different site (Section 7.8.6 and Section 7.9). This result was not unexpected, given that TbPLK exhibits divergent roles in the cell cycle in comparison to other

organisms, particularly with regards to mitosis, which does not appear to require PLK (Graffenried et al., 2008; Hammarton et al., 2007; Kumar and Wang, 2006). The localisation and regulation of PLK in other organisms is tightly associated with the mitotic function of this protein (Section 7.2) and given the divergent role of PLK in trypanosomes, it is highly probable that regulation occurs through alternative means.

The involvement of TbPLK in cytokinesis may indicate that kinases involved in cytokinesis could be candidates as upstream regulators of TbPLK. PK50 and PK53 and MOB1B, like TbPLK have been shown to have roles in cytokinesis in bloodstream form *T. brucei* (Hammarton et al., 2005; Ma et al., 2010) and it would be interesting to establish whether these proteins are involved in the same regulatory pathways (either as upstream kinases (PK50 or PK53), or as substrates of PLK (PK50, PK53, MOB1B). TbLRTP, which is a negative regulator of basal body biogenesis could be a potential substrate for TbPLK, as TbPLK is important for basal body duplication (Hammarton et al., 2007), although *in vitro* kinase assays performed using 6XHis:PLK WT and recombinant GST:TbLRTP during the course of this study did not detect any phosphorylation of TbLRTP by PLK (data not shown).

Investigations into the potential role of the PBD in the regulation of PLK activity revealed that there is an interaction between the PBD and the full length protein (Section 7.10.1); however, no inhibitory effect of the PBD on autophosphorylation or *trans*-phosphorylation of PLK could be determined through *in vitro* studies (Section 7.10.2 and Section 7.10.3). The ability of the full length protein to phosphorylate the PBD confirmed that autophosphorylation can occur at the C-terminal region of the protein, and revealed that this can happen through *trans* mechanisms (Section 7.10.2 and Section 7.10.3). A recombinant GST-tagged protein corresponding to the kinase domain of PLK was purified during the course of this study, but was inactive (Section 7.10.4), hampering efforts to investigate potential autoinhibition by the PBD through other means. Mutation of the putative 'His-Lys pincer' within the polo-box domain had no apparent effect on *in vitro* activity (Section 7.10.3). It is more likely that the function of these residues will be identified through future *in vivo* investigations, as the main role for this motif is believed to be association of the full length protein with phosphorylated substrates, rather than association with

the kinase domain of the protein (which could potentially be investigated *in vitro*).

Cytokinesis in *T. brucei* has been shown to involve unique mechanisms, and it is likely that substrates of TbPLK could be functionally divergent or novel proteins. The identification of these substrates and elucidation of how TbPLK is regulated *in vivo* will greatly improve the current knowledge of how these processes occur.

8 General discussion

8.1 Mechanisms of cytokinesis

8.1.1 Furrow ingression in T. brucei

Cytokinesis in *T. brucei* occurs via the longitudinal ingression of a cleavage furrow, and does not involve the formation of an actomyosin contractile ring. Initiation of furrow ingression occurs at the anterior end of the new FAZ, which is known to involve the molecular regulators: PLK and AUK1. At S phase, PLK localises to the extending FAZ, dissociating from the anterior tip of the new FAZ at anaphase which coincides with the translocation of the CPC (comprising AUK1, CPC1 and CPC2) to the site vacated by PLK. Furrow initiation occurs at the site of CPC localisation, and the CPC migrates with the furrow during furrow ingression apparently guiding the furrow along the dividing cell. It has been speculated that PLK phosphorylates a component of the flagellum attachment zone to mark the site for CPC translocation and therefore furrow initiation.

Whilst some molecular regulators associated with the site of furrow initiation and the furrow apex have been identified, how these molecular regulators mediate furrow ingression is not understood, and there are many questions remaining as to what occurs during ingression of the cleavage furrow. Firstly, furrow ingression is constrained by the heavily cross-linked and stable subpellicular microtubules, which must presumably disassemble to allow membrane to coalesce dividing the cytoplasm of the daughter cells. Disassembly of microtubules at the furrow has not been observed, although it is possible that this involves very small numbers of microtubules. Secondly, before the furrow is initiated cells display a ‘piggy back’ phenotype, characterised by localised indentation of the cell surface demarcating the outline of the new daughter cell. This suggests that the cleavage axis is determined before furrow ingression occurs and it is not known what proteins are involved in the remodelling of the cytoskeleton to produce the ‘piggy back’ phenoptype.

There are several models to explain the mechanisms of furrow ingression in mammalian cells, which may contribute towards an explanation of how furrow ingression in *T. brucei* might occur.

8.1.2 Models for furrow ingression in mammalian cells

8.1.2.1 Forces in cytokinesis

Mechanical factors which affect furrow ingression in mammalian cells include inward constriction or contraction forces, hydrostatic pressures in the cytoplasm, and elastic forces of the cell cortex (reviewed in (Wang, 2005)). Forces can be generated by cytoskeletal proteins and motor proteins, which are regulated by a variety of other proteins during furrow ingression. The mechanical properties of cells can be measured using a number of techniques for example, micropipette aspiration, atomic force microscopy and laser-tracking microheology (reviewed in (Reichl et al., 2005)). The roles of different cytoskeletal proteins and structures in cytokinesis can be investigated through the application of inhibitors such as cytochalasin D which inhibits actin polymerisation, or monastrol which inhibits centrosome separation to generate monopolar spindles. In addition, micromanipulation experiments for example, removal of centrosomes, severing of spindle microtubules, and the application of glass beads to cell surfaces have proved effective in identifying structures important for cleavage furrowing (reviewed in (Maddox and Oegema, 2003)).

Determination of furrow ingression mechanisms using these and other approaches has led to the belief that models other than the contractile ring hypothesis can describe the mechanics of furrow ingression (reviewed in (Pollard, 2010;Wang, 2005)).

8.1.2.2 Models for furrow ingression in eukaryotic cells

The contractile ring hypothesis describes a process where the accumulation of actin and myosin II at the equator of the cell is followed by sliding of antiparallel actin filaments, which are cross linked to myosin II filaments. This results in constriction of the contractile ring and membrane ingression. This ‘purse string’ model involves a localised increase in constriction forces, however, cortical

sinking describes how the contraction of actin filaments, when associated with the cell membrane in addition to myosin II filaments, could produce perpendicular forces resulting in furrow ingression. This implies that the actomyosin ring could alternatively cause furrow ingression through the generation of contractile forces. The ‘global contraction-equatorial deformation mechanism’ describes how signalling from the central spindle might trigger localised deformation of the cell equator, disrupting the balance of outward elastic and inward contractile forces within the cytoskeleton causing a net inward contractile force and ingression of a cleavage furrow.

In contrast to the previous three models, the polar relaxation model emphasises the importance of signals from the spindle asters. Whilst signals emanating from the central spindle lead to the formation of the actomyosin contractile ring, signalling from the spindle asters at opposite poles of the cell triggers polar relaxation and expansion of the cell poles. This generates a tension differential between the cell poles and equator. It has been proposed that the changes in hydrostatic pressures resulting from the production of a tension differential in a cell with a finite volume, could lead to equatorial shrinkage and accumulation of contractile elements at the cell equator (by cortical flow) generating a ‘crumple zone’ of filaments which would then become organised to form the contractile ring (He and Dembo, 1997).

More specific models have been proposed to explain cleavage furrow ingression in motile cells. The cortical ripping model describes how the definition of cell polarity in the new daughter cell could lead to the equator marking the posterior of both daughters, and motile forces pulling the cell in opposite directions would literally rip the cell apart. Also, adherence of the cell to the substratum at the equatorial region and the production of stress fibres emanating from the point of attachment to the cell cortex would generate a net inward force causing furrow ingression.

8.1.3 Thoughts on furrow ingression in T. brucei

The lack of an actomyosin contractile ring, lateral ingression of the cleavage furrow and apparent independence of furrow ingression from mitosis in procyclic form cells, precludes the involvement of the central spindle microtubules,

spindle asters and actomyosin contractile rings in furrow ingression in *T. brucei*. In addition whilst it is attractive to speculate that flagella motility could be involved in furrow ingression through a process similar to the cortical ripping model described above, the fact that procyclic form cells can still produce furrows without flagella motility contradicts this. The 'global contraction-equatorial deformation mechanism' which involves localised deformation of the cell may well be applicable to *T. brucei* cytokinesis: changes in the membrane/cytoskeleton association and microtubule depolymerisation could be mediated by microtubule-associated proteins, causing localised deformation generating the inward forces required for furrow ingression. Potentially this might involve furrow associated proteins for example, components of the CPC; microtubule-associated proteins, or post-translational modifications of tubulin.

During furrow ingression it is likely that remodelling occurs at the furrow apex. Membrane and cytoskeletal modelling could potentially involve kinesins, as over 40 kinesins have been identified in the *T. brucei* genome (Berriman et al., 2005), and already two have been assigned to roles in cytokinesis (Li et al., 2008a). These motor proteins may be involved in targeting proteins to the site of the furrow apex for remodelling of the cytoskeleton and membrane at this location.

Unfortunately analysis of *T. brucei* cells using the methods described in Section 8.1.2.1 are unlikely to be useful in investigating mechanisms of *T. brucei* cytokinesis due to the highly motile nature of these cells and it remains to be seen whether changes in microtubule dynamics occur, or whether changes in microtubule dynamics alone could be sufficient to cause furrow ingression.

8.1.4 Aims of this study

This study aimed to investigate different aspects of furrow ingression in *T. brucei* cytokinesis. Firstly, an orthologue of a microtubule-associated protein required for cytokinesis in plants, AIR9 was characterised to explore the potential that in *T. brucei* this protein could localise to the cytoskeleton and regulate cytokinesis. Secondly, the importance of microtubule dynamics in furrow ingression was assessed through inhibitor studies. Finally, this study aimed to further understanding of the regulation of cytokinesis by PLK by investigating how its activity is regulated *in vitro* and *in vivo*.

8.2 The role of AIR9 in *T. brucei*

Prior to this study, the localisation and function of AIR9 had only been investigated in plants (Buschmann et al., 2006), although the identification of Trypanosomatid homologues was reported (Buschmann et al., 2007). RNAi was used to evaluate the role of AIR9 in *T. brucei*. Depletion of AIR9 caused a growth arrest in bloodstream form cells, indicating that AIR9 is essential in this life cycle stage. AIR9 was also shown to be required for normal growth rates of procyclic populations. Following AIR9 depletion, cell cycle progression was affected in both life cycle stages, as evidenced by their flow cytometry profiles that indicated the presence of cells with an abnormally low or excessive DNA content. Analysis of nucleus and kinetoplast (N-K) configurations in these cells established that this was a result of the production of both anucleate (0N1K) and multinucleate cells. Additionally, sizeable numbers of 2N1K cells were also detected. In both life cycle stages, post-mitotic (2N2K) cells with cleavage plane positioning defects were observed, indicating that these 2N2K cells were likely to be the parents of the observed 0N1K and 2N1K daughters following an asymmetrical division, and that depletion of AIR9 results in defects in cytokinesis.

Depletion of AIR9 was also found to result in abnormal relative positioning of nuclei and kinetoplasts. This phenotype was found to be the most striking in procyclic trypanosomes, where organelle positioning defects were apparent in cells at all cell cycle stages. Detailed morphometric analyses of 1N1K cells in AIR9-depleted procyclic populations revealed that nuclei were displaced posteriorly, while kinetoplasts were malpositioned anteriorly relative to the posterior end of the cell. This was found to be the result of an increase in cell length (by posterior end extension) and posterior directed movement of the nucleus.The positions of other organelles were not determined in this study, and future work would involve investigations into whether the organelle positioning defect was specific to nucleus positioning, or whether a general disruption in polarity had occurred. It is also necessary to confirm that the increase in cell length was indeed at the posterior end of the cell through staining induced cells with anti-tyrosinated tubulin antibody.

In bloodstream form *AIR9* RNAi cell lines, organelle positioning defects were only observed in post-mitotic cells, suggesting that the organelle positioning defect at this life cycle stage could be cell cycle associated. It was not determined whether for this life cycle stage kinetoplasts or nuclei were abnormally positioned, or indeed whether the kinetoplasts apparently anterior to the adjacent nucleus was associated more frequently with the old or new flagellum. The association of an abnormally positioned kinetoplast and new flagellum has been observed previously during the downregulation of the axonemal protein PACRG (Dawe et al., 2005). Whilst no obvious motility defects were observed following AIR9 downregulation, suggesting that reduced motility is unlikely to account for the positioning defect, a higher proportion of abnormally positioned posterior kinetoplasts could suggest that the newly positioned basal body needs to be anchored into position following segregation, and as AIR9 is a cytoskeletal protein (see below), it could potentially be involved in anchoring organelles to the cytoskeleton.

AIR9 therefore plays a role in organelle positioning, predominantly in the procyclic life cycle stage, and while cytokinesis is also affected in this stage, it is likely that this represents a downstream effect of the organelle positioning defects. In the bloodstream form, organelle positioning was normal up until mitosis, and only a subset of post-mitotic cells showed abnormal relative positioning of nuclei and kinetoplasts. Thus the organelle positioning defect is more minor in this life cycle stage, and the cytokinesis furrowing defects observed, may occur as a direct effect of the downregulation of AIR9, particularly as some 2N2K cells with apparently normal N-K positioning were observed to be undergoing unequal furrow ingression. The observation of different *AIR9* RNAi phenotypes for different life cycle stages was not unexpected, as many aspects of the cell biology, and cell cycle regulation of procyclic and bloodstream form parasites are different.

Expression of AIR9 with an N-terminal tyGFP tag or C-terminal HA tag from the endogenous locus revealed that AIR9 is localised to the cytoskeleton but not to the flagella in both life cycle stages, which was confirmed through both microscopical analyses and cell fractionation studies. In addition, analysis of the dynamics of AIR9 depletion through endogenous expression of tyGFP:AIR9 in *AIR9* RNAi cell lines concurred with these observations, as depletion was first

observed at the posterior ends of cells where there is a greater turnover of microtubules. However, it cannot be concluded from these data whether AIR9 interacts directly with microtubules, or is localised to the microtubules by interaction with another MAP. Indeed, depletion of AIR9 did not cause obvious abnormalities in the organisation of subpellicular microtubules, as analysed by transmission electron microscopy, indicating that AIR9 is not crucial to the structure or stability of microtubules in *T. brucei*. To confirm the localisation of AIR9 it would be necessary to analyse the localisation of native AIR9 through the production of an antibody, as epitope tagging may have caused impairment of localisation. It is of great interest to determine how localisation to the cytoskeleton occurs. Given that the N-terminal microtubule binding domain of Trypanosoma AIR9 proteins is not conserved it would be interesting to see whether TbAIR9 can bind to microtubules, and if so which region of the protein is involved in the interaction. Attempts to determine a more specific localisation for AIR9 by immuno transmission electron microscopy were unsuccessful. Therefore, it was not possible to determine whether AIR9 decorates microtubules as has been previously observed for other microtubule-associated proteins. Potentially, investigations into the microtubule binding ability of AIR9 could involve binding assays using preformed microtubules and recombinant versions of AIR9.

Localisation of AIR9 to the cytoskeleton may allow AIR9 to have roles in cell polarity, or anchoring of organelles to the cytoskeleton. Given that the C-terminal A9 domains of AIR9 are conserved in *T. brucei* AIR9, it is possible that AIR9 is a scaffold protein whose potential binding partners could include signalling proteins, such as those involved in cytokinesis. PLK, which has been shown to bind and phosphorylate microtubule-associated proteins in other organisms (Yarm, 2002;Archambault et al., 2008), and components of the CPC could be potential binding partners. The global cytoskeletal localisation does not preclude a specific role for AIR9 at the furrow, as potentially post-translational modifications of AIR9 or association with particular binding partners may specifically occur at the future site of furrow ingression.

8.3 Microtubule inhibitors

Application of inhibitors of microtubule dynamics in other Trypanosomatid species has been shown previously to inhibit cytokinesis (Baum et al., 1981;Grellier et al., 1999); although phenotype analysis of *T. brucei* cells treated with different inhibitors of microtubule dynamics has not previously been reported.

Treatment of *T. brucei* cells with both destabilising and stabilising agents led to inhibition of cytokinesis. Treatment of bloodstream form cells with Vinca alkaloids led to an accumulation of post mitotic cells displaying stalled furrow ingression. Vincristine treated cells were examined by scanning electron microscopy, and qualitative analysis revealed that the furrow had ingressed approximately 75 % of the whole cell length. Furrow ingression may be subject to regulation by checkpoints at specific points, as downregulation of molecular regulators PLK, PK50 and MOB1B similarly caused arrested furrow ingression (Hammarton et al., 2007;Ma et al., 2010;Hammarton et al., 2005). However detailed analysis is required in order to determine whether furrow ingression arrested at a similar point in these RNAi cell lines, and for vincristine treated cells. Treatment of bloodstream and procyclic form cells with taxol caused different cytokinesis defects. Bloodstream form cells displayed impaired cytokinesis initiation, whilst procyclic form cells displayed abnormal cleavage plane positioning. Taxol treatment caused paralysis in both cell types, and it is possible that taxol has a potent effect on flagellar tubulin, and that impaired motility contributed to the cytokinesis defects observed, as flagellar motility is important for cytokinesis in *T. brucei* (section X). However, the effect of microtubule inhibitors on cell morphology whereby cells became rounded (taxol) or exhibited bulging at the central regions and long pointed tips (vinblastine), suggested that these inhibitors were interacting directly with subpellicular microtubules, implying that inhibition of microtubule dynamics caused the cytokinesis defects described.

Application of the microtubule inhibitor vinblastine to procyclic form cells expressing tyGFP:AIR9 affected the localisation of AIR9. Instead of brightly staining the outline of the cell, tyGFP:AIR9 exhibited a diffuse staining pattern,

similar to cytoplasmic proteins. It is possible that vinblastine could displace microtubule-associated proteins which share the same binding site within tubulin heterodimers. These could potentially include AIR9, or alternatively, other microtubule associated proteins involved in AIR9 localisation at the cytoskeleton. Vinca alkaloid treatment may also affect the localisation of microtubule-associated proteins in *T. cruzi*. Treatment of *T. cruzi* epimastigotes with Vincristine caused a decrease in staining with anti-polyglutamylated tubulin antibody. This was thought to result from displacement of microtubule-associated proteins from microtubules as oppose to a decrease in post-translational modification of tubulin, as the total amount of polyglutamylated tubulin in cell lysates was unchanged (Grellier et al., 1999).

8.4 Regulation of Polo-like kinase activity *in vitro* and *in vivo*

PLK has previously been shown to be important for cytokinesis (Hammarton et al., 2007;Kumar and Wang, 2006), and to have additional roles in basal body and Golgi duplication (Hammarton et al., 2007;Graffenried et al., 2008). However it is not known how the activity of *T. brucei* PLK is regulated.

To investigate the regulation of PLK activity, a series of recombinant versions of PLK were generated. 6XHis:PLK was found to prolifically autophosphorylate, and removal of these phosphorylations through lambda protein phosphatase treatment impaired the ability of 6XHis:PLK to transphosphorylate generic kinase substrates. This could be an *in vitro* artefact, as bacterially expressed kinases have been known to lose substrate specificity (reviewed in (Peck, 2006)), and therefore attempts to perform mass spectrometry analysis on ty:PLK extracted from trypanosome lysates were attempted. Unfortunately these experiments were not successful, and to verify the relevance of these phosphorylation sites it may be necessary to mutate some of these residues and assess the activity of *T. brucei* expressed PLK. An ideal situation would be to express mutated versions of PLK in a null mutant genetic background, and verify whether the mutated proteins can compensate for the loss of function phenotype.

T. brucei PLK contains a conserved T198 residue at the T-loop. This residue is phosphorylated by upstream kinases in other organisms resulting in stimulation of PLK activity (section X). In humans, Aur-A is a major regulator at this site, and as AUK1 is conserved in *T. brucei* it was thought phosphorylation at this site by AUK1 may regulate the activity of *T. brucei* PLK. Substitution of T198 with non-polar (A/V) or phosphomimetic (D) residues revealed that T198 is important for *in vitro* activity. All three T-loop mutants displayed reduced auto and *trans* phosphorylation. Whilst this was expected for T198A and T198V 6XHis:PLK mutants, it was not expected for 6XHis:PLK T198D. However, phosphomimetic substitutions have previously been found to cause a reduction in kinase activity, and it was suggested this could be a result of steric constraints preventing effective mimicry of a phosphate group by a negatively charged amino acid side chain at the site of the substitution (Millward et al., 1999). Analysis of the activity of *T. brucei* expressed PLK T-loop mutants, and phenotype analysis of procyclic form cells overexpressing ty:PLK T198V or tyPLK T198D implied that T-loop is not a site of *in vivo* regulation. Alternatively, it may be the case that *T. brucei* PLK is constitutively active, and that activity of PLK may be influenced by other factors such as localisation or binding partners.

To assess whether activity is negatively regulated by *trans* association with the polo-box domain, binding experiments and kinase assays were carried out using ty:PLK and 6XHis:PLK proteins. Although tyPLK was found to bind to recombinant PBD, no inhibitory effect on the activity of 6XHis:PLK was detected. Further, the PBD was found to be phosphorylated by the full length kinase, which has not previously been reported, but was consistent with the identification of autophosphorylated residues within the PBD. Recombinant kinase domain (GST:KD) was not active, and it was therefore not possible to assess whether deletion of the PBD stimulates activity. Given the time constraints of this study it was not possible to attempt other recombinant versions of the KD, and it is likely that the KD requires downstream structural motifs for correct folding and activity. As PLK localises to the FAZ in *T. brucei* cells, it is possible that PLK phosphorylates cytoskeletal proteins. Future investigations could involve determination of substrates through *in vitro* kinase assays with cytoskeletal preparations and recombinant AIR9.

Generation of recombinant active PLK was important step towards assessing whether PLK could be a good drug target, and although high throughput inhibitor screening using 6XHis:PLK purified in this study failed to identify suitable compounds (work carried out by Raffaella Grimaldi, University of Dundee). PLK is a major drug target in a number of human cancers due to the association of elevated levels of PLK1 in various human tumours, and it is now known that PLK1 is a negative regulator of p53 in carcinogenisis (reviewed in (Strebhardt, 2010)). This may provide an opportunity to take the 'piggy back' approach to drug design. The potential for treating cancers using inhibitors of human PLK1 PBD are currently being explored (Liao et al., 2010), and it is possible that compounds directed towards the PBD might be effective at inhibiting *T. brucei* PLK through impairing its ability to localise to the FAZ or basal bodies *in vivo*. Also, new compounds are being developed to target PLK1 in its inactive conformation, which allows greater selectivity due to the accessibility of a hydrophobic pocket containing less well conserved residues when PLK1 is in the inactive conformation (Keppner et al., 2010). Such an approach could also be used in drug design for *T. brucei* PLK to increase specificity against the *T. brucei* as oppose to human PLK proteins.

8.5 Conclusions and future directions

Characterisation of a novel cytoskeleton associated protein: AIR9, revealed a role for this protein in cleavage plane determination and nuclear positioning. How the cleavage plane is determined is not well understood in *T. brucei*, and the identification of a protein involved in this process will hopefully lead to further understanding of how this occurs. An area for future study could be to establish whether AIR9 can bind to microtubules, and to determine possible binding partners. It is also important to verify the localisation of AIR9 through the generation of an antibody and analysis of localisation of natively expressed AIR9.

Inhibition of microtubule dynamics through the application of inhibitors of microtubule stability revealed a role for microtubule dynamics in both furrow ingression and cleavage plane positioning. Furrow ingression in *T. brucei* occurs by divergent mechanisms, and increasing knowledge of this process is crucial to

further understanding of *T. brucei* cytokinesis. A future focus for research into the role of microtubule dynamics in cytokinesis could involve analysis of vinca alkaloid treated bloodstream form cells stalled at furrow ingression by transmission electron microscopy, in order to observe the organisation of microtubules at the cleavage furrow. In addition, analysis of the extent of furrow ingression in vincristine treated bloodstream form cells and cells depleted of PLK or other regulators of furrow ingression may be a useful approach for investigations into the potential existence of a furrow ingression checkpoint. Vinca alkaloid treatment may prove to be a useful tool in enriching for cells with furrows, although as with all inhibitors, it must be taken into account that off target effects may cloud results.

Investigations into the regulation of PLK activity resulted in the generation of soluble and active recombinant protein, production of a series of mutant versions of recombinant PLK, and the generation of cell lines overexpressing versions of PLK where the T-loop residue T198 was substituted with valine or aspartic acid. PLK was found to exhibit prolific autophosphorylation which was shown to be important for activity. In addition, the T-loop residue T198 was found to be required for *in vitro* but not *in vivo* activity. Finally, regulation through autoinhibition via interaction with the PBD was shown to be unlikely. As PLK is an important regulator of cytokinesis in *T. brucei*, knowledge of how the activity of this protein is regulated could be important for furthering understanding of how molecular regulators are involved in directing the physical events which occur in cytokinesis. Also, given the importance of PLK1 in human cancers, there is real potential for drug development against *T. brucei* PLK using the ‘piggy back’ approach.

There are many areas for future research into the regulation and function of PLK. It is crucial that the relevance of the sites of autophosphorylation of recombinant PLK is established, as at present it is not known whether this is an *in vitro* artefact resulting from indiscriminate activity of the kinase, or whether these are real sites of autophosphorylation. This could be assessed by determination of the phosphorylation sites for ty:PLK. Whilst attempts to perform this experiment failed in this study, it may be useful in future investigations to extract PLK from cells which have been synchronised in order to enrich for PLK. It is also important to establish whether the PBD can direct

localisation of PLK. This could be achieved by analysing the localisation of a C-terminally truncated version of PLK *in vivo*. In addition, the effects of substituting residues H705 and K707 with alanine residues on the localisation of full length PLK may establish whether the potential 'His-Lys' pincer is important for localisation to phosphorylated substrates *in vivo*. Since a recombinant version of the PLK PBD was generated in this study, recombinant PBD could be used to identify binding partners of PLK from *T. brucei* cell lysates. Similarly 6XHis:PLK could be used to identify potential PLK substrates, potentially through the screening of a phage display library that was recently generated in the Hammarton lab.

9 References

Absalon, S., T.Blisnick, M.Bonhivers, L.Kohl, N.Cayet, G.Toutirais, J.Buisson, D.Robinson, and P.Bastin. 2008a. Flagellum elongation is required for correct structure, orientation and function of the flagellar pocket in Trypanosoma brucei. *J Cell Sci* 121:3704-3716.

Absalon, S., L.Kohl, C.Branche, T.Blisnick, G.Toutirais, F.Rusconi, J.Cosson, M.Bonhivers, D.Robinson, and P.Bastin. 2007a. Basal Body Positioning Is Controlled by Flagellum Formation in Trypanosoma brucei. *Plos One* 2.

Absalon, S., T.Blisnick, L.Kohl, G.Toutirais, G.Dore, D.Julkowska, A.Tavenet, and P.Bastin. 2008b. Intraflagellar Transport and Functional Analysis of Genes Required for Flagellum Formation in Trypanosomes. *Molecular Biology of the Cell* 19:929-944.

Absalon, S., L.Kohl, C.Branche, T.Blisnick, G.Toutirais, F.Rusconi, J.Cosson, M.Bonhivers, D.Robinson, and P.Bastin. 2007b. Basal body positioning is controlled by flagellum formation in Trypanosoma brucei. *Plos One* 2:1-16.

Affolter, M., A.Hemphill, I.Roditi, N.Muller, and T.Seebeck. 1994. The Repetitive Microtubule-Associated Proteins Marp-1 and Marp-2 of Trypanosoma-Brucei. *Journal of Structural Biology* 112:241-251.

Al Bassam, J., N.A.Larsen, A.A.Hyman, and S.C.Harrison. 2007. Crystal structure of a TOG domain: Conserved features of XMAP215/Dis1-family TOG domains and implications for tubulin binding. *Structure* 15:355-362.

Al Bassam, J., R.S.Ozer, D.Safer, S.Halpain, and R.A.Milligan. 2002. MAP2 and tau bind longitudinally along the outer ridges of microtubule protofilaments. *Journal of Cell Biology* 157:1187-1196.

Alexandru, G., F.Uhlmann, K.Mechtler, M.A.Poupart, and K.Nasmyth. 2001. Phosphorylation of the cohesin subunit Scc1 by Polo/Cdc5 kinase regulates sister chromatid separation in yeast. *Cell* 105:459-472.

Alsford, S. and D.Horn. 2008. Single-locus targeting constructs for reliable regulated RNAi and transgene expression in Trypanosoma brucei. *mbp* 161:76-79.

Alsford, S., T.Kawahara, L.Glover, and D.Horn. 2005. Tagging a T-brucei RRNA locus improves stable transfection efficiency and circumvents inducible expression position effects. *mbp* 144:142-148.

Alves, P.S., S.A.Godinho, and A.A.Tavares. 2006. The Drosophila orthologue of xPlkk1 is not essential for Polo activation and is necessary for proper contractile ring formation. *Experimental Cell Research* 312:308-321.

Amos, L.A. and D.Schlieper. 2005. Microtubules and maps. *Fibrous Proteins: Muscle and Molecular Motors* 71:257-+.

Angelopo, E. 1970. Pellicular Microtubules in Family Trypanosomatidae. *Journal of Protozoology* 17:39-&.

Archambault, V., P.P.D'Avino, M.J.Deery, K.S.Lilley, and D.M.Glover. 2008. Sequestration of Polo kinase to microtubules by phosphopriming-independent binding to Map205 is relieved by phosphorylation at a CDK site in mitosis. *Genes & Development* 22:2707-2720.

Archambault, V. and D.M.Glover. 2009. Polo-like kinases: conservation and divergence in their functions and regulation. *Nature Reviews Molecular Cell Biology* 10:265-275.

Bahler, J., A.B.Steever, S.Wheatley, Y.L.Wang, J.R.Pringle, K.L.Gould, and D.McCollum. 1998. Role of polo kinase and Mid1p in determining the site of cell division in fission yeast. *Journal of Cell Biology* 143:1603-1616.

Baines, A. and K.Gull. 2008. WCB is a C2 domain protein defining the plasma membrane - Sub-pellicular microtubule corset of kinetoplastid parasites. *Protist* 159:115-125.

Balaban, N. and R.Goldman. 1992. Isolation and Characterization of A Unique 15-Kilodalton Trypanosome Subpellicular Microtubule-Associated Protein. *Cell Motility and the Cytoskeleton* 21:138-146.

Balaban, N., H.K.Waithaka, A.R.Njogu, and R.Goldman. 1989. Isolation of A Subpellicular Microtubule Protein from Trypanosoma-Brucei That Mediates Crosslinking of Microtubules. *Cell Motility and the Cytoskeleton* 14:393-400.

Balaban, N., H.K.Waithaka, A.R.Njogu, and R.Goldman. 1995. Intracellular Antigens (Microtubule-Associated Protein Copurified with Glycosomal Enzymes) - Possible Vaccines Against Trypanosomiasis. *Journal of Infectious Diseases* 172:845-850.

Balasegaram, M., H.Young, F.Chappluis, G.Priotto, M.E.Raguenaud, and F.Checchi. 2009. Effectiveness of melarsoprol and eflornithine as first-line regimens for gambiense sleeping sickness in nine Medecins Sans Frontieres programmes. *Trans R Soc Trop Med Hyg* 103:280-290.

Baral, T.N., S.Magez, B.Stijlemans, K.Conrath, B.Vanhollebeke, E.Pays, S.Muyldermans, and P.De Baetselier. 2006. Experimental therapy of African trypanosomiasis with a nanobody-conjugated human trypanolytic factor. *Nature Medicine* 12:580-584.

Baron, D.M., Z.P.Kabututu, and K.L.Hill. 2007a. Stuck in reverse: loss of LC1 in Trypanosoma brucei disrupts outer dynein arms and leads to reverse flagellar beat and backward movement. *J Cell Sci* 120:1513-1520.

Baron, D.M., K.S.Ralston, Z.P.Kabututu, and K.L.Hill. 2007b. Functional genomics in Trypanosoma brucei identifies evolutionarily conserved components of motile flagella. *J Cell Sci* 120:478-491.

Barr, F.A., H.H.W.Sillje, and E.A.Nigg. 2004. Polo-like kinases and the orchestration of cell division. *Nature Reviews Molecular Cell Biology* 5:429-440.

Barrett, M.P., D.W.Boykin, R.Brun, and R.R.Tidwell. 2007. Human African trypanosomiasis: pharmacological re-engagement with a neglected disease. *British Journal of Pharmacology* 152:1155-1171.

Bastin, P., A.Bagherzadeh, K.R.Matthews, and K.Gull. 1996. A novel epitope tag system to study protein targeting and organelle biogenesis in Trypanosoma brucei. *mbp* 77:235-239.

Bastin, P., K.Ellis, L.Kohl, and K.Gull. 2000. Flagellum ontogeny in trypanosomes studied via an inherited and regulated RNA interference system. *J Cell Sci* 113:3321-3328.

Bastin, P., T.J.Pullen, T.Sherwin, and K.Gull. 1999. Protein transport and flagellum assembly dynamics revealed by analysis of the paralysed trypanosome mutant *snl*-1. *J Cell Sci* 112:3769-3777.

Bauer, B., S.Amslerdelafosse, P.H.Clausen, I.Kabore, and J.Petrichbauer. 1995. Successful Application of Deltamethrin Pour on to Cattle in A Campaign Against Tsetse-Flies (Glossina Spp) in the Pastoral Zone of Samorogouan, Burkina-Faso. *Tropical Medicine and Parasitology* 46:183-189.

Baum, S.G., M.Wittner, J.P.Nadler, S.B.Horwitz, J.E.Dennis, P.B.Schiff, and H.B.Tanowitz. 1981. Taxol, A Microtubule Stabilizing Agent, Blocks the Replication of Trypanosoma-Cruzi. *Proceedings of the National Academy of Sciences of the United States of America-Biological Sciences* 78:4571-4575.

Berriman, M., E.Ghedin, C.Hertz-Fowler, G.Blandin, H.Renauld, D.C.Bartholomeu, N.J.Lennard, E.Caler, N.E.Hamlin, B.Haas, W.Bohme, L.Hannick, M.A.Aslett, J.Shallom, L.Marcello, L.H.Hou, B.Wickstead, U.C.M.Alsmark, C.Arrowsmith, R.J.Atkin, A.J.Barron, F.Bringaud, K.Brooks, M.Carrington, I.Cherevach, T.J.Chillingworth, C.Churcher, L.N.Clark, C.H.Corton, A.Cronin, R.M.Davies, J.Doggett, A.Djikeng, T.Feldblyum, M.C.Field, A.Fraser, I.Goodhead, Z.Hance, D.Harper, B.R.Harris, H.Hauser, J.Hostetter, A.Ivens, K.Jagels, D.Johnson, J.Johnson, K.Jones, A.X.Kerhornou, H.Koo, N.Larke, S.Landfear, C.Larkin, V.Leech, A.Line, A.Lord, A.MacLeod, P.J.Mooney, S.Moule, D.M.A.Martin, G.W.Morgan, K.Mungall, H.Norbertczak, D.Ormond, G.Pai, C.S.Peacock, J.Peterson, M.A.Quail, E.Rabbinowitsch, M.A.Rajandream, C.Reitter, S.L.Salzberg, M.Sanders, S.Schobel, S.Sharp, M.Simmonds, A.J.Simpson, L.Talton, C.M.R.Turner, A.Tait, A.R.Tivey, S.Van Aken, D.Walker, D.Wanless, S.L.Wang, B.White, O.White, S.Whitehead, J.Woodward, J.Wortman, M.D.Adams, T.M.Embley, K.Gull, E.Ullu, J.D.Barry, A.H.Fairlamb, F.Opperdoes, B.G.Barret, J.E.Donelson, N.Hall, C.M.Fraser, S.E.Melville, and N.M.El Sayed. 2005. The genome of the African trypanosome Trypanosoma brucei. *Science* 309:416-422.

Bhattacharya, G., J.Herman, D.Delfin, M.M.Salem, T.Barszcz, M.Mollet, G.Riccio, R.Brun, and K.A.Werbovetz. 2004. Synthesis and antitubulin activity of N-1- and N-4-substituted 3,5-dinitro sulfanilamides against African trypanosomes and Leishmania. *Journal of Medicinal Chemistry* 47:1823-1832.

Biebinger, S., L.E.Wirtz, P.Lorenz, and C.Clayton. 1997. Vectors for inducible expression of toxic gene products in bloodstream and procyclic Trypanosoma brucei. *mbp* 85:99-112.

Bodyl, A., P.Mackiewicz, and R.Milanowski. 2010. Did Trypanosomatid Parasites Contain a Eukaryotic Alga-Derived Plastid in Their Evolutionary Past? *J. Parasitol.* 96:465-475.

Bonhivers, M., S.Nowacki, N.Landrein, and D.R.Robinson. 2008. Biogenesis of the trypanosome endo-exocytotic organelle is cytoskeleton mediated. *Plos Biology* 6:1033-1046.

Bonnet, C., D.Boucher, S.Lazereg, B.Pedrotti, K.Islam, P.Denoulet, and J.C.Larcher. 2001. Differential binding regulation of microtubule-associated proteins MAP1A, MAP1B, and MAP2 by tubulin polyglutamylation. *J. Biol. Chem.* 276:12839-12848.

Branche, C., L.Kohl, G.Toutirais, J.Buisson, J.Cosson, and P.Bastin. 2006. Conserved and specific functions of axoneme components in trypanosome motility. *J Cell Sci* 119:3443-3455.

Briggs, L.J., P.G.McKean, A.Baines, F.Moreira-Leite, J.Davidge, S.Vaughan, and K.Gull. 2004. The flagella connector of Trypanosoma brucei: an unusual mobile transmembrane junction. *J Cell Sci* 117:1641-1651.

Broadhead, R., H.R.Dawe, H.Farr, S.Griffiths, S.R.Hart, N.Portman, M.K.Shaw, M.L.Ginger, S.J.Gaskell, P.G.Mckean, and K.Gull. 2006. Flagellar motility is required for the viability of the bloodstream trypanosome. *Nature* 440:224-227.

Brun, R. and M.Schonenberger. 1979. Cultivation and *in vitro* cloning of procyclic forms of *Trypanosoma brucei* in a semi-defined medium. *Acta Trop.* 36:289-292.

Burchmore, R.J.S., P.O.J.Ogbunude, B.Enanga, and M.P.Barrett. 2002. Chemotherapy of human African trypanosomiasis. *Current Pharmaceutical Design* 8:257-267.

Burkard, M.E., C.L.Randall, S.Larochelle, C.Zhang, K.M.Shokat, R.P.Fisher, and P.V.Jallepalli. 2007. Chemical genetics reveals the requirement for Polo-like kinase 1 activity in positioning RhoA and triggering cytokinesis in human cells. *Proceedings of the National Academy of Sciences of the United States of America* 104:4383-4388.

Buschmann, H., J.Chan, L.Sanchez-Pulido, M.A.Andrade-Navarro, J.H.Doonan, and C.W.Lloyd. 2006. Microtubule-associated AIR9 recognizes the cortical division site at preprophase and cell-plate insertion. *Current Biology* 16:1938-1943.

Buschmann, H., L.Sanchez-Pulido, M.A.Andrade-Navarro, and C.W.Lloyd. 2007. Homologues of Arabidopsis Microtubule-Associated AIR9 in Trypanosomatid Parasites: Hints on Evolution and Function. *Plant Signal Behav* 2:296-299.

Caljon, G., A.J.Van Den, B.Stijlemans, M.Coosemans, P.De Baetselier, and S.Magez. 2006. Tsetse fly saliva accelerates the onset of Trypanosoma brucei infection in a mouse model associated with a reduced host inflammatory response. *Infect. Immun.* 74:6324-6330.

Cerutti, H. and J.A.Casas-Mollano. 2006. On the origin and functions of RNA-mediated silencing: from protists to man. *Current Genetics* 50:81-99.

Chan, M.M. and D.Fong. 1990. Inhibition of leishmanias but not host macrophages by the antitubulin herbicide trifluralin. *Science* 249:924-926.

Chan, M.M. and D.Fong. 1994. Plant Microtubule Inhibitors Against Trypanosomatids. *Parasitology Today* 10:448-451.

Chan, M.M.Y., M.Grogl, C.C.Chen, E.J.Bienen, and D.Fong. 1993. Herbicides to Curb Human Parasitic Infections - Invitro and Invivo Effects of Trifluralin on the Trypanosomatid Protozoans. *Proceedings of the National Academy of Sciences of the United States of America* 90:5657-5661.

Chanez, A.L., A.B.Hehl, M.Engstler, and A.Schneider. 2006. Ablation of the single dynamin of T-brucei blocks mitochondrial fission and endocytosis and leads to a precise cytokinesis arrest. *J Cell Sci* 119:2968-2974.

Chen, Y.L., C.H.Hung, T.Burderer, and G.S.M.Lee. 2003. Development of RNA interference revertants in Trypanosoma brucei cell lines generated with a double stranded RNA expression construct driven by two opposing promoters. *mbp* 126:275-279.

Cheng, K.Y., E.D.Lowe, J.Sinclair, E.A.Nigg, and L.N.Johnson. 2003. The crystal structure of the human polo-like kinase-1 polo box domain and its phospho-peptide complex. *Embo Journal* 22:5757-5768.

Chowdhury, A.R., Z.Zhao, and P.T.Englund. 2007. Effect of hydroxyurea on procyclic Trypanosoma brucei: An unconventional mechanism for achieving synchronous growth. *Eukaryotic Cell*EC.

Clayton, C.E. 2002. Life without transcriptional control? From fly to man and back again. *Embo Journal* 21:1881-1888**.**

Cravchik, A., D.Reddy, and A.Matus. 1994. Identification of A Novel Microtubule-Binding Domain in Microtubule-Associated Protein-1A (Map1A). *J Cell Sci* 107:661-672.

Das, A., M.Gale, V.Carter, and M.Parsons. 1994. The Protein Phosphatase Inhibitor Okadaic Acid Induces Defects in Cytokinesis and Organellar Genome Segregation in Trypanosoma-Brucei. *J Cell Sci* 107:3477-3483.

Davidge, J.A., E.Chambers, H.A.Dickinson, K.Towers, M.L.Ginger, P.G.Mckean, and K.Gull. 2006. Trypanosome IFT mutants provide insight into the motor location for mobility of the flagella connector and flagellar membrane formation. *J Cell Sci* 119:3935-3943.

Dawe, H.R., H.Farr, N.Portman, M.K.Shaw, and K.Gull. 2005. The Parkin co-regulated gene product, PACRG, is an evolutionarily conserved axonemal protein that functions in outer-doublet microtubule morphogenesis. *J Cell Sci* 118:5421-5430.

De Luca, M., P.Lavia, and G.Guarguaglini. 2006. A functional interplay between Aurora-A, Plk1 and TPX2 at spindle poles - Plk1 controls centrosomal localization of Aurora-A and TPX2 spindle association. *Cell Cycle* 5:296-303.

Dean, S., R.Marchetti, K.Kirk, and K.R.Matthews. 2009. A surface transporter family conveys the trypanosome differentiation signal. *Nature* 459:213-U93.

Deborggraeve, S., F.Claes, T.Laurent, P.Mertens, T.Leclipteux, J.C.Dujardin, P.Herdewijn, and P.Buscher. 2006. Molecular dipstick test for diagnosis of sleeping sickness. *Journal of Clinical Microbiology* 44:2884-2889.

Delgado, M., P.Anderson, J.A.Garcia-Salcedo, M.Caro, and E.Gonzalez-Rey. 2008. Neuropeptides kill African trypanosomes by targeting intracellular compartments and inducing autophagic-like cell death. *Cell Death Differ* 16:406-416.

Dolan, M.T., C.G.Reid, and H.P.Voorheis. 1986. Calcium ions initiate the selective depolymerization of the pellicular microtubules in bloodstream forms of Trypanosoma brucei. *J Cell Sci* 80:123-140.

Durand-Dubief, M. and P.Bastin. 2003. TbAGO1, an argonaute protein required for RNA interference, is involved in mitosis and chromosome segregation in Trypanosoma brucei. *Bmc Biol* 1:2.

Elia, A.E.H., L.C.Cantley, and M.B.Yaffe. 2003a. Proteomic screen finds pSer/pThr-binding domain localizing Plk1 to mitotic substrates. *Science* 299:1228-1231.

Elia, A.E.H., P.Rellos, L.F.Haire, J.W.Chao, F.J.Ivins, K.Hoepker, D.Mohammad, L.C.Cantley, S.J.Smerdon, and M.B.Yaffe. 2003b. The molecular basis for phosphodependent substrate targeting and regulation of Plks by the Polo-box domain. *Cell* 115:83-95.

Ellinger-Ziegelbauer, H., H.Karasuyama, E.Yamada, K.Tsujikawa, K.Todokoro, and E.Nishida. 2000. Ste20-like kinase (SLK), a regulatory kinase for polo-like kinase (Plk) during the G2/M transition in somatic cells. *Genes to Cells* 5:491-498.

Elowe, S., S.Huemmer, A.Uldschmid, X.Li, and E.A.Nigg. 2007. Tension-sensitive Plk1 phosphorylation on BubR1 regulates the stability of kinetochore-microtubule interactions. *Genes & Development* 21:2205-2219.

Engstler, M., T.Pfohl, S.Herminghaus. Hydrodynamic flow-mediated protein sorting on the cell surface of trypanosomes. *Cell* 131:505-515, M.Boshart, G.Wiegertjes, N.Heddergott, and P.Overath. 2007. Hydrodynamic flow-mediated protein sorting on the cell surface of trypanosomes. *Cell* 131:505-515.

Erikson, E., T.A.J.Haystead, Y.W.Qian, and J.L.Maller. 2004. A feedback loop in the polo-like kinase activation pathway. *J. Biol. Chem.* 279:32219-32224.

Ersfeld, K., K.Asbeck, and K.Gull. 1998. Direct visualisation of individual gene organisation in *Trypanosoma brucei* by high-resolution in situ hybridisation. *Chromosoma* 107:237-240.

Farr, H. and K.Gull. 2009. Functional Studies of an Evolutionarily Conserved, Cytochrome b5 Domain Protein Reveal a Specific Role in Axonemal Organisation and the General Phenomenon of Post-division Axonemal Growth in Trypanosomes. *Cell Motility and the Cytoskeleton* 66:24-35.

Fennell, B.J., J.A.Naughton, J.Barlow, G.Brennan, I.Fairweather, E.Hoey, N.McFerran, A.Trudgett, and A.Bell. 2008. Microtubules as antiparasitic drug targets. *Expert Opinion on Drug Discovery* 3:501-518.

Fevre, E.M., P.G.Coleman, M.Odiit, J.W.Magona, S.C.Welburn, and M.E.J.Woolhouse. 2001. The origins of a new Trypanosoma brucei rhodesiense sleeping sickness outbreak in eastern Uganda. *Lancet* 358:625-628.

Field, M.C. and M.Carrington. 2004. Intracellular membrane transport systems in Trypanosoma brucei. *Traffic* 5:905-913.

Field, M.C. and M.Carrington. 2009. The trypanosome flagellar pocket. *Nature Reviews Microbiology* 7:775-786.

Figueiredo, L.M., G.A.M.Cross, and C.J.Janzen. 2009. Epigenetic regulation in African trypanosomes: a new kid on the block. *Nature Reviews Microbiology* 7:504-513.

Fijolek, A., A.Hofer, and L.Thelander. 2007. Expression, purification, characterization, and in vivo targeting of trypanosome CTP synthetase for treatment of African sleeping sickness. *J. Biol. **Chem.*** **282:11858-11865.**

Forsythe, G., R.McCulloch, and T.Hammarton. 2009. Hydroxyurea-induced synchronisation of bloodstream stage Trypanosoma brucei. *mbp* 164:131-136.

Frearson, J.A., S.Brand, S.P.McElroy, L.A.T.Cleghorn, O.Smid, L.Stojanovski, H.P.Price, M.L.Guther, L.S.Torrie, D.A.Robinson, I.Hallyburton, C.P.Mpamhanga, J.A.Brannigan, A.J.Wilkinson, M.Hodgkinson, R.Hui, W.Qiu, O.G.Raimi, D.M.F.van Aalten, R.Brenk, I.H.Gilbert, K.D.Read, A.H.Fairlamb, M.A.J.Ferguson, D.F.Smith, and P.G.Wyatt. 2010. N-myristoyltransferase inhibitors as new leads to treat sleeping sickness. *Nature* 464:728-732.

Gadelha, C., S.Rothery, M.Morphew, J.R.McIntosh, N.J.Severs, and K.Gull. 2009. Membrane domains and flagellar pocket boundaries are influenced by the cytoskeleton in African trypanosomes. *Proceedings of the National Academy of Sciences of the United States of America* 106:17425-17430.

Galanti, N., M.Galindo, V.Sabaj, I.Espinoza, and G.C.Toro. 1998. Histone Genes in Trypanosomatids. *Parasitology Today* 14:64-70.

Garcia-Alvarez, B., G.de Carcer, S.Ibanez, E.Bragado-Nilsson, and G.Montoya. 2007. Molecular and structural basis of polo-like kinase 1 substrate recognition: Implications in centrosomal localization. *Proceedings of the National Academy of Sciences of the United States of America* 104:3107-3112.

Genovese, G., D.J.Friedman, M.D.Ross, L.Lecordier, P.Uzureau, B.I.Freedman, D.W.Bowden, C.D.Langefeld, T.K.Oleksyk, A.L.U.Knob, A.J.Bernhardy, P.J.Hicks, G.W.Nelson, B.Vanhollebeke, C.A.Winkler,

J.B.Kopp, E.Pays, and M.R.Pollak. 2010. Association of Trypanolytic ApoL1 Variants with Kidney Disease in African Americans. *Science* 329:841-845.

Gibson, W., L.Peacock, V.Ferris, K.Williams, and M.Bailey. 2008. The use of yellow fluorescent hybrids to indicate mating in Trypanosoma brucei. *Parasites & Vectors* 1:4.

Gourguechon, S., J.M.Savich, and C.C.Wang. 2007. The multiple roles of cyclin E1 in controlling cell cycle progression and cellular morphology of Trypanosoma brucei. *Journal of Molecular Biology* 368:939-950.

Gourguechon, S. and C.C.Wang. 2009. CRK9 contributes to regulation of mitosis and cytokinesis in the procyclic form of Trypanosoma brucei. *Bmc Cell Biology* 10.

Graffenried, C., H.Ho, and G.Warren. 2008. Polo-like kinase is required for Golgi and bilobe biogenesis in Trypanosoma brucei. *Journal of Cell Biology* 181:431-438.

Graham, T.M., A.Tait, and G.Hide. 1998. Characterisation of a polo-like protein kinase gene homologue from an evolutionary divergent eukaryote, Trypanosoma brucei. *Gene* 207:71-77**.**

Grellier, P., V.Sinou, N.Garreau-de Loubresse, E.Bylen, Y.Boulard, and J.Schrevel. 1999. Selective and reversible effects of vinca alkaloids on Trypanosoma cruzi epimastigote forms: Blockage of cytokinesis without inhibition of the organelle duplication. *Cell Motility and the Cytoskeleton* 42:36-47.

Griffiths, S., N.Portman, P.R.Taylor, S.Gordon, M.L.Ginger, and K.Gull. 2007. RNA interference mutant induction in vivo demonstrates the essential nature of trypanosome flagellar function during mammalian infection. *Eukaryotic Cell* 6:1248-1250.

Gull, K., S.Alsford, and K.Ersfeld. 1998. Segregation of minichromosomes in trypanosomes: implications for mitotic mechanisms. *Trends in Microbiology* 6:319-323.

Haines, L.R., J.M.Thomas, A.M.Jackson, B.A.Eyford, M.Razavi, C.N.Watson, B.Gowen, R.E.W.Hancock, and T.W.Pearson. 2009. Killing of Trypanosomatid Parasites by a Modified Bovine Host Defense Peptide, BMAP-18. *Plos Neglected Tropical Diseases* 3.

Hait, W., E.Rubin, E.Alli, and S.Goodin. 2007. Tubulin Targeting Agents. *Update on Cancer Therapeutics* 2:1-18.

Hammarton, T.C. 2007. Cell cycle regulation in Trypanosoma brucei. *mbp* 153:1-8.

Hammarton, T.C., J.Clark, F.Douglas, M.Boshart, and J.C.Mottram. 2003. Stage-specific differences in cell cycle control in *Trypanosoma brucei* revealed by RNA interference of a mitotic cyclin. *J. Biol. Chem*. 278:22877-22886.

Hammarton, T.C., M.Engstler, and J.C.Mottram. 2004. The *Trypanosoma brucei* cyclin, CYC2, is required for cell cycle progression through G1 phase and maintenance of procyclic **form cell morphology. *J. Biol. Chem.* 279:24757-24764.**

Hammarton, T.C., S.Kramer, L.Tetley, M.Boshart, and J.C.Mottram. 2007. Trypanosoma brucei Polo-like kinase is essential for basal body duplication, kDNA segregation and cytokinesis. *Mol. Microbiol.* 65:1229-1248.

Hammarton, T.C., S.G.Lillico, S.C.Welburn, and J.C.Mottram. 2005. Trypanosoma brucei MOB1 is required for accurate and efficient cytokinesis but not for exit from mitosis. *Mol. Microbiol.* 56:104-116.

Hannaert, V., E.Saavedra, F.Duffieux, J.P.Szikora, D.J.Rigden, P.A.M.Michels, and F.R.Opperdoes. 2003a. Plant-like traits associated with metabolism of Trypanosoma parasites. *Proceedings of the National Academy of Sciences of the United States of America* 100:1067-1071.

Hannaert, V., F.Bringaud, F.R.Opperdoes, and P.A.Michels. 2003b. Evolution of energy metabolism and its compartmentation in Kinetoplastida. *Kinetoplastid Biology and Disease* 2:Unpaginated.

Harrington, J., J.Widener, S.Stephens, T.Johnson, M.Francia, P.Capewell, A.Macleod, and S.Hajduk. 2010. The Plasma Membrane of Bloodstream-form African Trypanosomes Confers Susceptibility and Specificity to Killing by Hydrophobic Peptides. *J. Biol. Chem.* 285:28659-28666.

He, C.Y., H.H.Ho, H.Malsam, C.Chalouni, C.M.West, E.Ullu, D.Toomre, and G.Warren. 2004. Golgi duplication in Trypanosoma brucei. *Journal of Cell Biology* 165:313-321.

He, C.Y., M.Pypaert, and G.Warren. 2005. Golgi duplication in Trypanosoma brucei requires Centrin2. *Science* 310:1196-1198.

He, X.Y. and M.Dembo. 1997. On the mechanics of the first cleavage division of the sea urchin egg. *Experimental Cell Research* 233:252-273.

Hemphill, A., T.Seebeck, and D.Lawson. 1991. The Trypanosoma-Brucei Cytoskeleton - Ultrastructure and Localization of Microtubule-Associated and Spectrin-Like Proteins Using Quick-Freeze, Deep-Etch, Immunogold Electron-Microscopy. *Journal of Structural Biology* 107:211-220.

Hertz-Fowler, C., K.Ersfeld, and K.Gull. 2001. CAP5.5, a life-cycle-regulated, cytoskeleton-associated protein is a member of a novel family of calpain-related proteins in Trypanosoma brucei. *mbp* 116:25-34**.**

Hillen, W. and C.Berens. 1994. Mechanisms Underlying Expression of TN10 Encoded Tetracycline Resistance. *Annual Review of Microbiology* 48:345-369.

Hirumi, H. and K.Hirumi. 1989. Continuous cultivation of *Trypanosoma brucei* blood stream forms in a medium containing a low concentration of serum-protein without feeder cell-layers. *J. Parasitol.* 75:985-989.

Hochegger, H., S.Takeda, and T.Hunt. 2008. Cyclin-dependent kinases and cell-cycle transitions: does one fit all? *Nat Rev Mol Cell Biol* 9:910-916.

Horton, R.M., Z.L.Cai, S.N.Ho, and L.R.Pease. 1990. Gene-Splicing by Overlap Extension - Tailor-Made Genes Using the Polymerase Chain-Reaction. *Biotechniques* 8:528-&.

Howard, J. and A.A.Hyman. 2003. Dynamics and mechanics of the microtubule plus end. *Nature* 422:753-758.

Hutchings, N.R., J.E.Donelson, and K.L.Hill. 2002. Trypanin is a cytoskeletal linker protein and is required for cell motility in African trypanosomes. *Journal of Cell Biology* 156:867-877.

Ilemobade, A.A. 2009. Tsetse and trypanosomosis in Africa: The challenges, the opportunities. *Onderstepoort Journal of Veterinary Research* 76:35-40.

Jang, Y.J., C.Y.Lin, S.Ma, and R.L.Erikson. 2002a Functional studies on the role of the C-terminal domain of mammalian polo-like kinase. *Proceedings of the National Academy of Sciences of the United States of America* 99:1984-1989.

Jang, Y.J., S.Ma, Y.Terada, and R.L.Erikson. 2002b. Phosphorylation of threonine 210 and the role of serine 137 in the regulation of mammalian polo-like kinase. *J. Biol. Chem.* 277:44115-44120.

Janzen, C.J., S.B.Hake, J.E.Lowell, and G.A.M.Cross. 2006. Selective di- or trimethylation of histone H3 lysine 76 by two DOT1 homologs is important for cell cycle regulation in Trypanosoma brucei. *Molecular Cell* 23:497-507.

Job, D., O.Valiron, and B.Oakley. 2003. Microtubule nucleation. *Curr Opin Cell Biol* 15:111-117.

Johnson, T.M., R.Antrobus, and L.N.Johnson. 2008. Plk1 activation by Ste20-like kinase (Slk) phosphorylation and polo-box phosphopeptide binding assayed with the substrate translationally controlled tumor protein (TCTP). *Biochemistry* 47:3688-3696.

Jurgens, G. 2005. Cytokinesis in higher plants. *Annual Review of Plant Biology* 56:281-299.

Kabani, S., M.Waterfall, and K.R.Matthews. 2010. Cell-cycle synchronisation of bloodstream forms of Trypanosoma brucei using Vybrant DyeCycle Violet-based sorting. *mbp* 169:59-62.

Kar, S., J.Fan, M.J.Smith, M.Goedert, and L.A.Amos. 2003. Repeat motifs of tau bind to the insides of microtubules in the absence of taxol. *Embo Journal* 22:70-77.

Kelley, L.A. and M.J.E.Sternberg. 2009. Protein structure prediction on the Web: a case study using the Phyre server. *Nature Protocols* 4:363-371.

Kelly, S., J.Reed, S.Kramer, L.Ellis, H.Webb, J.Sunter, J.Salje, N.Marinsek, K.Gull, B.Wickstead, and M.Carrington. 2007. Functional genomics in Trypanosoma brucei: A collection of vectors for the expression of tagged proteins from endogenous and ectopic gene loci. *mbp* 154:103-109.

Kelm, O., M.Wind, W.D.Lehmann, and E.A.Nigg. 2002. Cell cycle-regulated phosphorylation of the Xenopus polo-like kinase Plx1. *J. Biol. Chem.* 277:25247-25256.

Keppner, S., E.Proschak, M.Kaufmann, K.Strebhardt, G.Schneider, and B.Spankuch. 2010. Biological impact of freezing Plk1 in its inactive conformation in cancer cells. *Cell Cycle* 9:761-774.

Kgori, P.M., S.Modo, and S.J.Torr. 2006. The use of aerial spraying to eliminate tsetse from the Okavango Delta of Botswana. *Acta Trop.* 99:184-199.

Kieft, R., P.Capewell, M.Turner, N.Veitch, A.MacLeod, and S.Hajduk. 2010. Mechanism of *Trypanosoma brucei gambiense* (group 1) resistance to human trypanosome lytic factor. *Proceedings of the National Academy of Sciences of the United States of America* 107:16137-16141.

Kivic, P.A. and P.L.Walne. 1984. An Evaluation of A Possible Phylogenetic Relationship Between the Euglenophyta and Kinetoplastida. *Origins of Life and Evolution of the Biosphere* 13:269-288.

Kleinschmidt, A. and E.Kinder. 1950. Electro-nenoptische Befunde an Rattentrypanosomen. *Zentralbl Bakt Abt I Orig* 156:219-224.

Klingbeil, M.M. and P.T.Englund. 2004. Closing the gaps in kinetoplast DNA network replication. *Proceedings of the National Academy of Sciences of the United States of America* 101:4333-4334.

Kohl, L., D.Robinson, and P.Bastin. 2003. Novel roles for the flagellum in cell morphogenesis and cytokinesis of trypanosomes. *Embo Journal* 22:5336-5346.

Kohl, L., T.Sherwin, and K.Gull. 1999. Assembly of the paraflagellar rod and the flagellum attachment zone complex during the Trypanosoma brucei cell cycle. *Journal of Eukaryotic Microbiology* 46:105-109.

Kothe, M., D.Kohls, S.Low, R.Coli, A.C.Cheng, S.L.Jacques, T.L.Johnson, C.Lewis, C.Loh, J.Nonomiya, A.L.Sheils, K.A.Verdries, T.A.Wynn, C.Kuhn, and Y.H.Ding. 2007. Structure of the catalytic domain of human polo-like kinase 1. *Biochemistry* 46:5960-5971.

Kumar, P. and C.C.Wang. 2006. Dissociation of cytokinesis initiation from mitotic control in a eukaryote. *Eukaryotic Cell* 5:92-102.

Lacomble, S., S.Vaughan, C.Gadelha, M.K.Morphew, M.K.Shaw, J.R.McIntosh, and K.Gull. 2010. Basal body movements orchestrate membrane organelle division and cell morphogenesis in Trypanosoma brucei. *J Cell Sci* 123:2884-2891.

LaCount, D.J., S.Bruse, K.L.Hill, and J.E.Donelson. 2000. Double-stranded RNA interference in Trypanosoma brucei using head-to-head promoters. *mbp* 111:67-76.

Lambrecht, F.L. 1985. Trypanosomes and Hominid Evolution. *Bioscience* 35:640-646.

Leander, B.S. 2004. Did trypanosomatid parasites have photosynthetic ancestors? *Trends in Microbiology* 12:251-258.

Lee, K.S., J.E.Park, Y.H.Kang, W.Zimmerman, N.K.Soung, Y.S.Seong, S.J.Kwak, and R.L.Erikson. 2008. Mechanisms of mammalian polo-like kinase 1 (Plk1) localization: Self-priming. *Cell Cycle* 7:141-145.

Lejon, V., V.Jamonneau, P.Solano, P.Atchade, D.Mumba, N.Nkoy, N.Bebronne, T.Kibonja, F.Balharbi, A.Wierckx, M.Boelaert, and P.Buscher. 2006. Detection of trypanosome-specific antibodies in saliva, towards non-invasive serological diagnosis of sleeping sickness. *Trop Med Int Health* 11:620-627.

Li, H., X.S.Liu, X.Yang, Y.Wang, Y.Wang, J.R.Turner, and X.Liu. 2010a. Phosphorylation of CLIP-170 by Plk1 and CK2 promotes timely formation of kinetochore-microtubule attachments. *EMBO J* 29:2953-2965.

Li, Z., T.Umeyama, Z.Y.Li, and C.C.Wang. 2010b. Polo-Like Kinase Guides Cytokinesis in Trypanosoma brucei through an Indirect Means. *Eukaryotic Cell* 9:705-716.

Li, Z., T.Umeyama, and C.C.Wang. 2008a. The chromosomal passenger complex and a mitotic kinesin interact with the Tousled-like kinase in trypanosomes to regulate mitosis and cytokinesis. *Plos One* 3:e3814.

Li, Z., T.Umeyama, and C.C.Wang. 2009. The Aurora kinase in *Trypanosoma brucei* plays distinctive roles in metaphase-anaphase transition and cytokinetic initiation. *Plos Pathogens* 5:e1000575.

Li, Z. and C.C.Wang. 2003. A PHO80-like cyclin and a B-type cyclin control the cell cycle of the procyclic form of *Trypanosoma brucei*. *J. Biol. Chem.* 278:20652-20658.

Li, Z.Y., X.M.Tu, and C.C.Wang. 2006. Okadaic acid overcomes the blocked cell cycle caused by depleting Cdc2-related kinases in Trypanosoma brucei. *Experimental Cell Research* 312:3504-3516.

Li, Z., J.H.Lee, F.Chu, A.L.Burlingame, A.Gunzl, and C.C.Wang. 2008b. Identification of a Novel Chromosomal Passenger Complex and Its Unique Localization during Cytokinesis in Trypanosoma brucei. *Plos One* 3:Article.

Li, Z. and C.C.Wang. 2008. KMP-11, a Basal Body and Flagellar Protein, Is Required for Cell Division in Trypanosoma brucei. *Eukaryotic Cell* 7:1941-1950.

Liao, C.Z., J.E.Park, J.K.Bang, M.C.Nicklaus, and K.S.Lee. 2010. Probing Binding Modes of Small Molecule Inhibitors to the Polo-Box Domain of Human Polo-like Kinase 1. *Acs Medicinal Chemistry Letters* 1:110-114.

Lowell, J.E. and G.A.M.Cross. 2004. A variant histone H3 is enriched at telomeres in Trypanosoma brucei. *J Cell Sci* 117:5937-5947.

Lowery, D.M., K.R.Clauser, M.Hjerrild, D.Lim, J.Alexander, K.Kishi, S.E.Ong, S.Gammeltoft, S.A.Carr, and M.B.Yaffe. 2007. Proteomic screen defines the Polo-box domain interactome and identifies Rock2 as a Plk1 substrate. *Embo Journal* 26:2262-2273.

Lowery, D.M., D.H.Mohammad, A.E.H.Elia, and M.B.Yaffe. 2004. The Polo-box domain - A molecular integrator of mitotic kinase cascades and Polo-like kinase function. *Cell Cycle* 3:128-131.

Lubega, G.W., D.K.Byarugaba, and R.K.Prichard. 2002. Immunization with a tubulin-rich preparation from Trypanosoma brucei confers broad protection against African trypanosomosis. *Experimental Parasitology* 102:9-22.

Lythgoe, K.A., L.J.Morrison, A.F.Read, and J.D.Barry. 2007. Parasite-intrinsic factors can explain ordered progression of trypanosome antigenic variation. *Proc Natl Acad Sci U S A* 104:8095-8100.

Ma, J.T., C.Benz, R.Grimaldi, C.Stockdale, P.Wyatt, J.Frearson, and T.C.Hammarton. 2010. Nuclear DBF-2-related Kinases Are Essential Regulators of Cytokinesis in Bloodstream Stage Trypanosoma brucei. *J. Biol. Chem.* 285:15356-15368.

Macrae, T.H. and K.Gull. 1990. Purification and Assembly Invitro of Tubulin from Trypanosoma-Brucei-Brucei. *Biochemical Journal* 265:87-93.

Maddox, A.S. and K.Oegema. 2003. Deconstructing cytokinesis. *Nature Cell Biology* 5:773-776.

Masocha, W., M.E.Rottenberg, and K.Kristensson. 2006. Minocycline impedes African trypanosome invasion of the brain in a murine model. *Antimicrob. Agents Chemother.* 50:1798-1804.

McCulloch, R. 2004. Antigenic variation in African trypanosomes: monitoring progress. *Trends in Parasitology* 20:117-121.

McGwire, B.S., C.L.Olson, B.F.Tack, and D.M.Engman. 2003. Killing of African trypanosomes by antimicrobial peptides. *Journal of Infectious Diseases* 188:146-152.

McGwire, B.S. and M.M.Kulkarni. 2010. Interactions of antimicrobial peptides with Leishmania and trypanosomes and their functional role in host parasitism. *Experimental Parasitology* 126:397-405.

Miller.J.H. 1972. Experiments in molecular genetics. Cold Spring Harbor Laboratory Press.

Millward, T.A., D.Hess, and B.A.Hemmings. 1999. Ndr protein kinase is regulated by phosphorylation on two conserved sequence motifs. *J. Biol. Chem.* 274:33847-33850.

Mineyuki, Y., J.Marc, and B.A.Palevitz. 1991. Relationship Between the Preprophase Band, Nucleus and Spindle in Dividing Allium Cotyledon Cells. *Journal of Plant Physiology* 138:640-649.

Moores, C.A., M.Perderiset, F.Francis, J.Chelly, A.Houdusse, and R.A.Milligan. 2004. Mechanism of microtubule stabilization by doublecortin. *Molecular Cell* 14:833-839.

Moores, C.A., F.Francis, M.Perderiset, and A.Houdusse. 2003. A double-take on MAPs. *Nat Struct Mol Biol* 10:314-316.

Moreira-Leite, F.F., T.Sherwin, L.Kohl, and K.Gull. 2001. A trypanosome structure involved in transmitting cytoplasmic information during cell division. *Science* 294:610-612.

Morrison, L.J., P.Majiwa, A.F.Read, and J.D.Barry. 2005. Probabilistic order in antigenic variation of Trypanosoma brucei. *International Journal for Parasitology* 35:961-972.

Mottram, J.C. and K.M.Grant. 1996. Leishmania mexicana p12(cks1), a homologue of fission yeast p13(suc1), associates with a stage-regulated histone H1 kinase. *Biochemical Journal* 316:833-839.

Motyka, S.A. and P.T.Englund. 2004. RNA interference for analysis of gene function in trypanosomatids. *Current Opinion in Microbiology* 7:362-368.

Muller, S., A.J.Wright, and L.G.Smith. 2009. Division plane control in plants: new players in the band. *Trends in Cell Biology* 19:180-188.

Murray, M., J.C.Trail, and G.D.D'leteren. 1990. Trypanotolerance in cattle and prospects for the control of trypanosomiasis by selective breeding. *Rev Sci Tech* 9:369-386.

Nare, B., S.Wring, C.Bacchi, B.Beaudet, T.Bowling, R.Brun, D.Chen, C.Ding, Y.Freund, E.Gaukel, A.Hussain, K.Jarnagin, M.Jenks, M.Kaiser, L.Mercer, E.Mejia, A.Noe, M.Orr, R.Parham, J.Plattner, R.Randolph, D.Rattendi, C.Rewerts, J.Sligar, N.Yarlett, R.Don, and R.Jacobs. 2010. Discovery of Novel Orally Bioavailable Oxaborole 6-carboxamides that Demonstrate Cure in a Murine Model of Late Stage Central Nervous System African Trypanosomiasis. *Antimicrob. Agents Chemother.*AAC.

Navarro, M. and K.Gull. 2001. A pol I transcriptional body associated with VSG mono-allelic expression in Trypanosoma brucei. *Nature* 414:759-763.

Neef, R., U.Gruneberg, R.Kopajtich, X.L.Li, E.A.Nigg, H.Sillje, and F.A.Barr. 2007. Choice of Plk1 docking partners during mitosis and cytokinesis is controlled by the activation state of Cdk1. *Nature Cell Biology* 9:436-U132.

Nett, I., D.Martin, D.Miranda-Saavedra, D.Lamont, J.Barber, A.Mehlert, and M.Ferguson. 2009. The phosphoproteome of bloodstream form Trypanosoma brucei, causative agent of African sleeping sickness. *Molecular & Cellular Proteomics* 8:1527-1538.

Ngo, H., C.Tschudi, K.Gull, and E.Ullu. 1998. Double-stranded RNA induces mRNA degradation in Trypanosoma brucei. *Proceedings of the National Academy of Sciences of the United States of America* 95:14687-14692.

Njiokou, F., C.Laveissiere, G.Simo, S.Nkinin, P.Grebaut, G.Cuny, and S.Herder. 2006. Wild fauna as a probable animal reservoir for Trypanosoma brucei gambiense in Cameroon. *Infect Genet Evol* 6:147-153.

Njiru, Z.K., A.S.J.Mikosza, E.Matovu, J.C.K.Enyaru, J.O.Ouma, S.N.Kibona, R.C.A.Thompson, and J.M.Ndung'u. 2008. African trypanosomiasis: Sensitive and rapid detection of the sub-genus Trypanozoon by loop-mediated isothermal

amplification (LAMP) of parasite DNA. *International Journal for Parasitology* 38:589-599.

Obado, S.O., C.Bot, D.Nilsson, B.Andersson, and J.M.Kelly. 2007. Repetitive DNA is associated with centromeric domains in Trypanosoma brucei but not Trypanosoma cruzi. *Genome Biology* 8:R37.

Ochola, D.O.K., R.K.Prichard, and G.W.Lubega. 2002. Classical ligands bind tubulin of trypanosomes and inhibit their growth in vitro. *J. Parasitol.* 88:600-604.

Ochsenreiter, T., S.Anderson, Z.A.Wood, and S.L.Hajduk. 2008. Alternative RNA Editing Produces a Novel Protein Involved in Mitochondrial DNA Maintenance in Trypanosomes. *Mol. Cell. Biol.* 28:5595-5604.

Ogbadoyi, E., K.Ersfeld, D.Robinson, T.Sherwin, and K.Gull. 2000. Architecture of the Trypanosoma brucei nucleus during interphase and mitosis. *Chromosoma* 108:501-513.

Ogbadoyi, E.O., D.R.Robinson, and K.Gull. 2003. A high-order trans-membrane structural linkage is responsible for mitochondrial genome positioning and segregation by flagellar basal bodies in trypanosomes. *Mol. Biol. Cell* 14:1769-1779.

Ohkura, H., M.A.Garcia, and T.Toda. 2001. Dis1/TOG universal microtubule adaptors - one MAP for all? *J Cell Sci* 114:3805-3812.

Olego-Fernandez, S., S.Vaughan, M.K.Shaw, K.Gull, and M.L.Ginger. 2009. Cell Morphogenesis of Trypanosoma brucei Requires the Paralogous, Differentially Expressed Calpain-related Proteins CAP5.5 and CAP5.5V. *Protist* 160:576-590.

Opperdoes, F.R. and P.A.M.Michels. 2007. Horizontal gene transfer in trypanosomatids. *Trends in Parasitology* 23:470-476.

Overath, P. and M.Engstler. 2004. Endocytosis, membrane recycling and sorting of GPI-anchored proteins: Trypanosoma brucei as a model system. *Mol Microbiol* 53:735-744.

Park, J.E., N.K.Soung, Y.Johmura, Y.H.Kang, C.Liao, K.H.Lee, C.H.Park, M.C.Nicklaus, and K.S.Lee. 2010. Polo-box domain: a versatile mediator of polo-like kinase function. *Cellular and Molecular Life Sciences* 67:1957-1970.

Parsons, M., E.Worthey, P.Ward, and J.Mottram. 2005. Comparative analysis of the kinomes of three pathogenic trypanosomatids: Leishmania major, Trypanosoma brucei and Trypanosoma cruzi. *BMC Genomics* 6:15.

Patrick, K., H.Shi, N.Kolev, K.Ersfeld, C.Tschudi, and E.Ullu. 2009. Distinct and overlapping roles for two Dicer-like proteins in the RNA interference pathways of the ancient eukaryote Trypanosoma brucei. *Proceedings of the National Academy of Sciences of the United States of America* 106:17933-17938.

Peck, S.C. 2006. Analysis of protein phosphorylation: methods and strategies for studying kinases and substrates. *Plant Journal* 45:512-522.

Perez-Morga, D., B.Vanhollebeke, F.Paturiaux-Hanocq, D.P.Nolan, L.Lins, F.Homble, L.Vanhamme, P.Tebabi, A.Pays, P.Poelvoorde, A.Jacquet, R.Brasseur, and E.Pays. 2005. Apolipoprotein L-1 promotes trypanosome lysis by forming pores in lysosomal membranes. *Science* 309:469-472.

Petronczki, M., P.Lenart, and J.M.Peters. 2008. Polo on the rise - from mitotic entry to cytokinesis with Plk1. *Developmental Cell* 14:646-659.

Pfister, D.D., G.Burkard, S.Morand, C.K.Renggli, I.Roditi, and E.Vassella. 2006. A mitogen-activated protein kinase controls differentiation of bloodstream forms of Trypanosoma brucei. *Eukaryotic Cell* 5:1126-1135.

Ploubidou, A., D.R.Robinson, R.C.Docherty, E.O.Ogbadoyi, and K.Gull. 1999. Evidence for novel cell cycle checkpoints in trypanosomes: kinetoplast segregation and cytokinesis in the absence of mitosis. *J Cell Sci* 112:4641-4650.

Pollard, T.D. 2010. Mechanics of cytokinesis in eukaryotes. *Curr Opin Cell Biol* 22:50-56.

Portman, N. and K.Gull. 2010. The paraflagellar rod of kinetoplastid parasites: From structure to components and function. *International Journal for Parasitology* 40:135-148.

Priotto, G., C.Fogg, M.Balasegaram, O.Erphas, A.Louga, F.Checchi, S.Ghabri, and P.Piola. 2006. Three drug combinations for late-stage Trypanosoma brucei gambiense sleeping sickness: a randomized clinical trial in Uganda. *PLoS Clin. Trials* 1:e39.

Qian, Y.W., E.Erikson, and J.L.Maller. 1998. Purification and cloning of a protein kinase that phosphorylates and activates the polo-like kinase Plx1. *Science* 282:1701-1704.

Radwanska, M., M.Chamekh, L.Vanhamme, F.Claes, S.Magez, E.Magnus, P.De Baetselier, P.Buscher, and E.Pays. 2002. The serum resistance-associated gene as a diagnostic tool for the detection of Trypanosoma brucei rhodesiense. *Am. J Trop Med Hyg.* 67:684-690.

Ralston, K.S., Z.P.Kabututu, J.H.Melehani, M.Oberholzer, and K.L.Hill. 2009. The Trypanosoma brucei Flagellum: Moving Parasites in New Directions. *Annual Review of Microbiology* 63:335-362.

Ralston, K.S., A.G.Lerner, D.R.Diener, and K.L.Hill. 2006. Flagellar motility contributes to cytokinesis in Trypanosoma brucei and is modulated by an evolutionarily conserved dynein regulatory system. *Eukaryotic Cell* 5:696-711.

Rasooly, R. and N.Balaban. 2002. Structure of p15 trypanosome microtubule associated protein. *Parasitology Research* 88:1034-1039**.**

Rasooly, R. and N.Balaban. 2004. Trypanosome microtubule-associated protein p15 as a vaccine for the prevention of African sleeping sickness. *Vaccine* 22:1007-1015.

Redmond, S., J.Vadivelu, and M.C.Field. 2003. RNAit: an automated web-based tool for the selection of RNAi targets in Trypanosoma brucei. *mbp* 128:115-118.

Reichl, E.M., J.C.Effler, and D.N.Robinson. 2005. The stress and strain of cytokinesis. *Trends in Cell Biology* 15:200-206.

Rindisbacher, L., A.Hemphill, and T.Seebeck. 1993. A repetitive protein from *Trypanosoma brucei* which caps the microtubules at the posterior end of the cytoskeleton. *Mol. Biochem. Parasitol.* 58:83-96.

Robinson, D.R., T.Sherwin, A.Ploubidou, E.H.Byard, and K.Gull. 1995. Microtubule Polarity and Dynamics in the Control of Organelle Positioning, Segregation, and Cytokinesis in the Trypanosome Cell-Cycle. *Journal of Cell Biology* 128:1163-1172.

Robinson, D.R. and K.Gull. 1991. Basal body movements as a mechanism for mitochondrial genome segregation in the trypanosome cell cycle. *Nature* 352:731-733.

Schneider, A., W.Eichenberger, and T.Seebeck. 1988a. A Microtubule-Binding Protein of Trypanosoma-Brucei Which Contains Covalently Bound Fatty-Acid. *J. Biol. Chem.* 263:6472-6475.

Schneider, A., A.Hemphill, T.Wyler, and T.Seebeck. 1988b. Large Microtubule-Associated Protein of T-Brucei Has Tandemly Repeated, Near-Identical Sequences. *Science* 241:459-462.

Schneider, A., U.Plessmann, and K.Weber. 1997. Subpellicular and flagellar microtubules of Trypanosoma brucei are extensively glutamylated. *J Cell Sci* 110:431-437.

Schneider, A., T.Sherwin, R.Sasse, D.G.Russell, K.Gull, and T.Seebeck. 1987. Subpellicular and Flagellar Microtubules of Trypanosoma-Brucei-Brucei Contain the Same Alpha-Tubulin Isoforms. *Journal of Cell Biology* 104:431-438.

Scott, V., T.Sherwin, and K.Gull. 1997. gamma-tubulin in trypanosomes: molecular characterisation and localisation to multiple and diverse microtubule organising centres. *J Cell Sci* 110:157-168.

Seong, Y.S., K.Kamijo, J.S.Lee, E.Fernandez, R.Kuriyama, T.Miki, and K.S.Lee. 2002. A spindle checkpoint arrest and a cytokinesis failure by the dominant-negative polo-box domain of plk1 in u-2 OS cells. *J. Biol. Chem.* 277:32282-32293.

Shaner, N.C., G.H.Patterson, and M.W.Davidson. 2007. Advances in fluorescent protein technology. *J Cell Sci* 120:4247-4260.

Sharma, R., L.Peacock, E.Gluenz, K.Gull, W.Gibson, and M.Carrington. 2008. Asymmetric cell division as a route to reduction in cell length and change in cell morphology in trypanosomes. *Protist* 159:137-151.

Sherwin, T. and K.Gull. 1989a. The Cell-Division Cycle of Trypanosoma-Brucei-Brucei - Timing of Event Markers and Cytoskeletal Modulations. *Philosophical*

Transactions of the Royal Society of London Series B-Biological Sciences 323:573-&.

Sherwin, T. and K.Gull. 1989b. Visualization of detyrosination along single microtubules reveals novel mechanisms of assembly during cytoskeletal duplication in trypanosomes. *Cell* 57:211-221.

Sherwin, T., A.Schneider, R.Sasse, T.Seebeck, and K.Gull. 1987. Distinct Localization and Cell-Cycle Dependence of Cooh Terminally Tyrosinolated Alpha-Tubulin in the Microtubules of Trypanosoma-Brucei-Brucei. *Journal of Cell Biology* 104:439-446.

Shi, H.F., A.Djikeng, T.Mark, E.Wirtz, C.Tschudi, and E.Ullu. 2000b. Genetic interference in Trypanosoma brucei by heritable and inducible double-stranded RNA. *Rna-A Publication of the Rna Society* 6:1069-1076.

Shi, H.F., A.Djikeng, T.Mark, E.Wirtz, C.Tschudi, and E.Ullu. 2000a. Genetic interference in Trypanosoma brucei by heritable and inducible double-stranded RNA. *Rna-A Publication of the Rna Society* 6:1069-1076.

Shi, J., J.B.Franklin, J.T.Yelinek, I.Ebersberger, G.Warren, and C.Y.He. 2008. Centrin4 coordinates cell and nuclear division in T-brucei. *J Cell Sci* 121:3062-3070.

Siegel, T.N., D.R.Hekstra, and G.A.M.Cross. 2008. Analysis of the Trypanosoma brucei cell cycle by quantitative DAPI imaging. *mbp* 160:171-174.

Simarro, P.P., J.Jannin, and P.Cattand. 2008. Eliminating human African trypanosomiasis: Where do we stand and what comes next? *Plos Medicine* 5:174-180.

Sonneborn, T.M. 1964. Differentiation of Cells. *Proceedings of the National Academy of Sciences of the United States of America* 51:915-&.

Stephan, A., S.Vaughan, M.K.Shaw, K.Gull, and P.G.Mckean. 2007. An essential quality control mechanism at the eukaryotic basal body prior to intraflagellar transport. *Traffic* 8:1323-1330.

Sternberg, J.M. 1998. Immunobiology of African trypanosomiasis. *Chem. Immunol*. 70:186-199.

Sternberg, J.M.L. 2010. A spectrum of disease in Human African trypanosomiasis: the host and parasite genetics of virulence. *Parasitology*1-9.

Stevens, J.R. and W.Gibson. 1999. The Molecular Evolution of Trypanosomes. *Parasitology Today* 15:432-437.

Steverding, D. 2008. The history of African trypanosomiasis. *Parasites & Vectors* 1:3.

Strebhardt, K. 2010. Multifaceted polo-like kinases: drug targets and antitargets for cancer therapy. *Nature Reviews Drug Discovery* 9:643-U24.

Sumara, I., J.F.Gimenez-Abian, D.Gerlich, T.Hirota, C.Kraft, C.de la Torre, J.Ellenberg, and J.M.Peters. 2004. Roles of polo-like kinase 1 in the assembly of functional mitotic spindles. *Current Biology* 14:1712-1722.

Sumara, I., E.Vorlaufer, P.T.Stukenberg, O.Kelm, N.Redemann, E.A.Nigg, and J.M.Peters. 2002. The dissociation of cohesin from chromosomes in prophase is regulated by polo-like kinase. *Molecular Cell* 9:515-525.

Sunkel, C.E. and D.M.Glover. 1988. Polo, A Mitotic Mutant of Drosophila Displaying Abnormal Spindle Poles. *J Cell Sci* 89:25-38.

Szoor, B., I.Ruberto, R.Burchmore, and K.R.Matthews. 2010. A novel phosphatase cascade regulates differentiation in Trypanosoma brucei via a glycosomal signaling pathway. *Genes & Development* 24:1306-1316.

Szoor, B., J.Wilson, H.McElhinney, L.Tabernero, and K.R.Matthews. 2006. Protein tyrosine phosphatase TbPTP1: a molecular switch controlling life cycle differentiation in trypanosomes. *Journal of Cell Biology* 175:293-303.

Taylor, A.E.R. and D.G.Godfrey. 1969. A New Organelle of Bloodstream Salivarian Trypanosomes. *Journal of Protozoology* 16:466-&.

Tetley, L., C.M.Turner, J.D.Barry, J.S.Crowe, and K.Vickerman. 1987. Onset of expression of the variant surface glycoproteins of Trypanosoma brucei in the tsetse fly studied using immunoelectron microscopy. *J Cell Sci* 87:363-372.

Torr,S.2005 Integrated vector management: Controlling malaria and trypanosomiasis with insecticide-treated cattle.
Ref Type: Report

Torrie, L., S.Wyllie, D.Spinks, S.Oza, S.Thompson, J.Harrison, I.Gilbert, P.Wyatt, A.Fairlamb, and J.Frearson. 2009. Chemical validation of trypanothione synthetase: a potential drug target for human trypanosomiasis. *J. Biol. Chem.* 284:36137-36145.

Tu, X. and C.C.Wang. 2005. Coupling of posterior cytoskeletal morphogenesis to the G1/S transition in the Trypanosoma brucei cell cycle. *Mol. Biol. Cell* 16:97-105.

Turner, C.M. and J.D.Barry. 1989. High frequency of antigenic variation in Trypanosoma brucei rhodesiense infections. *Parasitology* 99 Pt 1:67-75.

Turner, C.M.R., J.D.Barry, I.Maudlin, and K.Vickerman. 1988. An Estimate of the Size of the Metacyclic Variable Antigen Repertoire of Trypanosoma-Brucei-Rhodesiense. *Parasitology* 97:269-276.

Tyler, K.M., P.G.Higgs, K.R.Matthews, and K.Gull. 2001a. Limitation of Trypanosoma brucei parasitaemia results from density-dependent parasite differentiation and parasite killing by the host immune response. *Proc. R. Soc. Lon.* 268:2235-2243.

Tyler, K.M., K.R.Matthews, and K.Gull. 2001b. Anisomorphic cell division by African trypanosomes. *Protist* 152:367-378.

Urwyler, S., E.Studer, C.K.Renggli, and I.Roditi. 2007. A family of stage-specific alanine-rich proteins on the surface of epimastigote forms of Trypanosoma brucei. *Mol. Microbiol.* 63:218-228.

Valiron, O., N.Caudron, and D.Job. 2001. Microtubule dynamics. *Cellular and Molecular Life Sciences* 58:2069-2084.

Van Damme, D. and D.Geelen. 2008. Demarcation of the cortical division zone in dividing plant cells. *Cell Biology International* 32:178-187.

Van den Bossche, P., S.d.L.Rocque, G.Hendrickx, and J.Bouyer. 2010. A changing environment and the epidemiology of tsetse-transmitted livestock trypanosomiasis. *Trends in Parasitology* 26:236-243.

Van Hellemond, J.J., P.Neuville, R.T.Schwarz, K.R.Matthews, and J.C.Mottram. 2000. Isolation of Trypanosoma brucei CYC2 and CYC3 cyclin genes by rescue of a yeast G(1) cyclin mutant - Functional characterization of CYC2. *J. Biol. Chem.* 275:8315-8323.

Vanhamme, L., F.Paturiaux-Hanocq, P.Poelvoorde, D.P.Nolan, L.Lins, J.Van den Abbeele, A.Pays, P.Tebabi, H.Van Xong, A.Jacquet, N.Moguilevsky, M.Dieu, and E.Pays. 2003a. Apolipoprotein L-I is the trypanosome lytic factor of human serum. *Nature* 422:83-87.

Vanhamme, L., F.Paturiaux-Hanocq, P.Poelvoorde, D.P.Nolan, L.Lins, J.Van Den Abbeele, A.Pays, P.Tebabi, H.Van Xong, A.Jacquet, N.Moguilevsky, M.Dieu, J.P.Kane, P.De Baetselier, R.Brasseur, and E.Pays. 2003b. Apolipoprotein L-I is the trypanosome lytic factor of human serum. *Nature* 422:83-87.

Vassella, E., R.Kramer, C.M.R.Turner, M.Wankell, C.Modes, M.van den Bogaard, and M.Boshart. 2001. Deletion of a novel protein kinase with PX and FYVE-related domains increases the rate of differentiation of Trypanosoma brucei. *Mol. Microbiol.* 41:33-46.

Vaughan, S., L.Kohl, I.Ngai, R.J.Wheeler, and K.Gull. 2008. A Repetitive Protein Essential for the Flagellum Attachment Zone Filament Structure and Function in Trypanosoma brucei. *Protist* 159:127-136.

Vedrenne, C., C.Giroud, D.R.Robinson, S.B.Besteiro, C.Bosc, F.Bringaud, and T.Baltz. 2002. Two related subpellicular cytoskeleton-associated proteins in Trypanosoma brucei stabilize microtubules. *Mol. Biol. Cell* 13:1058-1070.

Vickerman,K. The mechanism of cyclical development in trypanosomes of the Trypanosoma brucei sub-group: An hypothesis based on ultrastructural observations. Transactions of the Royal Society of Tropical Medicine and Hygiene 56[6], 487-495. 1962.
Ref Type: Abstract

Vickerman, K. 1965. Polymorphism and Mitochondrial Activity In Sleeping Sickness Trypanosomes. *Nature* 208:762-766.

Vickerman, K. 1969. On The Surface Coat and Flagellar Adhesion in Trypanosomes. *J Cell Sci* 5:163-193.

Vickerman, K. 1985. Developmental Cycles and Biology of Pathogenic Trypanosomes. *British Medical Bulletin* 41:105-114.

Vickerman, K., L.Tetley, K.A.K.Hendry, and C.M.R.Turner. 1988. Biology of African Trypanosomes in the Tsetse-Fly. *Biology of the Cell* 64:109-119.

Vreysen, M.J., K.M.Saleh, M.Y.Ali, A.M.Abdulla, Z.R.Zhu, K.G.Juma, V.A.Dyck, A.R.Msangi, P.A.Mkonyi, and H.U.Feldmann. 2000. Glossina austeni (Diptera: Glossinidae) eradicated on the island of Unguja, Zanzibar, using the sterile insect technique. *J Econ Entomol* 93:123-135.

Walter, S.A., R.E.Cutler, R.Martinez, M.Gishizky, and R.J.Hill. 2003. Stk10, a new member of the polo-like kinase kinase family highly expressed in hematopoietic tissue. *J. Biol. Chem.* 278:18221-18228.

Wang, Y.L. 2005. The mechanism of cortical ingression during early cytokinesis: Thinking beyond the contractile ring hypothesis. *Trends in Cell Biology* 15:581-588.

Wenzler, T., D.W.Boykin, M.A.Ismail, J.E.Hall, R.R.Tidwell, and R.Brun. 2009. New Treatment Option for Second-Stage African Sleeping Sickness: In Vitro and In Vivo Efficacy of Aza Analogs of DB289. *Antimicrob. Agents Chemother.* 53:4185-4192.

Wheeler, R.J. 2010. The trypanolytic factor-mechanism, impacts and applications. *Trends in Parasitology* 26:457-464.

Wirtz, E. and C.Clayton. 1995. Inducible Gene-Expression in Trypanosomes Mediated by A Prokaryotic Repressor. *Science* 268:1179-1183.

Wirtz, E., S.Leal, C.Ochatt, and G.A.M.Cross. 1999. A tightly regulated inducible expression system for conditional gene knock-outs and dominant-negative genetics in Trypanosoma brucei. *mbp* 99:89-101.

Wong, O.K. and G.W.Fang. 2007. Cdk1 phosphorylation of BubR1 controls spindle checkpoint arrest and Plk1-mediated formation of the 3F3/2 epitope. *Journal of Cell Biology* 179:611-617.

Woods, A., A.J.Baines, and K.Gull. 1992. A High Molecular Mass Phosphoprotein Defined by A Novel Monoclonal-Antibody Is Closely Associated with the Intermicrotubule Cross Bridges in the Trypanosoma-Brucei Cytoskeleton. *J Cell Sci* 103:665-675.

Woods, A., T.Sherwin, R.Sasse, T.H.Macrae, A.J.Baines, and K.Gull. 1989. Definition of Individual Components Within the Cytoskeleton of Trypanosoma-Brucei by A Library of Monoclonal-Antibodies. *J Cell Sci* 93:491-500.

Woodward, R. and K.Gull. 1990. Timing of Nuclear and Kinetoplast Dna-Replication and Early Morphological Events in the Cell-Cycle of Trypanosoma-Brucei. *J Cell Sci* 95:49-57.

World Health Organisation. WHO includes combination of eflornithine and nifurtimox in its Essential List of Medicines for the treatment of human African trypanosomiasis. 2009.

Ref Type: Report

World Health Organisation. Human African trypanosomiasis: number of new cases drops to historically low level in 50 years. 2010.
Ref Type: Report

Yamashiro, S., Y.Yamakita, G.Totsukawa, H.Goto, K.Kaibuchi, M.Ito, D.J.Hartshome, and F.Matsumura. 2008. Myosin phosphatase-targeting subunit 1 regulates mitosis by antagonizing polo-like kinase 1. *Developmental Cell* 14:787-797.

Yarm, F.R. 2002. Plk phosphorylation regulates the microtubule-stabilizing protein TCTP. *Mol. Cell. Biol.* 22:6209-6221.